Shear Strengthening of RC beams by means of NSM laminates: experimental evidence and predictive models

Vincenzo Bianco, Joaquim Barros and Giorgio Monti

Report 06-DEC/E-18

Date: October of 2006
N. of pages: 170
Keywords: CFRP, NSM, Shear Strengthening, Reinforced Concrete

Universidade do Minho

Escola de Engenharia
Departamento de Engenharia Civil

Sapienza University of Rome

Department of Structural Engineering and Geotechnics

Table of Contents

Notation

$A_{fi}\left(L_{fi};\alpha_{fi}\right)$	Area of the projection of the i-th semi-conical surface on a plane orthogonal to the laminate
A_{fi}^{lin}	area ascribed to the i-th semi-ellipse underlying the line whose equation is $Y = b_w/2$
$A_{fi,k}^{lin}$	area ascribed to the i-th semi-ellipse of the k-th configuration underlying the line whose equation is $Y = b_w/2$
A_{fi}^{nlin}	Area ascribed to the i-th semi-ellipse underlying the i-th semi-elliptic curve $Y_i\left(X\right)$
$A_{fi,k}^{nlin}$	area ascribed to the i-th semi-ellipse of the k-th configuration underlying the i-th semi-elliptic curve $Y_{i,k}\left(X\right)$
$\underline{A}_k$	Matrix of the area ascribed to each ellipse in the k-th configuration
A_{fv}	Area of the FRP shear reinforcement within spacing s_f (after ACI 440.2R 2002)
C_E	Environmental-exposition reduction factor (after ACI 440.2R 2002)
$C_{fi}\left(L_{fi};\alpha_{fi}\right)$	Equation of the semi-conical surface associated to the i-th laminate
D_c	Diameter of the circular cross section of the strengthened member
$\underline{E}$	Matrix of the coefficients of the equation of the semi-ellipses
E_{ep}	Young's Modulus of the epoxy adhesive
E_f	Young's Modulus of the FRP
$E_{fi}\left(L_{fi};\alpha_{fi}\right)$	Equation of the semi-ellipse intersection of the i-th semi-conical surface with the assumed crack plane
$E_{i1,k}$	First coefficient of the equation of the i-th semi-ellipse in the k-th configuration
$E_{i2,k}$	Second coefficient of the equation of the i-th semi-ellipse in the k-th configuration
$E_{i3,k}$	Third coefficient of the equation of the i-th semi-ellipse in the k-th configuration
$E_{i4,k}$	Fourth coefficient of the equation of the i-th semi-ellipse in the k-th configuration
$\underline{E}_k$	Matrix of the coefficients of the equation of the semi-ellipses in the k-th configuration
E_0	Young's Modulus of the concrete in tension
E_s	Steel Young's Modulus
$\underline{F}$	Matrix of the position x_{fi} in the global reference system and the available bond length L_{fi} of each laminate
$\underline{F}_k$	matrix $\underline{F}$ in the k-th configuration
$\underline{G}$	Matrix of the geometrical properties associated to each i-th semi-cone, in the crack plane reference system $OXYZ$
G_f	FRP bond stress-slip fracture energy

G_{fk}	FRP bond stress-slip characteristic fracture energy
$\underline{G}_k$	Matrix $\underline{G}$ in the k-th configuration
L_{an}	Anchorage Length
$L_{an,SLS}$	Anchorage Length corresponding to the Serviceability Limit State (SLS)
$L_{an,ULS}$	Anchorage Length corresponding to the Ultimate Limit State (ULS)
L_d	Length of the shear crack in OXZ
L_e	FRP effective bond length (for Externally bonded, EB)
L_f	Actual total length of the FRP element
L_{fi}	Available bond length of the i-th laminate
$L_{fi,k}$	Available bond length of the i-th laminate in the k-th configuration
$L_{fi,\max}$	Maximum value of the available bond lengths for the specified case
$\overline{L}_f$	Effective length of an NSM laminate corresponding to an effective strain of 4‰
$L_{tot,\min}$	Minimum value of the sum of the effective length of all the NSM laminates/rods crossing the crack
$M_{ij,k}$	Auxiliary second order coefficient between the i-th and j-th semi-ellipses' equations in the k-th configuration
$\underline{M}_k$	Auxiliary matrix of the second order coefficients $M_{ij,k}$ in the k-th configuration
N_{eff}	Effective number of laminates intersecting the shear crack (after Nanni)
N_f	Number of laminates crossing the shear crack
$N_{f,k}$	Number of laminates crossing the shear crack in the k-th configuration on one side of the web
$N_{f,ev}$	Even integer number of laminates that can cross the CDC
$N_{f,odd}$	Odd integer number of laminates that can cross the CDC
$N^h_{f,\text{int}}$	Higher integer number of laminates that can cross the Critical Diagonal Crack
$N^l_{f,\text{int}}$	Lower integer number of laminates that can cross the Critical Diagonal Crack
$N_{f,real}$	Real number of laminates that cross the Critical Diagonal Crack (CDC)
$N_{ij,k}$	Auxiliary first order coefficient between the i-th and j-th semi-ellipses' equations in the k-th configuration
$\underline{N}_k$	Matrix of the first order coefficients $N_{ij,k}$ in the k-th configuration
$OXYZ$	Crack plane reference system
$Q_{ij,k}$	Auxiliary coefficient between the i-th and j-th semi-ellipses' equations in the k-th configuration
$\underline{Q}_k$	matrix of the coefficients $Q_{ij,k}$ in the k-th configuration
R_{fi}	Radius of the base of the semi-cone associated to the i-th laminate

$\underline{V}$	Matrix of the NSM shear strength contributions corresponding to each k-th configuration
V_c	Shear strength contribution provided by concrete
V_f	Ultimate shear strength contribution provided by the FRP system
V_{fi}	Ultimate shear strength contribution provided by th i-th element
$V_{f,k}$	NSM shear strength contribution in correspondence of the k-th configuration
$V_{f,k}^{DM}$	NSM CFRP laminate ultimate shear resistance according to the Debonding Model in the k-th configuration
V_{fi}^{p}	Ultimate force that can be resisted by the i-th element parallely to its axis
$V_{fi,k}^{p}$	Shear strength contribution provided by the i-th laminate of the k-th configuration parallely to its orientation
$V_{fi}^{p,cf}$	Ultimate force that can be resisted by the i-th element parallely to its axis due to concrete tensile fracture
$V_{fi}^{p,db}$	Ultimate force that can be resisted by the i-th element parallely to its axis due to debonding
$V_{fi}^{p,spl}$	Adhesive splitting-based component of the i-th laminate shear strength contribution parallely to its orientation
$V_{fi}^{p,tr}$	Ultimate force that can be resisted by the i-th element parallely to its axis due to tensile rupture of the element itself
$V_{f,\max}^{DM}$	Analytical maximum contribution to the overall shear resistance by NSM laminates according to the DM
$V_{f,\min}^{DM}$	Analytical minimum contribution to the overall shear resistance by NSM laminates according to the DM
V_{f}^{exp}	Experiemntal contribution to the overall shear resistance by NSM laminates
$V_{f,\max}^{PM}$	Analytical maximum contribution to the overall shear resistance by NSM laminates according to the PM
$V_{f,\min}^{PM}$	Analytical minimum contribution to the overall shear resistance by NSM laminates according to the PM
$\underline{V}_{k}^{p}$	Matrix of the shear strength contributions, for the k-th configutation, ascribed to each i-th laminate parallely to their orientation
V_s	Shear strength contribution provided by the existing steel stirrups
V_R	Ultimate shear resistance of the RC element
V_{Rd}	Design shear resistance of the strengthened RC element
$V_{Rd,c}$	Concrete contribution to the design shear resistance of the strengthened RC element
$V_{Rd,s}$	Stirrups contribution to the design shear resistance of the strengthened RC element
$V_{Rd,f}$	FRP contribution to the design shear resistance of the strengthened RC element
$V_{Rd,\max}$	Maximum value of design shear resistance of the strengthened RC element
V_{Sd}	Design shear force
V_{f1}	NSM FRP shear strength contribution according to debonding (after De Lorenzis)
V_{f2}	NSM FRP shear strength contribution according to aggregate interlock saving (after De

	Lorenzis)
X_{fi}	Position of the laminate along the OX axis
$X_{fi,k}$	X_{fi} in the k-th configuration
$X_{i1,k}^{lin3}$	Abscissa of the left intersection of the i-th semi-ellipse of the k-th configuration with the line $Y = b_w/2$ constituting effective integration extremity in the linear range
$X_{i2,k}^{lin3}$	Abscissa of the right intersection of the i-th semi-ellipse of the k-th configuration with the line $Y = b_w/2$ constituting effective integration extremity in the linear range
$X_{i1,k}^{lin4}$	Value of abscissa ($X = 0$) if constituting effective integration extremity in the linear range for the i-th semi-ellipse of the k-th configuration
$X_{i2,k}^{lin4}$	Value of abscissa ($X = L_d$) if constituting effective integration extremity in the linear range for the i-th semi-ellipse of the k-th configuration
$X_{ij,k}^{lin1/2}$	Abscissa of the first/second intersection point between the i-th and j-th semi-ellipses of the k-th configuration constituting integration extremities for the relevant i-th semi-ellipse in the linear range
$X_{ij,k}^{p1/2}$	Abscissa of the first/second intersection point between the i-th and j-th semi-ellipses in the k-th configuration
$\underline{X}_k^{lin}$	Matrix of the abscissa values of the integration extremities in the linear range, for the k-th configuration
$\underline{X}_k^{lin1}$	Matrix of the abscissa values of the first intersection point between couples of ellipses constituting effective integration extremities in the linear range
$\underline{X}_k^{lin2}$	Matrix of the abscissa values of the second intersection point between couples of ellipses constituting effective integration extremities in the linear range
$\underline{X}_k^{lin3}$	Matrix of the abscissa values of the intersection points of the semi-ellipses with the line
$\underline{X}_k^{lin4}$	Matrix of the abscissa values $X = 0$ or $X = L_d$ constituting effective integration extremity in the linear range
$\underline{X}_k^{nlin}$	Matrix of the abscissa values of the integration extremities in the non linear range
$\underline{X}_k^{nlin1}$	Matrix of the abscissa values of the first intersection point between couples of ellipses constituting effective integration extremities in the non linear range
$\underline{X}_k^{nlin2}$	Matrix of the abscissa values of the second intersection point between couples of ellipses constituting effective integration extremities in the non linear range
$X_{ij,k}^{nlin1/2}$	Abscissa of the first/second intersection point between the i-th and j-th semi-ellipses in the k-th configuration constituting integration extremities in the non linear range
$\underline{X}_k^{nlin3}$	Matrix of the abscissa values of the intersection points of the semi-ellipses with the line $Y = b_w/2$ constituting effective integration extremities in the non linear range
$X_{i1,k}^{nlin3}$	Abscissa of the left intersection of the i-th semi-ellipse of the k-th configuration with the line $Y = b_w/2$ constituting effective integration extremity in the non linear range
$X_{i2,k}^{nlin3}$	Abscissa of the right intersection of the i-th semi-ellipse of the k-th configuration with the line $Y = b_w/2$ constituting effective integration extremity in the non linear range
$\underline{X}_k^{nlin4}$	Matrix of the abscissa values $X = 0$ or $X = L_d$ constituting effective integration extremity in the non linear range
$X_{i1,k}^{nlin4}$	Value of abscissa ($X = 0$) if constituting effective integration extremity in the non linear range for the i-th semi-ellipse of the k-th configuration
$X_{i2,k}^{nlin4}$	Value of abscissa ($X = L_d$) if constituting effective integration extremity in the non linear

	range for the i-th semi-ellipse of the k-th configuration
$\underline{X}_k^{nlin5}$	Matrix of the abscissa values of the vertices of the semi-ellipses along their major semi-axis constituting effective integration extremity in the non linear range
$X_{i1,k}^{nlin5}$	Value of abscissa of the left vertex of the i-th semi ellipse of the k-th configuration if it constitutes an effective integration extremity in the non linear range of the relevant semi-ellipse
$X_{i2,k}^{nlin5}$	Value of abscissa of the right vertex of the i-th semi ellipse of the k-th configuration if it constitutes an effective integration extremity in the non linear range of the relevant semi-ellipse
$X_{i1,k}^{q}$	Abscissa of the left intersection point of the i-th semi-ellipse with the line $Y = b_w/2$
$X_{i2,k}^{q}$	Abscissa of the right intersection point of the i-th semi-ellipse with the line $Y = b_w/2$
$\underline{X}_k^{p1}$	Matrix storing the abscissa of the first intersection point between each couple of semi ellipses in the k-th configuration
$\underline{X}_k^{p2}$	Matrix storing the abscissa of the second intersection point between each couple of semi ellipses in the k-th configuration
$\underline{X}_k^{q}$	Matrix storing the abscissa of the left and right intersection points between each semi ellipse and the straight line $Y = b_w/2$ in the k-th configuration
X_o	Position of the center of the i-th semi-ellipse along the OX axis
$X_{oi,k}$	Position of the center of the i-th semi-ellipse along the OX axis in the tk-th configuration
$Y_i(X)$	General expression of the equation of the i-th semi-ellipse in the OXY crack plane reference system
$Y_{i,k}(X)$	Equation of the i-th semi-ellipse in the generic k-th configuration in OXY
$Y = b_w/2$	Equation of the line trace of the mean plane of the beam on the assumed crack plane
$Y_{i1,k}^{e}$	Ordinate of the i-th semi-ellipse in correspondence of $X = 0$ in the k-th configuration
$Y_{i2,k}^{e}$	Ordinate of the i-th semi-ellipse in correspondence of $X = L_d$ in the k-th configuration
$\underline{Y}_k^{e}$	Matrix storing the ordinate of each semi-ellipse in correspondence of $X = 0$ and $X = L_d$, in the k-th configuration
a	Shear Span
a_i	Major semi-axis of the i-th semi-ellipse
$a_{i,k}$	Major semi-axis of the i-th semi-ellipse in the k-th configuration
$a_e^{'}$	Distance of the laminate from the edge of the specimen
a_f	Thickness of the cross section of the adopted FRP element
b_i	Minor semi-axis of the i-th semi-ellipse
$b_{i,k}$	Minor semi-axis of the i-th semi-ellipse in the generic k-th configuration
d	Section effective depth
b_c	Width of the concrete specimen
b_f	Width of the cross section of the adopted FRP element
b_w	RC beam cross section web width

c	Concrete cover of the member cross section
d	Beam cross section effective depth
d_b	Diameter of the NSM rods
e_{1Pi}	Abscissa of an auxiliary point P in the local reference system $oe_{1i}e_{2i}e_{3i}$ associated to the i-th semi-ellipse
e_{2Pi}	Ordinate of an auxiliary point P in the local reference system $oe_{1i}e_{2i}e_{3i}$ associated to the i-th semi-ellipse
$e_{1Pi,k}$	Abscissa of an auxiliary point P in the local reference system $oe_{1i,k}e_{2i,k}e_{3i,k}$ associated to the i-th ellipse in the k-th configuration
$e_{2Pi,k}$	Ordinate of an auxiliary point P in the local reference system $oe_{1i,k}e_{2i,k}e_{3i,k}$ associated to the i-th ellipse in the k-th configuration
f_b	Bearing stress along the ribs of steel ribbed bars
f_c	Concrete mean cylindrical compressive strength
f_{ck}	Characteristic value of the concrete cylindrical compressive strength
f_{cm}	Concrete cylindrical mean compressive strength
f_{ctm}	Concrete mean tensile strength
$f_{ct,sp}$	Mean value of the concrete splitting tensile strength
$f_{ep,fl}$	Epoxy bending tensile strength
$f_{ep,c}$	Epoxy compressive strength
f_{fd}	FRP design ultimate strength
f_{fe}	Effective stress in the FRP
f_{fdd}	Ultimate debonding-based FRP design strength
$f_{fdd,rid}$	Reduced value of the ultimate FRP design strength
f_{fed}	Effective FRP design strength
f_{fu}	Design value of the ultimate tensile strength
f_{fu}^{*}	Value of the ultimate tensile strength provided by the supplier
h	Depth of beam cross section
h_w	Beam cross section web height
i	Counter of the FRP elements crossing the crack on one side of the web
j	Counter of the FRP elements crossing the crack on one side of the web
k	Counter for the three different dispositions of the laminates along the crack
k_f	FRP sheet geometric coefficient
n	Number of layers of FRP per strip in the EB wet lay-up technology
$\underline{n}_k^{lin}$	Matrix containing the number, integer, of real values constituting effective integration extremities for each semi-ellipse in the linear range

$n_{i,k}^{lin}$	Maximum number, integer, of real values constituting effective integration extremities for the i-th semi-ellipse of the k-th configuration in the linear range
$n_{i,k}^{nlin}$	Maximum number, integer, of real values constituting effective integration extremities for the i-th semi-ellipse of the k-th configuration in the non linear range
n_{k}^{lin}	Maximum number, integer, of real values constituting effective integration extremities among all the semi-ellipses of the k-th configuration in the linear range
$\underline{n}_{k}^{nlin}$	Matrix containing the integer number of real values constituting effective integration extremities for each semi-ellipse in the non linear range
n_{k}^{nlin}	Maximum number, integer, of real values constituting effective integration extremities among all the semi-ellipses of the k-th configuration in the non linear range
$oe_{1i}e_{2i}e_{3i}$	Local reference system of the i-th semi-ellipse
$oe_{1i,k}e_{2i,k}e_{3i,k}$	Local reference system of the i-th semi-ellipse in the generic k-th configuration
$oxyz$	Global reference system
r_c	Rounded corner radius of the RC member section
s_f	Spacing between subsequent FRP elements measured along the axis of the beam
$s_f^{'}$	Spacing between subsequent FRP elements measured orthogonally to their orientation
t_s	Thickness of the slab of the beam cross section
v_1	Position, along the OX axis, of the leftward vertex of the semi-ellipse along its major semi-axis
$v_{1i,k}$	Position of the leftward vertex of the i-th semi-ellipse along its major semi-axis in the k-th configuration
v_2	Position, along the OX axis, of the leftward vertex of the semi-ellipse along its major semi-axis
$v_{2i,k}$	Position of the leftward vertex of the i-th semi-ellipse along its major semi-axis in the k-th configuration
w	Crack width
w_0	Maximum crack opening at which concrete can no longer transfer tensile stress
$\underline{x}$	Matrix of the geometrical properties in the global reference system
x_{f1}	Position of the first laminate, along the web soffit, with respect to the assumed crack origin
$x_{f1,k}$	Position of the first laminate, along the web soffit, with respect to the assumed crack origin, in correspondence of the k-th configuration
$x_{fi,k}$	Position of the i-th laminate with respect to the crack origin in the global reference system $oxyz$ for the k-th configuration
z	Beam cross section internal lever arm
$\alpha_{fi}\left(L_{fi}\right)$	Angle between the genratrices and the axis of the semi-conical surface associated with the i-th laminate
$\alpha_{fi,k}$	Angle between the genratrices and the axis of the semi-conical surface associated with the i-th laminate in the k-th configuration
β	Inclination of the FRP element with respect to the beam axis
δ_{fu}	FRP ultimate slip beyond which shear stress can no longer be transferred (EBR)

δ_0	Maximum deformation at which concrete can no longer transfer force intension
δ_f	EB FRP slip at the peak of bond strength
ε_{fd}	Designvalue of the FRP ultimate strain
ε_{fdd}	FRP debonding-based ultimate design strain
ε_{fe}	Mean value of the effective strain present in the FRP
ε_{fed}	Design value of the effective strain of the FRP
ε_{fek}	Characteristic value of the FRP effective strain
ε_{fu}	FRP mean ultimate strain
ε_{fu}^{*}	Value of the ultimate strain of the FRP provided by the manufacturer
ϕ	Strength reduction factor required by ACI 318-02
γ	Angle between the rib face and the bar axis, in a ribbed bar
γ_c	Concrete material partial safety factor
γ_f	Partial safety factor for the FRP material
γ_s	Steel material partial safety factor
γ_{Rd}	Partial safety factor for resistance model
ν	Poisson's ratio
θ	Shear crack inclination with respect to the longitudinal axis of the beam
$\theta^{\exp}$	Experiemntal value for the critical diagonal crack inclination angle
ρ_{fw}	FRP shear reinforcement ratio
ρ_{sl}	Longitudinal steel reinforcement ratio
ρ_{sw}	Transversal steel reinforcement ratio
$\tau(\delta)$	Local Bond Stress-Slip Relationship
τ_a	Shear Stress developed along the surface of the steel bar through adhesion
τ_{af}	Shear Strength of the Epoxy
τ_b	NSM laminate average bond strength
$\tau_b(L_f)$	Relationship between the average bond strength and the laminate available bond length
τ_f	Peak stress of the FRP local bond stress-slip relationship
$\tau_{b,rod}(L_{fi})$	Adopted relationship between average bond strength and available bond length for the case of NSM rods
$\tau_{spl,rod}(L_{fi})$	Adopted relationship between adhesive splitting-based average bond strength and available bond length for the case of NSM rods
τ_c	Shear stresses in the concrete surrounding embedded steel bars
ψ_f	Reduction factor for the case of U-wraps according to the ACI 440-02

ΔF_b	Force transmitted by an elementary bond length ΔL_b
ΔX	Infinitesimal increment of the abscissa X

1 Employment of Near Surface Mounted CFRP Laminates

The Shear Strengthening of existing reinforced concrete beams has been traditionally carried out so far mainly by means of the following two techniques: 1) external reinforcement, based on gluing steel plates to the surface of RC elements by means of structural adhesives, mainly epoxies; 2) adding external reinforced concrete coats that consist on wrapping the element with a reinforced concrete layer.

The application of adhesive epoxy can be performed by either spreading the adhesive on both the surfaces to be pasted to each other or by injecting it in the voids in between. The bonded joint can also be improved by means of bolt shear connectors. In order to guarantee good bond conditions, a meticulous preparation is needed not only for the concrete surface but for the plate as well. It is a technique well known by technical community dealing with structural strengthening. It also involves the use of materials whose mechanical behaviour has already been extensively investigated. That technique, anyway, presents some drawbacks: due to the steel's susceptibility to corrosion, it is very likely for the glued zone to undergo high deterioration; difficulty to handle weighty elements in the construction yard, especially if curved surfaces are involved; necessity of temporary supports during the curing time of the adhesive; limited dimensions of the elements due to transportation reasons and the consequent need for in-place executed joints.

The coating technique is much more efficient as regards the protection of added reinforcement against both corrosion and fire exposition. Nevertheless, the increase in the cross sectional dimensions is not always admissible from an architectural point of view and it might also result incompatible with the use destination of the building to be retrofitted. Moreover, a deal of time is required for the concrete to gain an adequate value of strength before the structure can be put in service again.

In the recent years the use of Fibre Reinforced Polymers (CFRP) in the strengthening of existing structures has spread worldwide due to the possibility of overcoming some of the drawbacks shown by the traditional techniques described above. The FRPs present high stiffness and tensile strength, low specific weight and good resistance to fatigue. The reduced specific weight facilitates both its transport and handling. The availability of these materials in practically unlimited sizes excludes the necessity of joints *in situ*. Their high resistance to corrosion makes them particularly suitable for application in aggressive environments such as costal zones. Moreover, due to their high mechanical properties, FRPs can guarantee the attainment of considerable increase in resistance by means of low addictions thus preserving the original architectural conception of the building. Some FRPs can be easily applied in case of curved surfaces, objective difficult to pursue by means of steel plates. Furthermore, retrofitting techniques employing FRPs can be carried out easily and quickly.

Shear strength of existing reinforced concrete elements can be significantly increased by gluing FRP strips or sheets orthogonally to either their axis or the direction of the shear cracks, as already extensively recognised by the Research Community. In fact, different guidelines dealing with FRP strengthening of existing RC structures are available worldwide CNR DT 200 (2004), Australian Guidelines (2006), fib Model Code (2001), ACI Committee (2002). This technique, designated as externally bonded reinforcing (EBR), has already been extensively investigated. A huge amount of experimental programs (Monti and Liotta 2006, Liotta 2007, Bousselham and Chaalal 2004, Dias and Barros 2004a) have shown that the external gluing of Carbon Fibre Reinforced Polymers (CFRP) allows the shear strength of RC beams to be considerably increased. However, due to the premature debonding occurring to the externally bonded FRP strips or sheets, the maximum stress mobilized is quite lower than their ultimate strength. Moreover, the failure modes associated to debonding are generally sudden and brittle.

In order to overcome these drawbacks and reduce the EBRs' susceptibility to the action of fire or vandalism, new techniques of employment of FRPs have been proposed by the World Academic Community to date.

In 2002 De Lorenzis, with the purpose of enhancing the effectiveness of CFRPs in the shear strengthening of RC beams, introduced CFRP rods inside grooves opened in the concrete cover of the lateral faces of the beams. Among the advantages obtained with respect to the previous EBR there were: a significant increase of the shear strength and a higher protection of the reinforcing elements. Conversely, the necessity to open deep grooves for installing the bars, constituted a considerable disadvantage.

In 2004, Dias and Barros (2004b) proposed to introduce laminates into thin slits, thus extending to the case of shear strengthening the technique adopted till that moment mainly in the flexural strengthening of RC beams (Blaschko and Zilch (1999), Barros *et al.* (2006), El-Hacha and Rizkalla (2004)). The effectiveness of the insertion of CFRP strips in saw-cut slits within the concrete cover in fact, had been already acknowledged worldwide at that time, for flexural strengthening.

Definitely the reasons why the use of the NSM technique (acronym for Near Surface Mounted, extensively adopted hereafter) is desirable with respect to the previous EBR can be summarized as follows:

1. Avoiding the premature and brittle failure due to the phenomenon of debonding thus attaining more ductile failure modes;
2. Improving the exploitation of the material by mobilizing, for equal strengthening ratio, stresses much closer to the strength of the FRP material in virtue of averting debonding, with consequent economical benefits;
3. Possibility to have higher values of local bond strength with respect to EBR, so as remarked by Sena-Cruz and Barros (2002) and by Sena-Cruz (2004) by means of pull-out bending tests;
4. Possibility to improve the overall structural behaviour of the strengthened RC element. In fact, the employment of NSM laminates has proven (Barros and Dias 2005) to increase the stiffness, the ultimate load and the corresponding deflection of the shear strengthened element;
5. Extra protection against fire and vandalism.

The NSM shear-strengthening system is applied by the following procedure, (Dias and Barros (2005b, 2006)) (see Fig. 1.1):

1. using a diamond blade cutter, slits of about 5 mm width and 12 to 15 mm depth are opened in the concrete cover of the lateral surfaces of the beam's web, according to the pre-defined geometrical arrangement for the laminates;
2. slits are cleaned by compressed air in order to improve the bond performance of the adhesive to the concrete substrate;
3. laminates are cleaned by acetone;
4. epoxy adhesive is prepared according to supplier recommendations;
5. slits are filled with the epoxy adhesive;
6. epoxy adhesive is applied on the faces of the laminates;
7. laminates are introduced into the slits and epoxy adhesive in excess is removed;

The curing time for the adhesive, recommended by the supplier, should spend before testing.

1) Execution of the slits

2) Cleaning of the slits by compressed air

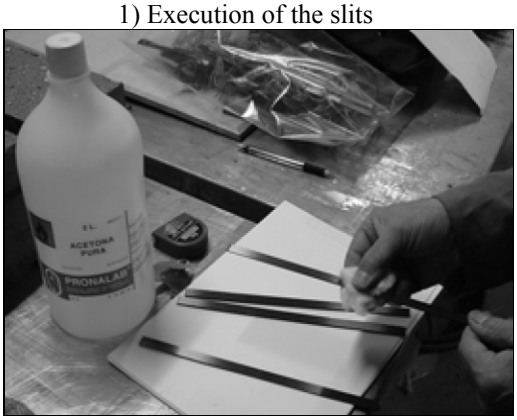

3) Cleaning of the laminates by acetone

4) Filling up the slits with adhesive

5) Application of the adhesive on the laminates

6) Introduction of the laminates

7) Removal of the adhesive in excess

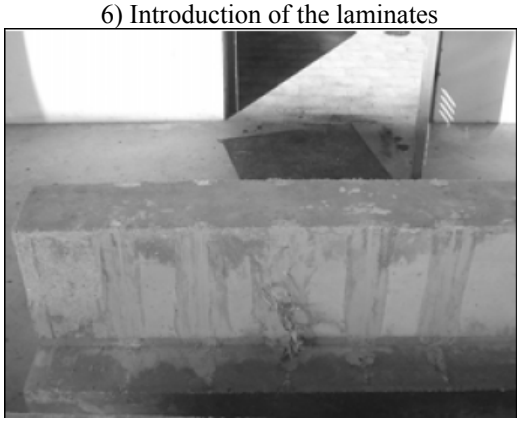

8) Curing time

Fig. 1.1 – Phases of the NSM CFRP laminate shear strengthening technology: phases (pictures taken from Dias and Barros (2005b))

As regards the procedure to open the slits, it is currently executed by means of round diamond blade cutters and refined manually in the zone of connection between the web and the slab of T cross section beams. In that respect, in order to shorten the amount of time required to execute the retrofitting intervention, the production of purposely intended devices with a small diameter round diamond blade cutter is desirable for further developments.

For the purpose of increasing the execution rapidity of the NSM technique, a device such as a gun-type applicator like those already in use in the field of the fastening technology, should be developed to fill the slits with the structural adhesive.

The first experimental programs, aiming at assessing the efficacy of the NSM technique, (De Lorenzis 2002, De Lorenzis and Nanni 2001), employed CFRP rods instead of laminates. More recently, El-Hacha and Rizkalla (2004) demonstrated that rectangular cross section bars are more effective than round rods.

2 Physical Phenomena, Resisting Mechanisms and Parameters affecting the Shear Strength

Before a method for calculating the shear resistance of NSM CFRP shear-strengthened RC members can be proposed, the main aspects influencing the FRP contribution to the shear-strength of RC beams strengthened by means of the NSM technique must be clearly singled out. This chapter is dedicated to this subject, taking into account the most accredited research findings currently available worldwide even if they are not strictly dedicated to the NSM but to the EBR, in case this latter comprehend similar mechanical behaviors. Moreover, some aspects, deemed important according to the "*structural feeling*" and "*intuition*" of the authors, are outlined and analyzed in depth even if they have not been taken into consideration by other researchers, up to now.

2.1 Bond between CFRP Laminates and Concrete

Bond performance is one of the main aspects affecting the ultimate load-carrying capacity of a strengthened reinforced concrete element, as well as its performance under serviceability limit state conditions.

An extensive experimental-analytical program, aimed at developing a better insight in the bond performance of NSM CFRP laminates was carried out by Sena-Cruz and Barros (2002 and 2004) by means of pull-out bending tests under both monotonic and cyclic loading. In that occasion the influence of parameters such as bond length, concrete compressive strength and load type was analysed by using CFRP laminates whose cross-section was 1.4 mm thick and 10 mm wide with smooth surface. In the tested specimens, a large slip in the laminate-concrete interface was observed.

From a physical point of view, a fish-spine cracking pattern occurred in the adhesive (see Fig.-2.1 and Sena-Cruz 2004) due to the tangential stresses developed at the adhesive-concrete and CFRP-adhesive interfaces as a consequence of the stress transfer between concrete and CFRP which gradually yielded its failure and the consequent slip at the laminate-concrete interface (see Fig. 2.2). The above described behaviour was pointed out by means of the photos taken by an optical microscope and reported hereafter.

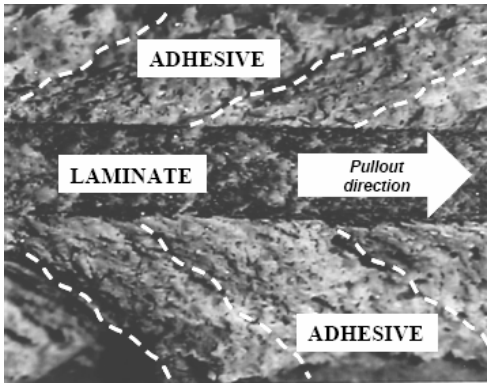

Fig. 2.1 – Crack pattern at the laminate-adhesive-concrete bonding zone

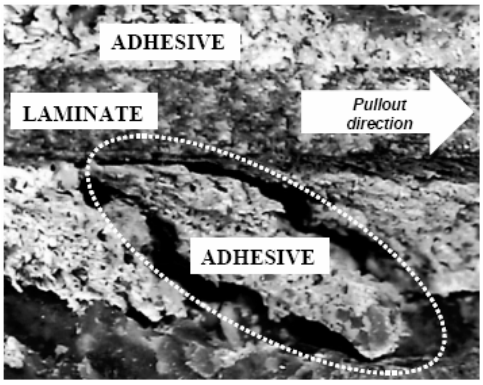

Fig. 2.2 – Failure of the epoxy adhesive

Figure 2.3 schematically depicts the micro-mechanism developed in the adhesive that yields the aforementioned fish-spine crack pattern.

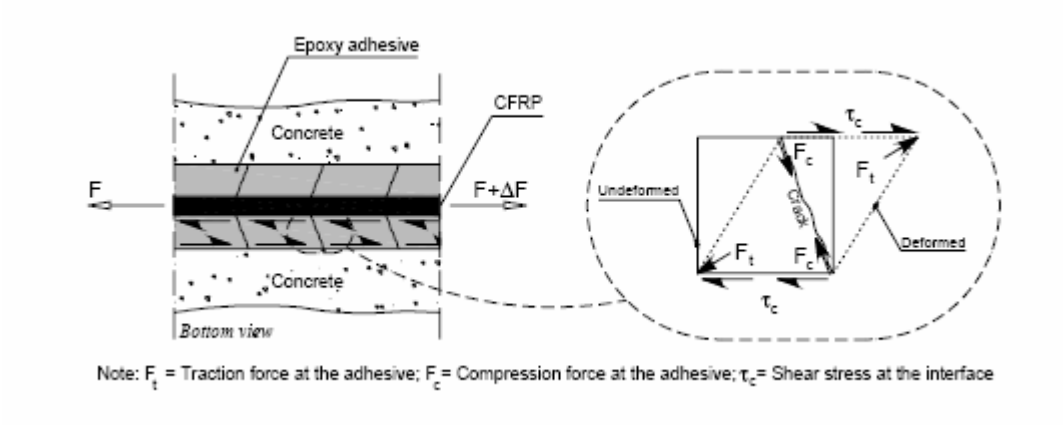

Fig. 2.3 – Force distribution corresponding to the crack pattern in the epoxy adhesive.
Note: F_t is the traction force at the adhesive; F_c is the compression force at the adhesive; τ_c is the shear stress at the interface.

As can be gathered from Figures 2.4 and 2.5, for the tested specimens, the concrete compressive strength did not show influence at all on the bond stress-slip relationship while a clear dependence on the bond length, L_b, emerged: both the peak pull-out force and the corresponding loaded end-slip increased with L_b (for further details see Sena-Cruz and Barros 2002).

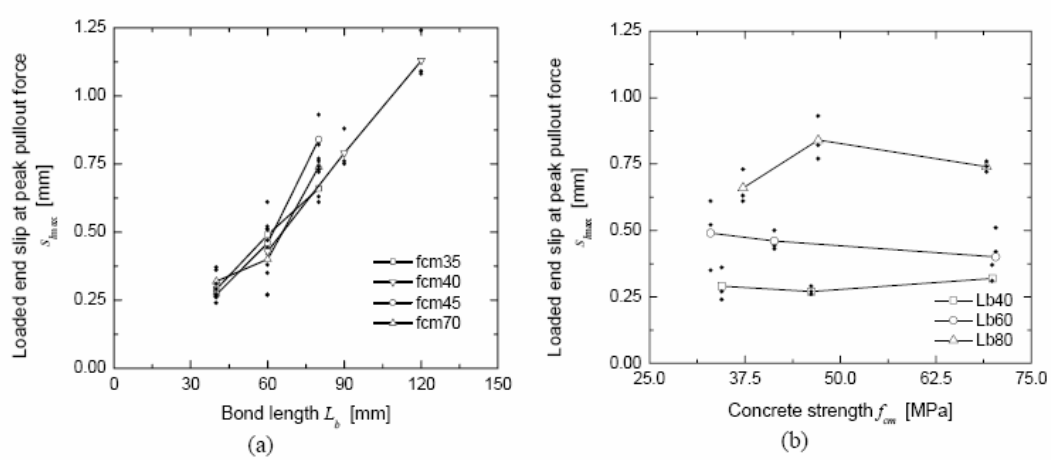

Fig. 2.4 – Influence of the bond length (a) and concrete strength (b) on the loaded end slip at peak pull-out force

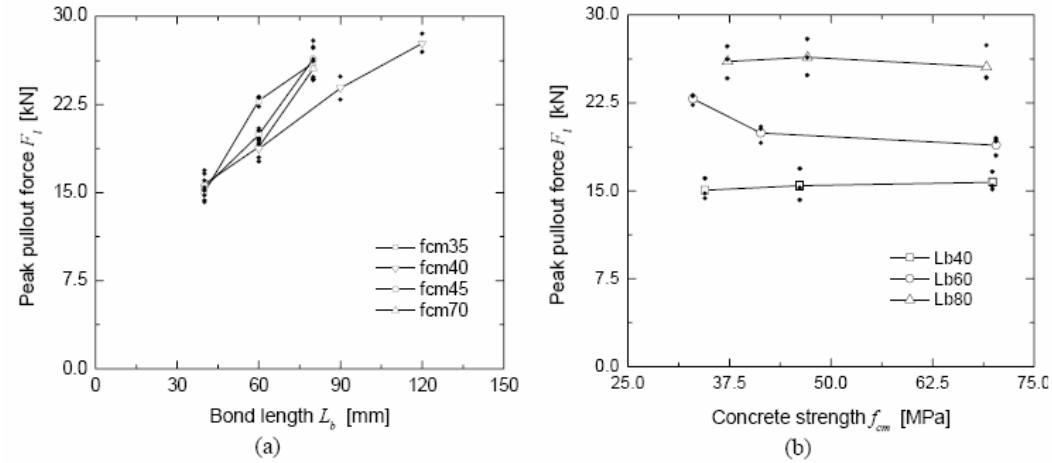

Fig. 2.5 – Influence of bond length (a) and concrete strength (b) on the pull-out force

Anyway it is worth underlying that, while the influence of concrete compressive strength on the bond is negligible for medium and high strength concretes whose mean compressive strength ranges from 30 to 70 MPa, the suspicion exists that this tendency can not be extrapolated for concretes of average compressive strength lower than 30 MPa.

Furthermore, in the experimental programs by Sena-Cruz and Barros (2004a), the concrete was reinforced by steel fibres, which might have contributed to avoid crack formation and propagation to the concrete surrounding the bond zone. Therefore, in the case of concrete strength classes of f_c lower than 50 MPa, without any fibres reinforcement, the concrete tensile strength might have influence on the CFRP-concrete behaviour. In that occasion (2004a), Sena-Cruz and Barros justified the use of fibre-reinforced concrete arguing that, for the amount of fibres used, only the concrete post cracking tensile residual strength could be affected but, since concrete cracking was not expected to occur in the bonding zone, the influence of the presence of fibres on the bond behavior, would be marginal. Anyway, in the authors' opinion, if the purpose is to isolate and study the phenomenon of debonding, the use of a fibre-reinforced concrete has no influence. In fact, the term "*debonding*" envisages failure occurring at the laminate/adhesive or adhesive/concrete interface, as well as within the adhesive. Debonding can be also regarded as a failure occurring along a surface parallel to the laminate, a few millimetres inside the surrounding concrete since a thin layer of concrete in contact with the adhesive has higher strength due to the adhesive penetration into its micro-structure. The pullout tests, currently underway, show that the debonding failure might be characterized by the simultaneous occurrence of more than one of these mechanisms.

In the work by Sena-Cruz & Barros, an increase in the slit dimensions showed to be absolutely detrimental for the bond performance. In fact, the increase in the peak pull-out force with L_b was higher with narrower slits. The same remark has been done by Blaschko (2003) who suggested that the depth and width of the cut groove should be at most about 3 mm larger than the width and thickness of the FRP laminate, so as to obtain an adhesive layer thickness of about 1-2 *mm*. In this respect, also Paretti and Nanni (2004) recommended that the minimum width of a groove be no less than $3\ a_f$ and the minimum depth be no less than $1.5\ b_f$. Where a_f is the thickness and b_f the width of the laminate cross section.

The local bond stress-slip $\tau(\delta)$ relationship is well represented by the following formulae (Sena-Cruz and Barros 2004a):

$$\tau(\delta)=\begin{cases}\tau_m \cdot \left(\dfrac{\delta}{\delta_m}\right)^{\alpha} & \text{if } \delta \le \delta_m \\ \tau_m \cdot \left(\dfrac{\delta}{\delta_m}\right)^{-\alpha'} & \text{if } \delta > \delta_m\end{cases} \tag{2.1}$$

where τ_m and δ_m are the peak bond strength and its corresponding slip, α and α' are parameters defining the shape of the curves. The equation for $\delta \le \delta_m$ was used by Eligehausen *et al.* (1983) and defines the bond behaviour up to peak stress (ascending branch). The equation for $\delta > \delta_m$ was also adopted by DeLorenzis & Nanni (2002) and reproduces the post-peak bond behaviour (descending branch). This law was selected due to its simplicity and ability to

simulate the phenomena under discussion: the gradual post-peak descending branch actually exists when bond failure occurs at an interface. In that case, a significant amount of post-peak friction develops, due to interfacial friction.

Sena Cruz & Barros (2004a) calibrated the main parameters of the above relationship on the basis of the collected experimental data and obtained the values indicated in Table 2.1, by a rigorous analytical approach.

Table 2.1 – Values for the parameters of Equation (2.1)

	τ_m	δ_m	α	α'
	[MPa]	[mm]	[ ]	[ ]
Average	19.81	0.25	0.21	0.32
C.O.V.	6.6	36.19	29.05	21.49

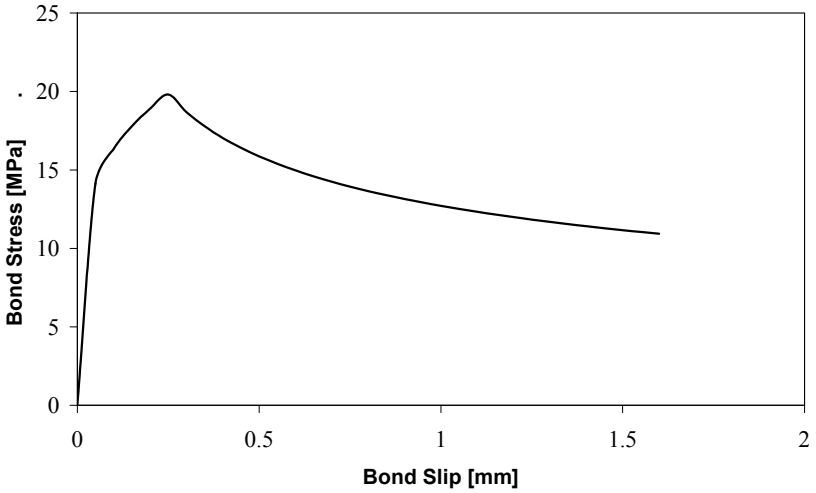

Fig. 2.6 – Bond stress-slip relationship calibrated by Sena & Barros (2004a)

The local bond stress-slip relationship, represented in Figure 2.6, is generally referred to as type-I curve by the International Academic Community in order to distinguish it from the other two types: type-II and type III, more suitable for round ribbed FRP rods with high protrusions and sand-blasted bars, respectively (De Lorenzis 2004).

Based on strain gauge intermediate points and free-end slip readings, Blaschko (2001) obtained local bond-slip curves for NSM strips very similar to the above mentioned type-I curve. However, by plotting the local bond-slip curves at different measurement locations along the bond length, he noted that the local bond strength tended to be larger close to the free end and smaller close to the loaded end. This was attributed to the influence of the transverse displacement of the surrounding concrete, which confirms the substantially three-dimensional and frictional nature of the bond.

The results obtained by Sena Cruz & Barros for the bond strength are in good agreement with the predictions attainable by means of the predictive formula by Blaschko (2003):

$$\tau_{\max} = 0.2 \sqrt{a_e'}\ \tau_{af} \quad \left(a_e' \le 150\ mm\right) \tag{2.2}$$

in which τ_{af} is the shear strength of the epoxy and a_e' is the distance of the centre of the laminate from the edge of the specimen.

In absence of edge effects (*i.e.* for $a_e^{'} \geq 150\,mm$) and for the typical values of the average shear strength of most common two-components epoxies ($22.5 \leq \tau_{af} \leq 28.1$ MPa) that equation yields a local bond strength ranging between 15.8 and 19.8 MPa, whose upper bound coincides with the one by Sena & Barros (19.81 MPa).

One of the aspects that it is worth emphasizing is the ductility of the local bond stress-slip relationship with respect to the one characterizing the externally bonded FRP sheets due to the presence of a residual friction that allows a better exploitation of the material properties.

In the case of EBR, the finite value of the area underlying the local bond stress-slip relationship (*i.e.* the fracture energy G_f) does not allow the tensile strength of the material to be fully exploited because this latter always exceeds the maximum value of stress that can be resisted by the bonded joint. Thus, an "*effective bond length*" exists in correspondence of which the maximum stress can be transmitted and beyond which any further increase in length does not produce any benefit (Monti *et al.* 2003).

In the case of NSM laminates, the infinite value of G_f allows the maximum force transmissible by the bonded joint to increase by increasing the bond length, until the tensile strength of the FRP is attained. In other words, the ultimate force resistible by the joint can be increased by increasing the bond length, until the FRP tensile strength is attained.

To assure a safe and economically valid design, the anchorage length should be evaluated so as to fulfil the requirements imposed by both serviceability and ultimate limit states:

$$L_{an} = \max\left\{ L_{an,SLS}; L_{an,ULS} \right\} \tag{2.3}$$

where $L_{an,SLS}$ and $L_{an,ULS}$ are the anchorage length at service and ultimate limit state, respectively (Sena-Cruz and Barros 2004b).

Conventionally the serviceability limit state occurs at the onset of the loaded end slip while the ultimate limit state is referred to as the instant in which the slip reaches the free end, *i.e.* in the instant in which the peak load that can be resisted by the joint is reached. Once the relationship $\tau(\delta)$ is reliably known, the aforementioned limit states can be easily determined by solving the differential equation governing the bond problem (Sena-Cruz and Barros 2004b).

2.2 Shear span to depth ratio a/d

The ratio a/d of the shear span, a, to the effective depth, d, of the beam cross section is one of the most important parameters affecting the shear resisting mechanisms.

Many Authors have been investigating (Bousselham and Chaalal (2004); Chao *et. al.* 2005) the influence of that ratio on the behaviour of EBR FRP shear-strengthened beams obtaining interesting and general results extendible to the case of NSM laminate strips.

The a/d ratio has great influence, in conjunction with other parameters such as the transverse steel reinforcement amount, on the inclination of the main shear failure crack *i.e.* on what the Australian Draft Guidelines (2006) designate as the Critical Diagonal Crack (CDC). The general observed trend is that the angle between the beam longitudinal axis and the CDC decreases with an increase in a/d. The CDC can be imagined as having its origin in correspondence of its intersection with the longitudinal tensile reinforcement and its end in correspondence of the loading point.

The ratio a/d can also have great influence on the distribution of the width of the CDC along its length. It has been observed that when the ratio a/d increases, the crack width is less evenly distributed and presents a maximum in the vicinity of its origin. On the contrary, for lower values of a/d, the crack with is evenly distributed along its length presenting a maximum at mid length (see Fig. 2.7).

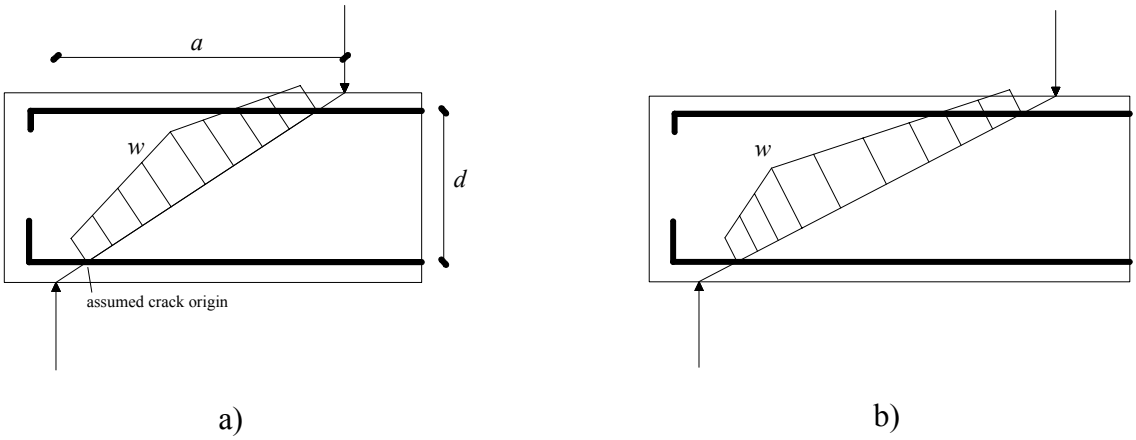

Fig. 2.7 – Distribution of the crack width along the crack length for low values a) and for high values b) of the ratio a/d

The value of a/d also influences the relative importance of the two main shear resisting mechanisms *i.e.*: arch mechanism and truss mechanism.

In that respect, the critical threshold is the value of a/d = 2.5. For values $a/d \geq 2.5$ the arch mechanism becomes negligible and contemporary the truss one becomes predominant while, on the contrary, for values $a/d < 2.5$ the arch mechanism becomes predominant.

Moreover, the influence of a/d on the gain in shear resistance ($\frac{V_f}{V_R - V_f} \cdot 100$) provided by the FRP system (V_f) to the overall shear resistance (V_R) has been extensively observed in the case of externally bonded FRP (Bousselham and Chaalal 2004).The gain in shear resistance increases by increasing a/d, which is due to the fact that, increasing the shear span to depth ratio, the relative importance of the truss mechanisms increases as well, thus outlining the inadequacy of the use of FRP to shear-strengthen deep beams whose prevailing resisting mechanism is the arch one.

2.3 Longitudinal reinforcement ratio

Te main aspects, regarding the importance of the amount of steel longitudinal reinforcement are: its influence on the concrete contribution to the overall shear strength of the RC element and its interaction with the FRP strengthening system.

As regards the influence on the concrete shear strength contribution, by increasing the longitudinal reinforcement ratio, ρ_{sl}, the amount of shear force resisted by concrete by means of: the resisting mechanism of aggregate interlock, the residual tensile stress along the crack, the shear resistance in the uncracked compression zone also increase. In fact, by increasing ρ_{sl} the average width of the critical diagonal crack diminishes and the depth of the compressed zone increases.

The amount of longitudinal reinforcing steel also influences the percentage of shear force resisted by dowel action: the relative transverse displacement of the two segments of the beam separated by the crack is resisted by the bridging reinforcement. Dowel action is particularly important in the case of using large size bars: their transverse rigidity and strength enhance that action.

In the case of externally bonded FRP, an interaction between the shear resistance gain, V_f, and the axial rigidity of the longitudinal reinforcement ($\rho_{sl} E_s$) was observed (Bousselham and Chaalal 2004): by increasing this latter, the enhancement of shear resistance provided by the strengthening system decreased. From a physical point of view, that observation can be explained as follows: by increasing the longitudinal reinforcement, resisting mechanisms proper to the concrete such as arch truss, aggregate interlock, plain concrete shear resistance become predominant so as the FRP contribution percentage becomes relatively less important. Moreover, when ρ_{sl} increases, the average crack width w decreases so as the FRP, either NSM or EBR, is activated at a less extent.

2.4 Bond between Steel Ribbed Bars and surrounding Concrete

Another resisting mechanism affecting the performance of reinforced concrete beams, in general, is the bond between steel reinforcing bars and the surrounding concrete (Park and Paulay 1975). The study of the bond between deformed steel bars and the surrounding concrete, can be extended to the case of the bond failure of NSM FRP rods. At the same, developing more insight in the understanding of the resisting mechanisms related to the bond between steel bars and concrete, can help singling out the physical behaviour of the interaction between the FRP system and the existing steel reinforcement, both longitudinal and transversal.

In case of plain round bars, the bond performance relies on the following resisting mechanisms:

- chemical adhesion between mortar paste and bar surface;
- friction;
- wedging action of small dislodged sand particles between the bars and the surrounding concrete.

Even low stresses generally cause sufficient slip to break the adhesion. Once slip occurs, further bond can be developed only by means of friction and by the above mentioned wedging action.

With the introduction of high strength steel and large diameter bars, the performance of bond has improved considerably but new problems have been introduced. Deformed bars have greatly increased bond capacity because of the interlocking of the ribs with the surrounding concrete.

The bond strength developed between two ribs of a bar is associated with the following stresses (see Fig. 2.8):

1. Shear stresses τ_a developed through adhesion along the surface of the bar;
2. Bearing stresses f_b along the ribs of the bar;
3. Shear stresses τ_c, acting on the cylindrical concrete surface between adjacent ribs.

The relation between these stresses and the force to be transferred to the concrete by bond over a short length of the bar between centers of subsequent ribs can be obtained from a simple equilibrium requirement as follows:

$$\Delta F_b = \pi \; d_b' \left(b + e\right) \tau_a + \pi \; \frac{d_b''^2 - d_b'^2}{4} f_b \;\approx\; \pi \; d_b'' \; e \; \tau_c \tag{2.4}$$

where (see Fig. 2.8): ΔF_b is the increment of force transmissible by the bond length comprehended between two consecutive ribs, d_b' is the diameter of the plain bar, d_b'' is the diameter of the ribs, d_b the nominal diameter of the ribbed bar, e is the distance between two consecutive ribs, b and a are, respectively, the width and height of a rib.

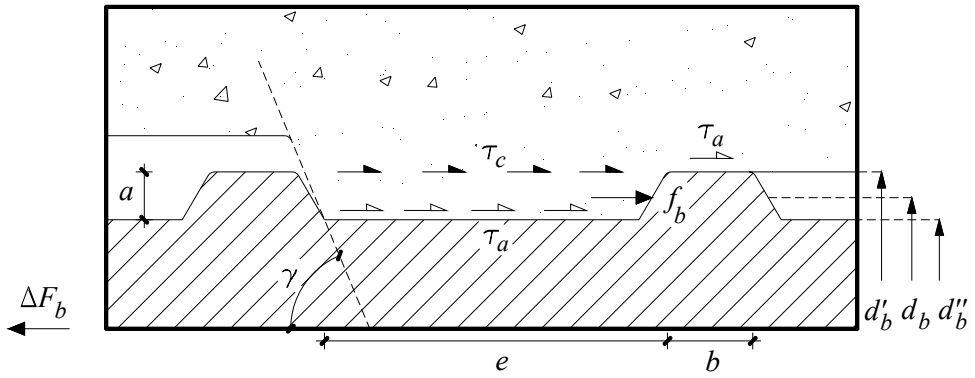

Fig. 2.8 – Stresses between two consecutive ribs of a deformed bar embedded in concrete

As the load is being increased, the adhesion along the bar surface inevitably breaks down. The remaining frictional shear strength is very small in comparison with the bearing strength developed around the ribs; therefore τ_a can be ignored for practical purposes. The relationship between the remaining two important components of bond force development, f_b and τ_c, can be simplified as follows: since $b \approx 0.1\, e$ the rib spacing is approximately e and, since $a \approx 0.05\ d_b'$, the bearing area of one rib is $\pi \dfrac{d_b''^2 - d_b'^2}{4} \approx \pi\ d_b\ a$.

Hence, from the equilibrium equation we obtain $\Delta F_b = \pi\ d_b\ a\ f_b \approx \pi\ d_b\ e\ \tau_c$; therefore,

$$\tau_c \approx \frac{a}{e} f_b \tag{2.5}$$

The most satisfactory performance of a bar embedded in concrete over the short length e was obtained when a/e is in the vicinity of 0.065. When the ribs are high and they are spaced too closely, the shear stress τ_c will govern the behaviour and the bar will pull out. When the rib spacing is larger than approximately 10 times the rib's height, the partly crushed concrete may form a wedge in front of the rib, and failure is normally brought about by splitting of the surrounding concrete. The concrete in front of the rib can sustain a bearing pressure several times the cylinder crushing strength because of the confined condition of the concrete (it was observed up to 4 times the concrete compressive strength). The two mechanisms associated with the rib, are illustrated in the Fig. 2.9.

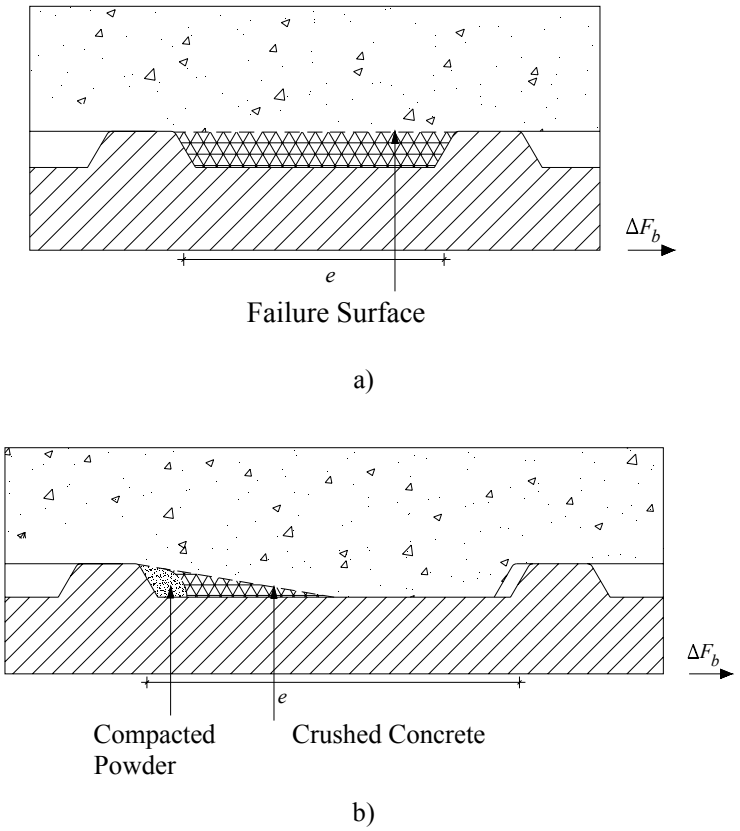

Fig. 2.9 – Failure mechanisms at the ribs of deformed bars: a) $a/e > 0.15$; b) $a/e < 0.1$

Clearly the geometry of deformed bars must be such that a shear pullout failure cannot occur.

Generally speaking, the parameters that may influence the bond performance are as follows:

- The position of the bars with respect to the placing of the surrounding concrete;
- Bar profiles and surface conditions;
- The state of stress in the surrounding concrete;
- The splitting failure.

As can be gathered from the above argumentations, a significant role in the bond of ribbed bars, is played by the bearing stresses that the concrete in front of the ribs is capable of resisting. In this respect, an important factor is the relative placing of the bars with respect to the direction of casting of the fresh mixture of concrete. Since water and air present in the fresh mixture tend to move upwards during the curing process, there could be a water and air gain beneath the bar that would contribute to have a layer of spongy and porous concrete. In that respect, for example, the bond behaviour of a horizontal bar is expected to be worse than that of a vertical one. Moreover, the downward movement of the fresh mixture, also contributes to increase the settlement of the particles in the bottom of the cast element with respect to the upper part so as, generally, the bond performance is better for bottom bars than for top ones. The settlement of the fresh mixture is influenced, in turn, by the amount of bleeding of fresh concrete and the rate at which water is permitted to escape from the formwork.

As regards the bar profile, it was demonstrated (Park and Paulay 1975) that, variations of the angle between the face of the rib and the axis of the bar (angle γ in Fig. 2.8) do not seem to affect the bond strength, provided this angle is larger

than 70°. The influence of the surface conditions of the bar, in terms of amount of superficial rust or mill scale, have a marginal effect on the bond performance.

The stresses in the concrete surrounding a deformed bar lead to cracks and deformations of the concrete, as illustrated in the Figure 2.10 for the case of a tension member.

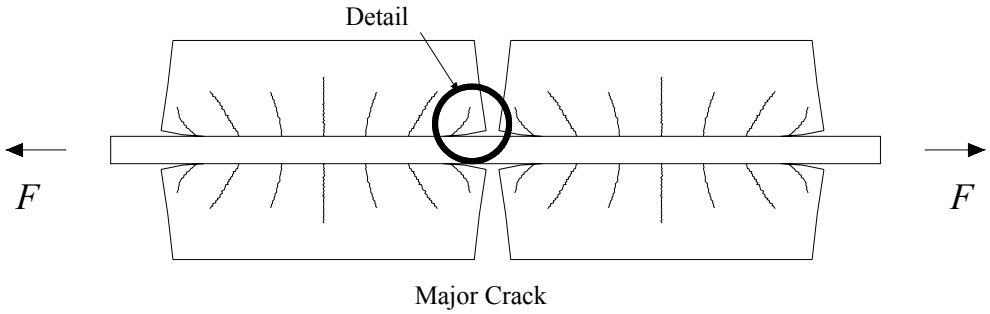

Fig. 2.10 – Deformed concrete between transverse cracks of a tension member

The bond stresses transmitted to the concrete, subject the cover thickness of concrete to eccentric tension. The deformations of the concrete resulting from the stresses so generated tend to pull the concrete away from this steel in the vicinity of the major crack (see Fig. 2.10). The tensile strength of the adhesive bond between steel and the mortar (orthogonally to the bar axis) is then reached and the surrounding concrete separates from the steel. Also numerous internal secondary cracks can form which may not propagate to the external surface of the concrete. In plain bars the bond stresses can be expected to disappear completely where separation between steel and concrete occurred. With deformed bars, bond forces have to be transmitted in this area solely by rib bearing as shown in Figure 2.11.

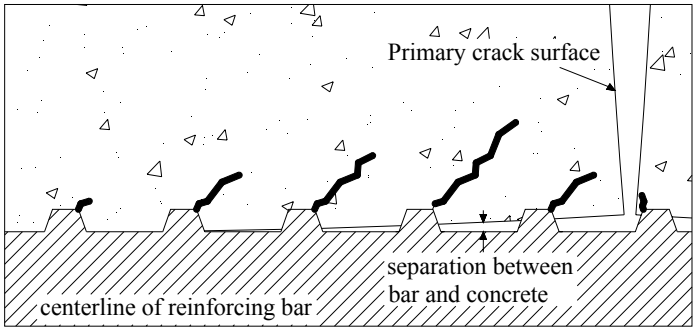

Fig. 2.11 – Detail of Fig. 2.10: section through reinforcing bar and concrete, showing separation that occurs near a primary crack

The separation between the bar and the concrete in the vicinity of the primary crack has been verified experimentally together with some sloping secondary cracks radiating from each rib.

When the concrete separates itself from around a bar at a primary crack, the circumference of the concrete surface, previously in contact with the bar, increases; hence circumferential tensile stresses are induced. These stresses can lead to longitudinal splitting cracks. When the ultimate capacity in bond transfer is being approached, there is crushing in front of the ribs. The compacted powder, extending in front of the ribs at a distance of up to three times the rib height,

forms a flat wedge (see Fig. 2.9b) and this tends to push the concrete further away from the bar. Hence additional circumferential tensile stresses are generated which may bring about a splitting failure.

Thus, one of the most important aspects is the splitting failure. Where adequate embedment length is provided in a large mass of concrete, it is not possible to produce a bond (pullout) failure with standard deformed bars. Rather, the bar will fracture at its loaded end. In most structural components, however, the area of concrete surrounding a bar or group of bars is relatively small (see Figure 2.12). In such a situation the common mode of failure is splitting, since the surrounding concrete cannot sustain the circumferential tensile stresses.

A particular severe situation arises in the shear span of beams, where splitting can be induced along the flexural reinforcement by the combination of the following events:

1. Circumferential tensile stresses generated in the vicinity of each flexural crack;
2. Circumferential or transverse tensile stresses induced by wedging action of the deformations and by the compressed concrete at the ribs (Fig. 2.12b) when large bond forces need to be transferred;
3. Transverse tensile stresses resulting from dowel action of the flexural reinforcement. This event is associated with shear displacement along diagonal cracks.

A group of bars, especially when closely spaced, will create a more adverse situation than a single bar. This is illustrated in Figure 2.12 which presents typical observed splitting cracks.

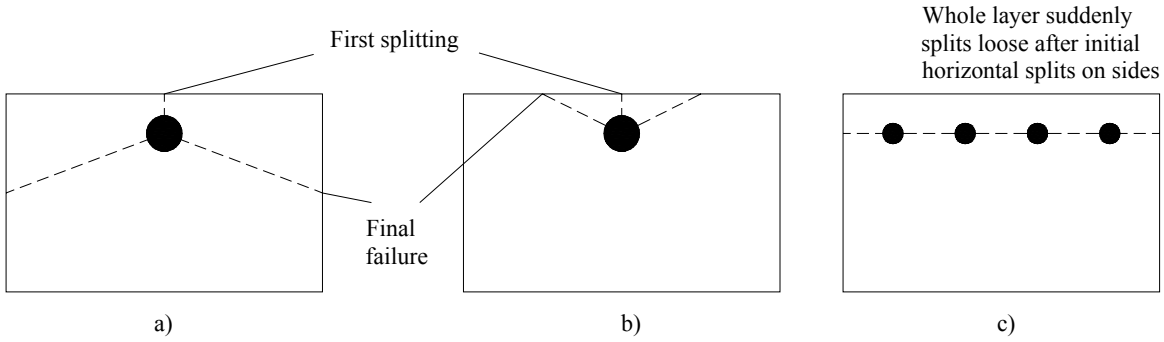

Fig. 2.12 – Splitting cracks at failure. (a) Typical case. (b) In very wide beams. (c) With closely spaced bars.

2.5 Amount of existing steel stirrups $\rho_{sw}E_s$ and spacing

A strong interaction exists between the transverse rigidity of pre-existent steel stirrups and the amount of FRP shear strengthening elements (Bousselham and Chaalal 2004). In fact, by increasing $\rho_{sw}E_s$, the FRP shear contribution diminishes.

The above observation has a huge importance not only as regards the complete understanding of the physical behaviour of a beam shear-strengthened by introducing FRPs but also as regards the proposal of a predictive formula.

In fact, most recent World Codes such as ACI 440 (2002), *fib* Bulletin 14 (2001) and CNR DT 200 (2004), dealing with the subject of FRP strengthening of existing RC structures, calculate the shear resistance by simply superimposing the contributions provided by concrete, steel stirrups and FRP, neglecting their mutual interaction, even if the Australian Guidelines (2006) explicitly warn about the importance of that issue and suggests the adoption of suitable reduction factors. It may happen that, due to the different mechanical properties of FRP and steel, their maximum contribution is

not reached contemporarily in terms of either instant or deflection. In this respect, it is worth outlining that in real cases of existing RC structures retrofitted by means of FRPs, at the moment of the application, stirrups are already loaded presenting a certain value of stress and deformation. This occurrence does not regard most of the tests currently curried out.

The existence of that interaction underlines the necessity of determining the optimum amount of FRP with respect to the existing transverse reinforcement in order to maximize the effectiveness of the strengthening technique.

Moreover, it has to be outlined that it is being observed, during the tests currently carried out at the Laboratory of Structural Engineering of the University of Minho by PhD Student Salvador Dias, that, after the failure of the laminates crossing the critical diagonal crack, this latter rotates, assuming, as function of the spacing between stirrups, a steeper inclination.

2.6 Concrete compressive strength

The concrete compressive strength is extremely important since the contribution provided by concrete V_c, to the beam overall shear strength V_r, results to be the highest, among the several contributions. In fact, the shear strength of the beam is generally calculated by adding the contributions V_c, V_f, V_s ascribed to concrete, FRPs and existing stirrups, respectively. The relative predominance of the term V_c increases for beams with a short value of the ratio a/d between the shear span and the effective depth since, for these beams, the resisting mechanism of the arch results to be the most important.

Anyway, it is worth outlining that generally, the term V_c, derived from the shear strength of the reference beam without stirrups at all, includes the contribution, not negligible, provided by the dowel effect of the tensile longitudinal reinforcement, ρ_{sl}. This is generally high enough since, the necessity to force the beam to fail in shear, prompts the adoption of large ρ_{sl}.

As observed by Sena-Cruz and Barros (2002), and already reported in paragraph 2.1, the concrete compressive strength has a negligible importance on the bond between CFRP laminates and concrete *i.e.* when NSM laminates fail by debonding.

2.7 Concrete tensile strength

Among the most recent works in the ambit of the shear strengthening of RC beams by means of the technique of NSM CFRP laminates, those by Dias and Barros (2005b) and by De Lorenzis and Rizzo (2006), outline the occurrence of a failure mode characterized by the separation of the cover of the beam, containing the glued laminates, from the underlying core. The occurrence of that phenomenon spotlights the importance of the tensile strength of the concrete as one of the commanding parameters for the shear strength contribution by the NSM technique and rises the suspicion that the commanding failure mode may not be debonding, in opposition to the International Academic Community belief to date.

Even if the tensile behaviour of concrete was formerly considered of minor importance to failure analysis, because of its higher capabilities to withstand compressive stresses, more recently, with the introduction of fracture mechanics, it has become clear that tensile properties play a dominant role in the failure of concrete structures. Prominent examples are anchorages and lap splices of reinforcing bars, slabs without shear reinforcement and the various kinds of anchors.

The tensile behaviour of concrete (CEB bulletin n° 210, 1996) is illustrated in Fig. 2.13. A deformation-controlled axial direct tension test may be performed on the specimen shown on the left side. The specimen is loaded with the force P and the total deformation is measured over the length l. At the left side the specimen is plotted for the load steps A, B and C. The load steps are also marked in the load-deformation curve at the right side. Load step A is before peak load, load step B at peak load and load step C after peak load in the descending branch of the load-displacement curve.

Already before the peak load is reached, some micro-cracking occurs (Fig. 2.13a). As the micro-cracking is uniformly distributed at the macro-level, a uniform strain over the length of the specimen may be assumed. The strain is plotted over the length of the specimen in Fig. 2.13 right next to the specimen.

Immediately before the peak load, an accumulation of micro-cracks occurs at the weakest part of the specimen. At the macro-level this leads to an additional strain over the length h of this weak part. A crack band of width h develops (see Fig. 2.13b).

Having passed the peak load, the crack band localizes more and more. The crack band width diminishes, and the deformation within the crack band increases. The final failure occurs due to one single crack. The total deformation of the specimen may be split up in the bulk deformation, which is almost linear elastic up to the peak, and the deformation at the crack band (see Fig. 2.13c).

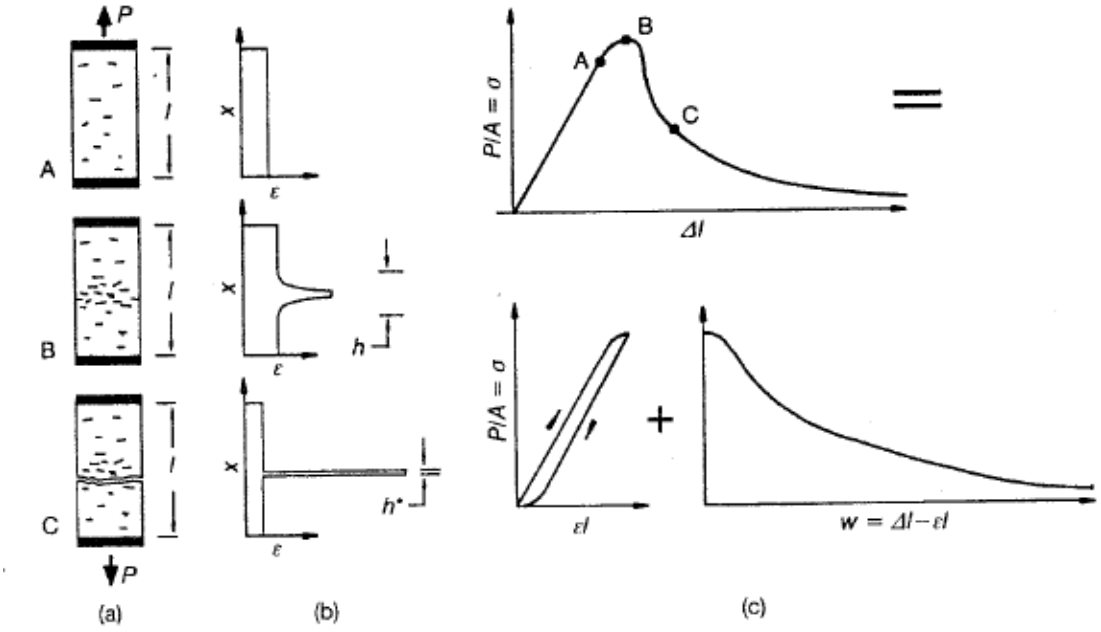

Fig. 2.13 – Tensile behaviour of concrete

Hillerborg *et al.* (1976) introduced the "*fictitious crack model*", according to which they collected the deformation of the crack band into the crack width w of one single "*fictitious*" crack. The relation between the width of the "fictitious" crack and the stress is the $\sigma - w$ relation. Two mechanisms contribute to the stress transfer over the crack. As mentioned, it is actually a fictitious crack: the crack width is the collected deformation of a band of micro-cracks. Within this crack band, material bridges transfer the load. After the formation of a real single crack, the stress transfer is possible due to aggregate interlock. In most cases a crack will run along the interface between the aggregate grains and the cement matrix. The grains are pulled out of the matrix and, due to this, friction forces between grains and matrix occur. The grains act like friction blocks and transfer friction forces over the crack.

The bulk behaviour is described by the $\sigma - \varepsilon$ relation of Fig. 2.13. This relation is linear almost up to the ultimate load. The modulus of elasticity is equal to the initial tangent modulus of elasticity in compression. Poisson's ratio is in the order of $\nu = 0.15 - 0.25$. Just before the ultimate load is reached, the $\sigma - \varepsilon$ relation bends off from the linear behaviour. For the stage of loading where the non linear behaviour starts showing, experimental results show great differences. In some experiments the nonlinearity starts at about half of the ultimate load, in other experiments the curve is linear up to the peak load. These differences in the experimental results are caused by different boundary test conditions. Any source of non-uniformity, like internal bending due to non-uniform cracking, eigenstresses due to differential shrinkage and temperature, notch effects, etc., cause non-linearities. The non-linear behaviour met in test specimens is more a structural behaviour than a material behaviour. Because of this, it seems acceptable to assume linear elastic material behaviour up to the ultimate load, for both the loading and unloading part.

A large number of analytical models exist in the literature to model the $\sigma - w$ relation. For instance, brief introduction to those models can be found in the CEB Bulletin n°210 (1996).

The typical load-displacement curve for concrete loaded axially in tension (CEB Bulletin n°201), measured in a displacement-controlled test is as shown in Fig. 2.14.

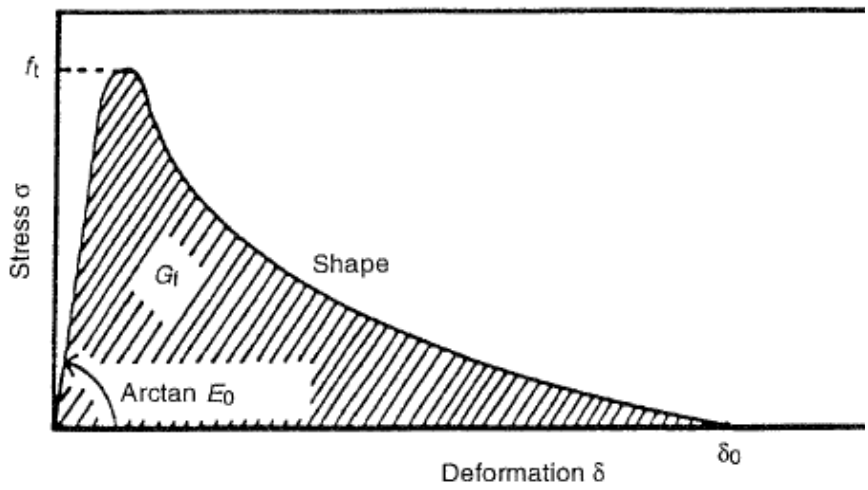

Fig. 2.14 – Stress-deformation relation and fracture mechanics parameters

The total behaviour can be characterized by the Young's Modulus E_0, the tensile strength f_t, the shape of the descending branch, the maximum deformation δ_0 at which stress can no longer be transferred and fracture energy G_f (defined as the amount of energy necessary to create one unit of crack area, equal to the area under the curve in Fig. 2.14). Another parameter characterizing the behaviour of concrete in tension is w_0, the maximum crack opening at which stress can no longer be transferred (see Fig. 2.15) whose value generally ranges between 0.1 and 0.2 mm.

As stated above, the stress transfer across the crack is explained by the phenomenon of aggregate interlock. In this context, aggregate interlock is the bonding action of aggregate particles across the crack that are being pulled out of matrix, and is accompanied by sliding forces. Because of this load-transfer mechanism, the contribution of interlock to the fracture energy can be expected to increase for more tortuous crack surfaces.

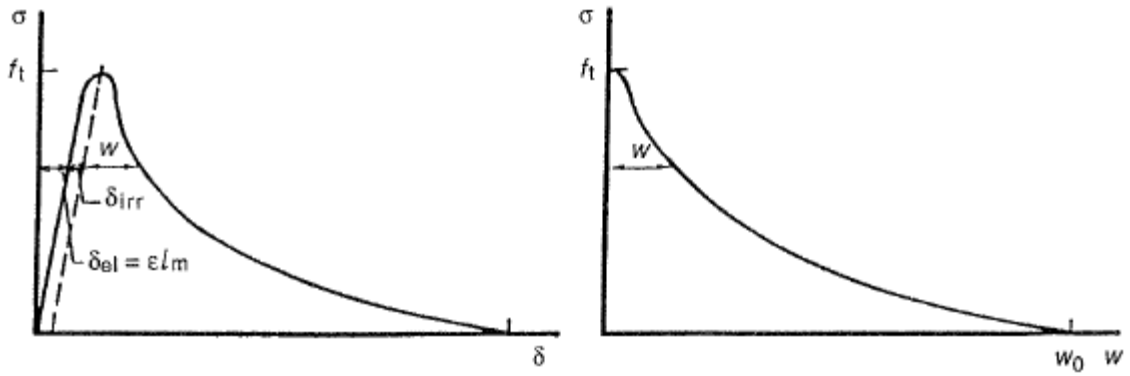

Fig. 2.15 – Stress-crack opening ($\sigma - w$) as derived from a stress-deformation ($\sigma - \delta$) relation

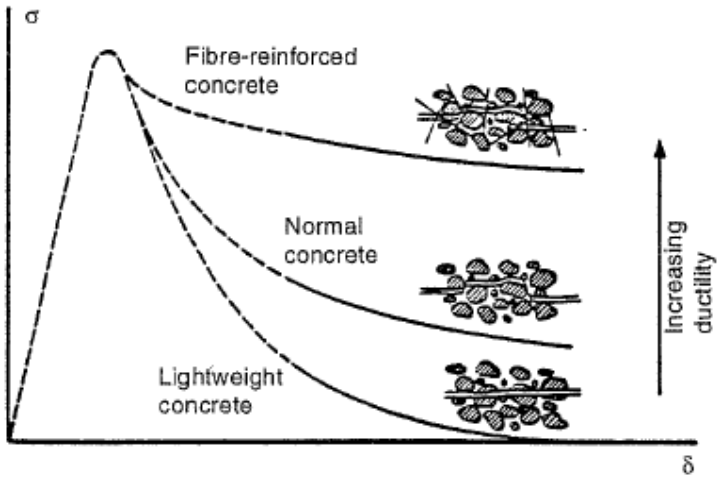

Fig. 2.16 – Influence of crack path tortuosity and fibre bridging on the stress-deformation relation

As shown in Fig. 2.16, in the case of a lightweight concrete in which cracks run through the aggregates, the crack path is smooth compared to the one of a normal concrete. For normal concrete, therefore, the descending branch lies above that for lightweight concrete. In fibre-reinforced concrete the crack surfaces are bridged through fibres, therefore the descending branch rises. Thus, the parameters that define the stress-deformation relation (Fig. 2.14) depend significantly on the concrete mix. In particular, the main influencing factors (CEB Bulletin n°201) are the maximum aggregate size, the type of aggregates (*e.g.* limestone or granite), the shape of aggregates (natural round or broken angular), their grading (fine or coarse grading curve), the water-cement ratio and the type of cement. Generally speaking, for a concrete with constant compressive strength the tensile strength and the fracture energy increase with increasing aggregate size (at least in the range 8-20 mm) and decreasing water-cement ratio. Also, the tensile strength and fracture energy may be higher for concrete made with crushed rock aggregates than with limestone aggregates. Thus, for constant compressive strength, the mechanical parameters characterizing the tensile behaviour of concrete may scatter considerably, depending on the concrete mix (grading curve, maximum aggregate size, size and type of aggregates).

The tensile strength is also affected by curing of the concrete, and may be lower for wet (saturated) concrete than for concrete dried over a long period without restriction of the deformations.

Another significant influence on the behaviour of tensioned concrete is the age at loading. In general, the ratio of tensile strength to compressive strength is much higher for a young concrete than for a 28 days old concrete. With increasing age, the ratio between the tensile strength and the compressive strength, decreases slightly further and seems to stabilize.

2.8 Beam size

A large amount of data is available in the technical literature regarding experimental tests carried out in order to systematically evaluate the influence of the beam size on the concrete contribution to the shear resistance.
In particular, Tompson and Frosch (2002) have been dedicated to the evaluation of the reliability of the concrete shear contribution predicted by means of the formulae provided by some Design Codes and too often obtained on the basis of regression of the experimental results regarding small cross-sectioned specimens. A fair influence of the beam effective depth on the concrete shear strength emerges: the larger the depth, the smaller the concrete contribution.

2.9 Quality of the epoxy adhesive

In most of the experimental programs carried out so far, in the ambit of the exploration of the NSM technique, the epoxy-based adhesive has been employed. Anyway, the suspicion exists, that the mechanical properties of the adhesive, and in particular the Young's modulus, influence the performance of the shear strengthening system by NSM laminates. In fact, the stiffness of the adhesive can influence the length of the laminate in which the stresses are transmitted to the surrounding concrete. In that regard, for example, it is desirable, for further developments, to explore the employment of structural epoxy-based adhesives characterised by different values of the stiffness or completely different adhesives such as vinyl or polyester-based organic resins. Besides, these latter, are characterised by a shorter curing time, aspect, this latter, that can positively influence the competitiveness of the NSM technique from a practical point of view.

3 State of the Art regarding Predictive Models and Design Formulae to assess the FRP Contribution to the Shear Strength of RC beams

Most of Design Codes currently available worldwide still lack both design formulae and predictive models as regards the evaluation of the NSM contribution to the overall shear resistance of retrofitted RC beams. On the contrary, the amount of research already carried out on the use of EBR FRP systems for the shear strengthening of RC beams is considerable, even if many aspects still need to be clarified.

In the present chapter, a critical review of the available formulae is presented even if, in some cases, they are not strictly devoted to the technique of NSM, that is the main interest of the present document, since it can help develop a good insight in the resisting mechanisms associated with the use of FRP for the shear strengthening of RC beams.

3.1 ACI Recommendations for EBR Technique

The design recommendations contained in the ACI 440.2R (2002) are based on limit-states design principles. They aim at setting acceptable levels of safety against the occurrence of both serviceability limit states (excessive deflections, cracking) and ultimate limit states (failure, stress rupture, fatigue). For general principles regarding strength and serviceability requirements, load factors and strength reduction factors they refer to ACI 318 (2002) document. Additional reduction factors for the contribution of the FRP reinforcement are recommended by ACI 440.2R (2002) to reflect the lesser information available, to date, for the FRP systems compared with reinforced and prestressed concrete.

The design ultimate mechanical properties of the adopted FRP material have to be first defined suitably reducing the values provided by the manufacturer as a function of the environmental conditions. In fact, the design ultimate tensile strength, f_{fd} , is obtained from:

$$f_{fd} = C_E \, f_{fu}^* \tag{3.1}$$

where C_E is the environmental reduction factor and f_{fu}^* is the value of the tensile strength provided by the manufacturer. The values of the environmental reduction factors are listed as function of both the type of material and environment in paragraph 8 of ACI 440.2R (2002).

Likewise, the design ultimate strain, ε_{fd} , is obtained from:

$$\varepsilon_{fd} = C_E \, \varepsilon_{fu}^* \tag{3.2}$$

where ε_{fu}^* is the value of the ultimate strain provided by the manufacturer.

The shear strength of existing concrete beams or columns is increased by wrapping or partially wrapping the members. The three types of FRP wrapping schemes used to increase the shear strength of prismatic, rectangular beams or columns are illustrated in Fig. 3.1.

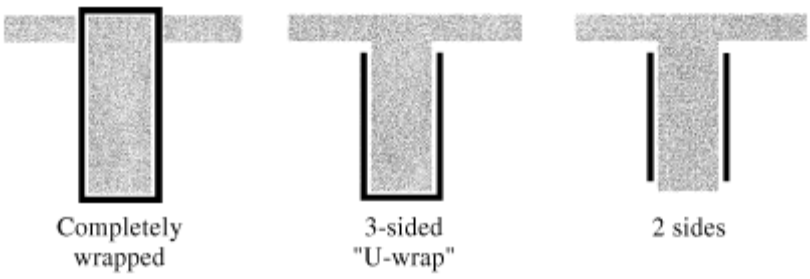

Fig. 3.1 – Typical wrapping schemes for shear strengthening using FRP laminates

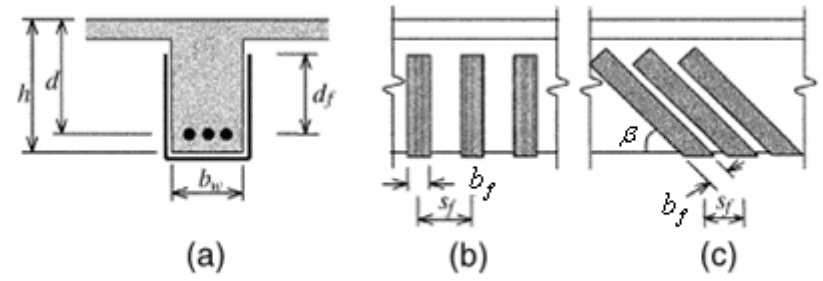

Fig. 3.2 – Illustration of the dimensional variables used in shear-strengthening calculations for repair, retrofit, or strengthening using FRP laminates

Completely wrapping the FRP system around the section on all four sides is the most efficient wrapping scheme and is most commonly used in column applications where access to all four sides of the column is usually available. In beam applications, where an integral slab makes it impractical to completely wrap the member, the shear strength can be improved by wrapping the FRP system around three sides of the member (U-wrap) or bonding to the two sides of the member. Although all the three techniques have been shown to improve the shear strength of a member, completely wrapping the section is the most efficient, followed by the three-sided U-wrap. Bonding to two sides of a beam is the least efficient scheme. In all wrapping schemes, the FRP system can be installed continuously along the span length of a member or placed as discrete strips. For external FRP reinforcement in the form of discrete strips, the center-to-center spacing between the strips should not exceed the sum of $d/4+b_f$, where d is the beam effective depth and b_f is the width of each strip.

The design valu of the ultimate shear resistance V_{Rd} of a RC member strengthened with an FRP system should exceed the design shear force V_{Sd} :

$$V_{Rd} = \phi \cdot V_R \geq V_{Sd} \tag{3.3}$$

where ϕ is the strength-reduction factor required by ACI 440.2R (2002).

The ultimate shear strength of an FRP-strengthened RC member V_R can be determined by adding the contribution of the FRP, V_f, to the contributions, V_c, from the concrete and, V_s, from the reinforcing steel (stirrups, ties or spirals). An additional reduction factor, ψ_f, is applied to the contribution of the FRP.

$$V_{Rd} = \phi \cdot \left(V_c + V_s + \psi_f \cdot V_f \right) \tag{3.4}$$

where ψ_f is equal to 0.95 for completely wrapped elements and 0.85 for three-sided U-wraps or bonded face piles. The contribution provided by the FRP reinforcement to the beam overall shear resistance is obtained by:

$$V_f = \frac{A_{fv} \cdot f_{fe} \cdot \left(\sin\beta + \cos\beta \right) \cdot d_f}{s_f} \tag{3.5}$$

where: s_f is the spacing of the wet lay-up strips of FRP evaluated along the axis of the beam; β is the inclination of FRP elements with respect to the beam axis; A_{fv} is the area of FRP shear reinforcement within spacing s_f:

$$A_{fv} = 2 \cdot n \cdot a_f \cdot b_f \tag{3.6}$$

with n, a_f and b_f being, respectively, the number of layers per strip, the thickness of a layer and the width of the strips. The FRP effective stress, f_{fe}, *i.e.* the tensile stress present in the reinforcement at ultimate state, is calculated in accordance to the value of the effective strain, ε_{fe}, that is the level of strain that can be developed in the FRP at ultimate:

$$f_{fe} = E_f \cdot \varepsilon_{fe} \tag{3.7}$$

The provisions recommend to determine ε_{fe} by taking into consideration all of the most likely failure modes and selecting the critical one. Anyway the recommendations also give guidance on determining that effective strain on the basis of the different configurations adopted.

For completely wrapped members, whose critical failure mode has been observed to be the loss of aggregate interlock, the allowable value of deformation should be limited to 4‰:

$$\varepsilon_{fe} = 0.004 \leq 0.75 \cdot \varepsilon_{fu} \tag{3.8}$$

For three and two side-bonded FRP wraps, the allowable value of the effective strain is intended to prevent the debonding failure and is calculated by means of a bond-reduction coefficient, κ_v:

$$\varepsilon_{fe} = \kappa_v \cdot \varepsilon_{fu} \leq 0.004 \tag{3.9}$$

The bond-reduction factor is a function of the concrete strength, the type of wrapping scheme used, and the stiffness of the laminate. It can be determined by:

$$\kappa_v = \frac{k_1 \cdot k_2 \cdot L_e}{468 \cdot \varepsilon_{fu}} \leq 0.75 \tag{3.10}$$

For the case of U-wrapping and by:

$$\kappa_v = \frac{k_1 \cdot k_2 \cdot L_e}{11900 \cdot \varepsilon_{fu}} \leq 0.75 \tag{3.11}$$

For the case of side-bonding.

The active bond length, L_e, *i.e.* the length over which the majority of the bond stress is maintained, is given by:

$$L_e = \frac{2500}{\left(n \cdot a_f \cdot E_f\right)^{0.58}} \tag{3.12}$$

For the U-wrapping and by:

$$L_e = \frac{23300}{\left(n \cdot a_f \cdot E_f\right)^{0.58}} \tag{3.13}$$

For the case of side-bonding, where E_f is the Young's modulus of the FRP.

The bond-reduction factor also relies on two modification factors, k_1 and k_2, that account for the concrete strength and the type of wrapping scheme used, respectively. The k_1 modification factor is calculated by:

$$k_1 = \left(\frac{f_{ck}}{4000}\right)^{\frac{2}{3}} \tag{3.14}$$

for the U-wrapping and by:

$$k_1 = \left(\frac{f_{ck}}{27}\right)^{\frac{2}{3}} \tag{3.15}$$

for the case of side-bonding, with f_{ck} being the characteristic value of the concrete compressive strength.

Likewise, the k_2 modification factor is calculated by:

$$k_2 = \frac{d_f - L_e}{d_f} \tag{3.16}$$

for the U-wrapping and by:

$$k_2 = \frac{d_f - 2 \cdot L_e}{d_f} \tag{3.17}$$

for the case of side-bonding.

The possibilty to adopt mechanical ancorages at the FRP extremities is allowed but it is also outlined that the effective strain in the FRP laminates should not overcome the limit value of 4‰.

In case of adoption of spaced FRP strips, spacing should adhere to the limits as set by ACI 318-02 for internal steel shear reinforcement where the spacing is defined as the distance between the centrelines of the strips.

The total shear reinforcement should be limited based on the criteria given for steel alone in ACI 318-02, *i.e.* V_f should be such as to satisfy the following limitations:

$$V_s + V_f \le 8 \cdot \sqrt{f_{ck}} \cdot b_w \cdot d \tag{3.18}$$

for the case of U-wrapping and:

$$V_s + V_f \le 0.66 \cdot \sqrt{f_{ck}} \cdot b_w \cdot d \tag{3.19}$$

for the side-donding.

It's worth noting that the resisting mechanism underlying the above formulation is the classical Mörsch Truss applied with the assumption that the critical diagonal crack inclination is 45° with respect to the beam axis and, consequently, the number of strips effectively intersecting the crack is accounted for.

3.2 fib Recommendations for EBR Technique

The design shear capacity of a RC strengthened element may be calculated, in accordance with the EC2, as follows:

$$V_{Rd} = \min\left\{ V_{Rd,c} + V_{Rd,s} + V_{Rd,f}; V_{Rd,\max} \right\} \tag{3.20}$$

in which: $V_{Rd,c}$, $V_{Rd,s}$, $V_{Rd,f}$ are the contributions provided, respectively, by the concrete, the steel stirrups and the FRP reinforcement, and $V_{Rd,\max}$ is the resistance of the concrete compression strut.

According to *fib* recommendations, the design FRP contribution to shear capacity can be estimated by means of the following formulation:

$$V_{Rd,f} = 0.9 \cdot \varepsilon_{fed} \cdot E_f \cdot \rho_{fw} \cdot b_w \cdot d \cdot \left(\cot\theta + \cot\beta\right) \cdot \sin\beta \tag{3.21}$$

where b_w is the width of the beam cross-section, d is the beam cross section effective depth, θ is the inclination of the shear crack assumed as 45°, β is the angle between the principal fibre orientation and the longitudinal axis of the beam, ε_{fed} is the design value of the FRP effective strain, E_f is the Young's modulus of the FRP element, ρ_{fw} is the reinforcement ratio equal to:

$$\rho_{fw} = \frac{2 \cdot a_f \cdot b_f}{b_w \cdot s_f} \tag{3.22}$$

for the case of FRP reinforcement in the form of strips or sheets of width b_f at a spacing s_f, and given by:

$$\rho_{fw} = \frac{2 \cdot a_f \cdot \sin\beta}{b_w} \tag{3.23}$$

for the case of continuously bonded shear reinforcement of thickness a_f.

The design effective strain can be computed, from its mean value ε_{fe} by applying two partial safety factors:

$$\varepsilon_{fed} = \frac{0.8 \cdot \varepsilon_{fe}}{\gamma_f} = \frac{\varepsilon_{fek}}{\gamma_f} \tag{3.24}$$

0.8, that is necessary to obtain, in absence of sufficient data, the corresponding characteristic value, ε_{fek}, and the material safety factor, γ_f, that, if failure involves FRP fracture, is listed in function of the type of fibres and, if debonding dominates, can be assumed equal to 1.3. Some researchers have proposed that the effective strain be limited to a maximum value, in the order of 6‰, to maintain the integrity of concrete and secure activation of aggregate interlock mechanism (*e.g.* Priestley and Seible 1995, Khalifa *et al.* 1998, Triantafillou and Antonopoulos 2000). Such limitation should be considered only if activation of this mechanism is of crucial importance.

For the case of fully wrapped CFRP, in which the controlling mechanism is the FRP rupture, the mean value of the effective strain, ε_{fe}, is calculated by:

$$\varepsilon_{fe} = 0.17 \cdot \left(\frac{f_{cm}^{2/3}}{E_f \cdot \rho_{fw}} \right)^{0.3} \cdot \varepsilon_{fu} \tag{3.25}$$

in which f_{cm} is the mean cylindrical concrete compressive strength and ε_{fu} is the ultimate FRP strain.

For the case of side or U-shaped CFRP strips, the mean value of the effective strain, ε_{fe}, is calculated by:

$$\varepsilon_{fe} = \min \left[0.65 \cdot \left(\frac{f_{cm}^{2/3}}{E_f \cdot \rho_{fw}} \right)^{0.56} \cdot 10^{-3}; 0.17 \cdot \left(\frac{f_{cm}^{2/3}}{E_f \cdot \rho_{fw}} \right)^{0.3} \cdot \varepsilon_{fu} \right] \tag{3.26}$$

in which the two expressions in parentheses contemplate, respectively, debonding and rupture failure modes of the FRP.
For the case of fully wrapped AFRP, in which case the fracture failure mode controls, ε_{fe} is calculated by:

$$\varepsilon_{fe} = 0.048 \cdot \left(\frac{f_{cm}^{2/3}}{E_f \cdot \rho_{fw}} \right)^{0.47} \cdot \varepsilon_{fu} \tag{3.27}$$

Note that in all equations f_{cm} is in MPa and E_f is in GPa.

For most practical cases, the above equations for the effective FRP strain give values that are above the yield strain of internal stirrups. For the sake of completeness *fib* document stresses that, if this is not the case, than the value of the effective strain should also be used for the calculation of the contribution of the internal steel stirrups.

The spacing of strips, s_f, if they are used vertically, should not exceed $\left(0.9 \cdot d - b_f/2\right)$ for rectangular cross sections or $\left(d - t_s - b_f/2\right)$ for T-beams, where t_s is the slab thickness. This limitation is meant to avoid that a diagonal crack may form without intercepting a strip.

If the RC member has circular section, *e.g.* some columns, the FRP shear contribution (for FRP wrapped around the column) is controlled by the tensile rupture of the FRP jacket, but may be limited to a maximum value corresponding to excessive dilation of the concrete due to aggregate interlock (one of the key shear force transfer mechanism) at inclined cracks. By limiting the concrete dilation, that is the radical strain (which is equal to the FRP hoop strain) to a maximum value, say, $\varepsilon_{\max}$, one may easily show that for inclined cracks forming an angle of θ with the column axis, the FRP contribution to shear capacity is as given by the following equation:

$$V_{fd} = \frac{\varepsilon_{\max}}{\gamma_f} \cdot E_f \cdot \rho_{fw} \cdot \frac{1}{2} \cdot \frac{\pi \cdot D_c^2}{4} \cdot \cot\theta \tag{3.28}$$

where D_c is the column diameter.

The predictive formula proposed by *fib* derives from the plain application of the Mörsch truss resisting mechanism. The possibility to take into account a shear crack inclination different than 45° is explicitly allowed.
Barros & Dias (2005) have recently verified that a substantial overestimation is obtained when applying the fib formulation to some RC shear strengthened by the NSM technique.

3.3 CNR DT 200 Recommandations for EBR Technique

The Italian Recommendations CNR DT 200, recently issued by the Italian National Research Council, start by outlining the brittleness of the failure governed by debonding of the externally bonded FRP strips or sheets to the concrete surface in both cracked and uncracked zones.

In accordance with the most rigorous "*Capacity Design*" philosophy, an approach is proposed to avoid that bond failure occurrence precede either the shear or flexural ones.

The design shear resistance of the strengthened beam is calculated as follows:

$$V_{Rd} = \min\left\{ V_{Rd,c} + V_{Rd,s} + V_{Rd,f}; V_{Rd,\max} \right\} \tag{3.29}$$

in which $V_{Rd,c}$, $V_{Rd,s}$, $V_{Rd,f}$ are the design contributions provided respectively by the concrete, the steel stirrups and the FRP reinforcement and $V_{Rd,\max}$ is the resistance of the concrete compression strut to be calculated in accordance to the current building codes.

In case of a RC member with a rectangular cross-section and FRP side-bonding configuration, the design value of the FRP contribution to the shear capacity, $V_{Rd,f}$, is calculated by:

$$V_{Rd,f} = \frac{1}{\gamma_{Rd}} \cdot \min\left\{0.9 \cdot d, h_w\right\} \cdot f_{fed} \cdot 2 \cdot a_f \cdot \frac{\sin\beta}{\sin\theta} \cdot \frac{b_f}{s_f'} \tag{3.30}$$

where γ_{Rd} is the partial safety factor, accounting for the uncertainties of the adopted mechanical model, that should be taken equal to 1.20, d is the beam effective depth, h_w is the height of the beam web, f_{fed} is the effective FRP design strength to be calculated as further specified, a_f is the thickness of the adopted FRP system, β is the fibers angle with respect to the member longitudinal axis, θ represents the angle of shear crack (to be assumed equal to 45° unless a more detailed calculation is made), and b_f and s_f' are the FRP width and spacing, respectively, measured orthogonally to the fibre direction (see Fig. 3.3). For a contiunous strengthening configuration, the ratio b_f / s_f' should be set equal to one.

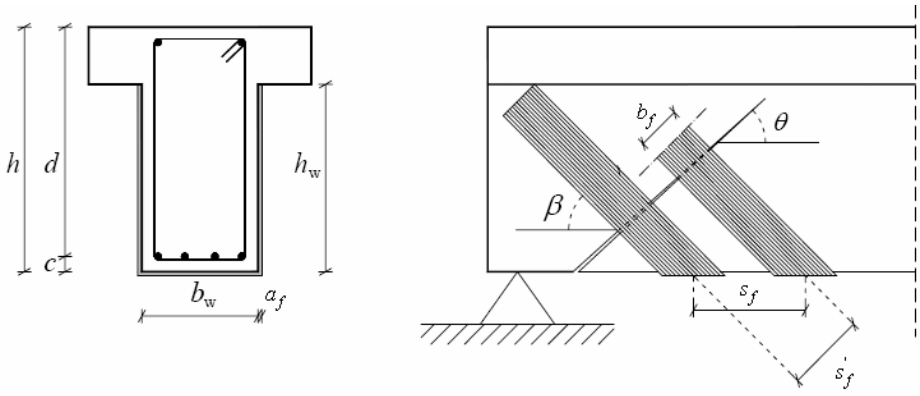

Fig. 3.3 – Notation for shear strengthening using FRP strips

In the case of a RC element with a rectangular cross section and U-wrapped or completely wrapped configurations, the FRP contribution to the shear capacity shall be calculated according to the Mörsch truss mechanism as follows:

$$V_{Rd,f} = \frac{1}{\gamma_{Rd}} \cdot 0.9 \cdot d \cdot f_{fed} \cdot 2 \cdot a_f \cdot \left(\cot\theta + \cot\beta\right) \cdot \frac{b_f}{s_f'} \tag{3.31}$$

where all symbols have the same meaning as those employed in the previous Eq. 3.30.

For completely wrapped members having circular cross-sections of diameter D_c when fibres are placed orthogonally to the axis of the member ($\beta = 90°$), the FRP contribution to the shear capacity, $V_{Rd,f}$, shall be calculated as follows:

$$V_{Rd,f} = \frac{1}{\gamma_{Rd}} \cdot D_c \cdot f_{fed} \cdot \frac{\pi}{2} \cdot a_f \cdot \cot\theta \tag{3.32}$$

In all Equations 3.30 to 3.32 it is allowed to replace the term s_f' with the term s_f measured along the member longitudinal axis, where $s_f' = s_f \cdot \sin\beta$.

The design effective strength of the FRPs is evaluated, for the side-bonded configuration, by means of the following equation:

$$f_{fed} = f_{fdd} \cdot \frac{z_{rid,eq}}{\min\left\{0.9 \cdot d, h_w\right\}} \cdot \left(1 - 0.6 \cdot \sqrt{\frac{l_{eq}}{z_{rid,eq}}}\right)^2 \tag{3.33}$$

in which f_{fdd} is the FRP design ultimate debonding-based strength to be determined as later specified, and:

$$z_{rid,eq} = z_{rid} + l_{eq}; \quad \mathrm{z_{rid}} = \min\left\{z, h_w\right\} - L_e \cdot \sin\beta; \quad l_{eq} = \frac{\delta_{fu}}{f_{fdd} / E_f} \cdot \sin\beta \tag{3.34}$$

with the following symbols: z_{rid} is the reduced value of the internal lever arm, z the internal lever arm ($z = 0.9 \cdot d$), h_w the web height , L_e is the effective bond length, l_{eq} is the vertical projection of the bonded length that would be necessary if the fabric strain $\varepsilon_{fdd} = f_{fdd} / E_f$ was uniform; δ_{fu} is the slip at debonding to be assumed equal to 0.2 mm, E_f the elasticity modulus in the fibres direction and $z_{rid,eq}$ the equivalent value of the reduced internal lever arm.

In case of U-shaped configuration, the effective design strength is evaluated as follows:

$$f_{fed} = f_{fdd} \cdot \left[1 - \frac{1}{3} \cdot \frac{L_e \cdot \sin\beta}{\min\left\{0.9 \cdot d; h_w\right\}}\right] \tag{3.35}$$

while, in case of wrapping:

$$f_{fed} = f_{fdd} \cdot \left[1 - \frac{1}{6} \cdot \frac{L_e \cdot \sin\beta}{\min\left\{0.9 \cdot d; h_w\right\}}\right] + \frac{1}{2} \cdot \left(\phi_R \cdot f_{fd} - f_{fdd}\right) \cdot \left[1 - \frac{L_e \cdot \sin\beta}{\min\left\{0.9 \cdot d; h_w\right\}}\right] \tag{3.36}$$

where f_{fd} is the design ultimate strength of the FRP and:

$$\phi_R = 0.2 + 1.6 \cdot \frac{r_c}{b_w}, \quad 0 \le \frac{r_c}{b_w} \le 0.5 \tag{3.37}$$

where r_c is the corner radius of the section to be wrapped. Moreover, in Eq. 3.36, the second term should be considered only if greater than zero.

The effective design strength, f_{fed} , *i.e.* a reduced value of the debonding-based ultimate design strength, f_{fdd} is introduced in order to prevent the FRP strips from debonding because of the brittleness of such failure mechanism.

For the case of a bond length value, L_f, higher or equal to the optimal bond length, L_e, and for the case of the FRP sheet end debonding failure mode (mode 1), the design effective strength is calculated by:

$$f_{fdd} = \frac{1}{\gamma_f \cdot \sqrt{\gamma_c}} \cdot \sqrt{\frac{2 \cdot E_f \cdot G_{fk}}{a_f}} \tag{3.38}$$

where γ_f is the FRP material partial safety factor, γ_c is the partial safety factor for concrete and G_{fk} is the characteristic value of the specific fracture energy for the FRP-concrete interface calculated as follows:

$$G_{fk} = 0.03 \cdot k_f \cdot \sqrt{f_{ck} \cdot f_{ctm}} \tag{3.39}$$

where f_{ck} is the characteristic cylindrical concrete compressive strength, f_{ctm} is the concrete mean tensile strength and k_f is the geometric coefficient.

The effective bond length is calculated as follows:

$$L_e = \sqrt{\frac{E_f \cdot a_f}{2 \cdot f_{ctm}}} \tag{3.40}$$

And the geometrical coefficient, k_f:

$$k_f = \sqrt{\frac{2 - \frac{b_f}{b_c}}{1 + \frac{b_f}{400}}} \geq 1 \tag{3.41}$$

in which b_f is the width of the FRP system and b_c is the width of the concrete element, see Fig. 3.4.

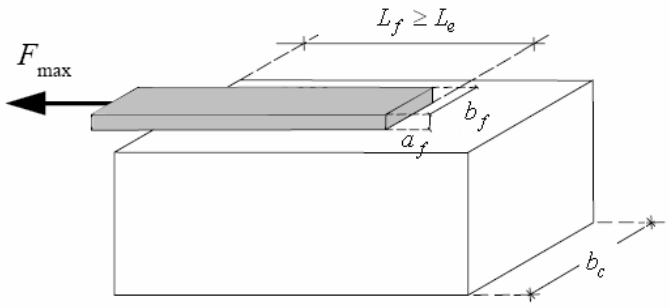

Fig. 3.4 – Maximum force transferred between FRP and concrete

For the cases in which the available bond length, L_f, is shorter than the effective bond length, L_e, the ultimate design strength shall be reduced according to the following equation:

$$f_{fdd,rid} = f_{fdd} \cdot \frac{L_f}{L_e} \cdot \left(2 - \frac{L_f}{L_e}\right) \tag{3.42}$$

To prevent failure from intermediate debonding mechanism (mode 2), the maximum strength calculated in the FRP system at ultimate shall be less than $f_{fdd,2}$:

$$f_{fdd,2} = k_{cr} \cdot f_{fdd} \tag{3.43}$$

where the reduction factor, k_{cr}, can be assumed equal to 3.0 if specific data are not available.

Among the construction details, it is recommended that: for U-wrapped and completely wrapped configurations, a minimum radius of 20 mm should be provided when FRP sheets are installed around outside corners; for external FRP reinforcement in the form of discrete strips, the strip width, b_f and centre to centre spacing between strips, $s_f^{'}$, should not exceed the following limitations, respectively:

$$50 \le b_f \le 250\ mm \text{ and } b_f \le s_f^{'} \le \min\left\{0.5 \cdot d, 3 \cdot b_f, b_f + 200\ mm\right\} \tag{3.44}$$

The above formulation was developed within a rigorous closed-form framework (Monti and Liotta 2006, Liotta 2007, Monti *et al.* 2004) by defining: a generalised failure criterion of an FRP strip/sheet bonded to a concrete surface; the local stress-slip constitutive law; the compatibility equations (*i.e.* the crack opening); the boundary conditions (*i.e.* the available bond lengths on both sides of the crack depending on the adopted configuration).

The above solution proposed by Italian Research Council has been determined with formal rigour and the predictions obtained accordingly have shown a more than satisfactory agreement with the experimental results (Liotta 2007, Monti *et al.* 2004).

This formulation has resulted absolutely innovative, in the ambit of the shear strengthening of RC concrete structures by means of EB FRP systems, mainly because of two points: first, it is based on the understanding of the mechanical failure modes, that, as stated above, can not always be modelled with the Mörsch truss and second, it was obtained in closed form taking into account not only equilibrium but also compatibility, constitutive law and boundary conditions.

3.4 De Lorenzis' analytical formulation for NSM Technique

The formulation by De Lorenzis (De Lorenzis and Nanni 2001, De Lorenzis 2002) was proposed within a general pioneering evaluation of the innovative strengthening technique by means of Near Surface Mounted (NSM) FRP rods.

The ultimate shear strength is calculated, in accordance with ACI provisions (ACI 318-95), by superimposing the contributions provided by the concrete, V_c, by the transverse steel reinforcement, V_s, and by the FRP rods, V_f. The strength reduction factors to be applied to the ultimate strength contributions above are: 0.85 for both concrete and steel and 0.7 for the FRP in order to implicitly take into account the major uncertainties due to the relative novelty of this technique. Thus, the design shear resistance of the strengthened RC element, V_{Rd}, will be as follows:

$$V_{Rd} = 0.85 \cdot \left(V_s + V_c\right) + 0.7 \cdot V_f \tag{3.45}$$

De Lorenzis also recommends the following limits to be respected:

$$V_f \le 4 \cdot \sqrt{f_{ck}} \cdot b_w \cdot d \tag{3.46}$$

$$V_s + V_f \le 8 \cdot \sqrt{f_{ck}} \cdot b_w \cdot d \tag{3.47}$$

where f_{ck} is the characteristic value of the concrete compressive strength, b_w the web width and d the cross section effective depth. The former limitation on the maximum amount of additional shear strength that may be achieved is defined as a percentage of the ultimate concrete shear strength contribution. It is a limitation that should get the designer

aware that it is better not to rely on additional FRP shear strength values that are too high with respect to the concrete shear strength. The latter limitation attempts to avoid excessive crack width by limiting the maximum shear resisted by stirrups.

According to De Lorenzis, the ultimate shear contribution by the NSM FRP Rods has to be assumed equal to the minimum of two values: V_{f1} determined taking into account the debonding failure mode (governed by splitting of the cover in the examined case of ribbed round bars) and V_{f2}, corresponding to the possibility that, avoided debonding, the maximum strain of 4‰ is reached in the rods. This latter is meant to avoid excessive width of the cracks to occur thus preserving the resisting contribution provided by concrete aggregate interlock.

In the calculations a reduced value of the height, d_{net}, of the cross-section is utilised:

$$d_{net} = d_r - 2 \cdot c \tag{3.48}$$

in which c is the concrete cover and d_r is the height of the shear-strengthened part of the cross-section. In the case of vertical NSM rods, d_r coincides with the length of the rods. This reduction is intended to approximately account for the height of the Mörsch truss being lower than the actual height of the section.

The term V_{f1} is computed based on the following assumptions:

- inclination angle of the shear cracks constant and equal to 45°;
- even distribution of bond stresses along the FRP rods' effective bond length, at ultimate;
- the ultimate bond strength is reached in all of the rods intersected by the crack at ultimate.

De Lorenzis adopted the assumption of evenly distributed bond strength on the basis of both experimental observations and analytical results: for low values of the bonded length (approximately less than 24 diameters), the ultimate load was observed to grow almost linearly with the bonded length thus justifying it. De Lorenzis also warns about the necessity to further verify the assumption of an even value of bond strength at ultimate in case of both bond stress-slip conditions $\tau(\delta)$ and bonded length values different than those she delt with.

De Lorenzis uses the term "*effective bond length*" to refer to the shorter of the two parts in which the crack divides the rod. Since troughout the present document, the comparison between NSM and EBR is made, we will refer the same quantity as "*available bond length*", to distinguish it from the effective bond length of the EBR technique.

The shear force can be computed as the sum of the forces resisted by each of the FRP rods intersected by the shear crack:

$$V_{1f} = 2 \cdot \pi \cdot d_b \cdot \tau_b \cdot L_{tot,\min} \tag{3.49}$$

in which d_b is the nominal diameter of the adopted FRP rods, τ_b is the average bond strength and $L_{tot,\min}$ is the minimum value of the effective lengths' sum, *i.e.* the minimum value, function of the geometrical disposition of the assumed crack with respect to the rods, of the sum of the available bond length of the rods crossing the crack.

Actually $L_{tot,\min}$ depends on: the reduced height of the beam cross section, d_{net}, the spacing of the rods calculated along the axis of the beam, s_f, and their inclination, β, and can be computed, on the basis of geometrical considerations, as follows:

$$L_{tot,\min} = d_{net} - s_f \quad \text{if} \quad \frac{d_{net}}{3} \le s_f \le d_{net} \tag{3.50}$$

$$L_{tot,\min} = 2 \cdot d_{net} - 4 \cdot s_f \quad \text{if} \quad \frac{d_{net}}{4} \le s_f < \frac{d_{net}}{3} \tag{3.51}$$

for vertical rods and:

$$L_{tot,\min} = \left(2 \cdot d_{net} - s_f\right) \cdot \frac{\sqrt{2}}{2} \quad \text{if} \quad \frac{2 \cdot d_{net}}{3} \le s_f \le 2 \cdot d_{net} \tag{3.52}$$

$$L_{tot,\min} = 2 \cdot \sqrt{2} \cdot \left(d_{net} - s_f\right) \quad \text{if} \quad \frac{d_{net}}{2} \le s_f \le \frac{2 \cdot d_{net}}{3} \tag{3.53}$$

for 45 degree-inclined rods.

The term V_{f2} is the NSM FRP shear strength contribution corresponding to a maximum effective strain of 4‰. It is calculated under the same assumptions adopted for V_{f1}, *i.e.*: 45-degree shear crack and even bond stress distribution at ultimate.

The effective length of an FRP rod crossed by the crack and corresponding to a strain of 4‰, $\overline{L}_f$, can be calculated, by equilibrium considerations, as follows:

$$\overline{L}_f = 0.001 \cdot \frac{d_b \cdot E_f}{\tau_b} \tag{3.54}$$

When the available bond length of the i-th laminate, L_{fi}, is higher than $\overline{L}_f$, this latter value will be considered.

According to De Lorenzis' provisions, if:

$$d_{net} < 0.002 \cdot \frac{d_b \cdot E_f}{\tau_b} \tag{3.55}$$

in the case of vertical rods or if:

$$d_{net} < \sqrt{2} \cdot 0.001 \cdot \frac{d_b \cdot E_f}{\tau_b} \tag{3.56}$$

for the 45 degree-inclined rods, the evaluation of V_{f2} is not necessary since the first term V_{f1} prevails.

V_{f2} has to be calculated in the most unfavourable position, that is in the position in which it is minimum. It can be shown that, the minimum value is:

$$V_{f2} = 2 \cdot \pi \cdot d_b \cdot \tau_b \cdot \overline{L}_f \quad \text{if} \quad \frac{d_{net}}{2} < s_f < d_{net} \tag{3.57}$$

$$V_{f2} = 2 \cdot \pi \cdot d_b \cdot \tau_b \cdot \overline{L}_f \cdot \frac{3 \cdot d_{net} - 4 \cdot s_f}{d_{net}} \quad \text{if} \quad \frac{d_{net}}{4} < s_f < \frac{d_{net}}{3} \tag{3.58}$$

for vertical rods and:

$$V_{f2} = 2 \cdot \pi \cdot d_b \cdot \tau_b \cdot \overline{L}_f \quad \text{if} \quad d_{net} < s_f < 2 \cdot d_{net} \tag{3.59}$$

$$V_{f2} = 2 \cdot \pi \cdot d_b \cdot \tau_b \cdot \overline{L}_f \cdot \frac{3 \cdot d_{net} - 2 \cdot s_f}{d_{net}} \quad \text{if} \quad \frac{d_{net}}{2} < s_f < d_{net} \tag{3.60}$$

for 45 degree-inclined rods.

The formulation by De Lorenzis was recently adapted to the case of NSM CFRP laminates by Barros and Dias (2005). The term V_{f1} was calculated as follows:

$$V_{f1} = 4 \cdot \left(a_f + b_f \right) \cdot \tau_b \cdot L_{tot,\min} \tag{3.61}$$

where a_f and b_f are, respectively, the thickness and width of the NSM laminates cross section.

The formula for the evaluation of V_{f2} was also adapted to the case of rectangular cross-sectioned laminates by Barros and Dias (2005):

$$V_{f2} = 4 \cdot \left(a_f + b_f \right) \cdot \tau_b \cdot \bar{L}_f \qquad \text{if} \qquad \frac{d_{net}}{2} < s_f < d_{net} \tag{3.62}$$

$$V_{f2} = 4 \cdot \left(a_f + b_f \right) \cdot \tau_b \cdot \bar{L}_f \cdot \frac{3 \cdot d_{net} - 4 \cdot s_f}{d_{net}} \qquad \text{if} \qquad \frac{d_{net}}{4} < s_f < \frac{d_{net}}{3} \tag{3.63}$$

for vertical rods and:

$$V_{f2} = 4 \cdot \left(a_f + b_f \right) \cdot \tau_b \cdot \bar{L}_f \qquad \text{if} \qquad d_{net} < s_f < 2 \cdot d_{net} \tag{3.64}$$

$$V_{f2} = 4 \cdot \left(a_f + b_f \right) \cdot \tau_b \cdot \bar{L}_f \cdot \frac{3 \cdot d_{net} - 2 \cdot s_f}{d_{net}} \qquad \text{if} \qquad \frac{d_{net}}{2} < s_f < d_{net} \tag{3.65}$$

for 45 degree-inclined rods.

Likewise, if:

$$d_{net} < 2 \cdot \bar{L}_f \tag{3.66}$$

in the case of vertical laminates, or if:

$$d_{net} < \sqrt{2} \cdot \bar{L}_f \tag{3.67}$$

in the case of laminates at 45 degrees, it is not necessary for V_{f2} to be calculated being V_{f1} the commanding, minimum value.

Within a work mainly devoted to the appraisal of the performance by the available predictive formulae, Barros and Dias Barros and Dias (2005) obtained a good agreement between experimental results and the predictions by De Lorenzis' formula even if they had to modify the value of some parameters to take into account the specificities related to the use of NSM laminates instead of rods. In particular, they assumed a value of 16.1 MPa as average bond strength and an average strain at peak pullout force of 5.9‰.

3.5 Formulation by Nanni et al. for NSM Technique

In the ambit of a proposal for shear-strengthening existent Pre-stressed Concrete (PC) bridge girders by means of NSM CFRP rectangular cross-sectioned bars, Nanni *et al.* (2004) proposed a formulation to estimate the CFRP contribution to the overall shear resistance of the strengthened RC member, which was derived from the formulation of De Lorenzis, described in the previous section. The ultimate contribution of the laminates, V_f, is obtained by the following equation:

$$V_f = 4 \cdot \left(a_f + b_f \right) \cdot \tau_b \cdot L_{tot,\min} \tag{3.68}$$

in which a_f and b_f are, respectively, the thickness and width of the bar cross section, τ_b is the average bond strength of the elements crossing the shear crack and $L_{tot,\min}$ is the minimum possible value of the sum of the "*effective length*" of all the elements intersected by the shear crack:

$$L_{tot,\min} = \sum_{i=1}^{N_{eff}} L_{fi} \tag{3.69}$$

The "*effective length*", L_{fi}, as for De Lorenzis' formulation, is the shorter of the two parts in which the crack divides the i-th intersected laminate. Hereinafter, it will be referred to as "*available bond length*". The minimum value L_{fi}, for the i-th laminate, is determined as follows:

$$L_{fi} = \begin{cases} \min\left(\dfrac{s_f}{\cos\beta + \sin\beta} \cdot i;\ \overline{L}_f \right) & i = 1;...;\dfrac{N_{eff}}{2} \\ \min\left(l_{net} - \dfrac{s_f}{\cos\beta + \sin\beta} \cdot i;\ \overline{L}_f \right) & i = \left(\dfrac{N_{eff}}{2} + 1 \right);..;N_{eff} \end{cases} \tag{3.70}$$

where β is the inclination angle of the laminates with respect to the beam axis, i is the ordinal number of the laminates crossing the crack and counted starting from the crack origin (see Fig. 3.5), s_f is the spacing of the laminates calculated along the beam axis. l_{net} is the net length of the laminates, intended to account for eventual cracking of the concrete cover and installation tolerances, calculated as follows:

$$l_{net} = L_f - \frac{2 \cdot c}{\sin\beta} \tag{3.71}$$

where L_f is the actual length of a laminate and c is the thickness of the concrete cover.

N_{eff} is the effective number of the FRP bars intersected by the crack obtained by rounding off its actual value to the lowest integer:

$$N_{eff} = \text{lowest integer of } \frac{l_{eff} \cdot \left(1 + \cot\beta\right)}{s_f} \tag{3.72}$$

in which: l_{eff} is the vertical projection of the net length of the laminates, l_{net}.

The value $\overline{L}_f$ is determined by equilibrium conditions of the case in which the maximum allowable value of the effective strain ($\varepsilon_{fe} = 0.004$) is reached in the bar:

$$l_{\max} = \frac{\varepsilon_{fe}}{2} \cdot \frac{a_f \cdot b_f}{a_f + b_f} \cdot \frac{E_f}{\tau_b} \tag{3.73}$$

The limitation of the effective strain is meant to limit the width of the crack thus preserving the amount of shear resistance provided by the aggregate interlock resisting mechanism.

The value suggested for the average bond strength is 6.90 MPa. The assumption of the inclination of 45° for the critical diagonal crack is implicit. Another implicit assumption is the even distribution of the bond strength along the length of the element: the limitations already outlined for the formulation by De Lorenzis are still valid.

The above geometrical expedient to determine the $L_{tot,\min}$ by calculating the minimum integer number of bars actually intersected by the crack looks extremely elegant from an analytical point of view, even if it seems to be simply a refinement of the previous formulation by De Lorenzis (see paragraph 3.4).

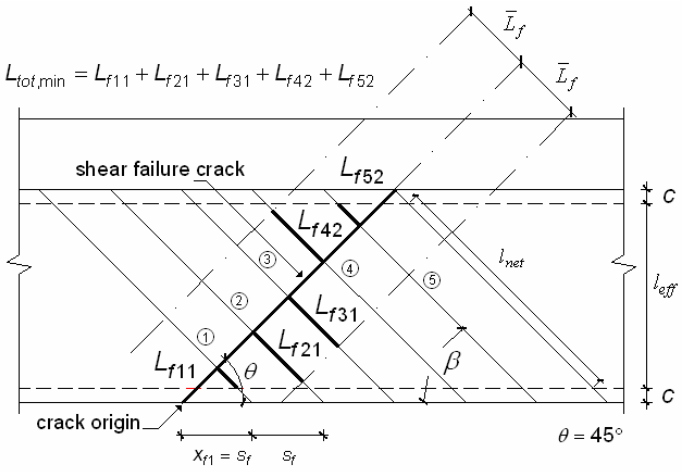

Fig. 3.5 – Concept of $L_{tot,\min}$

Barros and Dias (2006) already appraised the performance of the above formula in the case of NSM CFRP laminates obtaining too conservative results due to the low value of τ_b prescribed by Nanni *et al.* since it was determined in the case of FRP round bars glued by means of epoxy adhesive into square-sectioned grooves. In that case, the dominant bond mechanism was splitting of the epoxy cover that, for bigger dimensions of the cut slit, involved also the surrounding concrete (De Lorenzis and Nanni 2002). On the contrary, in the case of NSM CFRP laminates, the governing bond mechanism at failure is due to the damage of the interface laminate-epoxy (Sena-Cruz 2004). By using average bond strength and effective strain values obtained in pull-out bending tests carried out at the Structural Laboratory of the University of Minho, *i.e.* by using: $\tau_b = 16.1\,\text{MPa}$ and $\varepsilon_{fe} = 0.0059$, Barros and Dias obtained a more satisfactory average safety factor of about 1.39.

Apart from the improved formal elegance as regards the evaluation of the minimum total length with respect to the previous formulation by De Lorenzis, a conceptual limit seems not to be overcome yet: the resisting force is calculated by adding the contributions of the laminates crossing the crack evenly distributing the average bond strength on the shorter part of each bar irrespective of the length-dependence of the average bond strength. In that respect, it seems much more correct to multiply each effective length by the corresponding average bond strength. Moreover, it is not clear the reason why the shear resisting contribution provided by the NSM along the length of the bars is not projected on the vertical in order to obtain the vertical component.

3.6 Australian Guidelines Draft's Recommendations

These Recommendations deal with the strengthening of RC beams and slabs by means of FRP elements both Externally Bonded (EB) and Near Surface Mounted (NSM) and are composed of two parallel parts: the Guideline itself and the Commentary. In the former, the authors provide general informations aiming at developing a deep knowledge of the main specificities of the mechanical behaviour of RC elements strengthened in shear or flexure by FRP elements and, in

the latter, they provide some among the more advanced design analytical expressions available to date. The Commentary is only meant to assist in the design and the designer is free to use any other approach that has been shown to be correct and safe and which satisfies the generic and fundamental principles outlined in the Guideline.

The general formulation, reported in the Guideline, and applicable to both the case of EB and NSM, to evaluate the ultimate shear resistance of the strengthened beam, V_R , is the following:

$$V_u = V_c + \Delta V_c + k_f \cdot V_f + k_s \cdot V_s \tag{3.74}$$

where, V_c , is the contribution ascribed to concrete, V_f is the FRP contribution, V_s is the tranverse steel reinforcement contribution, ΔV_c is the increment of concrete shear contribution due to the presence, if any, of longitudinal FRP elements, glued either on the beam soffit or the web faces, crossing the Critical Diagonal Crack (CDC), k_f is a coefficient that accounts for the interaction between subsequent FRP elements and k_s is a coefficient that accounts for the interaction between FRP elements and existing stirrups. The CDC is defined as a crack across which there is a rigid body displacement between the two parts in which the beam is divided (see Fig. 3.6).

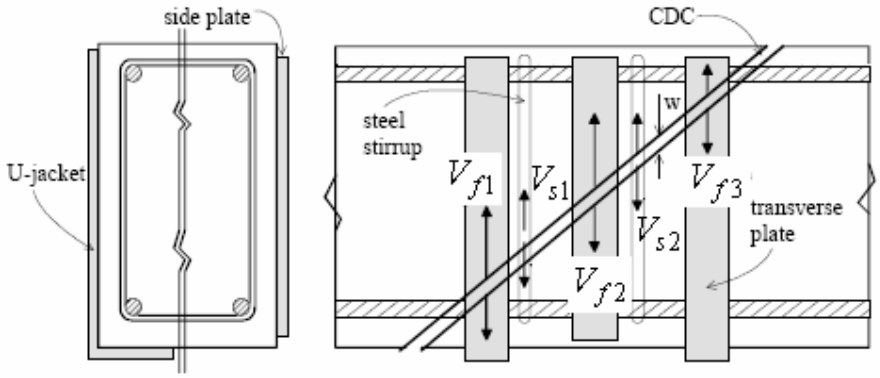

Fig. 3.6 – CDC and stress resultants in transveral plates

Critical diagonal cracks are neither flexural cracks nor inclined flexural-shear cracks that occur over a relatively small portion of the depth of the beam. In contrast, a critical diagonal crack occurs over the full depth, or nearly the full depth, of the beam cross section. The reduction factor k_s accounts for the possibility that, in correspondence of the beam peak load, the deformation already occurred in the stirrups is not large enough to have yielded them so that their maximum strength cannot be entirely added to the resisting forces V_c and V_f provided by concrete and FRP, respectively. The coefficient k_f accounts for the possibility that the FRP strips/laminates may debond as a whole for a value of the overall shear capacity which is less than the mere sum, V_f , of their individual capacities:

$$V_f = \sum_i^n V_{fi} = \sum_i^n V_{fi}^p \cdot \sin\beta \tag{3.75}$$

where n is the number of plates crossing the CDC, V_{fi} is the shear strength contribution that can be provided by a single i-th element, *i.e.* the component, orthogonal to the beam axis, of the maximum force that can be resisted by the element along its axis V_{fi}^p, and β is the inclination of the FRP element with respect to the beam axis. The term ΔV_c takes into account the possible presence of longitudinal FRP elements crossing the CDC whose beneficial effect is to

add extra resistance to the crack widening thus incrementing the value of the shear strength provided by concrete aggregate interlock. In the case of longitudinal NSM elements, as opposed to the case of EBR, the term ΔV_c is suggested to be taken equal to zero since the NSM elements, in virtue of a better bond behaviour, can bear higher deformations than EBR before debonding occurs.

The resistance provided by the i-th FRP element V_{fi}^{p} is calculated assuming that it is the minimum resisting value between those ascribed respectively to debonding, $V_{fi}^{p,db}$, and tensile rupture, $V_{fi}^{p,tr}$, of the element itself:

$$V_{fi}^{p} = \min\left\{V_{fi}^{p,tr}; V_{fi}^{p,db}\right\} \tag{3.76}$$

The commanding failure mechanism, on the basis of which the term $V_{fi}^{p,db}$ is calculated, is referred to as "*Intermediate Crack (IC) debonding*". The intermediate crak, in Fig. 3.7, can be any crack that intersects the plate such as a flexural crack, flexural-shear crack, or critical diagonal crack and the widening of the intermediate crack of width w can be due to flexural or shear deformations.

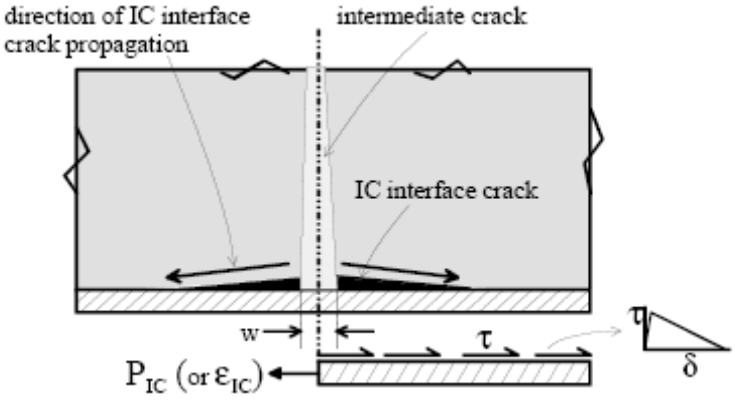

Fig. 3.7 – Concept of Intermediate Crack (IC)

When any new intermediate crack intersects a plate, localised debonding accompanied by interface slip δ occurs at the concrete/plate interface as shown in Fig. 3.7, which allows the crack to go on widening. These localized interface debonding cracks are referred to as IC interface cracks. If those IC interface cracks are allowed to grow due to widening of the intermediate crack w, they can cause the plate to debond at an axial force P_{IC} which is, throughout the Australian Guidelines, referred to as "*IC debonding resistance"*. The IC debonding resistance, P_{IC}, depends on the interface bond-slip characteristics shown as τ/δ in Fig. 3.7 and also shown in Fig. 3.9, where τ_f is the peak interface shear stress and δ_{fu} is the maximum interface slip that resists shear and beyond which the bond reduces to zero. These material interface characteristics, τ_f and δ_{fu}, and their corresponding energy term, $\tau_f \cdot \delta_{fu}$, are generally derived directly from tests, such as the push-pull test shown in Fig. 3.10, and are the fundamental properties that govern not only the IC debonding strength P_{IC} but also the ductility of the plated section at IC debonding.

It emerges that the authors of the Australian Guidelines adopt the definition of intermediate crack resistance P_{IC} in order to clearly distinguish this failure mechanism from the Plate End debonding (PE) that generally occurs for flexural strengthening elements at their free end, see Fig. 3.8.

Since in the case of shear, that is the main interest of the present document, the above intermediate crack debonding envisages debonding that starts propagating from the CDC, that is from the loaded end of the available bond length of the element crossing the crack, the corresponding resisting force, will be simply referred to throughout the text, in an attempt to uniformize the symbols, as debonding resistance and indicated by $V_{fi}^{p,db}$.

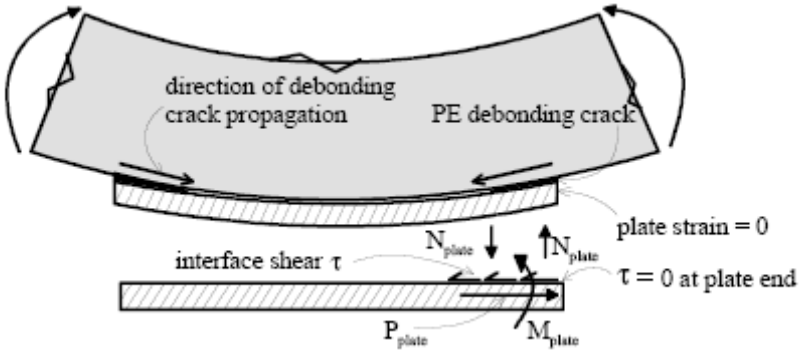

Fig. 3.8 – Plate End (PE) debonding mechanism

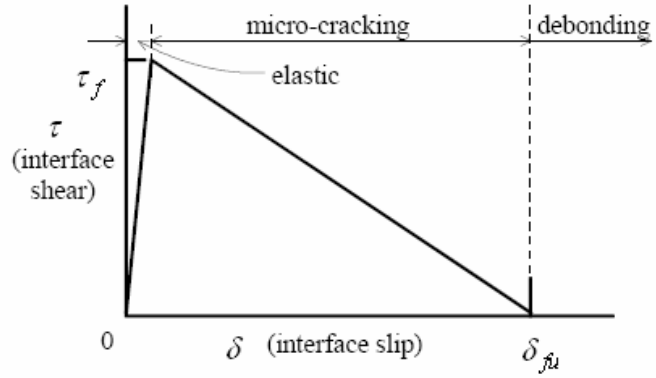

Fig. 3.9 – Fundamental interface bond-slip characteistics

The debonding resistance of the i-th element in beams, whose contour geometrical condition differ from the ones met in a simple push-pull test, and parallel to the element length, $V_{fi}^{p,db}$, can be assumed equal to the value obtainable by means of a simple push-pull test since this latter generally constitutes a lower bound. The maximum debonding resistance is given by (Seracino *et al.* 2006):

$$V_{fi}^{p,db} = \sqrt{\tau_f \cdot \delta_{fu}} \cdot \sqrt{L_{per,db} \cdot E_f \cdot \left(a_f \cdot b_f\right)} \tag{3.77}$$

where $L_{per,db}$ is the perimeter length of the cross section of the debonding failure plane as shown in Fig. 3.11, E_f is the Young's Modulus of the plate along its longitudinal axis and $a_f \cdot b_f$ is the plate cross sectional area.

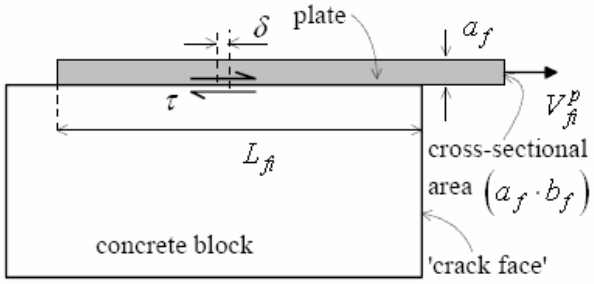

Fig. 3.10 – Fundamental interface bond-slip characteristics

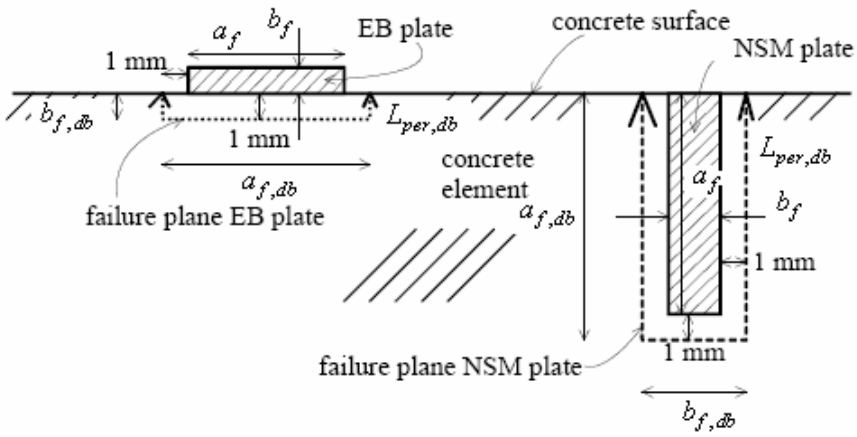

Fig. 3.11 – Perimeter length of idealised failure plane (cross section)

To achieve the maximum debonding resistance, $V_{fi}^{p,db}$, a minimum bond length, L_e, from the "crack face" in Fig. 3.12 is required that can be calculate by the following expression (Seracino *et al.* 2006):

$$L_e = \frac{\pi}{2 \cdot \sqrt{\frac{\tau_f \cdot L_{per,db}}{\delta_{fu} \cdot E_f \cdot a_f \cdot b_f}}} \tag{3.78}$$

It can be assumed that the variation of the debonding resistance is bilinear: being zero at $L_f = 0$, increasing to a maximum of $V_{fi}^{p,db}$ at $L_f = L_e$ and constant at $V_{fi}^{p,db}$ when $L_f \geq L_e$ as shown in Fig. 3.12.

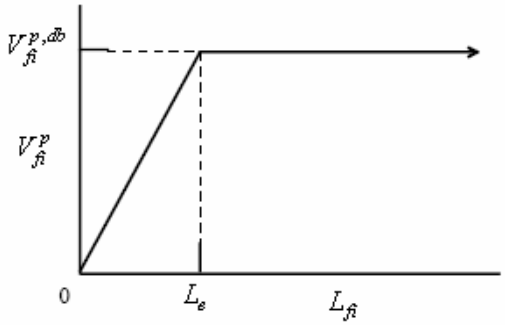

Fig. 3.12 – Idealized debonding resistance

The minimum bond length, L_e, is the minimum length of the element required to achieve the maximum debonding resistance $V_{fi}^{p,db}$. Unlike internal steel reinforcing bars, it is not always possible to increase the resisting force by increasing the bond length up to the tensile rupture of the element itself *i.e.* it can happen that, as function of the geometrical-mechanical parameters, the maximum load $V_{fi}^{p,db}$ is, in general, smaller than $V_{fi}^{p,tr}$.

In the parallel Commentary, it is suggested that the above values $V_{fi}^{p,db}$ and L_e can be calculated by the approach adopted at the University of Adelaide, valid for both EBR and NSM. The mean value of the fracture energy-related term, $\tau_f \cdot \delta_{fu}$, in Eq. 3.77, can be calculate by means of the following expression:

$$\tau_f \cdot \delta_{fu} = 0.73 \cdot \left(\frac{b_{f,db}}{a_{f,db}} \right)^{0.5} \cdot \left(f_{cm} \right)^{0.67} \tag{3.79}$$

where units are in N and mm and: f_{cm} is the average concrete cylindrical compressive strength, $b_{f,db}$ and $a_{f,db}$ are, respectively, the depth and width of the debonding failure plane (see Fig. 3.11). $b_{f,db}$ and $a_{f,db}$ are defined in Fig. 3.11 where the failure plane whose cross section perimeter is $L_{per,db}$ should be assumed to be 1 mm within concrete and from the plate (Seracino *et al.* 2006) as shown. The design characteristic value of the maximum force that can be reistsed by a single bonded element, which has a bond length equal at least to L_e, is:

$$V_{fki}^{p,db} = 0.725 \cdot \left(\frac{b_{f,db}}{a_{f,db}} \right)^{0.25} \cdot \left(f_c \right)^{0.33} \cdot \sqrt{L_{per,db} \cdot E_f \cdot a_f \cdot b_f} \tag{3.80}$$

where the corresponding mean value can be obtained substituting the coefficient 0.725 with 0.853.

For manufactured or pultruded plates, E_f and $\left(a_f \cdot b_f \right)$ are those of the plate itself. In case of wet lay-up systems, a_f and b_f are the dimensions of the FRP layers only, without considering the adhesive thickness and E_f is the Young's modulus of the FRP only.

The minimum bond length L_e can be obtained by Eq. 3.78 with τ_f taken as:

$$\tau_f = \left(0.8 + 0.078 \cdot \frac{b_{f,db}}{a_{f,db}} \right) \cdot \left(f_c \right)^{0.6} \tag{3.81}$$

where units are in N and mm and where δ_{fu}, also required in Eq. 3.78, can be obtaind substituting Eq. 3.81 into Eq. 3.79.

Alternatively, for the case of EBR only, the values of $V_{fi}^{p,db}$ and L_e can be calculated by the approach by Chen and Teng (Teng *et al.* 2002). In particular, $V_{fi}^{p,db}$ can be calculated by means of the following expression:

$$V_{fi}^{p,db} = \alpha_{EB} \cdot \beta_f \cdot b_f \cdot \sqrt{E_f \cdot a_f \cdot \sqrt{f_c}} \tag{3.82}$$

where units of N and mm must be used and where α_{EB} is equal to 0.427 for the mean value and 0.315 for the 95 percentile characteristic value. The factor β_f is a width coefficient given by:

$$\beta_f = \sqrt{\frac{2 - b_f / b_c}{1 + b_f / b_c}} \tag{3.83}$$

E_f is the Young's modulus of the plate, a_f is the thickness of the plate, b_c and b_f are the widths of the concrete element and the plate, respectively. When a number of parallel plates are bonded to a concrete surface or near the edge of a section, care must be taken to use an appropriate value of b_c as shown in Fig. 3.13.

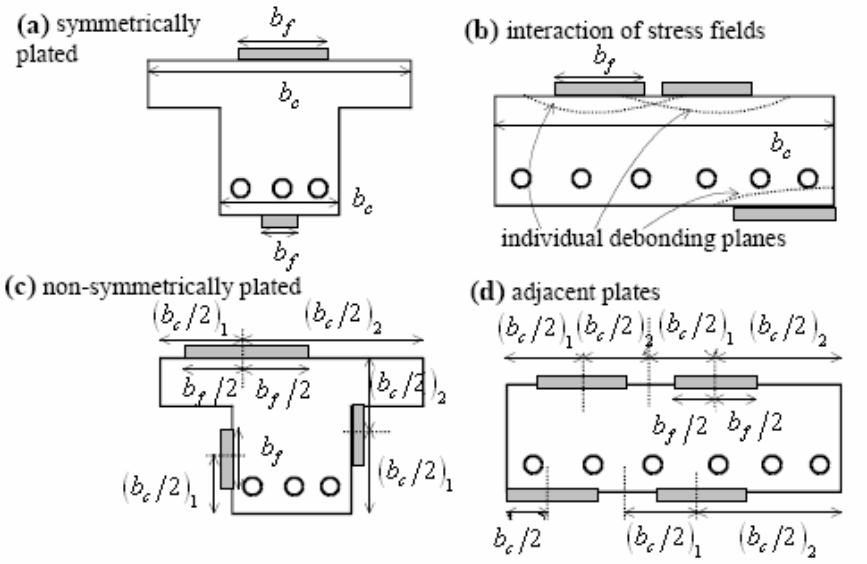

Fig. 3.13 – Recommended concrete widths (Oelehers and Seracino 2004)

It is not recommended to use Eq. 3.82 for plates thicker than 5 mm such as may be required when using thick steel plates to increase the beam stiffness. The effective bond length L_e required to achieve the maximum $V_{fi}^{p,db}$ is given by:

$$L_e = \sqrt{\frac{E_f \cdot a_f}{\sqrt{f_c}}} \tag{3.84}$$

where units are in N and mm.

When a vertical or transverse plate spans a CDC, as in Fig. 3.6, the rigid body shear deformations widen the CDC inducing axial forces in the crossing plates that are limited by $V_{fi}^{p,db}$.

At this point the recommendations dissert about the suitability and efficiency of the several shear strengthening techniques. The wrapping and U-jacketing configurations are best suited for the externally bonded wet lay-up FRP technique. The side bonded configuration is suited for EB FRP or metal plates and NSM strips. In terms of efficiency, the wrapping configuration is best as failure is typically by FRP rupture. However, the wrapping configuration is often unpossible (unpractical) due to the presence of the integrally cast concrete slab unless narrow strips are used at a given spacing which are taken through the slab. In terms of the externally bonded technique, the next most efficient configuration is U-jacketing and failure is typically associated with debonding of the plates. However, due to the better interface shear stress transfer mechanism of near surface mounted strips, NSM strips bonded on the sides may be just as efficient as U-jacketing EB plates. It is important to note that when using the wrapping or U-jacketing technique, the corners of the concrete section must be properly rounded to avoid FRP rupture due to high bending stresses around the corners; usually a 10 mm minimum radius is recommended. U-jacketing plates must be continuous around the sides and tension face. If a U-jacket goes across the compression face, it should be treated as a side bonded plate. In wrapped FRP the overlap should preferably be in the compression face and of sufficient length. The free ends of externally bonded plates in the U-jacketing or side bonded configuration may be mechanically anchored so that rupture of the FRP is possible. However, local failure of the FRP and failure of the anchor must be considered.

At this point, the Guideline, after having extensively argued the maximum axial force that can be resisted by a single bonded plate, either EB or NSM, lacks a coherent conclusion, that is, a final formulation, coherent with the term calculated so far, $V_{fi}^{p,db}$, is missing. The Guidelines also briefly say that the plates can be considered as stirrups but they do not provide informations at all on how to adapt the stirrups formulation, based on the Mörsch truss, to the case of the length-dependent ultimate strength of plates unless all elements are assumed to have a bond lengh, across the CDC, long enough to let them reach the value $V_{fi}^{p,db}$. Anyway, in the parallel Commentary, it is suggested to use, expressly for the case of the EBR only, the formulation by Teng *et al.* (Teng *et al.* 2002). Thus, even if not explicitely suggested, maybe, the authors implicitely suggest to use, for the time being, the formulation by Teng *et al.* also for the case of NSM.

According to the formulation by Teng *et al.*, the FRP shear contribution V_f, in Eq. 3.14, can be calculated, in the assumption of a CDC inclination of 45 degrees, as follows:

$$V_f = 2 \cdot f_{fe} \cdot a_f \cdot b_f \cdot \frac{h_{f,e} \cdot (\sin\beta + \cos\beta)}{s_f} \tag{3.85}$$

where a_f is the thickness of the strip, b_f is the width of the strip (perpendicular to the fibre orientation), s_f is the horizontal centre-to-centre spacing of the strips and β is the inclination of the fibres in the FRP to the longitudinal axis of the beam (see Fig. 3.14). For continuous FRP sheets it is:

$$s_f = \frac{b_f}{\sin\beta} \tag{3.86}$$

In Eq. 3.85, the term $h_{f,e}$ is the effective height of the sheet/plate bonded on the web of the RC beam and is given by the following expression:

$$h_{f,e} = z_b - z_t \tag{3.87}$$

where:

$$z_b = d_{fb} - h + 0.9 \cdot d \tag{3.88}$$

and:

$$z_t = d_{ft} \tag{3.89}$$

which is based on the assumption that the shear crack terminates $0.1 \cdot d$ from the compression face of the beam and where d is the effective depth of the beam to the centroid of the internal tensile reinforcement, h is the total depth of the beam, d_{ft} is the distance from the compression face of the beam to the "top" of the plate (that is, $d_{ft} = 0$ for the wrapping technique) and d_{fb} is the distance from the compression face of the beam to the "bottom" of the plate (that is, $d_{fb} = h$ for wrapping and U-jacketing techniques).

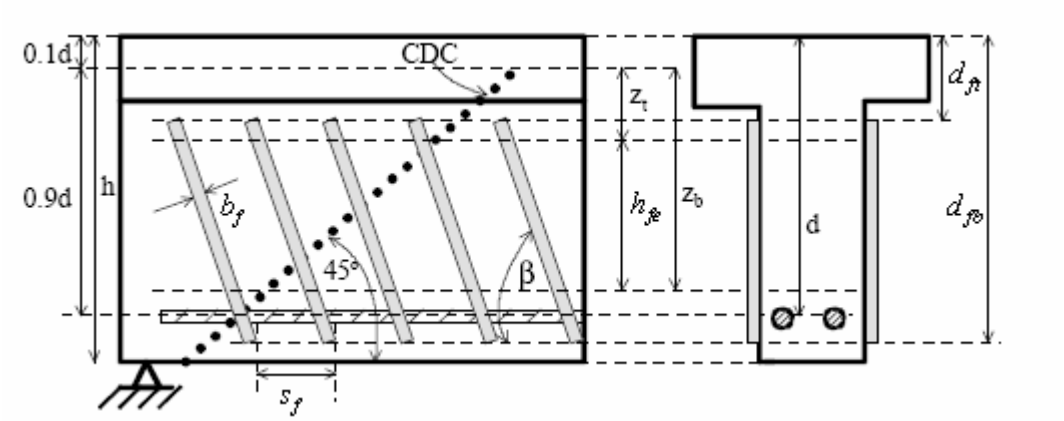

Fig. 3.14. – Notation for general shear strengthening scheme

As the stress distribution in the plates intersecting the shear crack at ultimate is non-uniform, the term f_{fe} in Eq. 3.85 is used to define the average stress in the plates and is given by:

$$f_{fe} = D \cdot \sigma_{f,\max} \tag{3.90}$$

where $\sigma_{f,\max}$ is the maximum stress that can be reached in the plate and D is a stress distribution factor, both depending on whether failure is governed by rupture or debonding.

If failure is governed by debonding, typically the case for the side bonded technique (and possible for U-jacketing), the stress distribution factor is given by:

$$D = \begin{cases} \dfrac{2}{\pi \cdot \lambda} \cdot \dfrac{1-\cos(\pi/2)\cdot\lambda}{\sin(\pi/2)\cdot\lambda} & \text{if } \lambda \le 1 \\ 1 - \dfrac{\pi - 2}{\pi \cdot \lambda} & \text{if } \lambda > 1 \end{cases} \tag{3.91}$$

in which:

$$\lambda = L_{fi,\max} / L_e \tag{3.92}$$

where L_e is the effective bond length already defined earlier and:

$$L_{fi,\max} = \begin{cases} \dfrac{h_{fe}}{\sin\beta} & \text{for U-jacketing} \\ \dfrac{h_{fe}}{2\cdot\sin\beta} & \text{for side bonding} \end{cases} \tag{3.93}$$

The maximum stress is given by:

$$\sigma_{f,\max} = \min \begin{cases} 0.8 \cdot f_{\max} \\ \sigma_{IC} \end{cases} \tag{3.94}$$

where σ_{IC} is the 95 percentile IC characteristic debonding stress as given in the Hong Kong approach, determinable by Eq. 3.82 *i.e.* $\sigma_{IC} = V_f^{p,db} / \left(a_f \cdot b_f\right)$ and $f_{\max}$ is the ultimate strength of the element f_{fu}. Note that, if $L_{fi,\max} < L_e$, a

linear variation of the debonding resistance should be used as illustrated in Fig. 3.12. For EB FRP plates or sheets using Chen and Teng's approach, the width coefficient to give σ_{IC} is given by:

$$\beta_f = \sqrt{\frac{2 - b_f / \left(s_f \cdot \sin\beta\right)}{1 + b_f / \left(s_f \cdot \sin\beta\right)}} \tag{3.95}$$

where $\beta_f = 0.707$ for continuous FRP sheets.

If failure is governed by FRP rupture, typically the case for the wrapping technique (and possibly for U-jacketing) the stress distribution factor is given by:

$$D = 0.5 \cdot \left(1 + \frac{z_t}{z_b}\right) \tag{3.96}$$

and the maximum stress is:

$$\sigma_{f,\max} = \begin{cases} 0.8 \cdot f_{fu} & if\ \varepsilon_{fu} \le \varepsilon_{\max} \\ 0.8 \cdot \varepsilon_{\max} \cdot E_f & if\ \varepsilon_{fu} > \varepsilon_{\max} \end{cases} \tag{3.97}$$

where ε_{fu} is the rupture strain of the plate and for $\varepsilon_{\max}$, which represents the maximum usable strain to control the shear crack width, it is recommended to take $\varepsilon_{\max} = 1.5\%$. The 0.8 factor in Eq. 3.94 and 3.97, allows for factors not explicitly considered in the shear strength model.

The formulation shown above, is intended for the shear spans in which the bending moment is positive. For negative moment regions, the various dimensional quantities employed, and respresented in Fig. 3.14, have to be measured from the bottom (compression) face of the beam. Furthermore, U-jackets wrapped around the bottom (compression) face of the beam should be considered as side-bonded only since, the part of the wrapping located in the compressed soffit, because of the transversal compression stresses, is expected to unglue from the concrete surface due to buckling.

As regards the calculation of the term ΔV_c in Eq. 3.74, the recommendations warn about the effective reliability of this term if only the length of the longitudinal plates, either on the soffit or on the web lateral faces, is such as to assure that their extension, on either side of the hypothetical CDC is such as to reach the minimum bond length L_e. For those cases, and only if the longitudinal plates are externally bonded, ΔV_c can be calculated as follows:

$$\Delta V_c = 0.15 \cdot \sum_{i=1}^{n_l} V_{fi}^{p} = 0.15 \cdot \sum_{i=1}^{n_l} \min\left\{V_{fi}^{p,db}; V_{fi}^{p,tr}\right\} \tag{3.98}$$

Where V_{fi}^{p} is the maximum axial force that can be resisted by an FRP element along its length and n_l is the number of longitudinal FRP elements crossing the CDC.

For a shear strengthening scheme using strips (that is, not continuous sheets) to be effective, it should be ensured that the strip spacing is less than half the horizontal distance spanned by the shear crack. This ensures that at least two strips intersect the shear crack, with at least one being effective. Hence, the maximum clear strip spacing is given by (Chen and Teng 2003):

$$\left(s_f - \frac{b_f}{\sin\beta}\right) \le \min\begin{cases} \dfrac{h_{fe}\cdot(1+\cot\beta)}{2} \\ 300\ mm \end{cases} \tag{3.99}$$

3.7 Conclusions

Among the formulations analyzed in the present Chapter, the one provided by the Italian National Reasearch Council results to be the most satisfactory for the EBR shear strengthening of RC beams. It results to be innovative since it is a correct, closed-form, mathematical interpretation of the physical phenomena affecting the EBR systems at ultimate. On the contrary, the formulations proposed by the ACI 440 and *fib* seem to solve the problem in a simplistic way. In fact, they simply adopt the formula for steel stirrups to the case of externally bonded FRP regardless of the changed physical behaviour. Anyway, the Codes by ACI 440, *fib* and Italian National Research Council completely neglect the case of the NSM, for the time being.

The Australian Guidelines result interesting since they highlight the importance of issues such as the interaction between FRP elements and between FRP elements and existing stirrups. They also contemplate the possibility of using NSM FRP elements and provide, in that regard, some argumentations very useful to help develop insight in the subject. As regards the proposal of a formulation useful to predict, with enough accuracy, the FRP shear strength contribution, they suggest, in the parallel commentary, to adopt the one by Teng *et al.* (2002), expressly for the case of EBR while they do not explicitly say if the same formula can be extended to the case of NSM.

Moreover, the Australian Guidelines stress the importance of verifying if there might be failure in the surrounding concrete and provide designers with some possibile formulae.

Among the formulations specifically dedicated to the NSM technique, the formulation by Nanni *et al.* (2004) results to be a refinement of the previous formulation by De Lorenzis (2002). Anyway, given the observed failure modes recently observed by both De Lorenzis and Rizzo (2006) and Dias and Barros (2006), consisting in the detachment of the strengthened concrete cover from the core of the beam, those formulations do not seem to interpret the physical behavior consistently. In fact, both of them are based on the assumption that debonding is the only possible failure mode. Moreover, both the formulations by Nanni *et al.* and by De Lorenzis suggest calculating the NSM shear strength contribution as the minimum between two values: one based on the assumption that the NSM elements fail by debonding and the other on the limitation of the effective strain. They suggest adopting a maximum value of 4‰ so as to limit the crack width to such an extent that lets the concrete contribution by aggregate interlock to be preserved.

In this respect, anyway, there is a big discrepancy between the values proposed by the several authors. In fact, for example, the *fib* document suggests to limit the effective strain to a value of 6‰ while, for instance, tha Australian Guidelines suggest to adopt a maximum value of 1.5% in order to control the crack width. Thus, in that respect, a unique trend can not be clearly singled out.

4 Debonding-based Predictive Model

The Debonding-based Model (DM) herein developed to simulate the contribution provided by the NSM laminates to the shear resistance of the tested beams is derived from the design approach proposed by Nanni *et al.* (2004), discarding some details deemed suitable for a safe design rather than for a predictive model, such as:

- a limitation on the laminate available bond length in order to limit its maximum effective strain to 4‰.
- the reduction of the length of the laminate by twice the projection of the concrete cover thickness;

The DM assumes debonding of laminates as the prevailing failure mechanism. This latter envisages failure occurring at the laminate/adhesive or adhesive/concrete interface, as well as within the adhesive (Sena Cruz and Barros 2004a). Debonding can be also regarded as a failure occurring along a surface parallel to the laminate, a few millimetres inside the surrounding concrete since a thin layer of concrete in contact with the adhesive has higher strength due to the adhesive penetration into its micro-structure. The pullout tests currently carried out show that the debonding failure might be characterized by the simultaneous occurrence of more than one of these mechanisms.

Due to the post-peak residual bond strength of the local bond stress-slip relationship (see paragraph 2.1 and Sena-Cruz and Barros 2004a), it is possible to increase the available resisting force by increasing the bonded length until the laminate tensile strength is attained. Note that, for the EBR technique, the finite value of the area underlying the local bond stress-slip relationship (Monti *et al.* 2003, Monti 2006), *i.e.* the fracture energy, G_f, does not allow the tensile strength of the material to be fully exploited since this latter nearly always exceeds the maximum value of stress that can be resisted by the bonded joint. For those cases, an "*effective bond length*" exists in correspondence of which the maximum stress can be transmitted and beyond which any further increase in length does not produce any benefit in terms of further increment of resisting force.

As opposed to EBR, in the case of NSM laminates, the diagram of peak pull-out force versus bond length, $V_f^{p,db} - L_f$, (Fig.°4.1) is expected to present an hardening branch until the laminate fails in tension. When peak pull-out force is converted into average bond strength, τ_b, the resulting relationship between τ_b and L_f is characterized by two boundary values connected by a non linear descending branch, see Fig. 4.2.

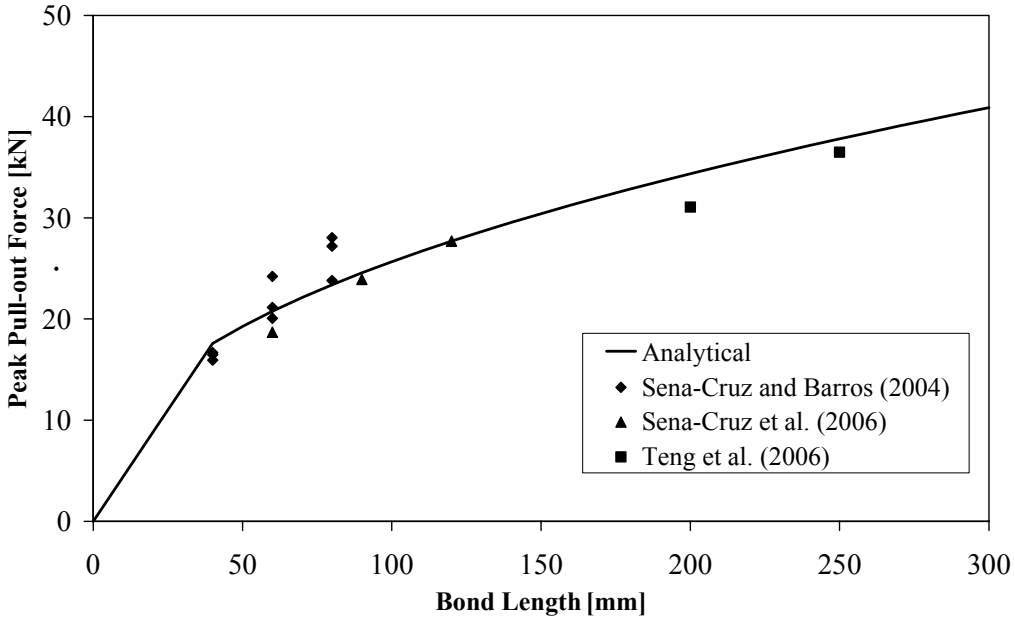

Fig. 4.1 – Peak pull-out force versus bonded length

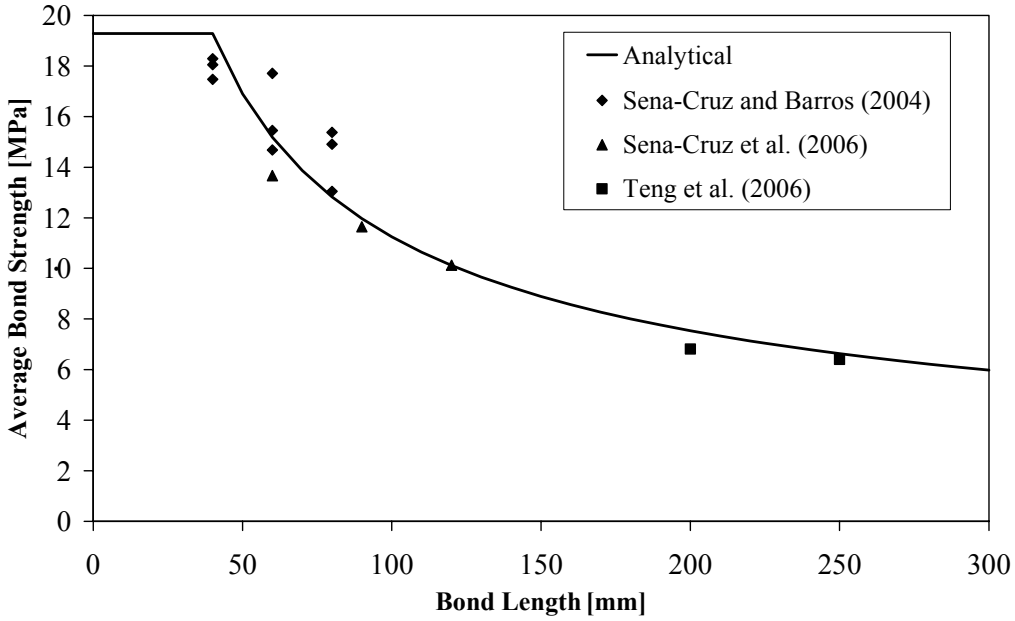

Fig. 4.2 – Average bond strength force versus bond length

The above statement is, however, based on limited experimental evidence and further investigations on the bond behaviour between concrete and NSM CFRP laminates are required to confirm.

In the following analytical developments, a relationship $\tau_b(L_f)$, calibrated on bond test results internationally available to date is taken into consideration (see Tables 4.1 to 4.2 and Fig. 4.2).

Table 4.1 – Bond test results available in literature to date.

Tests by	L_f [mm]	$V_{fi}^{p,db}$ [kN]	τ_b [MPa]
Sena-Cruz and Barros 2004a	40.00	15.00	17.47
	"	15.50	18.06
	"	15.70	18.29
	60.00	22.80	17.71
	"	19.90	15.46
	"	18.90	14.68
	80.00	22.40	13.05
	"	26.40	15.38
	"	25.60	14.91
Sena-Cruz *et al.* 2006	60.00	18.70	13.67
	90.00	23.90	11.65
	120.00	27.70	10.12
Teng *et al.* 2006	200.00	54.50	6.81
	250.00	64.00	6.40

Table 4.2 – Material properties in bond tests.

Tests by	CFRP laminates				Adhesive Epoxy		
	b_f [mm]	a_f [mm]	E_f [GPa]	f_{fu} [GPa]	E_{ep} [GPa]	$f_{ep,fl}$* [MPa]	$f_{ep,c}$** [MPa]
Sena-Cruz and Barros 2004a	9.34	1.39	158.30	2.74	5.1	25.80	44.40
Sena-Cruz *et al.* 2006	10.00	1.40	171.00	2.83	-	21.80	67.50
Teng *et al.* 2006	16.00	4.00	151.00	2.07	2.62	42.60	-

* bending tensile strength; ** compressive strength

For the sake of generality of the model, the possibility for the diagonal crack angle to be different than 45° (the value adopted by Nanni *el al.* 2004) is assumed.

The "*available bond length*" of each laminate, L_{fi}, is accounted for, *i.e.*, the shorter length on either side of the crossing crack (see Figs. 4.3 to 4.5). Moreover, three different configurations of the laminates with respect to the assumed crack origin are considered in order to get a general approach for the relative position between the shear failure crack and the intersected laminates.

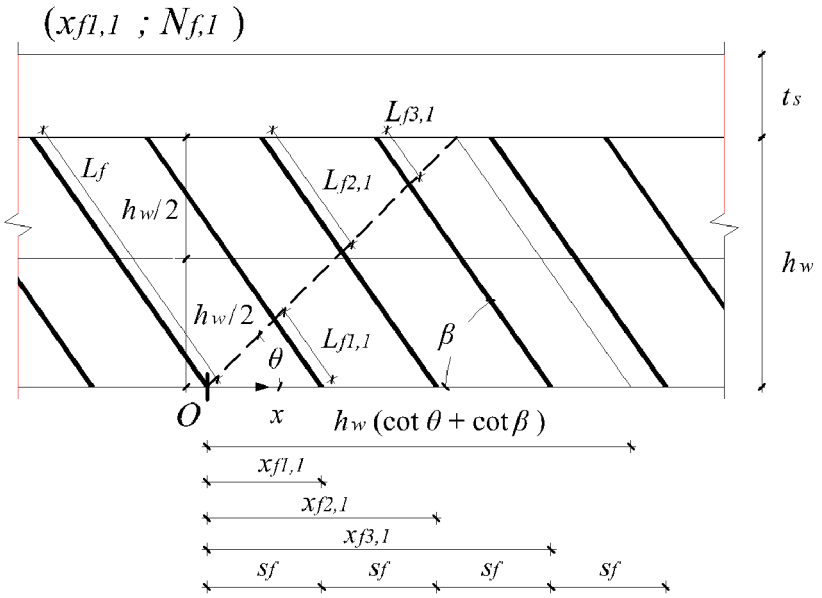

Fig. 4.3 – First geometrical configuration examined

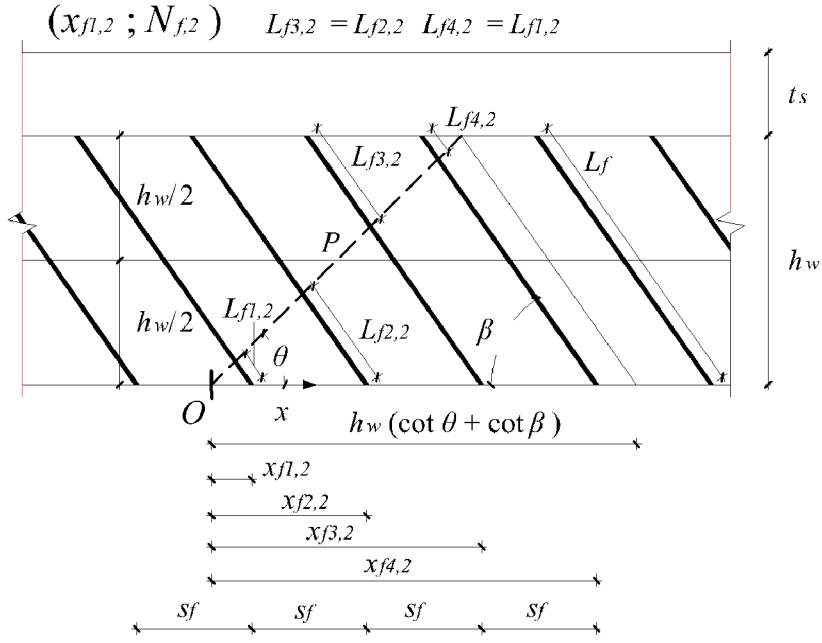

Fig. 4.4 – Second configuration examined.

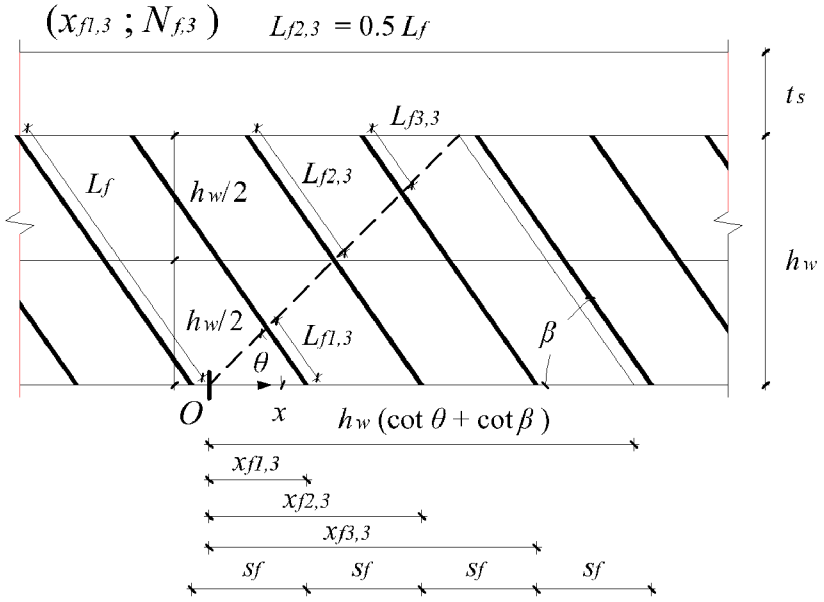

Fig. 4.5 – Third configuration examined.

Formulation

The general parameters taking part in the assumed approach are (see Figs. 4.3 to 4.5):

- a_f thickness of the laminates' cross section;
- b_f width of the laminates' cross section;
- h_w the height of the web of the beam cross section;
- β the inclination of the laminates with respect to the beam axis;
- s_f the spacing of the laminates along the beam axis;
- f_{fu} the laminates' average tensile strength;
- θ the assumed crack angle that is, according to experimental evidence, dependent on both the beam "shear span-to-depth" ratio and the amount of existing steel stirrups (if the shear crack was not formed when CFRP laminates are applied, the CFRP shear strengthening configuration also affects the value of θ);
- $\tau_b(L_f)$ relationship between the average bond strength and the available bond length of the laminate;
- $x_{f1,k}$ the position of the first laminate with respect to the assumed crack origin with $k = 1,2,3$ *i.e.*, the possible configurations of the laminates to identify the upper and lower bound of the NSM shear contribution;

- $N_{f,k}$ the effective integer number of laminates crossing the shear crack in the k^{th} configuration with $k = 1,2,3$ (see Appendix A).

The analytical expression adopted to determine the contribution provided by the NSM laminates to the shear resistance of the strengthened beam is:

$$V_{f,k}^{DM} = 2 \cdot \sin\beta \cdot \sum_{i=1}^{N_{f,k}} \min\left\{2 \cdot \left(a_f + b_f\right) \cdot L_{fi,k} \cdot \tau_b\left(L_{fi,k}\right);\ a_f \cdot b_f \cdot f_{fu}\right\} \tag{4.1}$$

This expression takes into account the contribution of the laminates at both lateral faces of the beam web. The debonding-based maximum force is limited by the tensile rupture of the laminate itself.

The number of laminates that can intersect the shear critical diagonal crack, constituted by a real number, can be determined by the following Eq. 4.2 (see Fig. 4.3):

$$N_{f,real} = \frac{h_w \cdot \left(\cot\theta + \cot\beta\right)}{s_f} \tag{4.2}$$

The number of laminates that can actually cross the shear crack is constituted by an integer that can assume two values: $N_{f,\text{int}}^{l}$ and $N_{f,\text{int}}^{h}$, differing by one unit and determinable respectively by rounding off $N_{f,real}$ to the lowest and to the highest integer. In the case in which $N_{f,real}$ is an integer, $N_{f,\text{int}}^{h} = N_{f,real}$ and $N_{f,\text{int}}^{l} = N_{f,real} - 1$. The above numbers $N_{f,\text{int}}^{l}$ and $N_{f,\text{int}}^{h}$ result to be, in an order not definable *a priori* and function of the values assumed by h_w, θ, and s_f, an odd and an even number or vice-versa, herein indicated as $N_{f,odd}$ and $N_{f,ev}$. Even if the possible values of the number of laminates that can effectively intersect the crack are two only, it is necessary to maintain both the above denominations ($N_{f,\text{int}}^{l}$ and $N_{f,\text{int}}^{h}$ or $N_{f,odd}$ and $N_{f,ev}$) in order to single out more easily the possible configurations assumed by the laminates with respect to the crack, as further specified hereafter.

Given the crack angle, $V_{f,k}^{DM}$ is computed for three different laminates arrangements, identified by the parameters $x_{f1,k}$ and $N_{f,k}$, in order to evaluate its possible variation as function of the laminates/crack geometrical configuration.

The pair $(x_{f1,k}; N_{f,k})$ can assume the following values, as function of $k = 1,2,3$:

$$(x_{f1,k}; N_{f,k}) = \begin{cases} \left[s_f; N_{f,\text{int}}^{l}\right] \\ \left[\dfrac{L_f}{2} \cdot \dfrac{\sin(\theta+\beta)}{\sin\theta} - \dfrac{(N_{f,ev}-1)}{2} \cdot s_f; N_{f,ev}\right] \\ \left[\dfrac{h_w}{2} \cdot \left(\cot\theta + \cot\beta\right) - \dfrac{(N_{f,odd}-1)}{2} \cdot s_f; N_{f,odd}\right] \end{cases} \tag{4.3}$$

The above three pairs include, respectively:

- the possibility for the laminates to attain the minimum total available bond length (Fig. 4.3);
- the possibility that an even number of laminates be disposed symmetrically with respect to the crack axis (Fig. 4.4);
- the case in which one laminate has the maximum length *i.e.*, it intersects the crack at its mid-length (Fig. 4.5).

For each of the above configurations, a value of the NSM shear contribution can be computed: $V_{f,k}^{ana}$ with $k = 1,2,3$. Among those three values, the maximum, $V_{f,\max}^{ana}$, and the minimum, $V_{f,\min}^{ana}$, can be selected to define the actual contribution range for each analyzed beam.

The position of each laminate along the assumed *x*-axis is (see Figs. 4.3 to 4.5):

$$x_{fi,k} = x_{f1,k} + (i-1)s_f \qquad \text{for} \qquad i = 1;.....;N_{f,k} \tag{4.4}$$

and its available bond length, *i.e.* the shorter length on either side of the crossing crack, is obtained by (see Appendix A):

$$L_{fi,k} = \begin{cases} [x_{f1,k} + (i-1)s_f]\dfrac{\sin\theta}{\sin(\theta+\beta)} & \text{for} \quad x_{fi,k} < \dfrac{h_w}{2}(\cot\theta + \cot\beta) \\ L_f - [x_{f1,k} + (i-1)s_f]\dfrac{\sin\theta}{\sin(\theta+\beta)} & \text{for} \quad x_{fi,k} \geq \dfrac{h_w}{2}(\cot\theta + \cot\beta) \end{cases} \tag{4.5}$$

The adopted relationship between average bond strength (in MPa) and bond length (in mm) is the following (Fig. 4.2):

$$\tau_b\left(L_f\right) = \begin{cases} 19.28 & 0 < L_f < 40 \\ 0.355 + 174.613 \,.\, \left(L_f\right)^{-0.60233} & L_f \geq 40 \end{cases} \tag{4.6}$$

Table 4.2 shows that the laminates used in the pull-out tests taken to calibrate the $\tau_b(L_f)$ law had similar mechanical properties. However, the properties of the adhesive used in the experimental programs by Sena-Cruz and Barros (2004a) and by Sena-Cruz *et al.* (2006) differ from those by Teng *et al.* (2006), but the data of Table 4.1 represented in Fig. 4.2, indicate that these differences had marginal influence on the $\tau_b(L_f)$ trend. Since a pure debonding failure mechanism occurred in the tests of all these programs, the concrete strength class had no influence on the $\tau_b\left(L_f\right)$ (Sena-Cruz and Barros 2004a, Sena-Cruz *et al.* 2006).

At the same time, for each one of the three configurations taken into consideration, the effective strain in the laminates can be computed from equilibrium, resulting:

$$\varepsilon_{f,k} = \frac{2\left(a_f + b_f\right)}{N_{f,k}\, a_f\, b_f E_f} \sum_{i=1}^{N_{f,k}} \tau_b\left(L_{fi,k}\right) L_{fi,k} \qquad \text{for} \qquad k = 1,2,3 \tag{4.7}$$

where E_f is the Young's modulus of the CFRP laminates.

5 In search for confirmations

By attending both the tests currently carried out by PhD Student Salvador Dias in the Laboratory for Structures of the Department of Civil Engineering at the University of Minho and the fruitful discussions held weekly with Prof. Joaquim Barros, an idea started to catch our attention. Hereinafter, the main features of the above mentioned physical-analytical idea are shown by means of experimental observations, analogies with literature findings and comparisons with other analytical models worldwide available to date.

5.1 Experimental Relevance and Literature Analogies

In most of the NSM shear strengthened beams tested so far (*e.g.* Dias and Barros 2005b), the failure governed by pure debonding mechanism was observed only for low percentage of laminates while the failure governed by the separation of the NSM reinforced concrete cover on both the sides of the web often occurred for high percentages of CFRP reinforcement. From a physical point of view, the former is reasonably expected to occur when the spacing between subsequent laminates is high meanwhile the latter is more likely to occur when the NSM laminates are closer to each other. Those two main failure mechanisms observed can be clearly supported by the photographic documentation collected at UMinho, as shown by the pictures in Figs. from 5.1 to 5.6 (Dias and Barros 2005b).

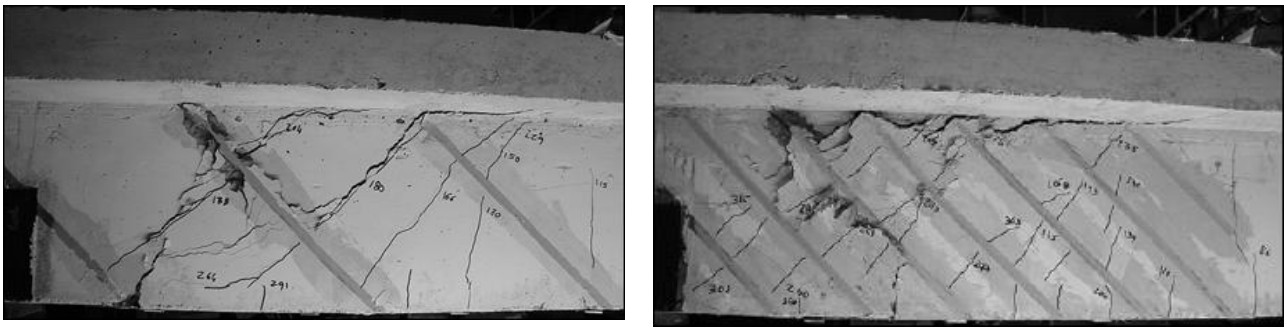

Fig. 5.1 – Laminates inclined at 45° (Dias and Barros 2005b): a) debonding (beam 2S_3LI45); b) concrete tensile failure (beam 2S_8LI45)

Fig. 5.2 – Further detail of beam 2S_8LI45

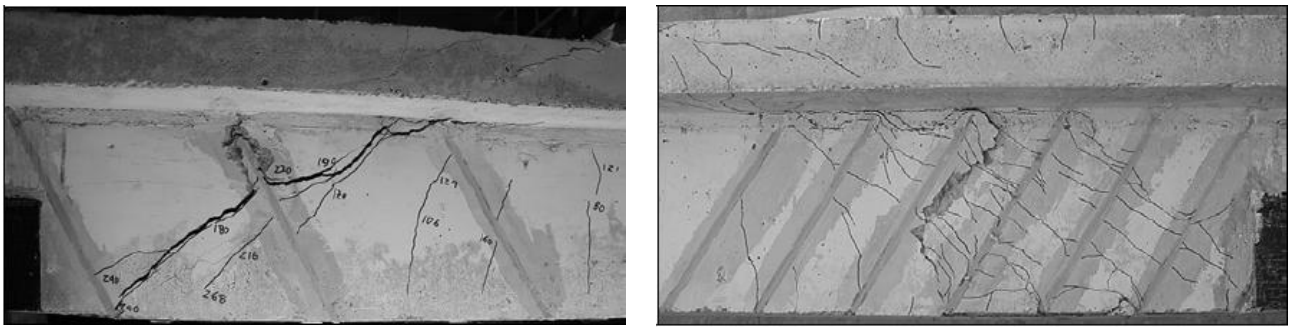

Fig. 5.3 – Laminates inclination of 60°: a) debonding (beam 2S_3LI60); b) concrete tensile failure (beam 2S_8LI60)

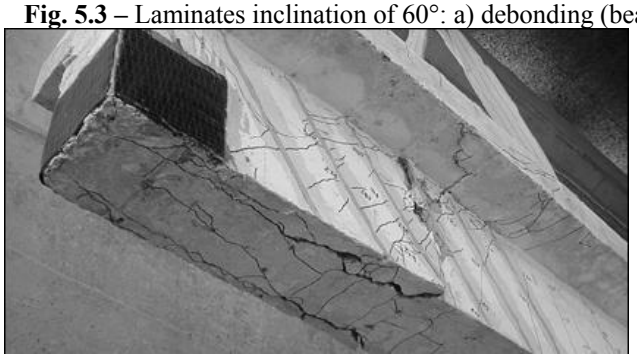

Fig. 5.4 – Further detail of beam 2S_8LI60

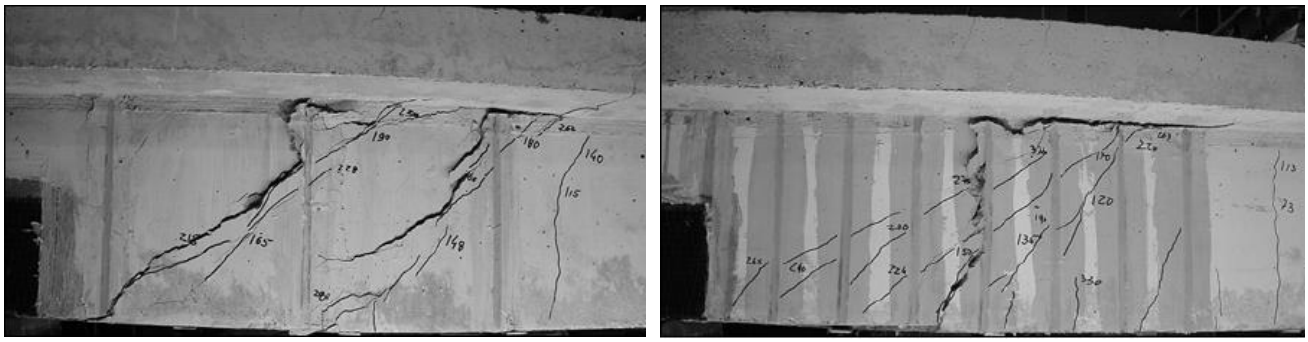

Fig. 5.5 – Laminates inclined at 90°: a) debonding (beam 2S_3LV); b) concrete tensile failure (beam 2S_8LV)

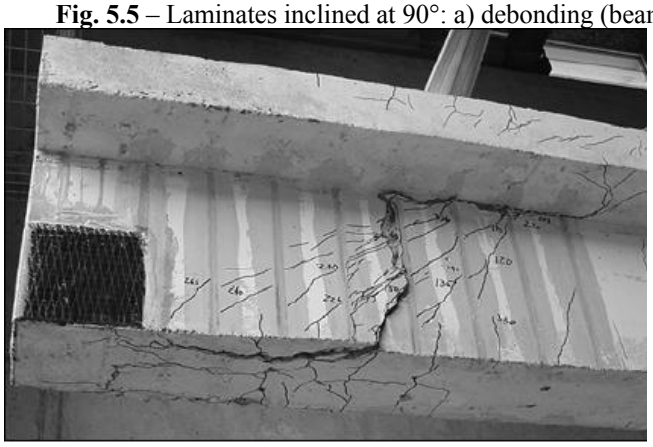

Fig. 5.6 – Further detail of beam 2S_8LV

Observing the tested beams much closer, it can be unequivocally realized that, for high amount of laminates, failure is characterized by concrete tensile fracture. By extensively searching the literature available to date, a physical similitude with failure modes already observed in the experiments carried out in the field of the Fastening Technology, arises.

Among the fastenings, those showing much more similitude with the NSM technique are the adhesive bonded ones: consisting of steel rods installed into holes drilled generally in the soffit of RC elements and filled with a structural adhesive. The transfer of tensile stresses form the bar to the surrounding concrete relies on the bond characteristics rod-adhesive-concrete.

In the case of adhesive anchors (Cook *et al.* 1993, Cook *et al.* 1998, CEB Bulletin n°201-1994) three failure modes have been observed: fracture of the steel anchor, cone failure of the surrounding concrete with or without pullout of an adhesive core, pull-out of an adhesive core, see Fig. 5.7.

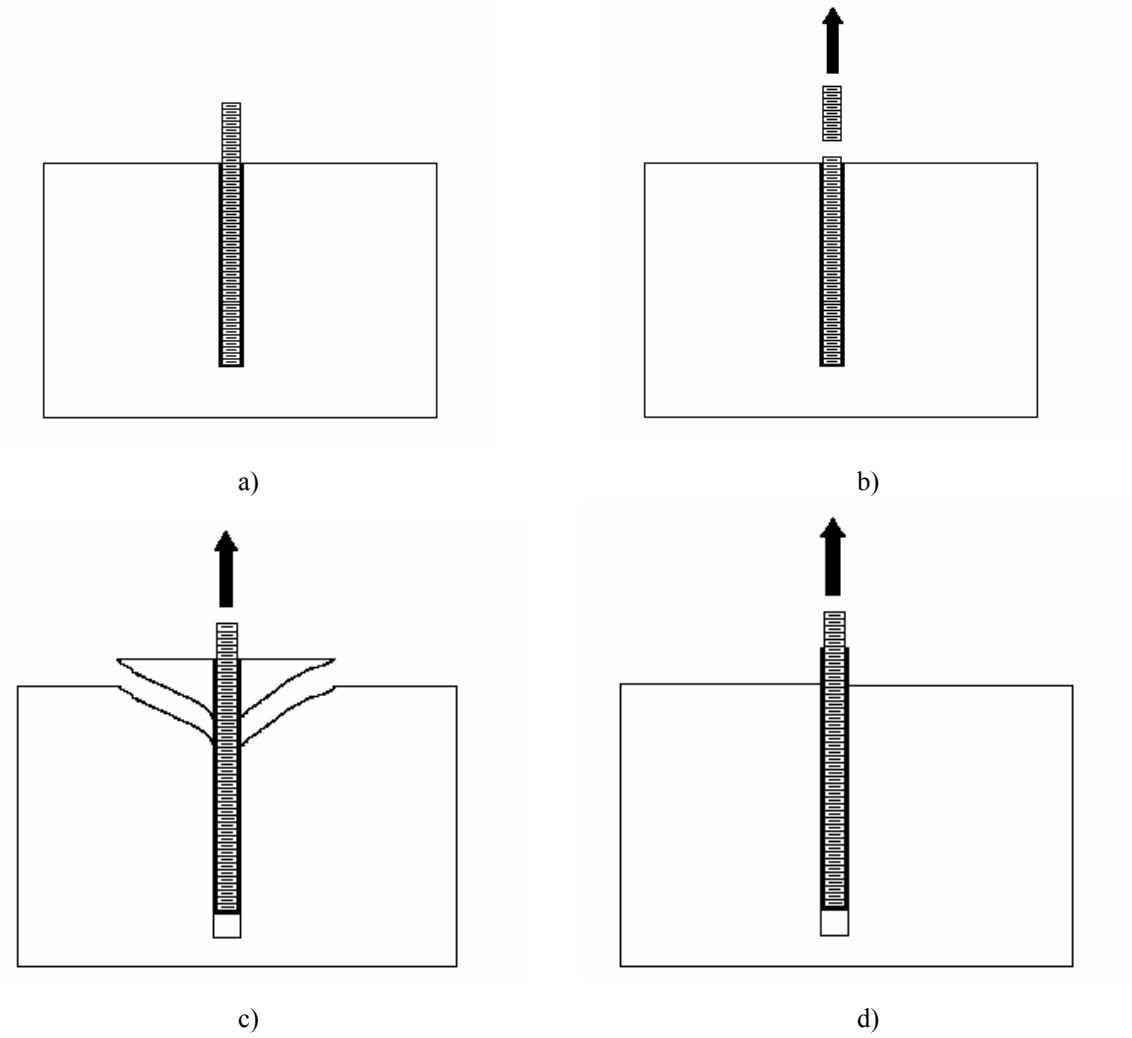

Fig. 5.7 – Failure modes for adhesive anchors: a) adhesive anchor; b) steel failure; c) concrete cone failure with or without pullout of an adhesive core; d) pull-out of adhesive anchor (Cook *et al.* 1993)

In the case of the NSM technique for shear strengthening, the fracture of the laminate was never observed, so far, due to the short length, for most of the small cross-sectioned RC beams tested up to now, of the laminates crossing the critical shear crack. The remaining two failure modes are absolutely identical to those observed in the tests carried out at UMinho.

The conical failure surface is the envelope of the tensile isostatic lines and the commanding parameter is the concrete tensile strength spread upon it. When the embedded length and the local bond stress-slip behaviour at both the bar-adhesive and adhesive-concrete interfaces is strong enough to prevent debonding from occurring, failure occurs in the concrete due to the overcoming of its tensile strength. This similitude has been extensively exploited hereinafter in

order to obtain analytical expressions capable to guarantee a good compromise between accuracy and computational simplicity. In the case of the NSM shear strengthened beams, it seems reasonable to expect the occurrence of the same phenomena as above. In fact, the shear crack can be thought as an inclined discontinuity plane slicing the web and crossed by the adhesive bonded NSM laminates which oppose to the crack opening and are consequently subjected mainly to axial tensile force. In the case of NSM laminates, the concrete fracture surface is expected to be semi-conical because of the changed geometrical contour conditions with respect to the fastenings (see Fig. 5.8). The concrete tensile strength is distributed throughout the semi-conical surface ascribed to each i-th laminate and orthogonally to the assumed fracture surface, see Fig. 5.9. Moreover, between the two parts in which the crack actually divides each laminate, the shorter one, herein named as "*available bond length*", results to be the weaker.

Figure 5.8 represents a simple scheme of the assumed model which, for the sake of simplicity, is shown for the simplifying case in which both the crack and the laminates are inclined at 45° with respect to the longitudinal axis of the beam.

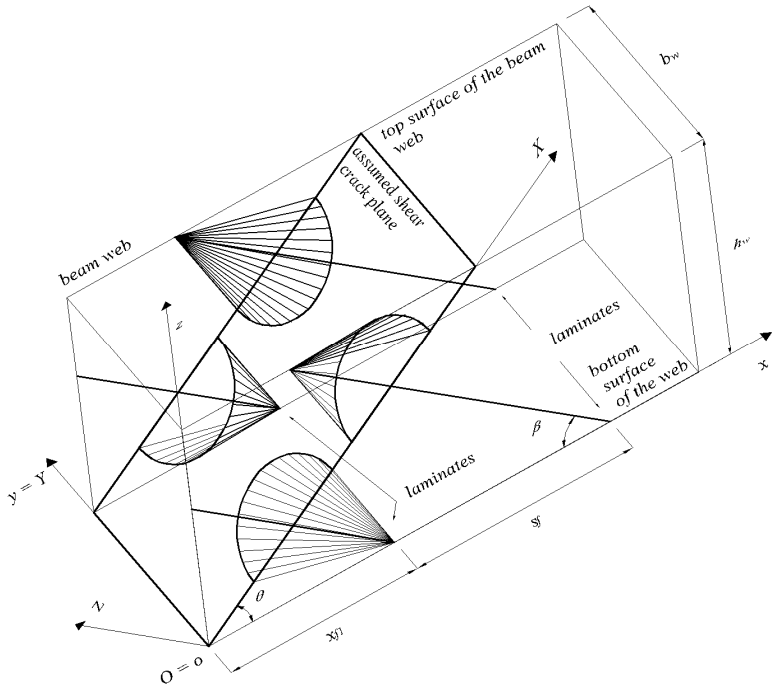

Fig. 5.8 – Scheme of the concrete fracture model

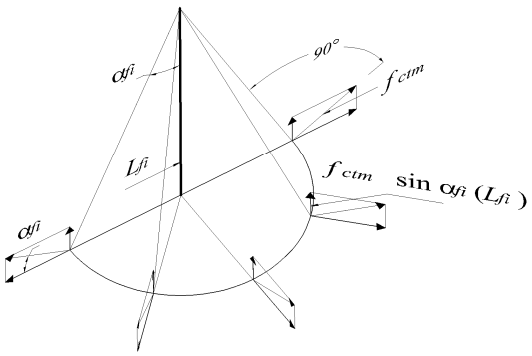

Fig. 5.9 – Concrete tensile strength distributed orthogonally in each point of the fracture surface and its components parallel to the laminate and to the crack plane (drawn in some points only, for sake of simplicity)

The hypothesis regarding the formation of a semi-conical fracture surface can be also supported by experimental relevance regarding another research project being currently carried out at UMinho by Master Student João Lima and aiming at the evaluation of the relation between the crack opening width and the strains effectively mobilized in the CFRP NSM Laminate. The above mentioned test program comprehends a specimen prototype that consists of a plain concrete cylinder presenting a thin notch along the loading plane, see Fig. 5.10 and 5.11. The CFRP NSM laminates are glued into thin slits to assess the influence of the inclination between the crack plane (forced to coincide with the loading plane) and the plane containing the laminates. The specimen is subjected to diametral compression similar to the Brasilian Test Configuration. Hereafter a simple scheme of the test set-up and some post-test inspection pictures are shown. (For further details see the Master Thesis by João Lima).

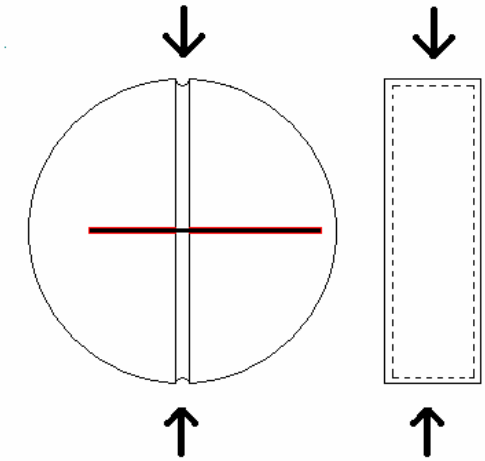

Fig. 5.10 – Test set-up with respectively front and lateral view (type A)

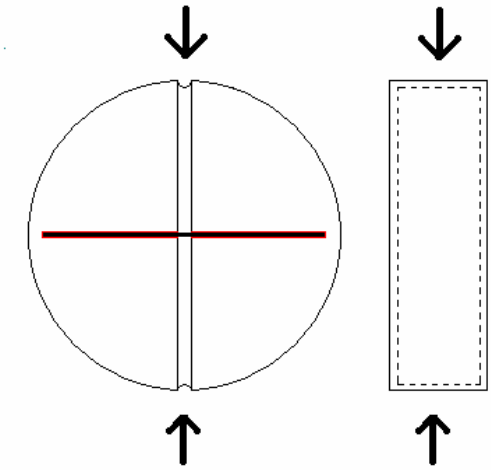

Fig. 5.11 – Test set-up with respectively front and lateral view (type B)

Fig. 5.12 – Specimen S2: semi-conical fracture surface (Master Thesis by João Lima)

Returning to the proposed model for the mechanical simulation of NSM shear strengthened RC beams, since the position of those semi-conical surfaces (Fig. 5.8) is symmetric with respect to the mean vertical plane of the cross section, the horizontal outward components of the tensile strength vectors are balanced only from an overall standpoint and not locally. In Fig. 5.13, a section of the semi-conical fracture surfaces by a plane parallel to the crack is shown for

the simple case in which the inclination of both the crack and the laminates with respect to the beam longitudinal axis results to be of 45°. In fact, in this case, the intersection of a semi-conical surface with the plane simulating the critical diagonal crack (CDC) is represented by a semi-circumference and not a semi-ellipse.

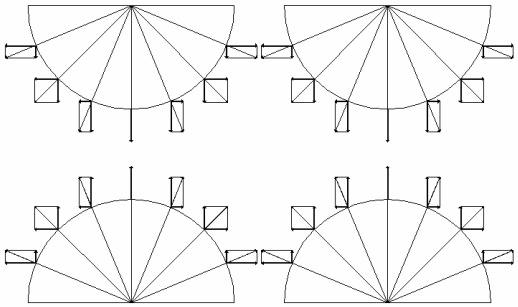

Fig. 5.13 – Section of semi-conical fracture surfaces by a plane parallel to the shear crack with horizontal components of tensile stresses respectively parallel and normal to the web faces.

The local unbalance of the horizontal tensile stress component orthogonal to the web can justify the outward expulsion of the concrete cover in both the uppermost and lowermost parts of the strengthened sides of the web. This can also be verified by observing the photographic documentation regarding the post-test inspection (see Figs. 5.2, 5.4 and 5.6).
The splitting circumferential tensile stresses developed around the longitudinal bars have also contributed to the outward expulsion of the concrete cover in the lowermost edge of the web lateral faces. This is more evident as larger is the diameter of the tensile longitudinal bars. In fact, in the tested beams, in order to make them fail by shear, the bottom longitudinal flexural reinforcement is composed of large diameter bars. For those reinforcing bars, the tensile circumferential stresses due to local wedge effect around the ribs (see paragraph 2.4), flexural cracks and dowel action, are very high and strongly contribute to circumscribe the vertical splitting cracks along the concrete cover at ultimate, see Fig. 5.14.

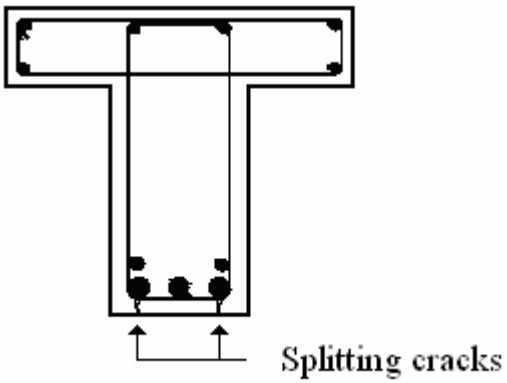

Fig. 5.14 – Cross-section of the tested beams and location of splitting cracks.

Moreover, there is the suspicion that the presence of a high amount of stirrups located almost in the same vertical plane as the longitudinal bars (see Figs. 5.14 and 5.15), also contributes, by means of the corresponding splitting circumferential tensile stresses, induced in the surrounding concrete, to circumscribe the concrete fracture at the interface between the concrete cover and the core of the beam. Higher is the amount of existing stirrups, due to their

circumferential splitting tensile stresses, more extended is a micro-crack plane, running parallel to the web faces and at a depth almost as large as the cover, within the web.

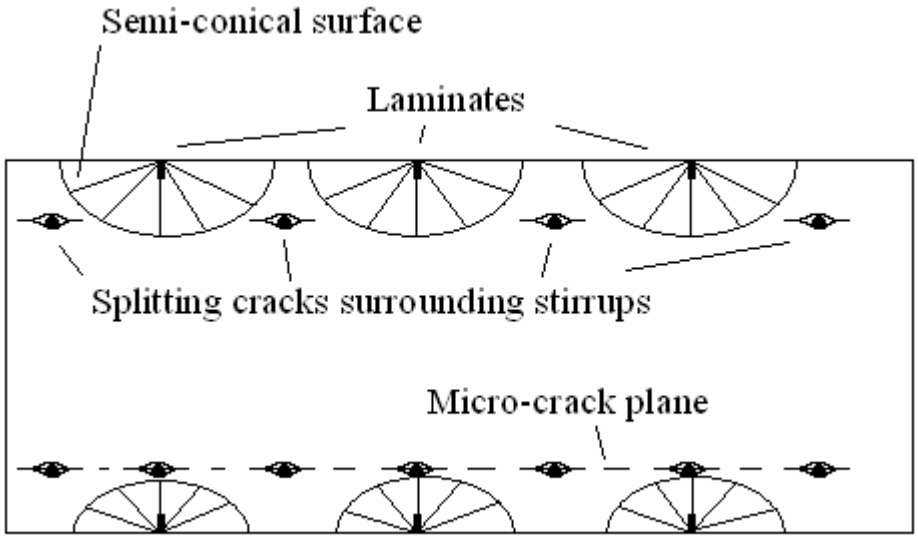

Fig. 5.15 – Section of a strengthened beam parallel to the shear crack and splitting cracks surrounding stirrups.

This micro-fracture surface, prevents the semi-conical surfaces to go deeper inside the core of the web, thus limiting the shear strength contribution that can be provided by the NSM system. On the contrary, when the amount of stirrups is limited, it is more likely for the semi-conical surfaces to develop deeper inside the core of the beam with a consequent increase of the NSM contribution to the shear resistance of the beam. From a computational standpoint, and in accordance with the modelling strategy herein proposed, when the amount of stirrups is limited, the envelope of the fracture surface is larger, thus providing a higher shear strength contribution, for an equal amount of laminates. In that respect, an analytical model in accordance with this approach, can simply take into account the interaction with stirrups by assuming semi-conical surfaces with a steeper inclination of their generatrices, when closer to the stirrups. As regards this interpretation of the phenomenon of interaction between stirrups and laminates, it has also to be outlined that, when applying the NSM technique to shear-strengthen an existing RC beam, stirrups are already loaded and deformed at a certain extent. Thus, the micro-fracture plane separating the concrete cover from the core, already exists. On the contrary, when testing an NSM shear strengthened RC beam in laboratory, generally stirrups and laminates start being loaded contemporarirly. In this respect, it is aspected that the interaction between stirrups and laminates be higher in the restoration of a real RC structure.

This approach also permits to easily take into account the interaction between subsequent laminates because when they are very close to each other, the semi-conical surfaces intersect each other: thus the reduction in efficacy can easily be taken into account calculating the reduced overall fracture surface accordingly. In fact, as the spacing between subsequent laminates is reduced, their semi-conical fracture surfaces overlap each other and the resulting envelope fracture surface progressively becomes smaller than the mere summation of each of them (see Fig. 5.16). This detrimental interaction between laminates can be easily taken into account by calculating the resulting semi-conical surface ascribed to each laminate accordingly. For very short values of the spacing, the resulting concrete failure surface

is almost parallel to the web face of the beam, which is in agreement with the failure mode observed experimentally, consisting in the detachment of the concrete cover from the underlying core of the beam (see Figs. 5.2,5.4,5.6).

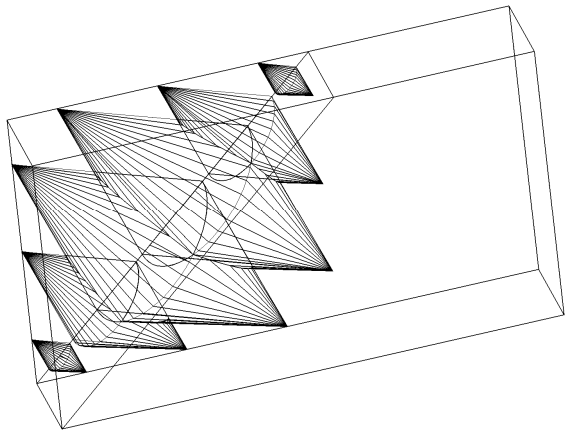

Fig. 5.16 – Interaction between laminates: inside view of the fracture surface resulting from the overlapping of semi-conical fracture surfaces on one side of the web.

Given those observations, an analytical analysis was carried out in order to check the validity of that approach, by comparing the obtained analytical values with experimental data. If confirmed by fitting experimental values, the model herein described can be utilized to carry out parametric analyses by taking into account some of the most relevant aspects such as:

1. Interaction between subsequent laminates;
2. Variation of the assumed crack inclination angle.
3. Variation of the concrete tensile strength;
4. Variation of the semi-conical aperture angle;
5. Interaction with stirrups.

5.2 Some Analytical Details

To evaluate the maximum force actually transferable by NSM laminates, until concrete fracture failure mode occurs, it is necessary to determine the shorter part of each laminate crossing the crack, the corresponding semi-conical surface, multiply the resulting revolution area by the concrete tensile strength, project it on the direction of the laminates and consequently assume its vertical component as the shear strength contribution. By developing those calculations, (see Appendix A) it can be realized that, in order to determine the maximum resisting force in the direction of the laminates, the same result can be obtained by simply multiplying the absolute value of the concrete tensile strength by the area of the base of the semi-cone orthogonal to the laminate direction. Thus, for the i-th laminate the maximum force along its length, due to concrete fracture, $V_{fi}^{p,cf}$, can be simply calculated, for the case in which both the crack and the laminate are disposed at 45° with respect to the beam axis, as follows:

$$V_{fi}^{p,cf} = \frac{\pi \cdot R_{fi}^2}{2} \cdot f_{ctm} = \frac{\pi \cdot L_{fi}^2 \cdot tg^2 \alpha_{fi}}{2} \cdot f_{ctm} \tag{5.1}$$

where: R_{fi} is the radius of the base of the semi-conical surface asociated with the i-th laminate, f_{ctm} is the concrete mean tensile strength, L_{fi} is the available bond length associated with the i-th laminate and α_{fi} is the aperture angle of the i-th semi-conical surface.
Since the calculation of the semi-conical surface reduces to the calculation of the area of its intersection with a plane orthogonal to its axis, it can be shown (see Appendix A), that it results substantially independent of the effective shape of the surface, providing the method with a high generality.

The general parameters entering the assumed approach are: θ the assumed crack inclination angle that is, generally speaking, dependent on the shear span to depth ratio (see Paragraph 2.2) but can be assumed equal to 45° without introducing excessive mistakes; β the inclination of the NSM laminates with respect to the beam axis; the height, h_w, and width, b_w, of the web of the cross section; s_f the spacing of the laminates calculated along the axis of the beam; α_{fi} the angle between the axis and the generatrix of the semi-conical surface; f_{ctm} the concrete mean tensile strength.

In this phase of the present study, to appraise the validity of the proposed approach, it is worth evaluating the total area of the ellipses, intersection of the cones with the crack plane, in correspondence of several values of the position x_{f1} of the first laminate with respect to the assumed crack origin point in order to determine its maximum and minimum values. In that respect, some attempts have been carried out in order to single out the values of x_{f1} (with $0 \le x_{f1} \le s_f$) in correspondence of which it is necessary to position the first laminate to obtain the maximum, minimum and average values of the overall concrete fracture area above. It has been observed that a general rule cannot be drawn neither for maximum and minimum values nor for the average because the relationship between the total area (inclusive of eventual overlapping of the semi-conical surfaces associated with laminates placed at both lateral faces of the web) with respect to x_{f1} is non-linear and the singular points are not always located in the same position. One of the graphs employed for the attempts mentioned above is shown in Fig. 5.17 for the following values of the various parameters: $b_w = 180\,mm$; $h_w = 300\,mm$; $\alpha = 25°$; $\beta = 90°$; $\theta = 45°$; $s_f = 160\,mm$.

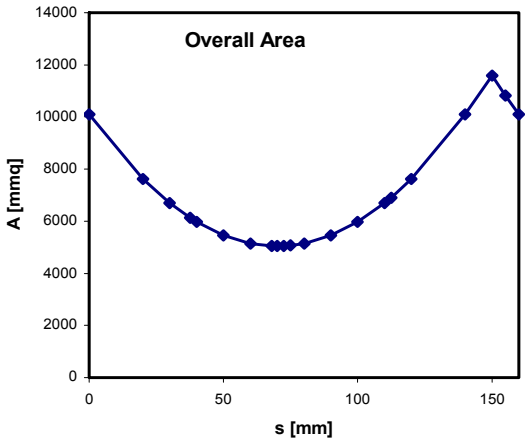

Fig. 5.17 – Determination of the position of the first laminate with respect to the crack origin to get the singular points of the envelope surface of the semi-cones associated with laminates.

Anyway, a general rule can be followed to determine the singular points in correspondence of which the maximum and minimum relatives are located.

The real number of laminates, $N_{f,real}$, crossing the crack can be determined as follows:

$$N_{f,real} = \frac{h_w \cdot (\cot\theta + \cot\beta)}{s_f} \tag{5.2}$$

where: h_w is the height of the cross section web; s_f is the spacing between laminates; θ is the assumed crack inclination angle and β is the inclination of the NSM laminates with respect to the beam axis.

The effective integer number of laminates, N_f, that can actually intersect the crack is $N^l_{f,\text{int}} \le N_f \le N^h_{f,\text{int}}$ where $N^l_{f,\text{int}}$ is the lower round off integer and $N^h_{f,\text{int}}$ is the higher round off one of $N_{f,real}$. In the case in which $N_{f,real}$ is an integer, it is: $N^h_{f,\text{int}} = N_{f,real}$ and $N^l_{f,\text{int}} = N_{f,real} - 1$. The above two integers are, in an order not definable *a priori*, an odd and an even number, herein indicated as $N_{f,odd}$ and $N_{f,ev}$, respectively.

The singular points of the overall area are in correspondence to one of the following values of x_{f1} (see Appendix A):

$$x_{f1} = \begin{cases} s_f \\ \dfrac{L_f}{2} \cdot \dfrac{\sin(\theta+\beta)}{\sin\theta} - \dfrac{(N_{f,ev}-1)}{2} \cdot s_f \\ \dfrac{h_w}{2} \cdot (\cot\theta + \cot\beta) - \dfrac{(N_{f,odd}-1)}{2} \cdot s_f \end{cases} \tag{5.3}$$

in which (see Chapter 4 and Figs. 4.3 to 4.5) the second case contemplates the possibility that the even number of laminates be disposed symmetrically with respect to the crack line's axis and the third case contemplates the case that one laminate has the maximum length *i.e.* it intersects the crack line at its mid-length. The term L_f is the actual total length of the employed laminate. For further details see also Appendix A.

In a general way, the available bond length of the i-th laminate crossed by the crack can be calculated according to the analytical method already adopted by both De Lorenzis and Nanni *et al.* and summarized as follows:

$$\begin{cases} L_{fi} = \left[x_{f1} + (i-1) \cdot s_f \right] \cdot \dfrac{\sin\theta}{\sin(\theta+\beta)} & 1 \le i \le \dfrac{N_f}{2}; \\ L_{fi} = L_f - \left[x_{f1} + (i-1) \cdot s_f \right] \cdot \dfrac{\sin\theta}{\sin(\theta+\beta)} & \dfrac{N_f}{2} < i \le N_f \end{cases} \tag{5.4}$$

The formula above, when the shear crack angle is assumed equal to 45°, modifies as follows:

$$\begin{cases} L_{fi} = \dfrac{x_{f1} + (i-1) \cdot s_f}{\sin\beta + \cos\beta} & 1 \le i \le \dfrac{N_f}{2}; \\ L_{fi} = L_f - \dfrac{x_{f1} + (i-1) \cdot s_f}{\sin\beta + \cos\beta} & \dfrac{N_f}{2} < i \le N_f \end{cases} \tag{5.5}$$

For further details see Appendix A.

Since we are in the phase corresponding to the "*exploration*" of the truthfulness and reliability of the possibilities of the proposed approach, the overall area $E_{f,tot}$ of the intersection of the semi-cones with the crack plane has been computed, for the sake of simplicity and relative quickness, by means of tools such as AuoCAD and MathCAD.

The calculated area, has been subsequently projected on the plane normal $A_{f,tot}$ to the axis of the cones and multiplied by the concrete mean tensile strength, f_{ctm}, see Fig. 5.18. Thus, the contribution of the NSM laminates for the shear resistance of a RC beam has been calculated, then, by the following equations:

$$A_{f,tot} = E_{f,tot} \cdot \sin(\beta + \theta) \tag{5.6}$$

$$V_f = 2 \cdot A_{f,tot} \cdot f_{ctm} \cdot \sin\beta \tag{5.7}$$

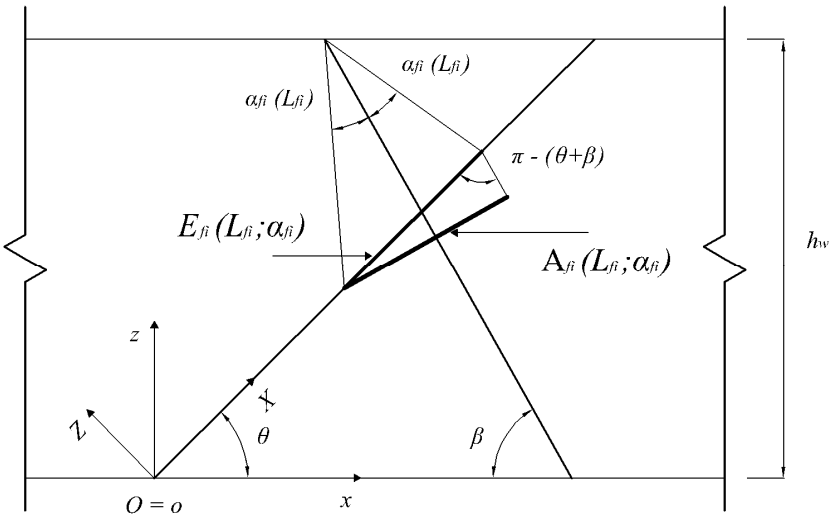

Fig. 5.18 – Projection of the semi-conical surface on a plane orthogonal to the laminate

5.3 Calibration of the semi-conical surface angle

By extensively searching the recent publications in the most qualified technical magazines about the employment of CFRP NSM Laminates, an interesting work (Teng *et al.* 2006) was found regarding some bond tests carried out in the Polytechnic University of Hong Kong, China. The details regarding both the test set-up and the characteristics of the materials employed in the above quoted article are summarized in the Appendix B of the present Report. In that work it is reported of two failure modes: debonding for the embedment lengths of 200 and 250 *mm* while the failure of the remaining specimens was by shear fracture within the concrete prism. The above mentioned work does not further explain the boundary conditions of the tested specimens affected by shear fracture but it is deemed reasonable thinking of a pseudo semi-conical concrete fracture surface.

The available results of those tests, together with the assumed assumption regarding the failure surface, was used to calibrate the projecting angle α between the axis and the generatrices of the semi-conical surface by means of a back-analysis. The above calibration was carried out as follows: since, from that article (Teng *et al.* 2006), it could not be gathered how the shear fracture surface looked like, some assumptions were made.

1st hypothesis

At first (see Fig. 5.19), it was assumed that the semi-conical surface was such as to intersect the front face of the prism-shaped specimen *i.e.* the base radius is within the minimum dimension of the cross-section: $0 < R \leq 75mm$.

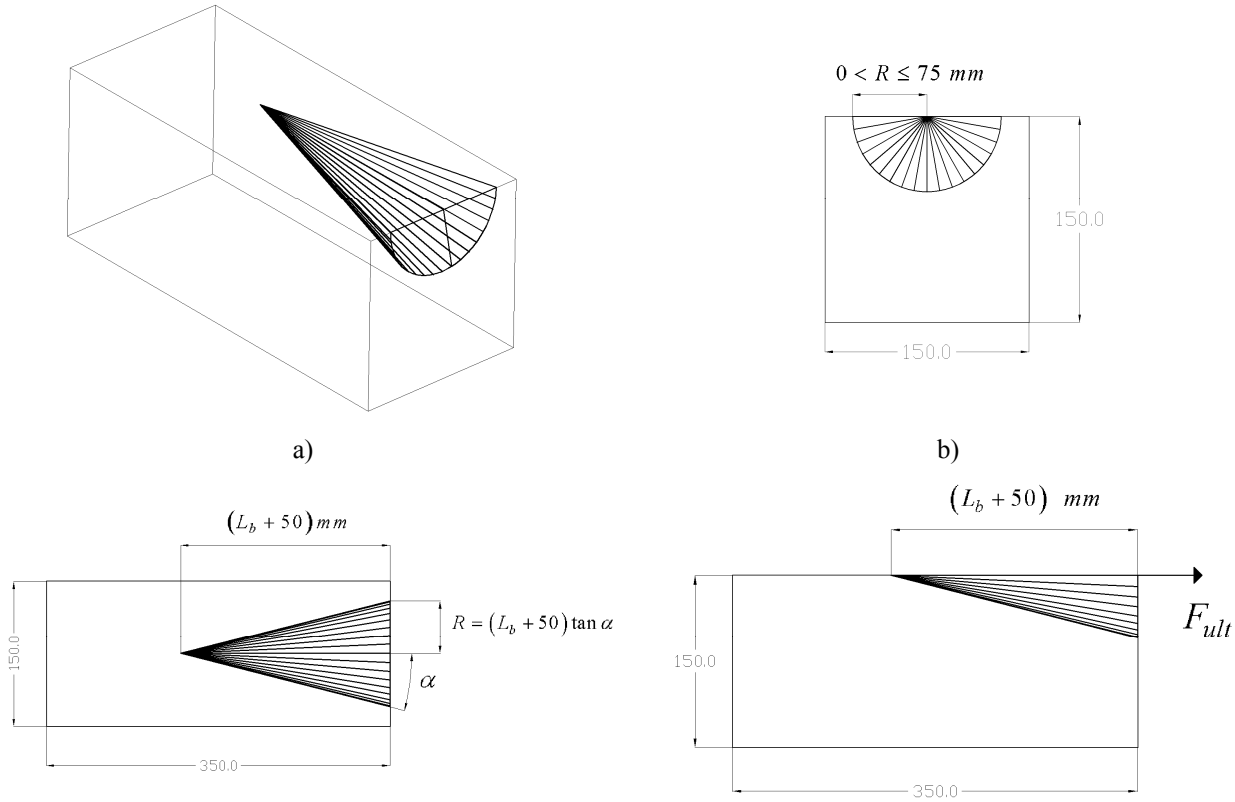

Fig. 5.19 – First hypothesis, adopted scheme: a) overall view; b) front view; c) top view; d) lateral view. (dimensions in mm)

In that case, the following formula was adopted to appraise the angle α:

$$F_{ult} = \frac{\pi}{2} \cdot R^2 \cdot f_{ctm} = \frac{\pi}{2} \cdot L^2 \cdot tg^2\alpha \cdot f_{ctm} \quad \rightarrow \quad \alpha = \text{arc}tg\sqrt{\frac{2 \cdot F_{ult}}{\pi \cdot L^2 \cdot f_{ctm}}} \tag{5.8}$$

If from the back-analysis of the obtained angle's value it results that the radius is larger than 75 *mm*, the above assumption is not valid and the we need to assume that the semi-conical surface intersects the lateral faces of the specimen. In this latter hypothesis, *i.e.* for $75 < R \leq 150$ *mm* another formula was adopted:

2nd Hypothesis

This second hypothesis contemplates the possibility that the semi-conical surface is such as to intersect the lateral faces of the prism, see Fig. 5.20.

Assuming the angle, β, between the radius and the median of the cross section (see Fig. 5.19 b), it results:

$$R = \frac{75}{sen\beta} \tag{5.9}$$

$$A = 75 \cdot h + \pi \cdot R^2 \cdot \frac{2 \cdot \beta}{360} \quad (\text{with } \beta \text{ measured in degrees}) \tag{5.10}$$

$$F_{ult} = A \cdot f_{ctm} = \left[(75)^2 \cdot \cot\beta + \frac{2 \cdot \beta}{360} \cdot \pi \cdot \frac{(75)^2}{sen^2 \beta} \right] \cdot f_{ctm} \tag{5.11}$$

and Eq. 5.11 was solved by attempts.

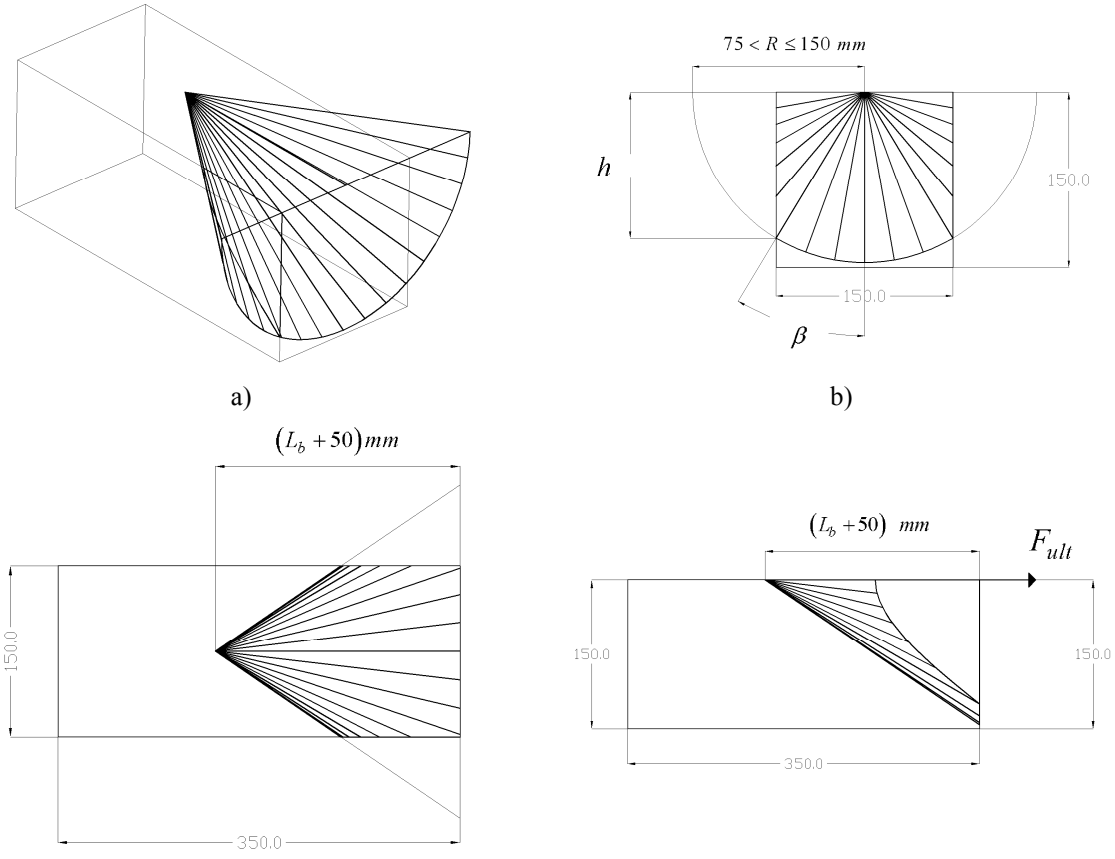

Fig. 5.20 – Second hypothesis, adopted scheme: a) overall view; b) front view; c) top view; d) lateral view. (dimensions in mm)

Since in the article by Teng *et al.* (2006), the value of the concrete mean splitting tensile strength is provided, in order to obtain the axial tensile strength, the conversion formula provided by the CEB Model Code 90 (1993) was used *i.e.*:

$$f_{ctm} = 0.9 \cdot f_{ct,sp} \tag{5.12}$$

obtaining a value of $f_{ctm} = 3.06\ MPa$ for the concrete mean tensile strength. By applying the simple method shown above, the values of the angle α listed in Table 5.1 were obtained.

Table 5.1 – Obtained estimates of the angle α.

L_b [mm]	α [°]
30,00	**32,26**
100,00	**27,98**
150,00	**25,23**
Mean	**28,49**

The above values are in agreement with the idea that the angle increases by reducing the embedment length. Obviously those values are only grossly indicative but in this phase of the study are deemed useful enough. On the basis of those data, the flowing relationship between the angle α_{fi} (in degrees) and the bond length L_{fi} (in mm) was adopted:

$$\alpha_{fi} = \begin{cases} 32.31 & \text{for} \quad 0 \le L_{fi} \le 30 \\ 33.973 - 0.0587 \,.\, L_{fi} & 30 < L_{fi} \le 150 \\ 25.17 & L_{fi} > 150 \end{cases} \tag{5.13}$$

That is represented in Fig. 5.21:

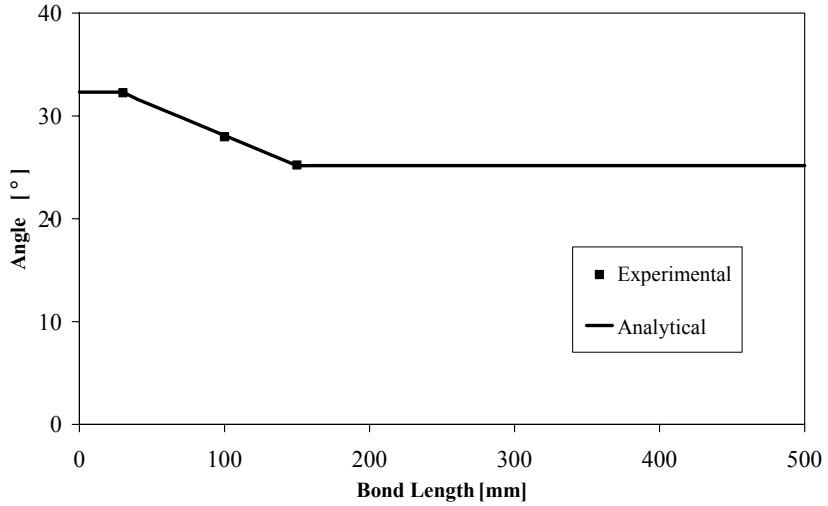

Fig. 5.21 – Length dependency of the angle $\alpha_{fi}\left(L_{fi}\right)$

Due to the narrowness of data available, for the ranges of bond lengths $L_{fi} < 30$ and $L_{fi} > 150$, a conservative constant value equal respectively to 32.31° and 25.17° was assumed.

5.4 Appraisal of the "idea"

To appraise the reliability of the above described approach, before developing the analytical details, the values of the increment of shear strength, for the beams tested up to now at UMinho, by Dias and Barros, were compared with the values obtained by both the pure debonding predictive model (DM of Chapter 4) and the one considering the concrete fracture surfaces as delineated above. Since the maximum value of the available bond length that can be reached in the beams tested is larger than the maximum value of bond length 150 *mm*, to which a value of $25.17°$ corresponds, a value of $\alpha = 25°$ was assumed.

It is worth outlining that in the following calculations, the adopted value of f_{ctm} was deduced from the mean compressive strength, according to CEB-FIP Model Code 90. This is not deemed a correct procedure because the concrete tensile strength itself generally presents a high scatter when it is measured directly (see Paragraph 2.7). When it is deduced by another quantity already affected by scatter like the compressive strength, the scatter increases and gets difficult to control, in statistical terms. Moreover, the beams analyzed, are those belonging to the first, explorative, series by Barros and Dias (2006), those belonging to the second series, by Dias and Barros (2005a), and the third series, by Dias and Barros (2006).

Note that the relationship $\tau_b\left(L_{fi}\right)$ adopted to draw the graphs reported hereafter (see Figs. 5.23-25) was a previous version slightly different than the one reported in Eq. 4.6 *i.e.*, the following.

$$\tau_b\left(L_{fi}\right)=\begin{cases}18.13 & 0<L_{fi}<40\\ 42.66-6.65\cdot\ln L_{fi} & 40\ \le L_{fi}\le 225\end{cases} \tag{5.14}$$

The beams of the several series are labelled according to the following scheme: the first letters indicate the type of section (if rectangular "Ret" or T-shaped "T"), then the height of the section in mm, the inclination of laminates and the value of concrete average tensile strength.

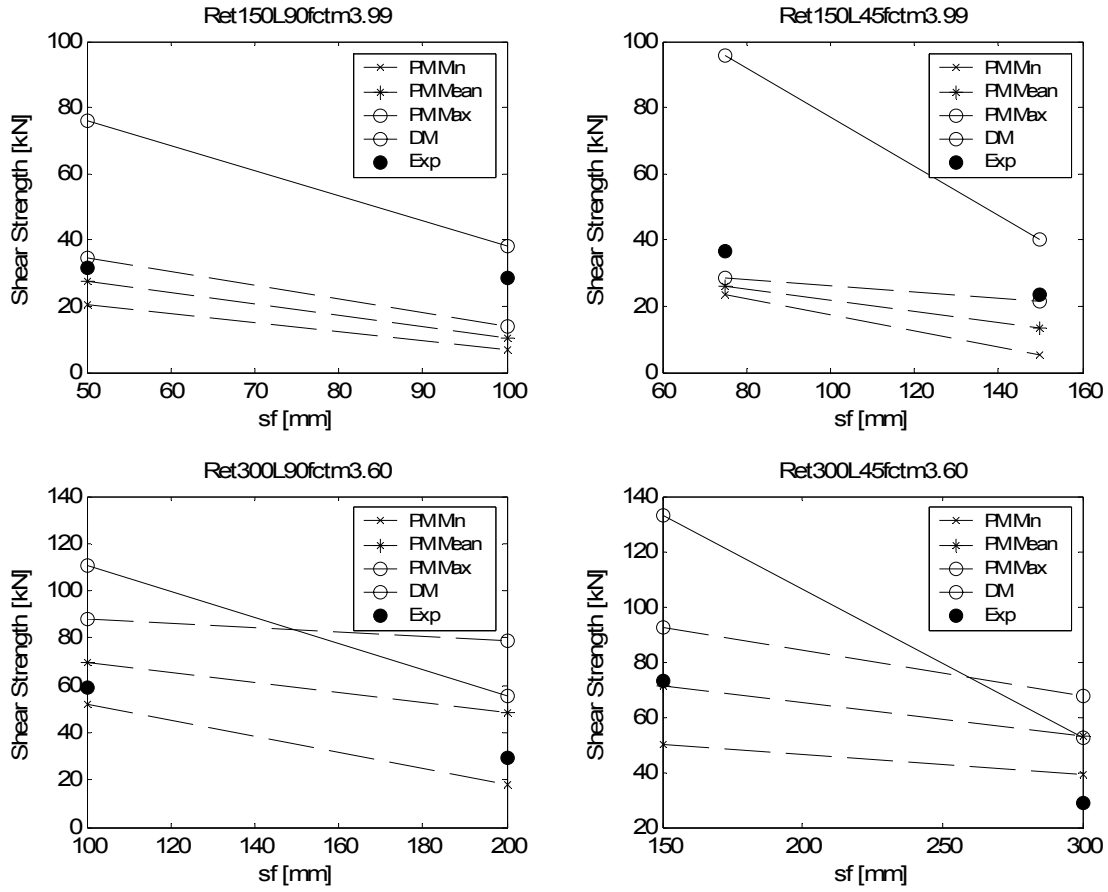

Fig. 5.23 – Beams of the 1st series, by Barros and Dias (2006)

Analyzing Figs. 5.23 to 5.25, it arises that, for the beams taken into consideration, independently of the shape and height of the cross section, the inclination of laminates and concrete mechanical properties, the estimates provided by the proposed modelling strategy are in better agreement with the experimentally recorded values of the NSM shear strength contribution with respect to the DM. In fact, in most of the analyzed cases, the experimental values lie within the range of analytical values. It can also be gathered that, for most of the beams analyzed, the values predicted by the DM overestimate the experimental ones, as more as smaller the spacing.

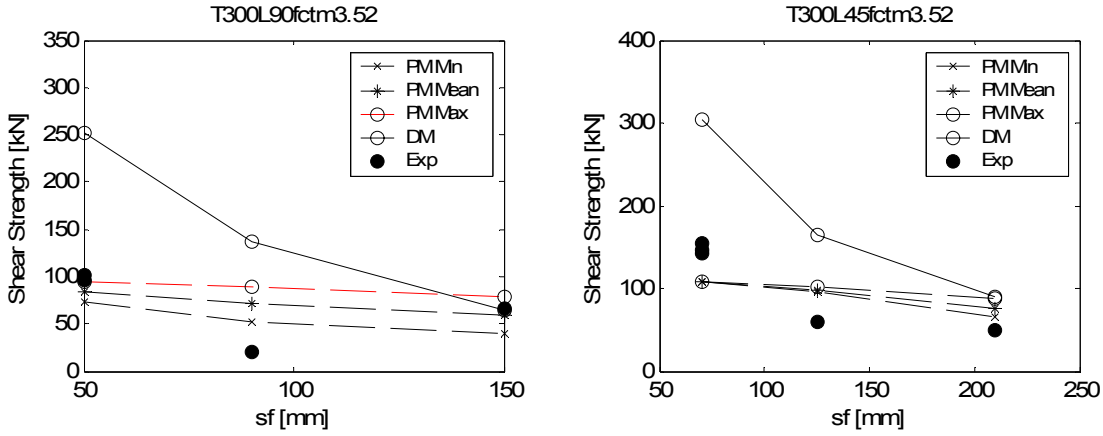

Fig. 5.24 – Beams of the 2nd series, by Dias and Barros (2005a)

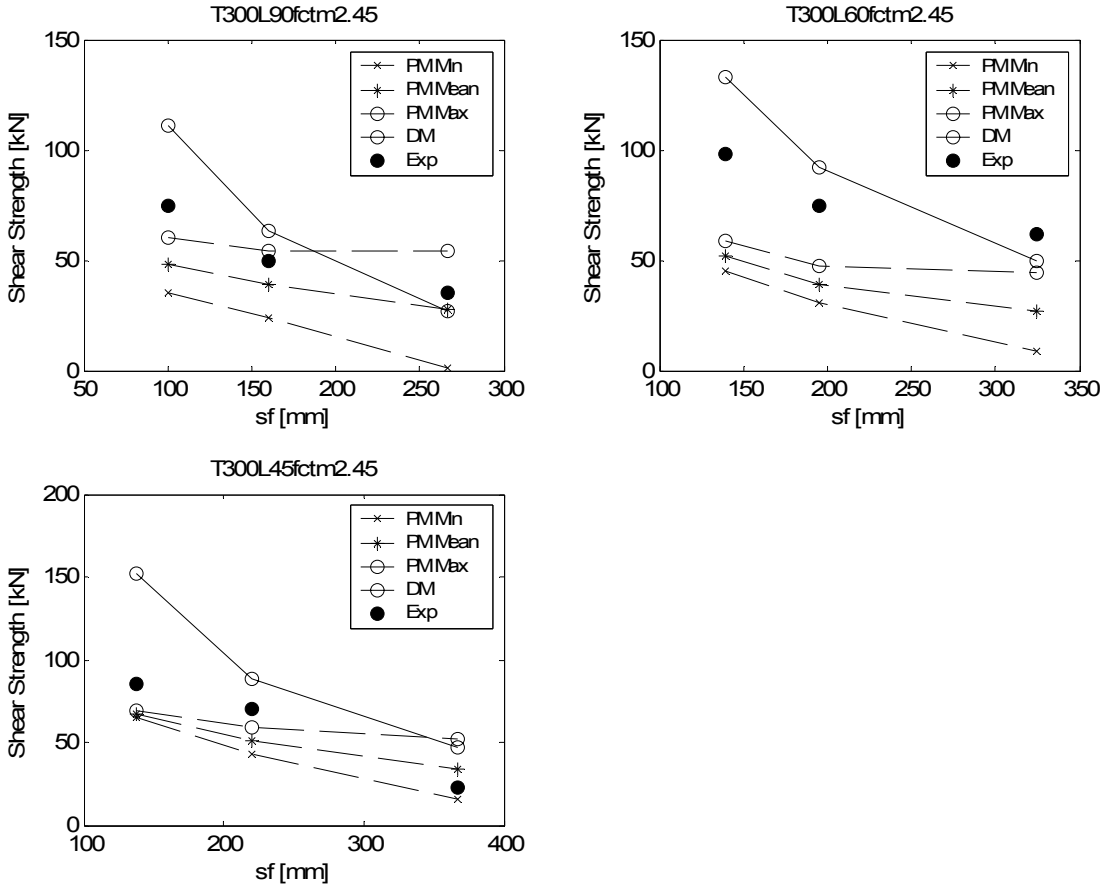

Fig. 5.25 – Beams of the 3rd series, by Dias and Barros (2006)

5.5 Influence of Concrete Tensile Strength

According to the model presented, for the following values of the various parameters: $\theta = 45°$; $\alpha = 25°$; $b_w = 180\,mm$; $h_w = 300\,mm$ and $\beta = 45°$, a parametric study was carried out by varying the mechanical properties of the concrete, see Fig. 5.26. In fact, the NSM shear strength contributions, calculated by the "*proposed approach*", for concrete classes C12, C20, C50, C70, according to the classification by CEB Model Code 90, are compared with those provided by the DM (Chapter 4). Note that, in graphs of Fig 5.26, the DM was applied according to the definition of the model as provided in Chapter 4 but the $\tau_b\left(L_f\right)$ adopted was slightly different than the one represented by Eq. 4.6 (see Eq. 5.14) but this is not detrimental to the main purpose of the present Chapter *i.e.* the evaluation of the "*idea*".

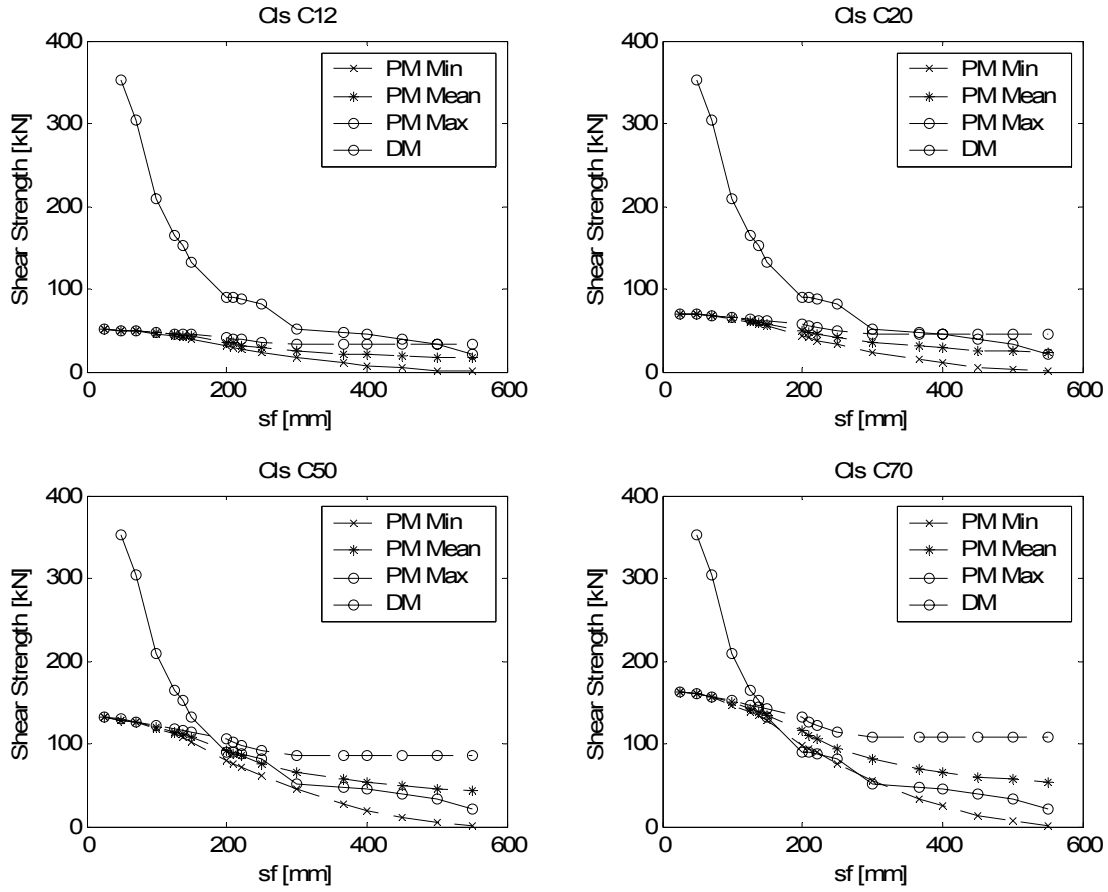

g)

Fig. 5.26 – Comparison between analytical values of V_f by the "*proposed approach*" and those by the DM for concrete classes C12, C20, C50, C70.

From this simple parametric study, it arises that, a formulation based on the assumption that debonding is the only possible failure mode, that completely neglects the mechanical properties of concrete, provides values of the NSM shear strength contribution that present a variable safety factor. In fact, for a concrete class C12, the DM dangerously overestimates the maximum concrete-fracture-based NSM shear strength contribution for a wide range of spacing values. For stronger concrete, such as C70, the DM provides reasonable estimates for a wider range of values of s_f but, for low values of the spacing, it still greatly overestimates the concrete-fracture-based NSM shear strength contribution.

5.6 Conclusions

From the study carried out in this Chapter it emerges that, the idea that CFRP laminates near surface mounted are susceptible to fail due to the concrete fracture is confirmed, by experimental evidence, literature analogies and analytical comparisons. Concrete surrounding laminates fails along semi-conical fracture surfaces, envelope of the tension isostatics, when its tensile strength is exceeded. This failure mode can highly limit the NSM shear strength contribution since it prevents debonding failure, to which higher strengths can be ascribed, to occur.

It also emerges that debonding can happen if only the mechanical properties of concrete are relatively very high and the percentage of laminates low. In this respect, a coherent analytical formulation should take into consideration all the possible failure modes undergone by NSM CFRP laminates.

The proposed modelling strategy allows the issue of the interaction between subsequent laminates to be easily taken into account. When the spacing between laminates is decreased, their semi-conical concrete fracture surfaces overlap and the fracture surface ascribed to each of them can be calculated accordingly.

It also has to be outlined that, according to the interpretation of the phenomena proposed, the interaction stirrups/laminates is a very important issue that needs to be further addressed. The higher the amount of stirrups (better: the closer their spacing) the lower is the NSM shear strength contribution provided by the same amount of laminates. This should be ascribed to the micro-splitting-cracks that form around the stirrups that, when they are very close to each other, almost form a discontinuity plane between the concrete cover and the core of the beam web. In this respect, the situation is even worse in the case of existing real structures since stirrups, at the moment of the strengthening intervention, are already loaded and strained, at a certain extent, so as a micro-crack plane that separates the concrete cover from the core of the beam already exists.

6 Analytical Predictive Model Proposed

Given both the complexity of the behaviour of RC beams failing in shear from a general point of view and the further complications introduced by the presence of brittle materials, such as the CFRP Laminates glued by an epoxy adhesive into thin shallow slits cut in the concrete cover, a complete 3D Finite Element Analysis allowing for the Non-Linear behaviour of both the various materials involved and the bond between these latter, remains the strongest tool for research purposes but too computational-time consuming and requiring expert users.

Provided that, hereafter a relatively simple analytical model is proposed on the basis of the observations shown in the previous chapter that, if confirmed by further investigations both experimental and numerical, can constitute a useful and computationally not excessively demanding analysis tool.

Some details already presented in the previous Chapter 5, where the main features of the Model physical fundamentals were delineated, are briefly repeated hereinafter, for the sake of an easy reading.

6.1 Neglecting the interaction with stirrups

The Proposed Model (PM) assumes as possible failure modes: tensile rupture of the laminate, debonding and concrete tensile fracture, see Fig. 6.1 and Chapter 5.

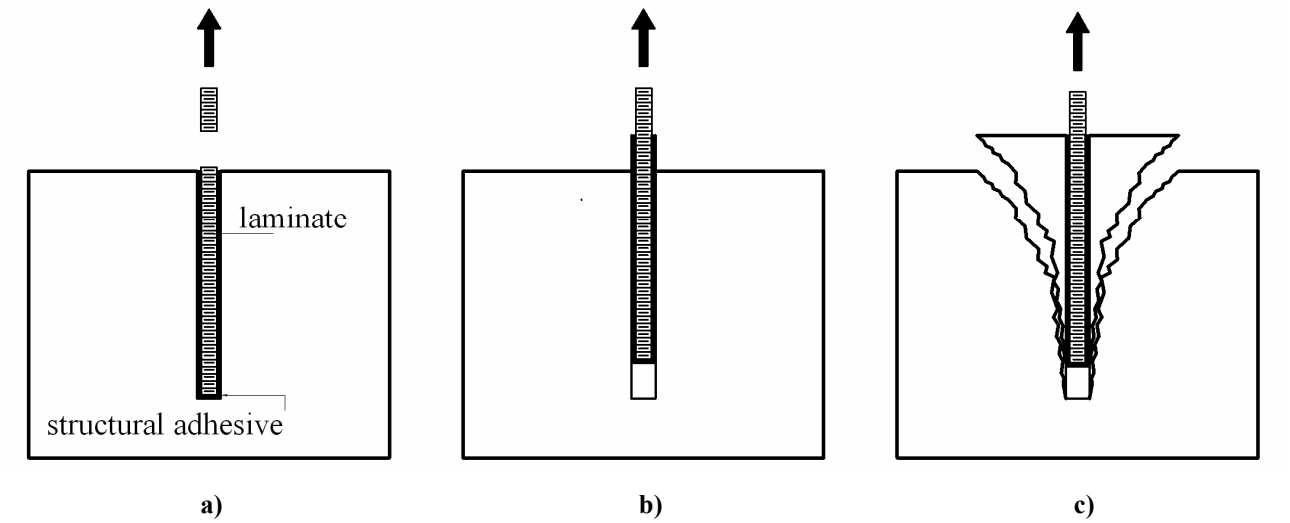

Fig. 6.1 – Assumed possible failure modes undergone by the NSM laminates: a) laminate tensile rupture; b) debonding; c) concrete semi-conical tensile fracture

As regards the RC beam strengthened in shear by the NSM technique, the critical diagonal crack can be schematized like a plane slicing the web of the beam in two parts sewn together by the crossing laminates (see Fig. 5.8). The laminates may fail along their "*available bond length*" by one of the above failure modes. As regards the concrete tensile fracture failure mode, the assumption is done that the semi-conical fracture surface starts propagating from the inner tip of the available bond length, see Fig. 6.1c. The concrete average tensile strength, f_{ctm}, is distributed throughout each of the resulting semi-conical fracture surfaces and orthogonally to them in each point, see Fig. 5.9.

The NSM shear strength contribution, V_f, can be calculated by adding the contribution ascribed to each laminate, V_{fi}^{p}, and parallel to its orientation, and projecting the resulting force orthogonally to the beam axis, according to the following formula:

$$V_f = 2 \cdot \sin\beta \cdot \sum_{i=1}^{N_f} V_{fi}^{p} \tag{6.1}$$

where β is the inclination of the laminates and N_f is the number of laminates crossing the shear crack.

The contribution provided by each laminate, V_{fi}^{p}, can be assumed as the minimum among the three possible contributions ascribed, respectively, to debonding, $V_{fi}^{p,db}$, tensile rupture of the laminate, $V_{fi}^{p,tr}$, or concrete tensile fracture, $V_{fi}^{p,cf}$, *i.e.*:

$$V_{fi}^{p} = \min\left\{V_{fi}^{p,db}; V_{fi}^{p,tr}; V_{fi}^{p,cf}\right\} \tag{6.2}$$

The debonding-based term, $V_{fi}^{p,db}$, ascribed to each i-th laminate and parallel to its orientation can be computed as follows:

$$V_{fi}^{p,db} = 2 \cdot \left(a_f + b_f\right) \cdot \tau_b(L_f) \cdot L_{fi} \tag{6.3}$$

where a_f and b_f are, respectively, the thickness and width of the laminates' cross section and $\tau_b\left(L_f\right)$ is the length-dependent value of the average bond strength, determined based on the physical interpretation of the most recent experimental results regarding debonding, see Chapter 4, and equal to (L_f in mm and τ_b in MPa):

$$\tau_b\left(L_f\right) = \begin{cases} 19.28 & 0 < L_f < 40 \\ 0.355 + 174.613 \cdot \left(L_f\right)^{-0.60233} & L_f \geq 40 \end{cases} \tag{6.4}$$

The tensile rupture-based term, $V_{fi}^{p,tr}$, ascribed to each i-th laminate and parallel to its orientation is equal to:

$$V_{fi}^{p,tr} = a_f \cdot b_f \cdot f_{fu} \tag{6.5}$$

where f_{fu} is the adopted CFRP laminates' tensile strength.

The concrete fracture-based term, $V_{fi}^{p,cf}$, ascribed to each laminate and parallel to its orientation, can be calculated distributing the component of the concrete average tensile strength parallel to the laminate, *i.e.*, $f_{ctm} \cdot \sin\alpha_{fi}$, throughout the resulting relevant semi-conical surface and integrating, according to the following formula (Fig. 2b):

$$V_{fi}^{p,cf} = \int_{C_{fi}\left(L_{fi};\alpha_{fi}\right)} \left(f_{ctm} \cdot \sin\alpha_{fi}\right) \cdot dC_{fi} \tag{6.6}$$

where $C_{fi}\left(L_{fi};\alpha_{fi}\right)$ concisely denotes the semi-conical surface associated to the i-th laminate and α_{fi} is the angle between the generatrices and the axis of the semi-cone attributed to the i-th laminate.

The angle between the axis of the semi-conical surface and its generatrices, α_f, calibrated on the basis of the interpretation of some experimental results available to date (see Paragraph 5.3), ranges approximately between 20° and

30° and shows a length-dependency on the available bond length, L_f, but, in this respect, further investigations are required.

The relationship between the angle, α_{fi} (in degrees), and the available bond length, L_{fi} (in mm), assumed in the present work, is the following:

$$\alpha_{fi} = \begin{cases} 32.31 & \text{for} \quad 0 \le L_{fi} \le 30 \\ 33.973 - 0.0587 \cdot L_{fi} & 30 < L_{fi} \le 150 \\ 25.17 & L_{fi} > 150 \end{cases} \tag{6.7}$$

If attention is focused on one laminate only, in the case in which it results to be orthogonal to the crack plane and in complete absence of interaction with the contiguous ones, the shear strength contribution parallel to its orientation, V_{fi}^{p}, can be calculated by:

$$V_{fi}^{p} = \min\left\{2 \cdot \left(a_f + b_f\right) \cdot \tau_b(L_{fi}) \cdot L_{fi};\ a_f \cdot b_f \cdot f_{fu}\ ;\ \left(\frac{\pi}{2} \cdot f_{ctm}\right) \cdot tg^2\alpha_{fi} \cdot L_{fi}^2\right\} \tag{6.8}$$

that, for instance, for the materials adopted by Dias and Barros 2006, is plotted in Fig. 6.3. It arises that, in that case: for a value of the available bond length up to 200 *mm* the prevailing failure mode is the concrete semi-conical fracture; for a value between 200 and 310*mm* the failure mode is debonding, and for an available bond length higher than 310*mm* the laminates are expected to fail by tensile rupture. Due to the interaction between contiguous laminates, when laminates spacing decreases, the curve regarding the concrete tensile fracture opens downwards, thus reducing the range of length values in correspondence of which debonding is expected to be the commanding failure mode.

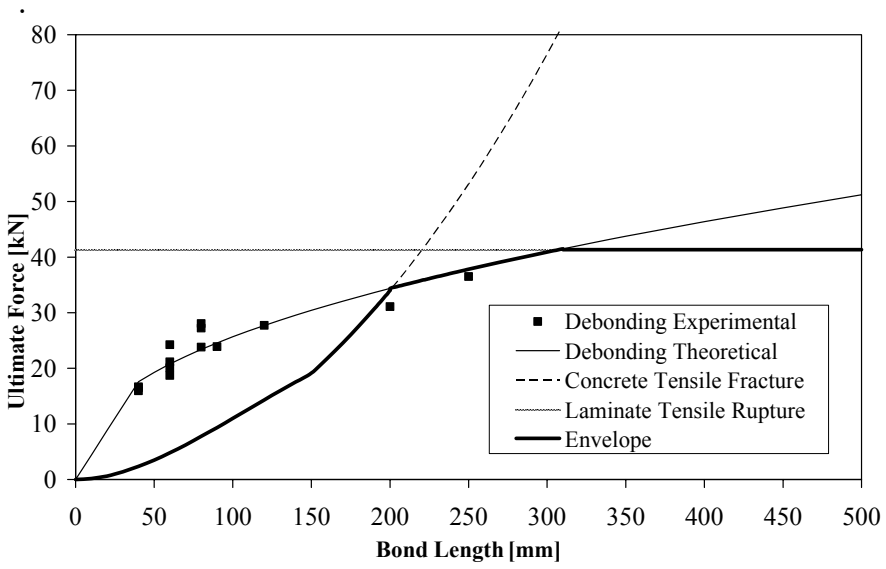

Fig. 6.3 – Expected failure mode as function of the available bond length

The terms $V_{fi}^{p,tr}$ and $V_{fi}^{p,db}$, based on the phenomenon of tensile rupture and debonding of the laminate, respectively, are intrinsically independent of the interaction between subsequent laminates that, on the contrary, affects the concrete fracture-based term, $V_{fi}^{p,cf}$.

As the spacing between subsequent laminates is reduced, their semi-conical fracture surfaces overlap and the resulting envelope area progressively becomes smaller than the mere summation of each of them (see Paragraph 5.1 and Fig. 5.15). This detrimental interaction between laminates can be easily taken into account by calculating the resulting semi-conical surface ascribed to each laminate accordingly.

In the above Eq. 6.6, the operation of integrating the component of the concrete tensile strength parallel to the laminate $\left(f_{ctm}\cdot\sin\alpha_{fi}\right)$ throughout the surface is equivalent to projecting the surface on a plane orthogonal to the laminate and multiplying it by the absolute value of the strength *i.e.* (see Paragraph 5.2 and Appendix A):

$$d\mathrm{A}_{fi} = dC_{fi}\cdot\sin\alpha_{fi} \tag{6.9}$$

Thus, introducing (6.9) into (6.6) results:

$$V_{fi}^{p,cf} = \int\limits_{C_{fi}\left(L_{fi};\alpha_{fi}\right)}\left(dC_{fi}\cdot\sin\alpha_{fi}\right)\cdot f_{ctm} = f_{ctm}\cdot\int\limits_{\mathrm{A}_{fi}\left(L_{fi};\alpha_{fi}\right)} d\mathrm{A}_{fi} = f_{ctm}\cdot\mathrm{A}_{fi}\left(L_{fi};\alpha_{fi}\right) \tag{6.10}$$

where $\mathrm{A}_{fi}\left(L_{fi};\alpha_{fi}\right)$ is the area, function of both the "*available bond length*" L_{fi} and the angle α_{fi}, obtained by projecting the semi-conical surface on a plane orthogonal to the laminate (see Fig. 5.18).

Since the intersection of each semi-conical surface with the crack plane is constituted by a semi-ellipse, that becomes a semi-circle in the particular case in which the laminate results to be orthogonal to the crack plane, the above area $\mathrm{A}_{fi}\left(L_{fi};\alpha_{fi}\right)$ can be evaluated by calculating the area of the semi-ellipse and then projecting this latter on the plane orthogonal to the laminate (see Fig. 5.17). Thus, the calculation of the contribution ascribed to the i-th laminate parallel to its length is reduced to the evaluation of the area underlying the relevant semi ellipse *i.e.*:

$$V_{fi}^{p,cf} = \sin\left(\theta+\beta\right)\cdot f_{ctm}\cdot\int\limits_{E_{fi}\left(L_{fi};\alpha_{fi}\right)} dE_{fi} \tag{6.11}$$

where $E_{fi}\left(L_{fi};\alpha_{fi}\right)$ is the equation of the semi-ellipse, intersection of the i-th semi-conical surface with the assumed crack plane.

This simplification is extremely powerful from a computational standpoint since allows the interaction between laminates to be easily accounted for. In function of the main geometrical parameters h_w, b_w, s_f, L_{fi} and $\alpha_{fi}\left(L_{fi}\right)$, see Fig. 6.2, that interaction can be either mono-directional, longitudinal or transversal, or bi-directional. The longitudinal interaction can occur when, due to the reduced spacing with respect to the height of the web, the semi-cones associated to adjacent laminates located at the same side of the web, and consequently their relevant semi-ellipses, overlap along their major semi-axis (see for instance the semi-ellipses 5 and 6 of the example of Fig. 6.4). The transversal interaction can occur when, for slender beam cross sections of high h_w/b_w ratio, the semi-ellipses symmetrically placed on the opposite sides of the web, intersect each other along their minor semi-axis (see the semi-ellipse 1 of Fig. 6.4). In this latter case, the area of the i-th semi-ellipse is limited, upwards, by the line $Y = b_w/2$, *i.e.* the trace, on the shear crack plane, of the vertical plane passing through the beam axis. In the most general case, in which bidirectional interaction might occur, the area on the shear crack plane associated to the i-th laminate, would be

composed of two terms: one, A_{fi}^{nlin}, limited upwards by the non-linear branch of the relevant semi-ellipse $Y_i(X)$ and another, A_{fi}^{lin}, limited by the line $Y = b_w/2$ (see the semi-ellipses 1, 6 and 7 of Fig. 6.4).

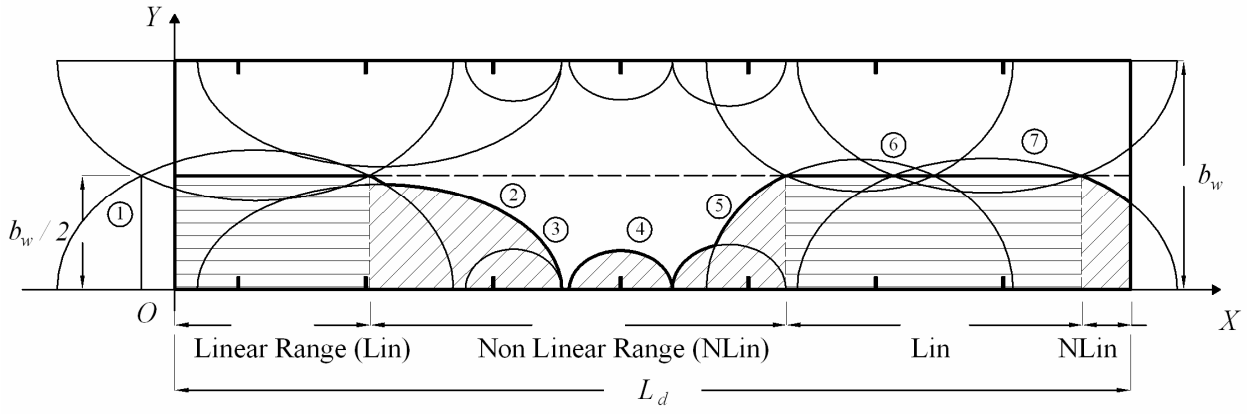

Fig. 6.4 – Example: definition of half crack plane and linear and non-linear range of integration for each ellipse

Hence, due to the most general case of bi-directional interaction, the area of the semi-ellipse associated to the i-th laminate is calculated as follows:

$$\int_{E_{fi}\left(L_{fi};\alpha_{fi}\right)} dE_{fi} = \left(A_{fi}^{nlin} + A_{fi}^{lin}\right) \tag{6.12}$$

Ultimately, Eq. (6.1) can be re-written as follows:

$$\begin{aligned} V_f &= 2\cdot\sin\beta\cdot\sum_{i=1}^{N_f} V_{fi}^{p} = \\ &= 2\cdot\sin\beta\cdot\sum_{i=1}^{N_f}\min\left\{2\cdot\left(a_f+b_f\right)\cdot L_{fi}\cdot\tau_b\left(L_{fi}\right);\ a_f\cdot b_f\cdot f_{fu};\left(A_i^{nlin}+A_i^{lin}\right)\cdot\sin\left(\theta+\beta\right)\cdot f_{ctm}\right\} \end{aligned} \tag{6.13}$$

In that expression, the most complicated task is represented by the evaluation of the term $\left(A_i^{nlin} + A_i^{lin}\right)$ ascribed to each i-th laminate. The algorithm, whose summarizing folw chart is represented in Fig. 6.5, is developed so as to make the above task easy by calculating the necessary informations step by step. This also makes the whole algorithm easy to be programmed.

Moreover, the model is developed taking into consideration the three geometrical configurations, for $k = 1,2,3$, already introduced in Chapter 4 (see Figs. 4.3 to 4.5), of the present work. This is reflected by the digit after comma present in the subscript of each configuration-dependent quantity.

Apart from the possible interaction of the laminates between each other, the analytical development of the PM takes all the necessary precautions in order to result the most robust, general and reliable as possible (see Appendix E).

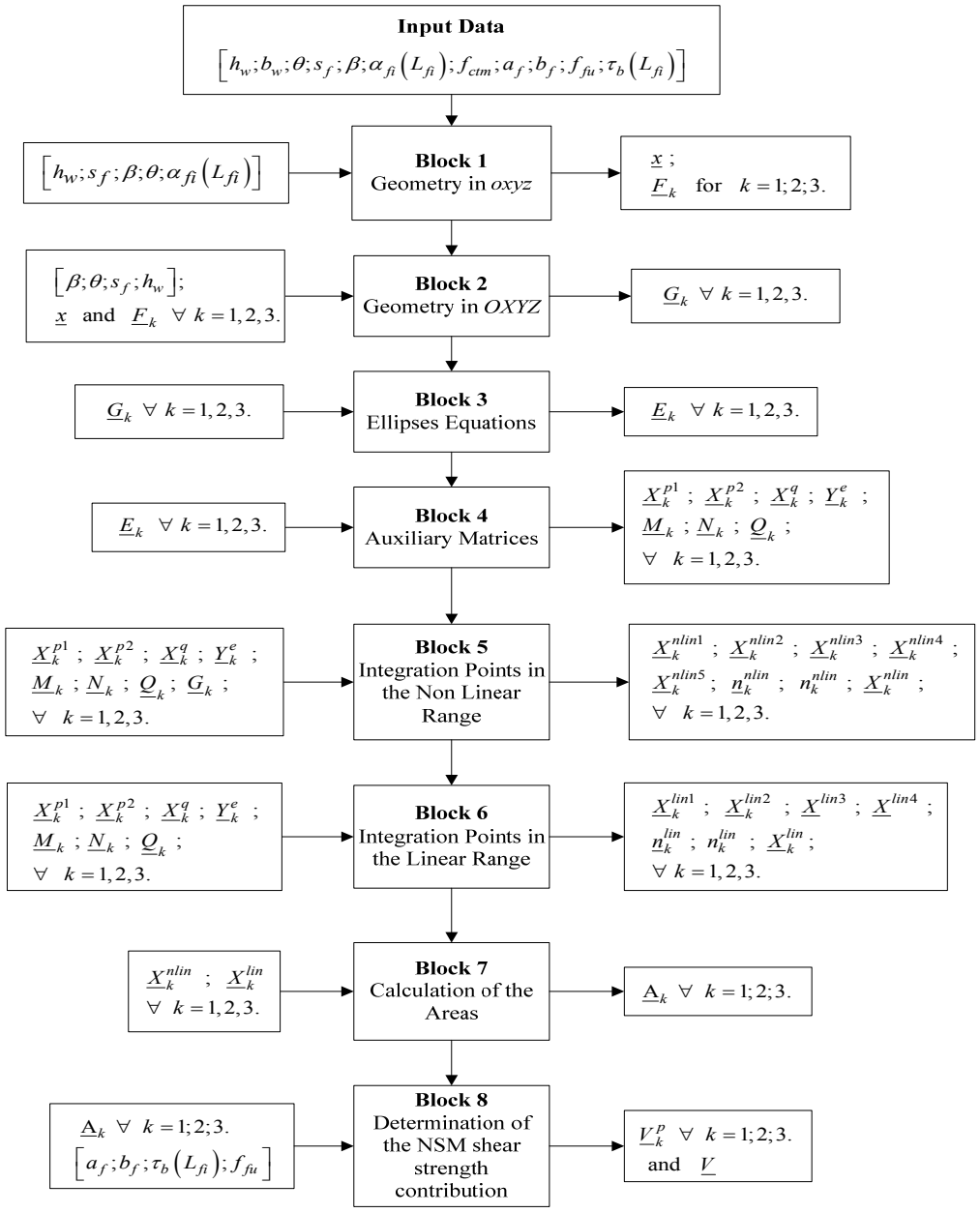

Fig. 6.5 – Flow chart of the several Blocks of operations to be execute in sequence

Input Data

The general parameters entering the assumed approach are:

- h_w, the height of the web in the case of a T cross section beam. For a rectangular cross section beam, h_w is the vertical component of the laminate length, *i.e.*, $h_w = L_f / \sin\beta$, where L_f is the laminate length;
- b_w, the width of the web of the beam cross section in the case of a T beam. For a rectangular cross section beam, b_w is the cross section width;
- β, the inclination of the laminates with respect to the beam axis;
- s_f, the spacing of the laminates along the beam axis;
- θ, the assumed crack angle;

- $\alpha_{fi}\left(L_{fi}\right)$, the relationship between the angle, formed by the axis and the generatrices of the i-th semi-conical surface, and the available bond length of the laminate;
- f_{ctm}, the concrete average tensile strength;
- a_f, the thickness of the laminate cross section;
- b_f, the width of the laminate cross section;
- f_{fu}, the laminate tensile strength;
- $\tau_b(L_f)$, the relationship between the average bond strength and the available bond length of the laminate.

The formulation requires the use of the following two cartesian reference systems (see Fig. 6.2a):

- *oxyz* the "*global reference system*" whose origin is placed in the assumed crack origin and whose plane *oxy* lies on the intrados of the prism schematizing the beam web;
- *OXYZ* the "*crack plane reference system*" whose origin is placed in the assumed crack origin and whose plane *OXY* lies on the plane schematizing the crack.

Moreover, it is necessary to define, in the plane *OXY*, the "*local reference system*", $o_i e_{1i} e_{2i}$, for each i-th semi-ellipse (see Fig. 6.6).

Block 1: Definition of the geometrical quantities in the global reference system *oxyz*

The output of this Block of calculation is composed of four matrices summarizing the prominent geometrical quantities defined in the global reference system:

- $\underline{x}$ is a 3×2 dimension matrix, the first column of which stores the position of the first laminate with respect to the assumed crack origin, for the three possible laminates' configurations, $x_{f1,k}$, see Figs. 4.3-4.5 and Eq. (4.3) of Chapter 4, while the second column includes the corresponding number of laminates crossing the shear failure crack, $N_{f,k}$, see Eq. (4.3);
- $\underline{F}$ is a $N_f \times 3$ dimension matrix. For a generic k-th configuration, the first column of $\underline{F}_k$ includes the position of the laminates, $x_{fi,k}$, the second column stores the available bond length of the laminates, $L_{fi,k}$ (see Eqs. (4.4) and (4.5) of Chapter 4), and the third column includes the values of the angle $\alpha_{fi,k}$. In the present model, the i char in the subscript of any symbol refers the i-th laminate and its associated semi-ellipse. For the generic k-th configuration it is $i = 1,.....,N_{f,k}$.

Block 2: Definition of the geometrical properties in the crack plane reference system *OXYZ*

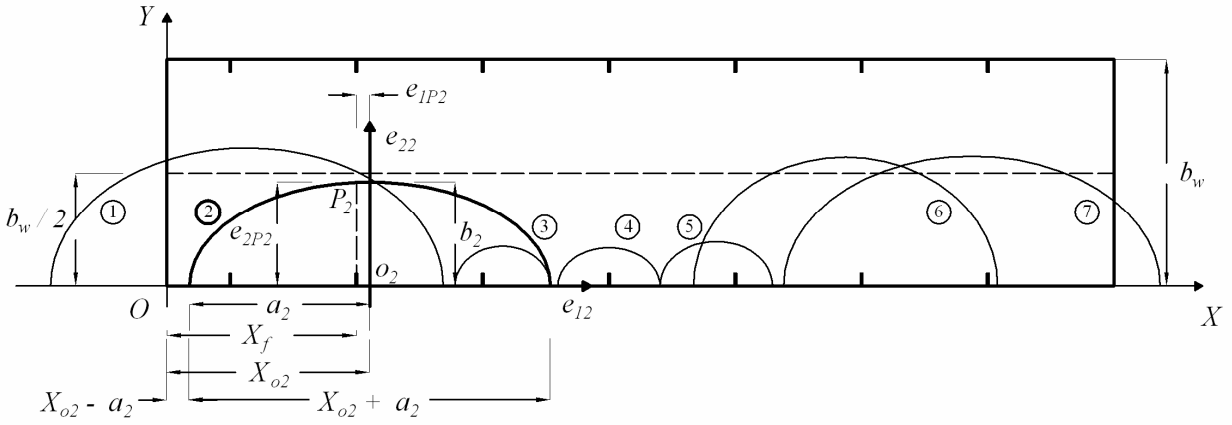

Fig. 6.6 – Example of Fig. 6.4: definition of the geometrical quantities in OXY and the ellipse local reference system $o_i e_{1i} e_{2i}$

Once the geometry and the number of laminates to be allowed for have been determined as described above, it is necessary, for the further developments, to determine the equations, in the plane OXY **,** of the semi-ellipses generated by slicing the semi-conical surfaces with the inclined plane simulating the major shear crack.

To easily determine the equations of the semi-ellipses in the crack plane reference system, the prominent geometrical quantities, for each i-th laminate, are stored in the corresponding i-th row of the $\underline{G}_k$ matrix, that is, the $\underline{G}$ matrix in the k-th configuration, of $N_{f,k} \times 8$ dimensions. The first column of the $\underline{G}_k$ matrix has the position of each laminate singled out along the OX axis of the crack plane reference system, X_{fi} (see Fig. 6.6). For a generic i-th laminate, $X_{fi,k}$ can be evaluated by, (for further details see Appendix D):

$$X_{fi,k} = \frac{\sin\beta}{\sin\left(\beta+\theta\right)} \cdot \left[x_{f1,k} + \left(i-1\right) \cdot s_f \right] \tag{6.14}$$

The second column includes the length of the major semi-axis of the semi-ellipse, a . For a generic i-th laminate, $a_{i,k}$ can be determined from:

$$a_{i,k} = \frac{L_{fi,k}}{2} \cdot \sin\alpha_{fi,k} \cdot \left[\frac{1}{\sin\left(\alpha_{fi,k}+\beta+\theta\right)} + \frac{1}{\sin\left(\theta+\beta-\alpha_{fi,k}\right)} \right] \tag{6.15}$$

The third column stores the values of the position, along the OX axis, of the center of the i-th ellipse X_o . For a generic i-th ellipse $X_{oi,k}$ can be calculated from (see Appendix D):

$$\begin{cases} X_{oi,k} = x_{fi,k} \cdot \dfrac{\sin\left(\beta-\alpha_{fi,k}\right)}{\sin\left(\beta+\theta-\alpha_{fi,k}\right)} + a_{i,k} & \text{for } \left(x_{fi,k} < \dfrac{h_w}{2} \cdot \left(\cot\theta+\cot\beta\right) \right) \\ X_{oi,k} = \dfrac{h_w}{\sin\theta} - \dfrac{\sin\left(\beta-\alpha_{fi,k}\right)}{\sin\left(\beta+\theta-\alpha_{fi,k}\right)} \cdot \left[h_w \cdot \left(\cot\theta+\cot\beta\right) - x_{fi,k} \right] - a_{i,k} & \text{for } \left(x_{fi,k} \geq \dfrac{h_w}{2} \cdot \left(\cot\theta+\cot\beta\right) \right) \end{cases} \tag{6.16}$$

The fourth column includes the values of the abscissa, e_{1P}, in the local reference system of the semi-ellipse $oe_1e_2e_3$, of an auxiliary point P necessary to write the equation of the relevant ellipse. For a generic i-th ellipse of the k-th geometrical configuration, $e_{1Pi,k}$ can be calculated from:

$$e_{1Pi,k} = X_{fi,k} - X_{oi,k} \tag{6.17}$$

The fifth column stores the values of the ordinate, in the local reference system of the semi-ellipse, $oe_1e_2e_3$, of an auxiliary point P necessary to write the equation of the relevant ellipse, e_{2P}. For a generic i-th ellipse, $e_{2Pi,k}$ can be calculated from:

$$e_{2Pi,k} = L_{fi,k} \cdot \tan \alpha_{fi,k} \tag{6.18}$$

The sixth column includes the values of the length of the minor semi-axis of the semi-ellipse, b. For a generic i-th semi-ellipse, $b_{i,k}$ can be calculated from:

$$b_{i,k} = \sqrt{\frac{a_{i,k}^2 \cdot e_{2Pi,k}^2}{\left(a_{i,k}^2 - e_{1Pi,k}^2\right)}} \tag{6.19}$$

The seventh column includes the values of the position, along the OX axis, of the leftward vertex of the semi-ellipse along its major axis, v_1. For a generic i-th semi-ellipse $v_{1i,k}$ can be calculated from:

$$v_{1i,k} = X_{oi,k} - a_{i,k} \tag{6.20}$$

The eight column includes the values of the position, along the OX axis, of the rightward vertex of the semi-ellipse along its major axis, v_2. For a generic i-th semi-ellipse $v_{2i,k}$ can be calculated from:

$$v_{2i,k} = X_{oi,k} + a_{i,k} \tag{6.21}$$

Block 3: Determination of the equations of the semi-ellipses in the crack plane reference system $OXYZ$

At this point, it's necessary to determine the analytical equation, in the $OXYZ$ reference system, of each semi-ellipse corresponding to the various laminates. The explicit form of $E_{fi}\left(L_{fi};\alpha_{fi}\right)$ of Eq. 6.11, is:

$$Y_{i,k}\left(X\right) = +\sqrt{-\frac{\left(E_{i1,k} \cdot X^2 + E_{i3,k} \cdot X + E_{i4,k}\right)}{E_{i2,k}}} \tag{6.22}$$

To determine the above equation in the crack plane reference system, it is only necessary to operate a change from the local reference system $o_i e_{1i} e_{2i}$ to OXY, once the analytical expression of the ellipse ha been written in the former (see Appendix D).

The coefficients of the semi-ellipses are stored in the $\underline{E}$ matrix that, for the k-th configuration ($\underline{E}_k$) has $N_{f,k} \times 4$ dimensions. The first to fourth columns of the $\underline{E}$ matrix store the values of the coefficients of the semi-ellipses. For a generic i-th semi-ellipse of the k-th configuration, these coefficients can be calculated from, see Appendix D:

$$E_{i1,k} = b_{i,k}^2 \tag{6.23}$$

$$E_{i2,k} = a_{i,k}^2 \tag{6.24}$$

$$E_{i3,k} = -2 \cdot b_{i,k}^2 \cdot X_{oi,k} \tag{6.25}$$

$$E_{i4,k} = b_{i,k}^2 \cdot X_{oi,k}^2 - a_{i,k}^2 \cdot b_{i,k}^2 \tag{6.26}$$

Block 4: Determination of the Auxiliary Matrices

It is worth determining, even if they are not strictly necessary for the implementation of the algorithm, some auxiliary matrices *i.e.* $\underline{X}_k^{p1}$, $\underline{X}_k^{p2}$, $\underline{X}_k^{q}$, $\underline{Y}_k^{e}$, $\underline{M}_k$, $\underline{N}_k$, $\underline{Q}_k$ since they condense some operations that, otherwise, should be repeated several times. These matrices, will be useful to determine, in the following steps, the matrices of the effective integration points' abscissa $\underline{X}_k^{nlin}$ and $\underline{X}_k^{lin}$ defining respectively the intervals of integration of each semi-ellipse in the "*non-linear*" and in the "*linear*" range.

Step 1: Determination of the auxiliary intersection points $\underline{X}_k^{p1}$ and $\underline{X}_k^{p2}$

The matrices $\underline{X}_k^{p1}$ and $\underline{X}_k^{p2}$, that are the matrices $\underline{X}^{p1}$ and $\underline{X}^{p2}$ in the k-th configuration, contain, in the i-th row, the abscissa value of all the intersection points, if any, of the i-th ellipse with the j-th one for $j = 1.....N_{f,k}$; $i = 1.....N_{f,k}$ and $k = 1,2,3$.

When the solving system for the intersection points between the i-th and j-th ellipses is written:

$$\begin{cases} E_{i1,k}X^2 + E_{i2,k}Y^2 + E_{i3,k}X + E_{i4,k} = 0 \\ E_{j1,k}X^2 + E_{j2,k}Y^2 + E_{j3,k}X + E_{j4,k} = 0 \end{cases} \tag{6.27}$$

the solving equation obtained by substituting the former, $Y^2 = -\dfrac{\left(E_{i1,k}X^2 + E_{i3,k}X + E_{i4,k}\right)}{E_{i2,k}}$, in the latter is as follows:

$$\left(E_{j1,k} \cdot E_{i2,k} - E_{i1,k} \cdot E_{j2,k}\right) \cdot X^2 + \left(E_{i2,k} \cdot E_{j3,k} - E_{j2,k} \cdot E_{i3,k}\right) \cdot X + \left(E_{i2,k} \cdot E_{j4,k} - E_{j2,k} \cdot E_{i4,k}\right) = 0 \tag{6.28}$$

that results to be, in general, a second-order equation, meaning that, in general, the two ellipses can intersect each other in two values of the abscissa, corresponding to a total of four points in the whole plane OXY composed of four quadrants, because of the symmetry with respect to the axis $Y = 0$ (see Fig. 6.7). Since we are interested in what regards the semi-ellipses located in the half crack plane, $Y \geq 0$, in case the solving equation results to be a second-order one, only two points are effectively useful for our purposes (see Fig. 6.7a).

There can also be the case in which the solving equation is of the first order and in that case there are a total of two points in the whole plane OXY but one point only meets our interest because located in the half-space $Y \geq 0$ (see Fig. 6.7b).

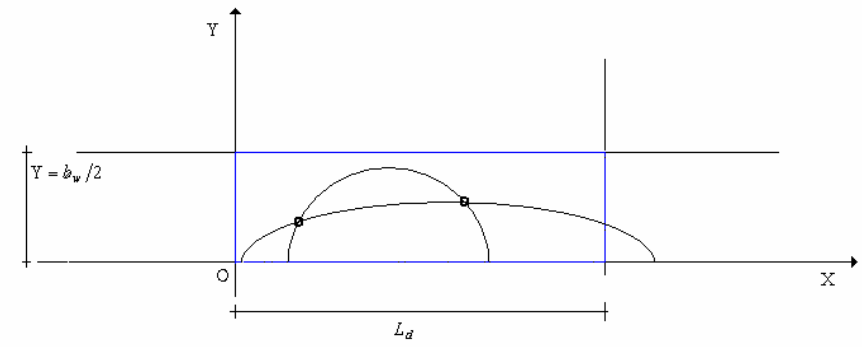

a)

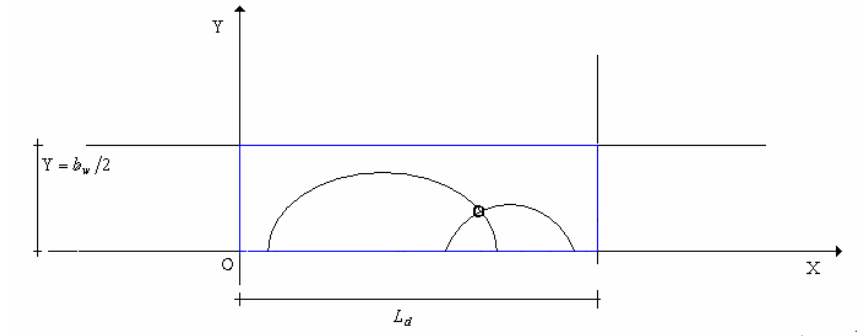

b)

Fig. 6.7 – Intersection between two semi-ellipses ellipses: a) two intersection point; b) one intersection point

In the general case of a second order solving equation, *i.e.* if the following condition is satisfied:

$$\left(E_{j1,k}\cdot E_{i2,k}-E_{i1,k}\cdot E_{j2,k}\right)\neq 0 \tag{6.29}$$

There are two real distinct solutions $X_{ij,k}^{p1}$ and $X_{ij,k}^{p2}$ equal respectively to:

$$X_{ij,k}^{p1}=\frac{-\left(E_{i2,k}\cdot E_{j3,k}-E_{j2,k}\cdot E_{i3,k}\right)-\sqrt{\Delta_{ij,k}}}{2\cdot\left(E_{j1,k}\cdot E_{i2,k}-E_{i1,k}\cdot E_{j2,k}\right)} \tag{6.30}$$

and

$$X_{ij,k}^{p2}=\frac{-\left(E_{i2,k}\cdot E_{j3,k}-E_{j2,k}\cdot E_{i3,k}\right)+\sqrt{\Delta_{ij,k}}}{2\cdot\left(E_{j1,k}\cdot E_{i2,k}-E_{i1,k}\cdot E_{j2,k}\right)} \tag{6.31}$$

where the radicand, $\Delta_{ij,k}$, of the above expressions should be positive:

$$\Delta_{ij,k}=\left[E_{i2,k}\cdot E_{j3,k}-E_{i3,k}\cdot E_{j2,k}\right]^2-4\cdot\left[E_{j1,k}\cdot E_{i2,k}-E_{i1,k}\cdot E_{j2,k}\right]\cdot\left[E_{i2,k}\cdot E_{j4,k}-E_{j2,k}\cdot E_{i4,k}\right]>0 \tag{6.32}$$

Note that in the above analytical expression the possibility, for $\Delta_{ij,k}=0$, that the i-th and j-th ellipses result to be tangent to each other is excluded because of no interest for our purposes. In fact, that tangency can happen in a point located along the X axis (see cases 3 and 5 of Appendix E) or in a point with $0<X<L_d$ and $0\le Y\le b_w/2$ (see cases 16-18 of Appendix E).

Anyway, the present algorithm, discarding the cases of double real root of Eq. (6.28), contemplating the possibility of internal tangency along the X axis or in another point ($0 < X < L_d$ and $Y \geq b_w/2$), works, as can be gathered from the above particular cases listed in Appendix E.

If the solving equation, Eq. (6.28), results to be of the first order, meaning that the two semi-ellipses intersect each other in one point only in the half plane $Y \geq 0$, *i.e.* if it is:

$$\left(E_{j1,k} \cdot E_{i2,k} - E_{i1,k} \cdot E_{j2,k}\right) = 0 \tag{6.33}$$

the solving equation is:

$$\left(E_{i2,k} \cdot E_{j3,k} - E_{j2,k} \cdot E_{i3,k}\right) \cdot X + \left(E_{i2,k} \cdot E_{j4,k} - E_{j2,k} \cdot E_{i4,k}\right) = 0 \tag{6.34}$$

The above equation provides a real value if the following condition is satisfied:

$$\left(E_{i2,k} \cdot E_{j3,k} - E_{j2,k} \cdot E_{i3,k}\right) \neq 0 \tag{6.35}$$

and the corresponding real and unique value of the abscissa is:

$$X_{ij,k}^{p1} = -\frac{\left(E_{i2,k} \cdot E_{j4,k} - E_{j2,k} \cdot E_{i4,k}\right)}{\left(E_{i2,k} \cdot E_{j3,k} - E_{j2,k} \cdot E_{i3,k}\right)} \tag{6.36}$$

and:

$$X_{ij,k}^{p2} = * \tag{6.37}$$

that is, the second solution is attributed a "*non-value*", *e.g.* an asterisk. Note that a "*non-value*" term is not zero since this latter has a physical meaning representing the position, in OXZ , of the assumed crack origin.

In general, one point in a two-dimensional space has two coordinates thus, it is necessary to verify if the value of the ordinate assumed by the i-th semi-ellipse $Y_{i,k}\left(X_{ij,k}^{p1/2}\right)$, in correspondence of $X_{ij,k}^{p1/2}$, is effectively a real number because it might happen that the above solving equations return a real value for the abscissa but in order for the point to actually exist, it is necessary that both coordinates be effectively real numbers. Where the symbol $X_{ij,k}^{p1/2}$ syntetically represents both $X_{ij,k}^{p1}$ and $X_{ij,k}^{p2}$.

The value of the ordinate $Y_{i,k}\left(X_{ij,k}^{p1/2}\right)$ results to be a real number if both of the following conditions are satisfied:

$$E_{i2,k} \neq 0 \tag{6.38}$$

and:

$$-\frac{\left[E_{i1,k} \cdot \left(X_{ij,k}^{p1/2}\right)^2 + E_{i3,k} \cdot \left(X_{ij,k}^{p1/2}\right) + E_{i4,k}\right]}{E_{i2,k}} > 0 \tag{6.39}$$

Moreover, this condition, excludes the points of intersection whose ordinate should be equal to zero because this case is contemplated in Block 5 in which the abscissa of the vertices along the axis $Y = 0$ are analysed *i.e.* $\left(X_{oi,k} \mp a_{i,k}\right)$.

If the value $X_{ij,k}^{p1/2}$ is real and it corresponds to a real value for the ordinate of the i-th ellipse $Y_{i,k}\left(X_{ij,k}^{p1/2}\right)$, and this latter is higher than zero, it is stored in the corresponding j-th column of thei-th row of the corresponding matrix of the

auxiliary intersection points, $\underline{X}_k^{p1}$ or $\underline{X}_k^{p2}$. The cells referring to intersections not existing have to be filled with a "*non-value*".

Note that Eq. (6.39) intentionally lacks the sign of equality in order to carry out a first selection of the points of intersection between ellipses since the points of intersection lying on the X axis are unuseful for our purposes. In fact, we will also take into consideration the vertices of the ellipses along the X axis and these latter are more useful and include, at the same time, the case in which two or more ellipses intersect each other along X.

Hence, in general, the output of this step is constituted of two square symmetric matrices $\underline{X}_k^{p1}$ and $\underline{X}_k^{p2}$ that for the Example of Fig. 6.4, will be as follows, see Fig. 6.8:

$$\underline{X}^{p1} = \begin{bmatrix} * & X_{12}^{p1} & * & * & * & * & * \\ X_{21}^{p1} & * & * & * & * & * & * \\ * & * & * & * & * & * & * \\ * & * & * & * & * & * & * \\ * & * & * & * & * & X_{56}^{p1} & * \\ * & * & * & * & X_{65}^{p1} & * & X_{67}^{p1} \\ * & * & * & * & * & X_{76}^{p1} & * \end{bmatrix}; \quad \underline{X}^{p2} = \begin{bmatrix} * & * & * & * & * & * & * \\ * & * & * & * & * & * & * \\ * & * & * & * & * & * & * \\ * & * & * & * & * & * & * \\ * & * & * & * & * & * & * \\ * & * & * & * & * & * & * \\ * & * & * & * & * & * & * \end{bmatrix} \tag{6.40}$$

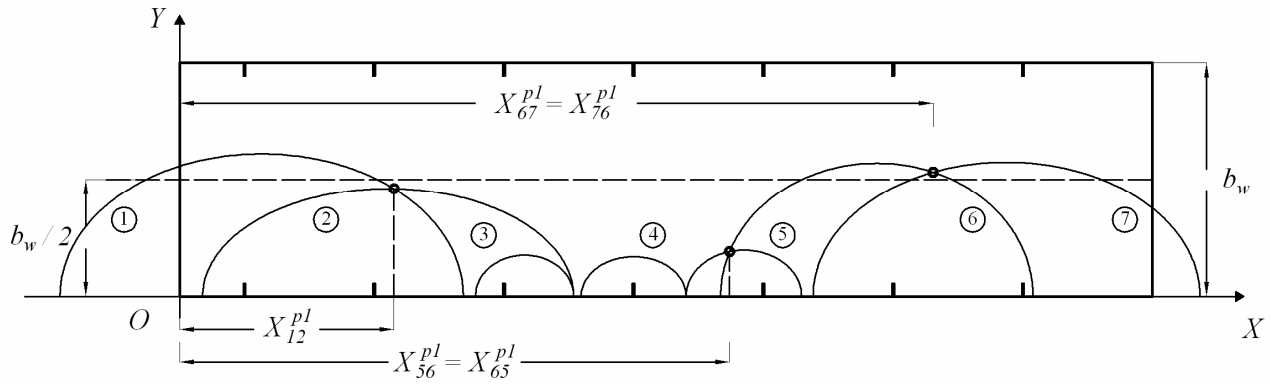

Fig. 6.8 – Intersection points of the ellipses between each other whose abscissa is contained in $\underline{X}^{p1}$ and $\underline{X}^{p2}$

Step 2: Determination of the auxiliary intersection points of each ellipse $\underline{X}^q$ with the straight line $Y = b_w/2$

$\underline{X}^q$ is a $N_f \times 2$ dimensions matrix containing, in each i-th row, the abscissa of the left X_{i1}^q and right X_{i2}^q intersection, if actually existing, of the relevant i-th semi-ellipse with the straight line $Y = b_w/2$. For the general k-th configuration, the first column term of the i-th row, $X_{i1,k}^q$, and the second column one, $X_{i2,k}^q$, of the $\underline{X}_k^q$ matrix are calculated, as follows.

The i-th semi-ellipse actually intersects the line $Y = b_w/2$ if the following conditions are satisfied:

$$\begin{cases} E_{i1,k} \neq 0 \\ \Delta_{i,k} = E_{i3,k}^2 - 4 \cdot E_{i1,k} \cdot \left(E_{i2,k} \cdot b_w^2/4 + E_{i4,k} \right) \geq 0 \end{cases} \tag{6.41}$$

and the corresponding abscissa values are determined as follows:

$$X_{i1,k}^{q} = \frac{-E_{i3,k} - \sqrt{E_{i3,k}^2 - 4E_{i1,k} \,.\left(E_{i2,k} \,.\, b_w^2/4 + E_{i4,k}\right)}}{2 \,.\, E_{i1,k}} \tag{6.42}$$

$$X_{i2,k}^{q} = \frac{-E_{i3,k} + \sqrt{E_{i3,k}^2 - 4 \,.\, E_{i1,k}\left(E_{i2,k} \,.\, b_w^2/4 + E_{i4,k}\right)}}{2 \,.\, E_{i1,k}} \tag{6.43}$$

In the eventuality that the second condition of Eq. (6.41) results to be equal to zero, the two values of the abscissa are equal contemplating the possibility that the semi-ellipse results tangent to the boundary line $Y = b_w/2$. This case is among the ones contemplated in Appendix D.

For the Example of Fig. 6.4, the matrix $\underline{X}^q$ will be as follows, see Fig. 6.9:

$$\underline{X}^q = \begin{bmatrix} X_{11}^q & X_{12}^q \\ * & * \\ * & * \\ * & * \\ * & * \\ X_{61}^q & X_{62}^q \\ X_{71}^q & X_{72}^q \end{bmatrix} \tag{6.44}$$

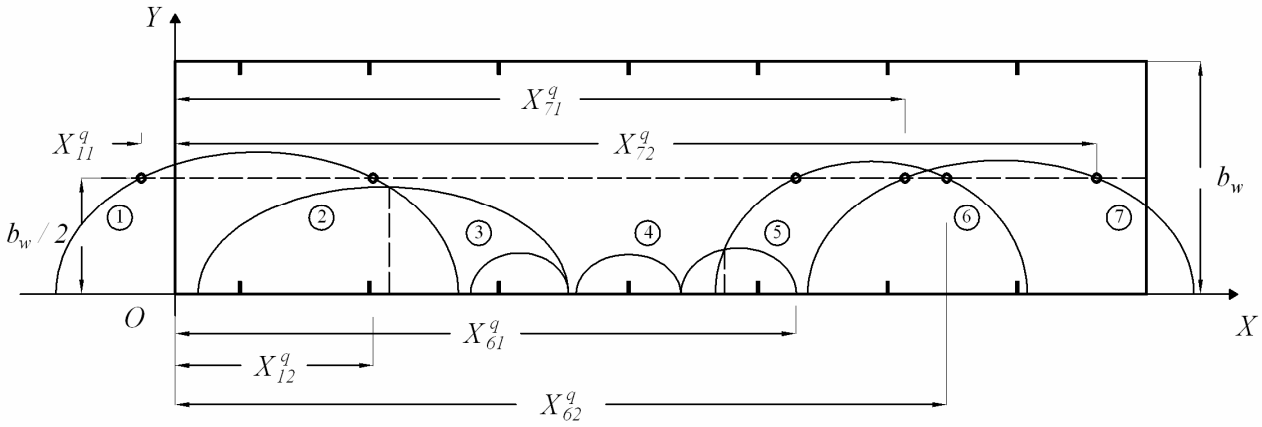

Fig. 6.9 – Intersection points of the semi-ellipses with line $Y = b_w/2$ whose abscissa is contained in $\underline{X}^q$

Step 3: Determination of the auxiliary intersection points $\underline{Y}_k^e$ of each semi-ellipse with the boundary lines $X = 0$ and $X = L_d$

$\underline{Y}^e$ is a $N_f \times 2$ dimensions matrix containing, in each i-th row, the ordinate assumed by the i-th semi-ellipse in correspondence of $X = 0$, and in correspondence of $X = L_d$, if the semi-ellipse actually passes through those abscissa values. For the generic k-th configuration, the first term $Y_{i1,k}^e$ of the i-th row of the $\underline{Y}_k^e$ matrix is a real number, indicating that the relevant semi-ellipse effectively passes through $X = 0$ if the following condition is satisfied:

$$\begin{cases} E_{i2,k} \neq 0 \\ -\dfrac{E_{i4,k}}{E_{i2,k}} \geq 0 \end{cases} \tag{6.45}$$

The latter of the conditions above also contemplates the possibility that the i-th ellipse intersects the line $X = 0$ in correspondence of the origin, *i.e.* in $Y = 0$.

If the above conditions of existence are satisfied, the value of the abscissa is obtained as follows:

$$Y_{i1,k}^{e} = +\sqrt{-\frac{E_{i4,k}}{E_{i2,k}}} \tag{6.46}$$

In which the positive sign in front of the square root is justified by the fact that we are only interested in the intersection point of the i-th ellipse with the boundary line $X = 0$ that lies above the axis $Y = 0$. Likewise, the conditions of existence for the second point of intersection, $Y_{i2,k}^{e}$, are the followings:

$$\begin{cases} E_{i2,k} \neq 0 \\ -\dfrac{\left(E_{i4,k} + E_{i3,k} \,.\, L_d + E_{i1,k} \,.\, L_d^2\right)}{E_{i2,k}} \geq 0 \end{cases} \tag{6.47}$$

If the conditions above are satisfied, the value $Y_{i2,k}^{e}$ is obtained as follows:

$$Y_{i2,k}^{e} = +\sqrt{-\frac{\left(E_{i1,k} \,.\, L_d^2 + E_{i3,k} \,.\, L_d + E_{i4,k}\right)}{E_{i2,k}}} \tag{6.48}$$

If the conditions above are not satisfied, the i-th semi-ellipse does not intersect the boundary line $X = L_d$ and the corresponding cell of the matrix $\underline{Y}_k^e$ has to be filled with a "*non-value*". For the Example of Fig. 6.4, the matrix $\underline{Y}^e$ will be as follows, see fig. 6.10:

$$\underline{Y}^{e} = \begin{bmatrix} Y_{11}^{e} & * \\ * & * \\ * & * \\ * & * \\ * & * \\ * & * \\ * & Y_{72}^{e} \end{bmatrix} \tag{6.49}$$

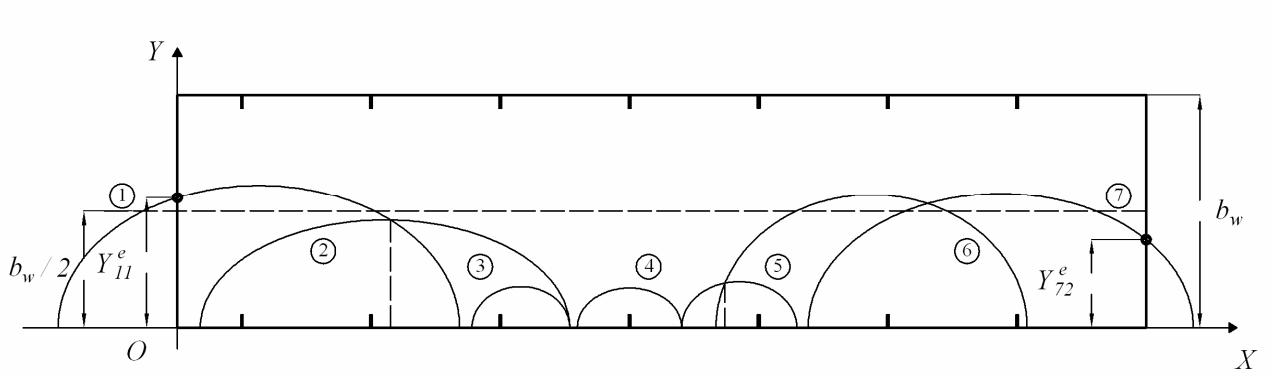

Fig. 6.10 – Intersection points of the semi-ellipses with boundary lines $X = 0$ and $X = L_d$ whose ordinate is contained in $\underline{Y}^e$

Step 3: Determination of the auxiliary matrices $\underline{M}_k$, $\underline{N}_k$ and $\underline{Q}_k$

$\underline{M}$, $\underline{N}$, $\underline{Q}$ are $N_f \times N_f$ dimensions matrices containing, respectively, the coefficients M_{ij}, N_{ij} and Q_{ij} with $i, j = 1,....,N_f$. For the generic k-th configuration, the general terms $M_{ij,k}$, $N_{ij,k}$, $Q_{ij,k}$ of the $\underline{M}_k$, $\underline{N}_k$ and $\underline{Q}_k$ matrices are calculated respectively by the following Eqs.:

$$M_{ij,k} = \left[\left(\frac{E_{i1,k}}{E_{i2,k}} - \frac{E_{j1,k}}{E_{j2,k}} \right) \right] \tag{6.50}$$

$$N_{ij,k} = \left[\left(\frac{E_{i3,k}}{E_{i2,k}} - \frac{E_{j3,k}}{E_{j2,k}} \right) \right] \tag{6.51}$$

$$Q_{ij,k} = \left[\left(\frac{E_{i4,k}}{E_{i2,k}} - \frac{E_{j4,k}}{E_{j2,k}} \right) \right] \tag{6.52}$$

where $E_{i1,k}$, $E_{i2,k}$, $E_{i3,k}$, $E_{i4,k}$ and $E_{j1,k}$, $E_{j2,k}$, $E_{j3,k}$, $E_{j4,k}$ are, respectively, the coefficients of the i-th and j-th semi-ellipses in the k-th configuration stored in the relevant rows of the $\underline{E}_k$ matrix.

Block 5: Determination of the Matrix of the Effective Integration Points in the non linear range $\underline{X}_k^{nlin}$

$\underline{X}^{nlin}$ is a $N_f \times n^{nlin}$ dimensions matrix containing, in the i-th row, the couples of abscissa values constituting limits of the integration intervals for the relevant i-th semi-ellipse equation $Y_i(X)$. For the k-th configuration, the matrix $\underline{X}_k^{nlin}$ has $N_{f,k} \times n_k^{nlin}$ dimensions where n_k^{nlin} is the maximum number of real values of integration limits amongst all the $N_{f,k}$ ellipses of that configuration (an even number). To evaluate $\underline{X}_k^{nlin}$, five other auxiliary matrices $\underline{X}_k^{nlin1}$, $\underline{X}_k^{nlin2}$, $\underline{X}_k^{nlin3}$, $\underline{X}_k^{nlin4}$, $\underline{X}_k^{nlin5}$ have to be determined, first, based on both the auxiliary ones $\underline{X}_k^{p1}$, $\underline{X}_k^{p2}$, $\underline{X}_k^{q}$, $\underline{Y}_k^{e}$, $\underline{M}_k$, $\underline{N}_k$, $\underline{Q}_k$, output of the previous block of calculations, and the matrix of the semi-ellipses geometrical properties, $\underline{G}_k$. Then, the Non Linear range auxiliary matrices, $\underline{X}_k^{nlin1}$, $\underline{X}_k^{nlin2}$, $\underline{X}_k^{nlin3}$, $\underline{X}_k^{nlin4}$, $\underline{X}_k^{nlin5}$, will be joined in the final one $\underline{X}_k^{nlin}$ with $k = 1,2,3$.

The several steps to be taken in sequence, in order to accept and store the abscissa of the aforementioned auxiliary points, are as indicated in the flow chart of Fig. 6.11. The scheme represented by the that flow chart is absolutely general and summarises the conceptual steps to be undertaken to get the abscissa values, among the auxiliary ones already calculated, that are useful to determine the area ascribed to each i-th semi-ellipse. Thus, it refers to both the Linear and Non-Linear ranges of integration. However, the acceptance conditions assume different formal features depending on what range of integration, Linear either Non Linear, we are taking into consideration.

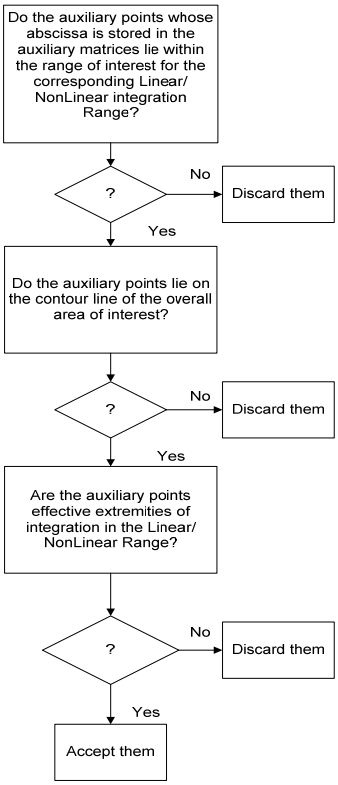

Fig. 6.11 – General steps to check the effectiveness of the Auxiliary points for the *Lin* or *NLin* integration ranges.

Step 1: Determination of the matrices of the effective intersection points between ellipses $\underline{X}_k^{nlin1}$ and $\underline{X}_k^{nlin2}$

$\underline{X}^{nlin1}$ and $\underline{X}^{nlin2}$ are two $N_f \times N_f$ dimensions matrices containing, in the i-th row, the abscissa values, amongst those already calculated and stored in the corresponding i-th row, respectively, of the auxiliary matrices $\underline{X}^{p1}$ and $\underline{X}^{p2}$, that, according to the acceptance conditions hereafter specified, effectively constitute useful integration limits for the relevant i-th semi-ellipse equation. In the following, the symbols $X_{ij,k}^{p1/2}$ and $X_{ij,k}^{nlin1/2}$ will be used to synthetically indicate both the first and second intersection between the i-th and j-th semi-ellipses (see Step 1 of Block 4). For the k-th configuration, the general j-th term $X_{ij,k}^{nlin1/2}$ of the i-th row of the $\underline{X}_k^{nlin1/2}$ matrix is set equal to the corresponding term $X_{ij,k}^{p1/2}$ of the corresponding auxiliary matrix $\underline{X}_k^{p1/2}$, *i.e.*:

$$X_{ij,k}^{nlin1/2} = X_{ij,k}^{p1/2} \tag{6.53}$$

if $X_{ij,k}^{p1/2}$ is such as to satisfy, for the i-th semi-ellipse, the following acceptance conditions:

1. The corresponding point has to be placed inside the range of interest for the Non Linear integration;

2. The corresponding point has to lie upon the upper contour line;
3. The corresponding point has to constitute effective integration extremity;
4. It has not to be equal to the values already stored in the i-th row.

The auxiliary intersection point between the i-th and the j-th semi-ellipses, whose abscissa value is $X_{ij,k}^{p1/2}$ is accepted, for the i-th semi-ellipse, if the following conditions are fulfilled:

$$\begin{cases} 1)\ 0 < X_{ij,k}^{p1/2} < L_d \ \text{ and } \ 0 < Y_{i,k}\left(X_{ij,k}^{p1/2}\right) < \dfrac{b_w}{2} \\ 2)\ Y_{i,k}\left(X_{ij,k}^{p1/2}\right) \geq Y_{h,k}\left(X_{ij,k}^{p1/2}\right) \quad \text{for } \forall\ h = 1....N_{f,k} \\ 3) \begin{cases} \begin{cases} 0 < \left(X_{ij,k}^{p1/2} + \Delta X\right) < L_d \ \text{ and} \\ 0 < Y_{i,k}\left(X_{ij,k}^{p1/2} + \Delta X\right) < \dfrac{b_w}{2} \ \text{ and} \\ Y_{i,k}\left(X_{ij,k}^{p1/2} + \Delta X\right) > Y_{h,k}\left(X_{ij,k}^{p1/2} + \Delta X\right) \ \forall\ h = 1,...,N_{f,k} \ \text{ and } \ h \neq i \end{cases} \\ \text{or} \\ \begin{cases} 0 < \left(X_{ij,k}^{p1/2} - \Delta X\right) < L_d \ \text{ and} \\ 0 < Y_{i,k}\left(X_{ij,k}^{p1/2} - \Delta X\right) < \dfrac{b_w}{2} \ \text{ and} \\ Y_{i,k}\left(X_{ij,k}^{p1/2} - \Delta X\right) > Y_{h,k}\left(X_{ij,k}^{p1/2} - \Delta X\right) \ \forall\ h = 1,...,N_{f,k} \ \text{ and } \ h \neq i \end{cases} \end{cases} \\ 4)\ X_{ij,k}^{p1/2} \neq X_{ig,k}^{nlin1/2} \ \text{ with } g = 1,.....,(j-1) \end{cases} \tag{6.54}$$

in which the term ΔX indicates an infinitesimally small length along the OX axis. If at least one of the above conditions is not fulfilled by the auxiliary value $X_{ij,k}^{p1/2}$, the corresponding effective term $X_{ij,k}^{nlin1/2}$ has to be set equal to "*non-value*".

As regards the first condition, actually it should be $0 < Y_{i,k}\left(X_{ij,k}^{p1/2}\right) < \dfrac{b_w}{2}$ but the left inequality is already contemplated in the calculations that select the auxiliary intersection points between ellipses (see Step 1 of Block 4) thus, in the following analytical expressions it will be omitted. The rightward inequality is necessary because the intersection between semi-ellipses in correspondence of the line $Y = \dfrac{b_w}{2}$ is not interesting for the integration of the semi-ellipses in their non-linear range and furthermore, that eventuality is already contemplated in the case of the intersections with $Y = \dfrac{b_w}{2}$.

The second condition checks if the the intersection point, whose abscissa is abscissa $X_{ij,k}^{p1/2}$, effectively lies on the border line and simply verifies if the value of the ordinate assumed by the i-th semi-ellipse is higher or equal to the ordinate that any other h-th semi-ellipse assumes there.

The third condition checks if the point effectively constitutes a useful integration extremity for the i-th ellipse *i.e.* if, on either the left side $\left(X_{ij,k}^{p1/2} - \Delta X\right)$ or on the right side $\left(X_{ij,k}^{p1/2} + \Delta X\right)$, the i-th semi-ellipse is higher than any other semi-ellipse passing through the point $\left(X_{ij,k}^{p1/2} \mp \Delta X\right)$ (see Fig.6. 12).

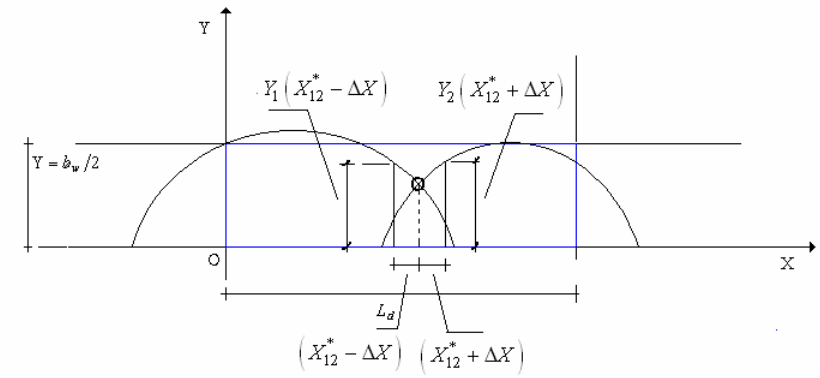

Fig. 6.12 – Check of the effectiveness of the intersection point between the i-th and j-th ellipses $X_{ij,k}^{p1/2}$ for the integration of $Y_{i,k}\left(X\right)$ in its non linear range

The fourth condition aims at avoiding to store, in the j-th column of the i-th row of the matrix $\underline{X}_k^{nlin1/2}$ of the effective points, a value that has already been stored in that row so far as for example could be the case of several ellipses intersecting each other in the same point. In that case, like the one shown by Fig. 6.13, the same value, ($X_{12}^{p1}=X_{13}^{p1}$), might be stored twice. On the contrary, the algorithm has to select couples of abscissa values. This selection could also be done in the final step of this Block 5 in which the final matrix $\underline{X}_k^{nlin}$ of the effective integration points is built but maybe it is preferable to carry out it now, while analyzing the values $X_{ij,k}^{p1/2}$ on the i-th row from left to right. In this way the determination, later on, of the number of columns n_k^{nlin} of the final matrix $\underline{X}_k^{nlin}$, will be carried out more easily.

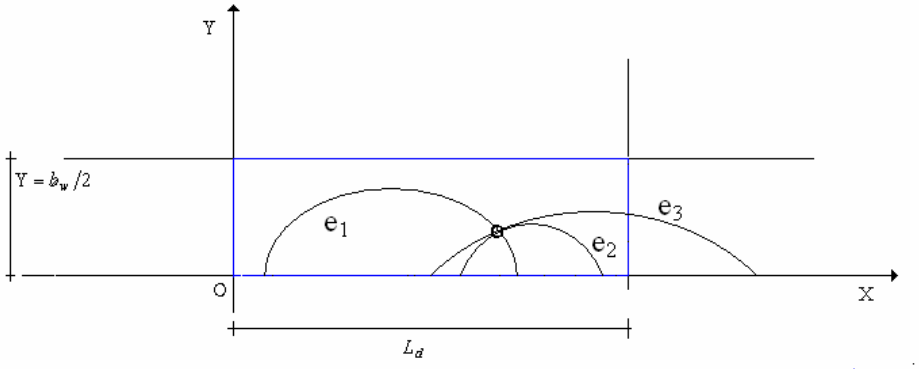

Fig. 6.13 – Necessity of the fourth condition

The conditions (6.54) yield the following analytical expressions:

$$\begin{cases} 0 < X_{ij,k}^{p1/2} < L_d \text{ and } Y_{i,k}\left(X_{ij,k}^{p1/2}\right) < \dfrac{b_w}{2} \\ M_{ih,k}\cdot\left(X_{ij,k}^{p1/2}\right)^2 + N_{ih,k}\cdot\left(X_{ij,k}^{p1/2}\right) + Q_{ih,k} \le 0 \qquad \text{for} \quad h = 1....N_{f,k} \\ \begin{cases} \begin{cases} 0 < \left(X_{ij,k}^{p1/2} + \Delta X\right) < L_d \quad \text{and} \\ 0 < Y_{i,k}\left(X_{ij,k}^{p1/2} + \Delta X\right) < \dfrac{b_w}{2} \quad \text{and} \\ M_{ih,k}\cdot\left(X_{ij,k}^{p1/2} + \Delta X\right)^2 + N_{ih,k}\cdot\left(X_{ij,k}^{p1/2} + \Delta X\right) + Q_{ih,k} < 0 \quad \forall\ h = 1....N_{f,k} \text{ and } h \neq i \end{cases} \\ \text{or} \\ \begin{cases} 0 < \left(X_{ij,k}^{p1/2} - \Delta X\right) < L_d \text{ and} \\ 0 < Y_{i,k}\left(X_{ij,k}^{p1/2} - \Delta X\right) < \dfrac{b_w}{2} \text{ and} \\ M_{ih,k}\cdot\left(X_{ij,k}^{p1/2} - \Delta X\right)^2 + N_{ih,k}\cdot\left(X_{ij,k}^{p1/2} - \Delta X\right) + Q_{ih,k} < 0 \quad \forall\ h = 1....N_{f,k} \text{ and } h \neq i \end{cases} \\ X_{ij,k}^{p1/2} \neq X_{ig,k}^{nlin1/2} \quad \text{with } g = 1,.....,(j-1) \end{cases} \end{cases} \tag{6.55}$$

For further details regarding the origin of the above formulae, see Appendix D. The output of this 1st step is constituted of the matrices $\underline{X}_k^{nlin1}$ and $\underline{X}_k^{nlin2}$, for $k = 1,2,3$, containing, in each i-th row, the values of the abscissa of the effective intersection points of the i-th ellipse with the j-th one for $j = 1....N_{f,k}$. The adjective "*effective*" is used to mean that it is a point effectively useful to determine the area corresponding to the i-th semi-ellipse and delimitated upwards by the relevant non-linear curve $Y_{i,k}(X)$. For the example of Fig. 6.4, they will be as follows, see Fig. 6.14:

$$\underline{X}^{nlin1} = \begin{bmatrix} * & X_{12}^{p1} & * & * & * & * & * \\ X_{21}^{p1} & * & * & * & * & * & * \\ * & * & * & * & * & * & * \\ * & * & * & * & * & * & * \\ * & * & * & * & * & X_{56}^{p1} & * \\ * & * & * & * & X_{65}^{p1} & * & * \\ * & * & * & * & * & * & * \end{bmatrix}; \quad \underline{X}^{nlin2} = \begin{bmatrix} * & * & * & * & * & * & * \\ * & * & * & * & * & * & * \\ * & * & * & * & * & * & * \\ * & * & * & * & * & * & * \\ * & * & * & * & * & * & * \\ * & * & * & * & * & * & * \\ * & * & * & * & * & * & * \end{bmatrix} \tag{6.56}$$

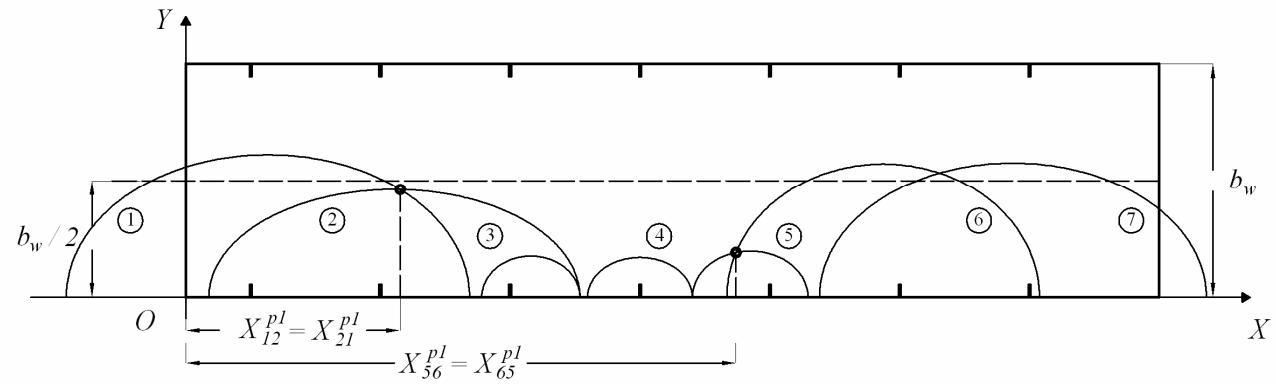

Fig. 6.14 – Intersection points between the semi-ellipses useful for the Non Linear integration, whose abscissa is stored in matrices $\underline{X}^{nlin1}$ and $\underline{X}^{nlin2}$

Step 2: Determination of the effective intersection points of each ellipse $\underline{X}_k^{nlin3}$ with the straight line $Y = b_w/2$

$\underline{X}^{nlin3}$ is a $N_f \times 2$ matrix containing, in the first and second column of the i-th row, X_{i1}^{nlin3} and X_{i2}^{nlin3}, the abscissa values of the left and right intersection points of the relevant semi-ellipse with the straight line $Y = b_w/2$ that result effective for the integration of the corresponding equation $Y_i(X)$. For the k-th configuration, the term $X_{i1,k}^{nlin3}$ of the i-th row of the $\underline{X}_k^{nlin3}$ matrix is set equal to the corresponding term $X_{i1,k}^{q}$, *i.e.*:

$$X_{i1,k}^{nlin3} = X_{i1,k}^{q} \tag{6.57}$$

if $X_{i1,k}^{q}$ is such as to satisfy the acceptance conditions.

Those general acceptance conditions, already introduced for the previous matrices, are as follows:

1. The corresponding point has to be placed inside the range of interest for the Non Linear integration;
2. The corresponding point has to lie upon the upper contour line;
3. It has to constitute effective integration extremity.

They yield the following analytical expressions:

$$\begin{cases} 1)\ \ 0 \le X_{i1,k}^{q} \le L_d \\ 2)\ \ Y_{i,k}\left(X_{i1,k}^{q}\right) \ge Y_{j,k}\left(X_{i1,k}^{q}\right) \quad \text{for } \forall\ j = 1,.,N_{f,k} \\ 3)\ \begin{cases} 0 < \left(X_{i1,k}^{q} - \Delta X\right) < L_d \ \text{ and} \\ Y_{i,k}\left(X_{i1,k}^{q} - \Delta X\right) < \dfrac{b_w}{2} \ \text{ and} \\ Y_{i,k}\left(X_{i1,k}^{q} - \Delta X\right) > Y_{j,k}\left(X_{i1,k}^{q} - \Delta X\right) \quad \forall\ j = 1,.,N_{f,k} \quad j \ne i \end{cases} \end{cases} \tag{6.58}$$

where the first condition simply defines the range of interest that comprehends the eventuality that the semi-ellipse intersects the straight line $Y = b_w/2$ in correspondence of the two vertices of the rectangle of interest $\left(0; \dfrac{b_w}{2}\right)$ and $\left(L_d; \dfrac{b_w}{2}\right)$. The equality signs are, in that respect required, even because this possibility is not contemplated in any of the other matrices of the present Block 5. The second condition checks if the point lies on the upper border line. The third condition checks if, on the left side of the abscissa $X_{i1,k}^{q}$, at an infinitesimal distance ΔX from it, the i-th ellipse results to be constituting the border. This latter is verified if the value of the ordinate there assumed by the i-th ellipse, results higher than any other ellipse and below $Y = b_w/2$. Moreover, as the first expression of the third condition shows, the decremented value of the abscissa has to be comprehended between, but not equal to, the extremities $X = 0$ and $X = L_d$. As to the second expression of the third condition, note that the limitation $Y_{i,k}\left(X_{i1,k}^{q} - \Delta X\right) > 0$ has been omitted because, since we are in a point infinitesimally left of $X_{i1,k}^{q}$, it is superfluous to verify that.

The conditions above yield the following analytical expressions:

$$\begin{cases} 0 \le X_{i1,k}^{q} \le L_d \\ M_{ij,k} \cdot \left(X_{i1,k}^{q} \right)^2 + N_{ij,k} \cdot \left(X_{i1,k}^{q} \right) + Q_{ij,k} \le 0 \quad \text{for } \forall \; j = 1,\ldots\ldots, N_{f,k} \\ 0 < \left(X_{i1,k}^{q} - \Delta X \right) < L_d \\ Y_{i,k} \left(X_{i1,k}^{q} - \Delta X \right) < \dfrac{b_w}{2} \\ M_{ij,k} \cdot \left(X_{i1,k}^{q} - \Delta X \right)^2 + N_{ij,k} \cdot \left(X_{i1,k}^{q} - \Delta X \right) + Q_{ij,k} < 0 \quad \forall \quad j = 1,\ldots\ldots, N_{f,k} \quad j \ne i \end{cases} \tag{6.59}$$

Likewise, the term $X_{i2,k}^{nlin3}$ is set equal to the corresponding auxiliary term $X_{i2,k}^{q}$, *i.e.*:

$$X_{i2,k}^{nlin3} = X_{i2,k}^{q} \tag{6.60}$$

if $X_{i2,k}^{q}$ meets the following acceptance condition:

$$\begin{cases} \\ 1) \;\; 0 \le X_{i2,k}^{q} \le L_d \\ 2) \;\; Y_{i,k} \left(X_{i2,k}^{q} \right) \ge Y_{j,k} \left(X_{i2,k}^{q} \right) \quad \text{for} \quad \forall \; j = 1 \ldots . N_{f,k} \\ \quad \begin{cases} 0 < \left(X_{i2,k}^{q} + \Delta X \right) < L_d \;\; \text{and} \\ 3) \; \begin{cases} Y_{i,k} \left(X_{i2,k}^{q} + \Delta X \right) < \dfrac{b_w}{2} \;\; \text{and} \\ Y_{i,k} \left(X_{i2,k}^{q} + \Delta X \right) > Y_{j,k} \left(X_{i2,k}^{q} + \Delta X \right) \;\; \forall \, j = 1..N_{f,k} \;\; j \ne i \end{cases} \end{cases} \end{cases} \tag{6.61}$$

The conditions above yield the following analytical expressions:

$$\begin{cases} 0 \le X_{i2,k}^{q} \le L_d \\ M_{ij,k} \cdot \left(X_{i2,k}^{q} \right)^2 + N_{ij,k} \cdot \left(X_{i2,k}^{q} \right) + Q_{ij,k} \le 0 \quad \forall \quad j = 1,\ldots., N_{f,k} \\ 0 < \left(X_{i2,k}^{q} + \Delta X \right) < L_d \\ Y_{i,k} \left(X_{i2,k}^{q} + \Delta X \right) < \dfrac{b_w}{2} \\ M_{ij,k} \cdot \left(X_{i2,k}^{q} + \Delta X \right)^2 + N_{ij,k} \cdot \left(X_{i2,k}^{q} + \Delta X \right) + Q_{ij,k} < 0 \quad \forall \quad j = 1,\ldots., N_{f,k} \quad j \ne i \end{cases} \tag{6.62}$$

If those conditions are not fulfilled, the corresponding cell $X_{i2,k}^{nlin3}$ has to be filled with a "*non-value*".

For the Example of Fig. 6.4, the matrix $\underline{X}^{nlin3}$ will be as follows, see Fig. 6.15:

$$\underline{X}^{nlin3} = \begin{bmatrix} X_{12}^{q} & * \\ * & * \\ * & * \\ * & * \\ * & * \\ X_{61}^{q} & * \\ * & X_{72}^{q} \end{bmatrix} \tag{6.63}$$

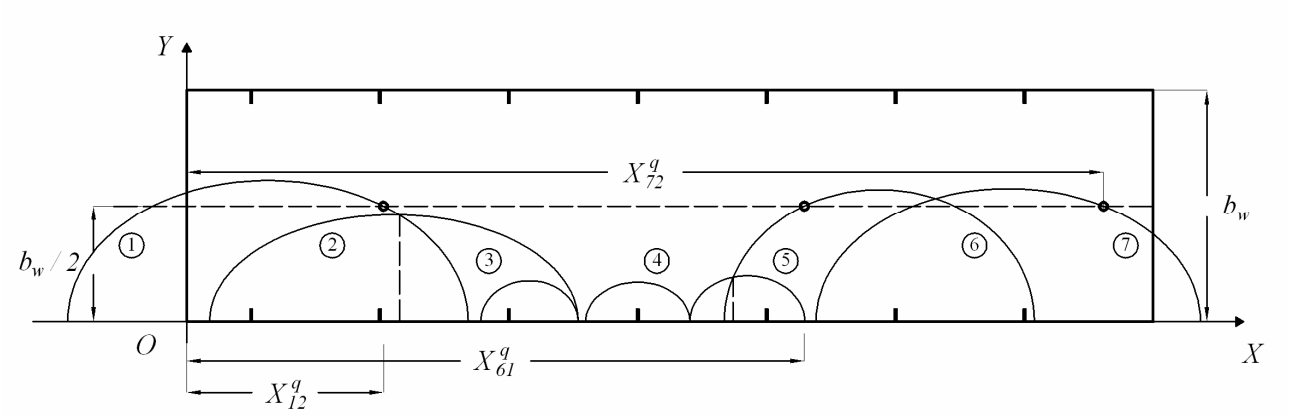

Fig. 6.15 – Intersection points of the semi-ellipses with line $Y = b_w/2$ useful for the Non Linear integration, whose abscissa is contained in $\underline{X}^{nlin3}$

Step 3: Determination of the effective intersection points of each ellipse with the boundary lines $X = 0$ and $X = L_d$

$\underline{X}^{nlin4}$ is a $N_f \times 2$ dimensions matrix containing, in the first cell of the i-th row, the null abscissa value, $X_{i1}^{nlin4} = 0$, and the L_d value in the second cell, $X_{i2}^{nlin4} = L_d$, if those values result to be effective integration limits for the relevant semi-ellipse $Y_i(X)$. The horizontal extremities of the crack plane, $X = 0$ and $X = L_d$ in correspondence of which, according to the above Block 4, the ordinates assumed by the i-th ellipse have been calculated and stored in the corresponding row of the matrix $\underline{Y}_k^e$, will constitute extremities of the non linear integration intervals if the intersection points are such as to satisfy the usual general conditions, repeated hereafter for the sake of clarity:

1. They have to be placed inside the range of interest for the Non Linear integration;
2. They have to lie upon the upper contour line;
3. They have to constitute effective integration extremities.

For the generic k-th configuration, the first column term of the i-th row, $X_{i1,k}^{nlin4}$, of the $\underline{X}_k^{nlin4}$ matrix has to be set equal to zero, *i.e.*:

$$X_{i1,k}^{nlin4} = 0 \tag{6.64}$$

if the ordinate value, $Y_{i1,k}^e$, contained in the corresponding cell of the $\underline{Y}_k^e$ matrix satisfies the above conditions, that, written in mathematical terms, are like follows:

$$\begin{cases} 1)\ \ 0 < Y_{i1,k}^e < \dfrac{b_w}{2} \\ 2)\ \ Y_{i1,k}^e \geq Y_{j1,k}^e \ \text{ for } \ \forall\ \ j = 1....N_{f,k} \\ 3)\ \begin{cases} 0 < Y_{i,k}(0 + \Delta X) < \dfrac{b_w}{2} \ \text{ and} \\ Y_{i,k}(0 + \Delta X) > Y_{j,k}(0 + \Delta X) \ \ \forall\ \ j = 1....N_{f,k} \ \ j \neq i \end{cases} \end{cases} \tag{6.65}$$

that yield the following analytical expressions:

$$\begin{cases} 0 < Y^{e}_{i1,k} < \dfrac{b_w}{2} \\ Q_{ij,k} \le 0 \qquad \forall \;\; j = 1,\ldots..,N_{f,k} \\ 0 < Y_{i,k}\left(\Delta X\right) < \dfrac{b_w}{2} \\ M_{ij,k}\,.\left(\Delta X\right)^2 + N_{ij,k}\,.\left(\Delta X\right) + Q_{ij,k} < 0 \qquad \forall \;\; j = 1,\ldots..,N_{f,k} \quad j \ne i \end{cases} \tag{6.66}$$

otherwise the value $X = 0$ has not to be taken into consideration for the respective i-th ellipse's non linear range, i.e. the corresponding cell $X^{nlin4}_{i1,k}$ ha sto be filled with a "*non-value*".

Likewise, for the generic k-th configuration, the second column term of the i-th row, $X^{nlin4}_{i2,k}$, of the $\underline{X}^{nlin4}_{k}$ matrix has to be set equal to L_d, *i.e.*:

$$X^{nlin4}_{i2,k} = L_d \tag{6.67}$$

if the ordinate value, $Y^{e}_{i2,k}$, contained in the corresponding cell of the $\underline{Y}^{e}_{k}$ matrix satisfies the following conditions:

$$\begin{cases} 1) \;\; 0 < Y^{e}_{i2,k} < \dfrac{b_w}{2} \\ 2) \;\; Y^{e}_{i2,k} \ge Y^{e}_{j2,k} \;\; \text{for} \;\; \forall \;\; j = 1....N_{f,k} \\ 3) \begin{cases} 0 < Y_{i,k}\left(L_d - \Delta X\right) < \dfrac{b_w}{2} \;\; \text{and} \\ Y_{i,k}\left(L_d - \Delta X\right) > Y_{j,k}\left(L_d - \Delta X\right) \;\; \forall \;\; j = 1....N_{f,k} \;\; j \ne i \end{cases} \end{cases} \tag{6.68}$$

that yield the following analytical expressions:

$$\begin{cases} 0 < Y^{e}_{i2,k} < \dfrac{b_w}{2} \\ M_{ij,k}\,.\,L_d^2 + N_{ij,k}\,.\,L_d + Q_{ij,k} \le 0 \qquad \forall \;\; j = 1,\ldots..,N_{f,k} \\ 0 < Y_{i,k}\left(L_d - \Delta X\right) < \dfrac{b_w}{2} \\ M_{ij,k}\,.\left(L_d - \Delta X\right)^2 + N_{ij,k}\,.\left(L_d - \Delta X\right) + Q_{ij,k} < 0 \qquad \forall \;\; j = 1,\ldots..,N_{f,k} \quad j \ne i \end{cases} \tag{6.69}$$

The final result of this step is a matrix $\underline{X}^{nlin4}_{k}$ with $k = 1,2,3$ in which, in general, there will be rows whose first value can be zero or "*non-value"* and whose second term can be L_d or "*non-value"*.

For the Example of Fig. 6.4, the matrix $\underline{X}^{nlin4}$ will be as follows, see Fig. 6.16:

$$\underline{X}^{nlin4} = \begin{bmatrix} * & * \\ * & * \\ * & * \\ * & * \\ * & * \\ * & * \\ * & L_d \end{bmatrix} \tag{6.70}$$

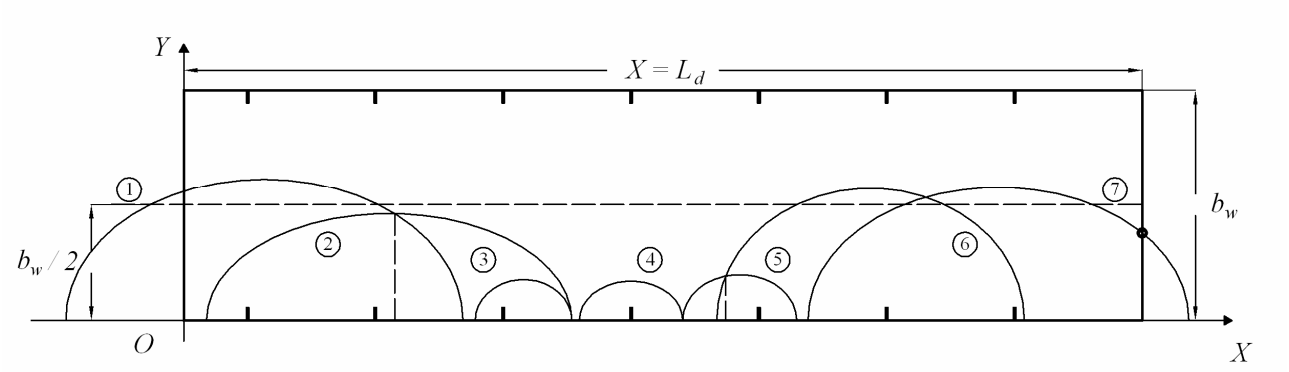

Fig. 6.16 – Intersection points of the semi-ellipses with boundary lines $X = 0$ and $X = L_d$ useful for the Non Linear integration, whose abscissa is contained in $\underline{X}^{nlin4}$

Step 4: Determination of the effective points of intersection $\underline{X}_k^{nlin5}$ of each ellipse with the axis $Y = 0$ of the crack plane reference system

From the output matrix $\underline{G}_k$ of the Block 2, it is necessary to process the abscissa $\left(X_{oi,k} \mp a_{i,k}\right)$ of the vertices of each ellipse with the X axis, *i.e.* its vertices on the major semi-axis, stored respectively in the 7th and 8th columns and accept or discard them if they result respectively useful or unuseful for the integration of the i-th ellipse in its non-linear range.

The points whose abscissa is $\left(X_{oi,k} - a_{i,k}\right)$ and $\left(X_{oi,k} + a_{i,k}\right)$ are effective points in the sense that they constitute integration limits for i-th ellipse, if they satisfy the following conditions of acceptance:

1. They are comprehended in the range of interest;
2. Any other j-th ellipse, with $j = 1.....N_f$, either does not pass through it or passes and assumes null ordinate $Y = 0$;
3. It constitutes an effective integration extremity.

As to the third condition, $\left(X_{oi,k} - a_{i,k}\right)$ results to be useful for the non linear integration of the i-th ellipse if, in an abscissa value infinitesimally more rightwards *i.e.* $\left(X_{oi,k} - a_{i,k}\right) + \Delta X$, the corresponding i-th ellipse constitutes the upper border line. Likewise, the vertex $\left(X_{oi,k} + a_{i,k}\right)$, results to be useful for the i-th ellipse if this latter constitutes the upper border line for $\left(X_{oi,k} + a_{i,k}\right) - \Delta X$.

$\underline{X}^{nlin5}$ is a $N_f \times 2$ dimensions matrix containing the abscissa of the vertices of the major semi-axis of the semi-ellipse that constitute effective integration extremities for the ellipses. For the k-th configuration, the first column term of the i-th row, $X_{i1,k}^{nlin5}$, of the $\underline{X}_k^{nlin5}$ matrix has to be set equal to the term $G_{i7,k}$, stored in the seventh column cell of the corresponding i-th row of the matrix $\underline{G}_k$ *i.e.*:

$$X_{i1,k}^{nlin5} = G_{i7,k} \tag{6.71}$$

if it is such as to satisfy the following conditions:

$$\begin{cases} 0 \le G_{i7,k} \le L_d \\ Y_{j,k}\left(G_{i7,k}\right) = 0 \text{ or } Y_{j,k}\left(G_{i7,k}\right) \text{ is not real} \quad \text{for} \quad j = 1;.....;\ N_{f,k} \\ \begin{cases} 0 < G_{i7,k} + \Delta X < L_d \\ Y_{i,k}\left(G_{i7,k} + \Delta X\right) > Y_{j,k}\left(G_{i7,k} + \Delta X\right) \quad \text{for } j = 1;.....;N_{f,k} \quad \text{and} \quad j \ne i \end{cases} \end{cases} \tag{6.72}$$

that yield the following analytical expressions:

$$\begin{cases} 0 \le G_{i7,k} \le L_d \\ -\dfrac{\left[E_{j1,k}.\left(G_{i7,k}\right)^2 + E_{j3,k}.\left(G_{i7,k}\right) + E_{j4,k}\right]}{E_{j2,k}} \le 0 \quad \forall \quad j = 1;.....;\ N_{f,k} \\ 0 < \left(G_{i7,k} + \Delta X\right) < L_d \\ M_{ij,k}.\left(G_{i7,k} + \Delta X\right)^2 + N_{ij,k}.\left(G_{i7,k} + \Delta X\right) + Q_{ij,k} < 0 \quad \forall\ j = 1;.....;N_{f,k} \quad \text{and} \quad j \ne i \end{cases} \tag{6.73}$$

If the above conditions are not met, it is necessary to assume "*non-value*" in order to discard the previous auxiliary value.

Likewise, for the k-th configuration, the second column term of the i-th row, $X_{i2,k}^{nlin5}$, of the $\underline{X}_k^{nlin5}$ matrix has to be set equal to the term $G_{i8,k}$, stored in the eight-th column cell of the corresponding i-th row of the matrix $\underline{G}_k$ *i.e.*:

$$X_{i2,k}^{nlin5} = G_{i8,k} \tag{6.74}$$

if it is such as to satisfy the following conditions:

$$\begin{cases} 0 \le G_{i8,k} \le L_d \\ Y_{j,k}\left(G_{i8,k}\right) \le 0 \quad \text{for} \quad j = 1;.....;\ N_{f,k} \\ \begin{cases} 0 < G_{i8,k} - \Delta X < L_d \\ Y_{i,k}\left(G_{i8,k} - \Delta X\right) > Y_{j,k}\left(G_{i8,k} - \Delta X\right) \quad \text{for } j = 1;.....;N_{f,k} \quad \text{and} \quad j \ne i \end{cases} \end{cases} \tag{6.75}$$

that yield the following analytical expressions:

$$\begin{cases} 0 \le G_{i8,k} \le L_d \\ -\dfrac{\left[E_{j1,k}.\left(G_{i8,k}\right)^2 + E_{j3,k}.\left(G_{i8,k}\right) + E_{j4,k}\right]}{E_{j2,k}} \le 0 \quad \forall \quad j = 1;.....;\ N_{f,k} \\ 0 < \left(G_{i8,k} - \Delta X\right) < L_d \\ M_{ij,k}.\left(G_{i8,k} - \Delta X\right)^2 + N_{ij,k}.\left(G_{i8,k} - \Delta X\right) + Q_{ij,k} < 0 \quad \forall\ j = 1;.....;N_{f,k} \quad \text{and} \quad j \ne i \end{cases} \tag{6.76}$$

If the above conditions are not met, it is necessary to fulfil the cell $X_{i2,k}^{nlin5}$ with a "*non-value*" in order to discard the previous auxiliary value. For the Example of Fig. 6.4, the matrix $\underline{X}^{nlin5}$ will be as follows, see Fig. 6.17:

$$\underline{X}^{nlin5} = \begin{bmatrix} * & * \\ * & X_{o2} + a_2 \\ * & * \\ X_{o4} - a_4 & X_{o4} + a_4 \\ X_{o5} - a_5 & * \\ * & * \\ * & * \end{bmatrix} \tag{6.77}$$

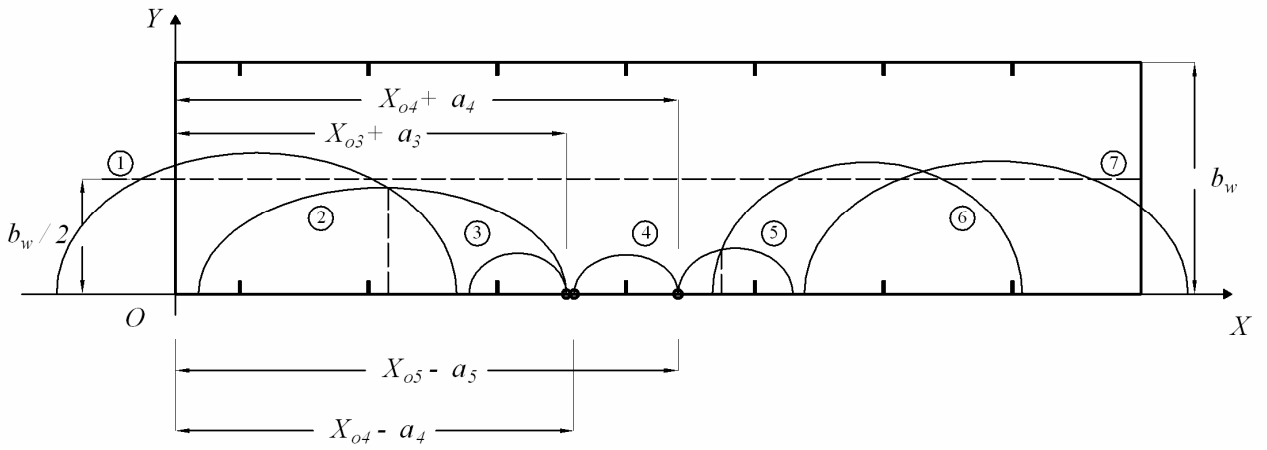

Fig. 6.17 – Vertices of the semi-ellipses on the line $Y = 0$ useful for the Non Linear integration, whose abscissa is contained in $\underline{X}^{nlin5}$

Step 5: Determination of the final matrix of the Non Linear effective integration points $\underline{X}_k^{nlin}$

Once all the auxiliary matrices for the integration points in the Non-Linear range $\underline{X}_k^{nlin1}$, $\underline{X}_k^{nlin2}$, $\underline{X}_k^{nlin3}$, $\underline{X}_k^{nlin4}$, $\underline{X}_k^{nlin5}$, are determined as above specified, they are ready to be joined in the matrix $\underline{X}_k^{nlin}$ containing, in each i-th row, the couples of points that define the integration intervals for the relevant i-th ellipse equation $Y_{i,k}(X)$.

It is necessary to determine, first, the vector $\underline{n}_k^{nlin}$ for $k = 1, 2, 3$.

$\underline{n}^{nlin}$ is a $N_f \times 1$ vector containing, in the i-th row, the maximum number of real abscissa values constituting effective integration limits for the relevant i-th semi-ellipse equation (the integrand function is nonlinear in the X variable). For the k-th configuration, the general i-th term, $n_{i,k}^{nlin}$, of the $\underline{n}_k^{nlin}$ vector is equal to the number of real values present amongst all the terms stored in the corresponding i-th row of all the auxiliary matrices, *i.e.*:

$$n_{i,k}^{nlin} = \text{real numbers}\left\{X_{i,k}^{nlin1}; X_{i,k}^{nlin2}; X_{i,k}^{nlin3}; X_{i,k}^{nlin4}; X_{i,k}^{nlin5}\right\} \tag{6.78}$$

The number of columns of the $\underline{X}_k^{nlin}$ matrix, n_k^{nlin}, is equal to the maximum number of effective values among all the semi-ellipses for the k-th configuration, *i.e.*:

$$n_k^{nlin} = \max\left\{n_{i,k}^{nlin}\right\} \quad \text{with } i = 1;...;N_{f,k} \tag{6.79}$$

The $\underline{X}_k^{nlin}$ matrix is then built by joining, for each i-th row corresponding to the i-th semi-ellipse, the effective terms, discarding the "non-values", present in the corresponding i-th row of the auxiliary matrices $\underline{X}_k^{nlin1}$, $\underline{X}_k^{nlin2}$, $\underline{X}_k^{nlin3}$,

$\underline{X}_k^{nlin4}$, $\underline{X}_k^{nlin5}$ and sorting them in increasing order. For instance, the intermediate informations $\underline{n}^{nlin}$, n^{nlin} and the final matrix $\underline{X}_k^{nlin}$ for the example of Fig. 6.4 are as follows, see Fig. 6.18:

$$\underline{n}^{nlin} = \begin{bmatrix} 2 \\ 2 \\ 0 \\ 2 \\ 2 \\ 2 \\ 2 \end{bmatrix}; \; n^{nlin} = 2; \; \underline{X}^{nlin} = \begin{bmatrix} X_{12}^{p1} & X_{12}^{q} \\ X_{21}^{p1} & X_{o2} + a_2 \\ * & * \\ X_{o4} - a_4 & X_{o4} + a_4 \\ X_{o5} - a_5 & X_{56}^{p1} \\ X_{65}^{p1} & X_{61}^{q} \\ X_{72}^{q} & L_d \end{bmatrix} \tag{6.80}$$

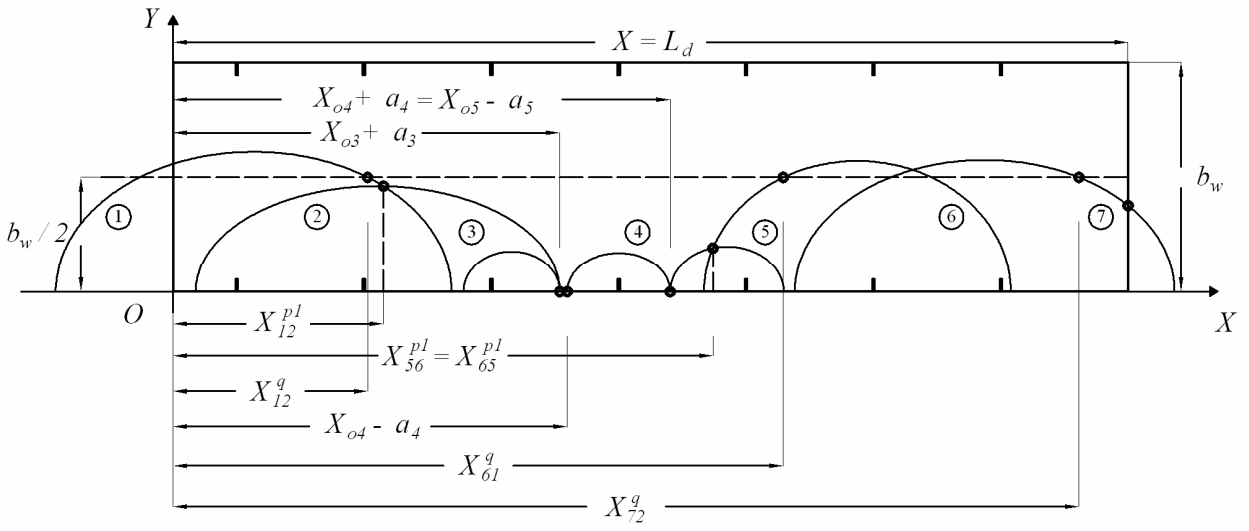

Fig. 6.18 – Determination of the effective matrix of the integration points in the non-linear range $\underline{X}^{nlin}$

Block 6: Determination of the Matrix of the Effective Integration Points in the Linear range $\underline{X}_k^{lin}$

The input of this Block is constituted of the previously determined auxiliary matrices: $\underline{X}_k^{p1}$, $\underline{X}_k^{p2}$, $\underline{X}_k^{q}$, $\underline{Y}_k^{e}$, $\underline{M}_k$, $\underline{N}_k$, $\underline{Q}_k$ with $k = 1,2,3$. The output will be composed of the auxiliary matrices containing the abscissa of the effective integration points for each semi-ellipse in its corresponding linear range of integration *i.e.*: $\underline{X}_k^{lin1}$, $\underline{X}_k^{lin2}$, $\underline{X}_k^{lin3}$, $\underline{X}_k^{lin4}$. Then, those four matrices will be joined in one only: $\underline{X}_k^{lin}$ with $k = 1,2,3$.

$\underline{X}^{lin}$ is a $N_f \times n^{lin}$ dimensions matrix containing, in the i-th row, the couples of abscissa values constituting limits of the integration intervals, in correspondence of the i-th semi-ellipse, of the equation $Y = b_w/2$. For the generic k-th configuration, the matrix $\underline{X}_k^{lin}$ has $N_{f,k} \times n_k^{lin}$ dimensions where n_k^{lin} is the maximum number (even) of real values of integration limits amongst all the $N_{f,k}$ semi-ellipses of that configuration. To evaluate $\underline{X}_k^{lin}$, four other auxiliary

matrices $\underline{X}_k^{lin1}$, $\underline{X}_k^{lin2}$, $\underline{X}_k^{lin3}$, $\underline{X}_k^{lin4}$ have to be determined, first, based on the auxiliary ones $\underline{X}_k^{p1}$, $\underline{X}_k^{p2}$, $\underline{X}_k^{q}$, $\underline{Y}_k^{e}$, $\underline{M}_k$, $\underline{N}_k$, $\underline{Q}_k$, already built.

Step 1: Determination of the matrices of the effective intersection points between ellipses $\underline{X}_k^{lin1}$ $\underline{X}_k^{lin2}$

$\underline{X}^{lin1}$ and $\underline{X}^{lin2}$ are two $N_f \times N_f$ dimensions matrices containing, in the i-th row, the abscissa values, amongst those already calculated and stored in the corresponding i-th row of the auxiliary matrices $\underline{X}^{p1}$ and $\underline{X}^{p2}$, respectively, that, according to the acceptance conditions hereafter specified, effectively constitute useful integration limits for the linear range ascribed to the relevant i-th semi-ellipse. For the k-th configuration, the general j-th term $X_{ij,k}^{lin1/2}$ of the i-th row of the $\underline{X}_k^{lin1/2}$ matrix is set equal to the corresponding term $X_{ij,k}^{p1/2}$ of the corresponding auxiliary matrix $\underline{X}_k^{p1/2}$, *i.e.*:

$$X_{ij,k}^{lin1/2} = X_{ij,k}^{p1/2} \tag{6.81}$$

if $X_{ij,k}^{p1/2}$ is such as to satisfy, for the i-th semi-ellipse, the following acceptance conditions:

1. The corresponding point is comprehended in the range of interest;
2. The point is located on the upper border line;
3. The point constitutes effective integration extremity for the i-th semi-ellipse in the linear integration range;
4. It is not equal to the values already stored in the i-th row.

The auxiliary intersection point between the i-th and j-th semi-ellipses, whose abscissa value is $X_{ij,k}^{p1/2}$, is accepted, for the i-th semi-ellipse, if the following conditions are fulfilled:

$$\begin{cases} 1)\ 0 < X_{ij,k}^{p1/2} < L_d \text{ and } Y_{i,k}\left(X_{ij,k}^{p1/2}\right) > \dfrac{b_w}{2} \\ 2)\ Y_{i,k}\left(X_{ij,k}^{p1/2}\right) \geq Y_{h,k}\left(X_{ij,k}^{p1/2}\right) \quad \text{for} \quad h = 1....N_{f,k} \\ 3) \begin{cases} \begin{cases} 0 < \left(X_{ij,k}^{p1/2} + \Delta X\right) < L_d \text{ and} \\ Y_{i,k}\left(X_{ij,k}^{p1/2} + \Delta X\right) > \dfrac{b_w}{2} \text{ and} \\ Y_{i,k}\left(X_{ij,k}^{p1/2} + \Delta X\right) > Y_{h,k}\left(X_{ij,k}^{p1/2} + \Delta X\right) \ \forall h = 1,...,N_{f,k} \text{ and } h \neq i \end{cases} \\ \text{or} \\ \begin{cases} 0 < \left(X_{ij,k}^{p1/2} - \Delta X\right) < L_d \text{ and} \\ Y_{i,k}\left(X_{ij,k}^{p1/2} - \Delta X\right) > \dfrac{b_w}{2} \text{ and} \\ Y_{i,k}\left(X_{ij,k}^{p1/2} - \Delta X\right) > Y_{h,k}\left(X_{ij,k}^{p1/2} - \Delta X\right) \ \forall h = 1,...,N_{f,k} \text{ and } h \neq i \end{cases} \end{cases} \\ 4)\ X_{ij,k}^{p1/2} \neq X_{ig,k}^{e1/2} \text{ with } g = 1,.....,(j-1) \end{cases} \tag{6.82}$$

The first condition verifies if the point lies within the range of interest. Note that the absence of equality signs in $0 < X_{ij,k}^{p1/2} < L_d$ means that points of intersection between semi-ellipses lying on the border lines $X = 0$ and $X = L_d$ are unuseful for this case since they have already been contemplated elsewhere (see Step 3 of the present Block 6 of

calculations). At the same time, for the Linear integration range, only the intersection points lying above the line $Y = b_w/2$ are useful.

The second condition checks if the point effectively lies on the upper border line and simply verifies if the value of the ordinate assumed by the i-th semi-ellipse is higher than or equal to the ordinate that any other h-th semi-ellipse assumes there.

The third condition checks if the general point $X_{ij,k}^{p1/2}$ effectively constitutes a useful integration extremity for the i-th semi-ellipse *i.e.* if, on either the left side $\left(X_{ij,k}^{p1/2} - \Delta X\right)$ or on the right side $\left(X_{ij,k}^{p1/2} - \Delta X\right)$, the i-th ellipse is higher than any other ellipse passing through it.

The fourth condition aims at avoiding to store, in the i-th row of the matrix of the effective points, $\underline{X}_k^{lin1/2}$ a value $X_{ij,k}^{p1/2}$ that has already been stored as intersection with another j-th ellipse whose ordinal number *g* is lower than the current value assumed by the counter *j*. This is for example the case in which several ellipses intersect each other in the same point (see, for instance, Fig. 6.13 for the Non-Linear case). In that case, the same value might be stored twice, creating problems in the next steps of the algorithm since there could be an odd number of integration extremities. On the contrary, the algorithm has to select couples of abscissa values. This selection could also be done in the final step of this Block in which the final matrix $\underline{X}_k^{lin}$ of the effective integration points is determined but maybe it is preferable to carry out it now (while analyzing the values $X_{ij,k}^{p1/2}$ on the i-th row from left to right).

Conditions (6.82) yield the following analytical expressions:

$$\begin{cases} 0 < X_{ij,k}^{p1/2} < L_d \ \text{ and } \ Y_{i,k}\left(X_{ij,k}^{p1/2}\right) > \dfrac{b_w}{2} \\ M_{ih,k}.\left(X_{ij,k}^{p1/2}\right)^2 + N_{ih,k}.\left(X_{ij,k}^{p1/2}\right) + Q_{ih,k} \le 0 \qquad \text{for} \quad h = 1....N_{f,k} \\ \begin{cases} \begin{cases} 0 < \left(X_{ij,k}^{p1/2} + \Delta X\right) < L_d \\ Y_{i,k}\left(X_{ij,k}^{p1/2} + \Delta X\right) > \dfrac{b_w}{2} \\ M_{ih,k}.\left(X_{ij,k}^{p1/2} + \Delta X\right)^2 + N_{ih,k}.\left(X_{ij,k}^{p1/2} + \Delta X\right) + Q_{ih,k} < 0 \quad \forall h \ne i \end{cases} \\ \text{or} \\ \begin{cases} 0 < \left(X_{ij,k}^{p1/2} - \Delta X\right) < L_d \ \text{ and} \\ Y_{i,k}\left(X_{ij,k}^{p1/2} - \Delta X\right) > \dfrac{b_w}{2} \ \text{ and} \\ M_{ih,k}.\left(X_{ij,k}^{p1/2} - \Delta X\right)^2 + N_{ih,k}.\left(X_{ij,k}^{p1/2} - \Delta X\right) + Q_{ih,k} < 0 \quad \forall h \ne i \end{cases} \\ X_{ij,k}^{p1/2} \ne X_{ig,k}^{lin1/2} \ \text{ with } \ g = 1,.....,(j-1) \end{cases} \end{cases} \tag{6.83}$$

as usual, if the auxiliary abscissa value $X_{ij,k}^{p1/2}$ does not fulfil all conditions (6.83), the corresponding cell $X_{ij,k}^{lin1/2}$ has to be filled with a "*non-value*". For further details on the origin of the above formulae, see Appendices A and D.

For the example of Fig. 6.4, they will be as follows, see Fig. 6.19:

$$\underline{X}^{lin1} = \begin{bmatrix} * & * & * & * & * & * & * \\ * & * & * & * & * & * & * \\ * & * & * & * & * & * & * \\ * & * & * & * & * & * & * \\ * & * & * & * & * & * & * \\ * & * & * & * & * & * & X_{56}^{p1} \\ * & * & * & * & * & X_{56}^{p1} & * \end{bmatrix}; \quad \underline{X}^{lin2} = \begin{bmatrix} * & * & * & * & * & * & * \\ * & * & * & * & * & * & * \\ * & * & * & * & * & * & * \\ * & * & * & * & * & * & * \\ * & * & * & * & * & * & * \\ * & * & * & * & * & * & * \\ * & * & * & * & * & * & * \end{bmatrix} \tag{6.84}$$

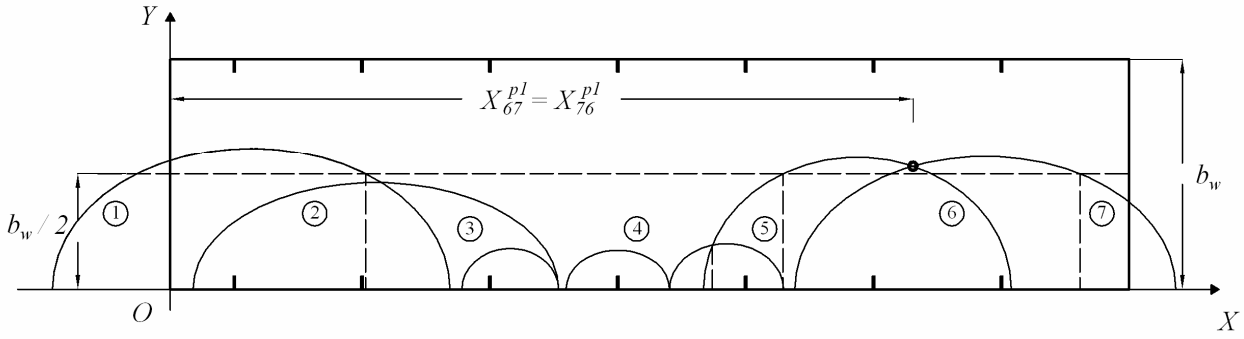

Fig. 6.19 – Intersection points between the semi-ellipses, useful for the Linear integration, whose abscissa is stored in matrices $\underline{X}^{lin1}$ and $\underline{X}^{lin2}$

Step 2: Determination of the effective intersection points of each ellipse $\underline{X}_k^{lin3}$ with the straight line $Y = b_w/2$

It is necessary to determine, among the previously determined auxiliary points of intersection of each ellipse with the straight line, whose abscissa is stored in $\underline{X}_k^q$, those satisfying the following conditions:

1. They have to be placed inside the range of interest for the Linear integration;
2. They have to lie upon the upper contour line;
3. They have to constitute effective linear integration extremities.

$\underline{X}^{lin3}$ is a $N_f \times 2$ matrix containing, in the first and second columns of the i-th row, X_{i1}^{lin3} and X_{i2}^{lin3}, respectively, the abscissa values of the left and right intersection points of the relevant semi-ellipse with the straight line $Y = b_w/2$ that result effective for the integration of the corresponding equation $Y = b_w/2$. For the k-th configuration, the first column term of the i-th row, $X_{i1,k}^{lin3}$, of the $\underline{X}_k^{lin3}$ matrix is set equal to the corresponding term $X_{i1,k}^q$ of the auxiliary matrix $\underline{X}_k^q$, *i.e.*:

$$X_{i1,k}^{lin3} = X_{i1,k}^q \tag{6.85}$$

if $X_{i1,k}^q$ satisfies the following conditions:

$$\begin{cases} 1)\ \ 0 \le X_{i1,k}^{q} \le L_d \\ 2)\ \ Y_{i,k}\left(X_{i1,k}^{q}\right) \ge Y_{j,k}\left(X_{i1,k}^{q}\right) \quad \text{for} \quad j = 1,.,N_{f,k} \\ 3)\ \begin{cases} 0 < \left(X_{i1,k}^{q} + \Delta X\right) < L_d \ \text{ and} \\ Y_{i,k}\left(X_{i1,k}^{q} + \Delta X\right) > \dfrac{b_w}{2} \ \text{ and} \\ Y_{i,k}\left(X_{i1,k}^{q} + \Delta X\right) > Y_{j,k}\left(X_{i1,k}^{q} + \Delta X\right) \ \forall\ j = 1,.,N_{f,k} \ \ j \ne i \end{cases} \end{cases} \tag{6.86}$$

where the first condition simply defines the range of interest that comprehends the eventuality that the semi-ellipse intersects the straight line $Y = b_w/2$ in correspondence of the two vertices of the rectangle of interest $\left(0; \frac{b_w}{2}\right)$ and $\left(L_d; \frac{b_w}{2}\right)$. The equality signs are in that respect, required, even because this possibility is contemplated in none of the other matrices of the effective integration points in the Linear Range analysed in the other steps of the present Block 6.

The second condition checks if the point lies on the upper border line.

The third condition checks if, on the right side of the abscissa $X_{i1,k}^{q}$, at an infinitesimal distance ΔX from it, the i-th semi-ellipse results to constitute the border. This latter condition is verified if $Y_{i,k}$ results higher than any other semi-ellipse and above $Y = b_w/2$. Note that the second inequality of the third condition is necessary because otherwise the algorithm would also select points of tangency of the ellipse with the straight line $Y = b_w/2$ (see cases 4-5 of Appendix E) . The conditions above yield the following analytical expressions:

$$\begin{cases} 0 \le X_{i1,k}^{q} \le L_d \\ M_{ij,k} \cdot \left(X_{i1,k}^{q}\right)^2 + N_{ij,k} \cdot \left(X_{i1,k}^{q}\right) + Q_{ij,k} \le 0 \quad \forall \quad j = 1....N_{f,k} \\ 0 < \left(X_{i1,k}^{q} + \Delta X\right) < L_d \\ Y_{i,k}\left(X_{i1,k}^{q} + \Delta X\right) > \dfrac{b_w}{2} \\ M_{ij,k} \cdot \left(X_{i1,k}^{q} + \Delta X\right)^2 + N_{ij,k} \cdot \left(X_{i1,k}^{q} + \Delta X\right) + Q_{ij,k} < 0 \quad \forall \quad j = 1..N_{f,k} \quad j \ne i \end{cases} \tag{6.87}$$

Thus, if those conditions are not fulfilled, the cell $X_{i1,k}^{lin3}$ has to be filled with a "*non-value*".

Likewise, the second column term of the i-th row $X_{i2,k}^{lin3}$ is set equal to the corresponding auxiliary term $X_{i2,k}^{q}$, *i.e.*:

$$X_{i2,k}^{lin3} = X_{i2,k}^{q} \tag{6.88}$$

if $X_{i2,k}^{q}$ meets the following acceptance condition:

$$\begin{cases} 1)\ \ 0 \le X_{i2,k}^{q} \le L_d \\ 2)\ \ Y_{i,k}\left(X_{i2,k}^{q}\right) \ge Y_{j,k}\left(X_{i2,k}^{q}\right) \quad \text{for} \quad \forall\ j = 1,.,N_{f,k} \\ 3) \begin{cases} 0 < \left(X_{i2,k}^{q} - \Delta X\right) < L_d \ \text{ and} \\ Y_{i,k}\left(X_{i2,k}^{q} - \Delta X\right) > \dfrac{b_w}{2} \ \text{and} \\ Y_{i,k}\left(X_{i2,k}^{q} - \Delta X\right) > Y_{j,k}\left(X_{i2,k}^{q} - \Delta X\right)\ \forall\ j = 1,.,N_{f,k}\ \ j \ne i \end{cases} \end{cases} \tag{6.89}$$

The conditions above yield the following analytical expressions:

$$\begin{cases} 0 \le X_{i2,k}^{q} \le L_d \\ M_{ij,k}\cdot\left(X_{i2,k}^{q}\right)^2 + N_{ij,k}\cdot\left(X_{i2,k}^{q}\right) + Q_{ij,k} \le 0 \quad \forall\ \ j = 1....N_{f,k} \\ 0 < \left(X_{i2,k}^{q} - \Delta X\right) < L_d \\ Y_{i,k}\left(X_{i2,k}^{q} - \Delta X\right) > \dfrac{b_w}{2} \\ M_{ij,k}\cdot\left(X_{i2,k}^{q} - \Delta X\right)^2 + N_{ij,k}\cdot\left(X_{i2,k}^{q} - \Delta X\right) + Q_{ij,k} < 0 \quad \forall\ \ j = 1..N_{f,k} \quad j \ne i \end{cases} \tag{6.90}$$

Thus, if those conditions are not fulfilled, the cell $X_{i2,k}^{lin3}$ has to be filled with a "*non-value*".

For the Example of Fig. 6.4, the matrix $\underline{X}^{lin3}$ will be as follows, see Fig. 6.20:

$$\underline{X}^{nlin3} = \begin{bmatrix} X_{12}^{q} & * \\ * & * \\ * & * \\ * & * \\ * & * \\ X_{61}^{q} & * \\ * & X_{72}^{q} \end{bmatrix} \tag{6.91}$$

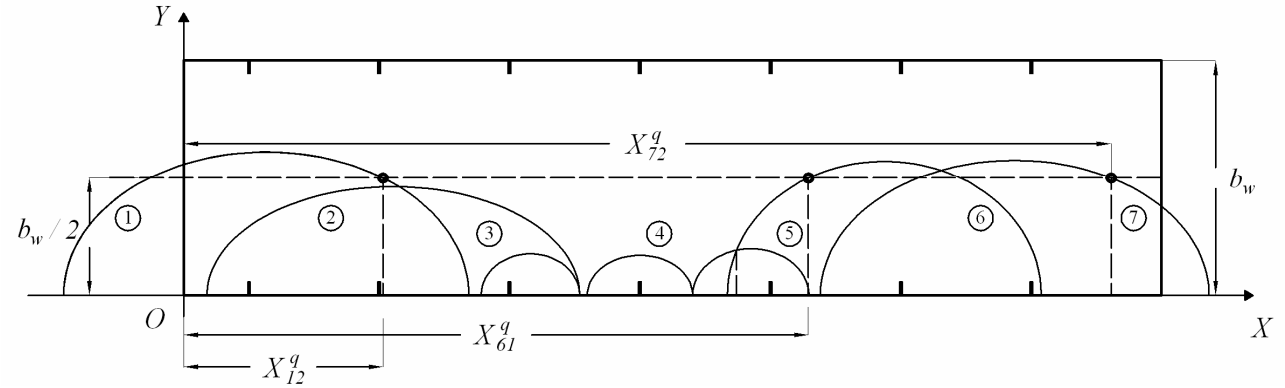

Fig. 6.20 – Intersection points of the semi-ellipses with line $Y = b_w/2$ useful for the Non Linear integration, whose abscissa is contained in $\underline{X}^{nlin3}$

Step 3: Determination of the effective intersection points $\underline{X}_k^{lin4}$ of each ellipse with the boundary lines $X = 0$ and $X = L_d$

The horizontal extremities of the crack plane, $X = 0$ and $X = L_d$ in correspondence of which, according to the above Block 4, the ordinates assumed by the i-th semi-ellipse have been calculated and stored in the corresponding i-th row of the matrix $\underline{Y}_k^e$, will constitute extremities of the linear integration intervals if the relevant points $\left(0; Y_{i1,k}^e\right)$ and $\left(L_d; Y_{i2,k}^e\right)$ are such as to satisfy the usual general conditions, repeated hereafter for the sake of clarity:

1. They have to be placed inside the range of interest for the Linear integration;
2. They have to lie upon the upper contour line;
3. They have to constitute effective integration extremities.

$\underline{X}^{lin4}$ is a $N_f \times 2$ dimensions matrix containing, in the first cell of the i-th row, the null abscissa value, $X_{i1}^{lin4} = 0$, and the L_d value in the second cell, $X_{i2}^{lin4} = L_d$, if those values result to be effective integration limits for the linear range ascribed to the relevant i-th semi-ellipse. For the generic k-th configuration, the first cell of the i-th row, $X_{i1,k}^{lin4}$, of the $\underline{X}_k^{lin4}$ matrix has to be set equal to zero, *i.e.*:

$$X_{i1,k}^{lin4} = 0 \tag{6.92}$$

if $Y_{i1,k}^e$ satisfies the above conditions, that, when re-written in mathematical terms, are like follows:

$$\begin{cases} 1) \;\; Y_{i1,k}^e > \dfrac{b_w}{2} \\ 2) \; Y_{i1,k}^e \geq Y_{j1,k}^e \;\; \text{for} \;\; \forall \;\; j = 1....N_{f,k} \\ 3) \; \begin{cases} Y_{i,k}\left(0 + \Delta X\right) > \dfrac{b_w}{2} \;\; \text{and} \\ Y_{i,k}\left(0 + \Delta X\right) > Y_{j,k}\left(0 + \Delta X\right) \;\; \forall \;\; j = 1....N_{f,k} \;\; j \neq i \end{cases} \end{cases} \tag{6.93}$$

That yield the following analytical expressions:

$$\begin{cases} Y_{i1,k}^e > \dfrac{b_w}{2} \\ Q_{ij,k} \leq 0 \quad \forall \;\; j = 1....N_{f,k} \\ Y_{i,k}\left(\Delta X\right) > \dfrac{b_w}{2} \\ M_{ij,k}.\left(\Delta X\right)^2 + N_{ij,k}.\left(\Delta X\right) + Q_{ij,k} < 0 \quad \forall \;\; j = 1....N_{f,k} \;\; j \neq i \end{cases} \tag{6.94}$$

otherwise the value $X = 0$ has not to be taken into consideration for the respective i-th ellipse's linear range.

Likewise, the second column term of the i-th row, $X_{i2,k}^{lin4}$, of the $\underline{X}_k^{lin4}$ matrix has to be set equal to L_d, *i.e.*:

$$X_{i2,k}^{lin4} = L_d \tag{6.95}$$

if the ordinate value, $Y_{i2,k}^e$, contained in the corresponding cell of the matrix $\underline{Y}_k^e$ satisfies the following conditions:

$$\begin{cases} 1)\ \ Y^{e}_{i2,k} > \dfrac{b_w}{2} \\ 2)\ \ Y^{e}_{i2,k} \geq Y^{e}_{j2,k} \ \ \text{for} \ \ \forall\ \ j = 1....N_{f,k} \\ 3) \begin{cases} Y_{i,k}\left(L_d - \Delta X\right) > \dfrac{b_w}{2} \ \ \text{and} \\ Y_{i,k}\left(L_d - \Delta X\right) > Y_{j,k}\left(L_d - \Delta X\right) \ \ \forall\ \ j = 1....N_{f,k} \ \ j \neq i \end{cases} \end{cases} \tag{6.96}$$

That yield the following analytical expressions:

$$\begin{cases} Y^{e}_{i2,k} > \dfrac{b_w}{2} \\ M_{ij,k}\ .L_d^2 + N_{ij,k}.L_d + Q_{ij,k} \leq 0 \quad \forall\ \ j = 1,....,N_{f,k} \\ Y_{i,k}\left(L_d - \Delta X\right) > \dfrac{b_w}{2} \\ M_{ij,k}.\left(L_d - \Delta X\right)^2 + N_{ij,k}.\left(L_d - \Delta X\right) + Q_{ij,k} < 0 \quad \forall\ \ j = 1,....,N_{f,k} \quad j \neq i \end{cases} \tag{6.97}$$

otherwise the value $X = L_d$ has not to be taken into consideration for the respective i-th ellipse's linear range.

The final result of this step is a matrix $\underline{X}^{lin4}_{k}$, with $k = 1,2,3$, in which, in general, there will be rows whose first value can be *zero* or "*non-value"* and whose second term can be L_d or "*non-value"*.

For the Example of Fig. 6.4, the matrix $\underline{X}^{lin4}$ will be as follows, see Fig. 6.21:

$$\underline{X}^{lin4} = \begin{bmatrix} 0 & * \\ * & * \\ * & * \\ * & * \\ * & * \\ * & * \\ * & * \end{bmatrix} \tag{6.98}$$

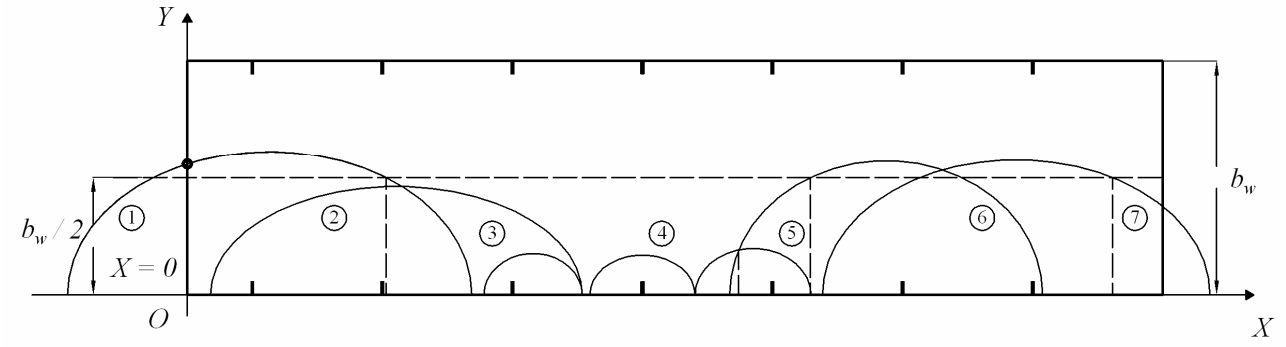

Fig. 6.21 – Intersection points of the semi-ellipses with boundary lines $X = 0$ and $X = L_d$ useful for the Non Linear integration, whose abscissa is contained in $\underline{X}^{nlin4}$

Step 4: Determination of the intervals of integration for the ellipses in the Linear range $\underline{X}^{lin}_{k}$

Once all the auxiliary matrices for the integration points in the Linear range, $\underline{X}_k^{lin1}$, $\underline{X}_k^{lin2}$, $\underline{X}_k^{lin3}$, $\underline{X}_k^{lin4}$, are determined as above specified, they are ready to be joined in the matrix $\underline{X}_k^{lin}$ containing, in each i-th row, the couples of abscissa that define the integration intervals of the equation $Y = \frac{b_w}{2}$ for the relevant i-th ellipse.

$\underline{n}^{lin}$ is a $N_f \times 1$ vector containing, in the i-th row, the maximum number of real abscissa values constituting effective integration limits for the corresponding i-th semi-ellipse in the linear range (the integrand function is independent of the X variable). For the k-th configuration, the general i-th term, $n_{i,k}^{lin}$, of the $\underline{n}_k^{lin}$ vector is equal to the number of real values present amongst all the terms stored in the corresponding i-th row of all the auxiliary matrices, *i.e.*:

$$n_{i,k}^{lin} = \text{real numbers}\left\{X_{i,k}^{lin1}; X_{i,k}^{lin2}; X_{i,k}^{lin3}; X_{i1,k}^{lin4}\right\} \tag{6.99}$$

The number of columns of the $\underline{X}_k^{lin}$ matrix, n_k^{lin}, is equal to the maximum number of effective values among all the semi-ellipses for the k-th configuration, *i.e.*:

$$n_k^{lin} = \max\left\{n_{i,k}^{lin}\right\} \text{ with } i = 1;...;N_{f,k} \tag{6.100}$$

The $\underline{X}_k^{lin}$ matrix is then built by joining, for each i-th row corresponding to the i-th semi-ellipse, the effective terms, discarding the "*non-values*" present in the corresponding i-th row of the auxiliary matrices $\underline{X}_k^{lin1}$, $\underline{X}_k^{lin2}$, $\underline{X}_k^{lin3}$, $\underline{X}_k^{lin4}$, and sorting them in increasing order. For instance, the final matrix $\underline{X}^{lin}$ for the example of Fig. 6.4 is as follows, see Fig. 6.22:

$$\underline{n}^{lin} = \begin{bmatrix} 2 \\ 0 \\ 0 \\ 0 \\ 0 \\ 2 \\ 2 \end{bmatrix}; \; n^{lin} = 2; \; \underline{X}^{lin} = \begin{bmatrix} 0 & X_{12}^{q} \\ * & * \\ * & * \\ * & * \\ * & * \\ X_{61}^{q} & X_{67}^{p1} \\ X_{76}^{p1} & X_{72}^{q} \end{bmatrix} \tag{6.101}$$

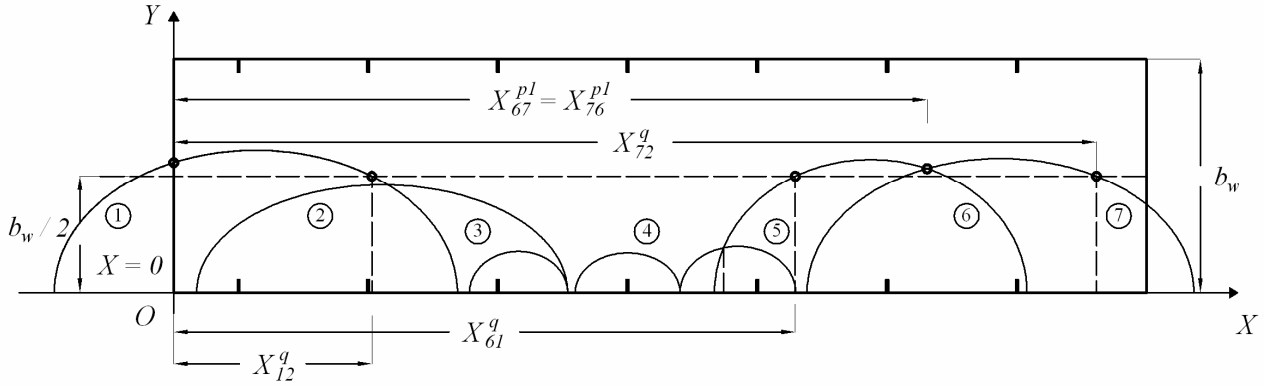

Fig. 6.22 – Determination of the effective matrix of the integration points in the linear range $\underline{X}^{lin}$

Block 7: Determination of the Areas

$\underline{\mathrm{A}}$ is a $N_f \times 1$ dimension vector containing, in the i-th cell, the area ascribed to the i-th semi-ellipse. For the k-th configuration, the term $\mathrm{A}_{i,k}$ of the $\underline{\mathrm{A}}_k$ matrix is equal to:

$$\mathrm{A}_{i,k} = \mathrm{A}_{i,k}^{nlin} + \mathrm{A}_{i,k}^{lin} \tag{6.102}$$

where $\mathrm{A}_{i,k}^{nlin}$ is determined by the following equation:

$$\mathrm{A}_{i,k}^{nlin} = \int_{X_{i1,k}^{nlin}}^{X_{i2,k}^{nlin}} Y_{i,k}(X).dX + \int_{X_{i3,k}^{nlin}}^{X_{i4,k}^{nlin}} Y_{i,k}(X).dX + ... \int_{X_{i\left(\left(n_k^{nlin}\right)-1\right),k}^{nlin}}^{X_{i\left(n_k^{nlin}\right),k}^{nlin}} Y_{i,k}(X).dX \tag{6.103}$$

The term $\mathrm{A}_{i,k}^{lin}$ can be obtained from:

$$\mathrm{A}_{i,k}^{lin} = \int_{X_{i1,k}^{lin}}^{X_{i2,k}^{lin}} \frac{b_w}{2}.dX + \int_{X_{i3,k}^{lin}}^{X_{i4,k}^{lin}} \frac{b_w}{2}.dX + ... \int_{X_{i\left(\left(n_k^{lin}\right)-1\right),k}^{lin}}^{X_{i\left(n_k^{lin}\right),k}^{lin}} \frac{b_w}{2}.dX \tag{6.104}$$

Note that in the above Eqs. (6.103) and (6.104) the abscissa values, already stored in the corresponding i-th row of $\underline{X}_k^{nlin}$ and $\underline{X}_k^{lin}$, respectively, have to be considered integration limits by pairs in sequence.

The equation of the semi-ellipse is like follows:

$$Y_{i,k}(X) = \sqrt{-\frac{E_{i1,k}X^2 + E_{i3,k}X + E_{i4,k}}{E_{i2,k}}} \tag{6.105}$$

The integration of the ellipse equation can be carried out in exact form, in fact Eq. (6.105) can be transformed into:

$$Y_{i,k}(X) = \sqrt{\left(-\frac{E_{i1,k}}{E_{i2,k}}\right)^2 \cdot X^2 + \left(-\frac{E_{i3,k}}{E_{i2,k}}\right) \cdot X + \left(-\frac{E_{i4,k}}{E_{i2,k}}\right)} = \sqrt{d_{i,k} \cdot X^2 + e_{i,k} \cdot X + f_{i,k}} \tag{6.106}$$

and solved:

$$\begin{aligned} &\int\left(\sqrt{d_{i,k} \cdot X^2 + e_{i,k} \cdot X + f_{i,k}}\right) \cdot dX = \\ &\left[\frac{\left(2 \cdot d_{i,k} \cdot X + e_{i,k}\right)}{4 \cdot d_{i,k}} \sqrt{\left(d_{i,k} \cdot X^2 + e_{i,k} \cdot X + f_{i,k}\right)} + \frac{4 \cdot d_{i,k} \cdot f_{i,k} - \left(e_{i,k}\right)^2}{8 \cdot d_{i,k}}\right] \times f(X) \end{aligned} \tag{6.107}$$

with $f(X)$:

$$\begin{aligned} &f(X) = \frac{1}{\sqrt{d_{i,k}}} \cdot \ln\left[2 \cdot \sqrt{d_{i,k}} \cdot \sqrt{\left(d_{i,k} \cdot X^2 + e_{i,k} \cdot X + f_{i,k}\right)} + 2 \cdot d_{i,k} \cdot X + e_{i,k}\right] \\ &\text{if } d_{i,k} \geq 0 \end{aligned} \tag{6.108}$$

or:

$$f(X) = -\frac{1}{\sqrt{-d_{i,k}}} \cdot \sin^{-1}\left[\frac{2 \cdot d_{i,k} \cdot X + e_{i,k}}{\sqrt{{e_{i,k}}^2 - 4 \cdot d_{i,k} \cdot f_{i,k}}}\right] \quad (6.109)$$

if $d_{i,k} < 0$ and ${e_{i,k}}^2 - 4 \cdot d_{i,k} \cdot f_{i,k} \geq 0$

or:

$$f(X) = \frac{1}{\sqrt{d_{i,k}}} \cdot \sinh^{-1}\left[\frac{2 \cdot d_{i,k} \cdot X + e_{i,k}}{\sqrt{4 \cdot d_{i,k} \cdot f_{i,k} - {e_{i,k}}^2}}\right] \quad (6.110)$$

if ${e_{i,k}}^2 - 4 \cdot d_{i,k} \cdot f_{i,k} < 0$

Block 8: Determination of the NSM shear strength contributions $\underline{V}_k^p$ and $\underline{V}$

$\underline{V}^p$ is a $N_f \times 1$ dimension vector containing, in the i-th cell, the shear strength contribution ascribed to the i-th laminate and parallel to its orientation. For the k-th configuration, the general i-th term, $V_{fi,k}^p$, of the $\underline{V}_k^p$ vector is calculated by the following equation:

$$V_{fi,k}^p = \min\left\{2 \,.\, \left(a_f + b_f\right) \,.\, L_{fi} \,.\, \tau_b\left(L_{fi}\right) \;;\; a_f \,.\, b_f \,.\, f_{fu} \;;\; A_{i,k} \,.\, f_{ctm} \,.\, \sin\left(\theta + \beta\right)\right\} \quad (6.111)$$

$\underline{V}$ is a $k \times 1$ dimension vector containing, in the k-th cell, the NSM shear strength contribution $V_{f,k}$ corresponding to the k-th configuration. The k-th term is equal to:

$$V_{f,k} = 2 \,.\, \sin\beta \,.\, \sum_{i=1}^{N_{f,k}} V_{fi,k}^p \quad (6.112)$$

6.2 Accounting for the interaction with stirrups

By simply introducing some modifications in the above simpler formulation of the proposed modelling approach, the interaction between stirrups and laminates can be, in a simplified way, taken into account. It is sufficient to modify the calculations preceding the determination of the angle between axis and generatrices of the semi-conical surface associated to each i-th laminate.

The idea is to model the interaction with stirrups by varying the projecting angle $\alpha_{fi,k}$ of the i-th semi-conical surface with the distance, along the crack development (*i.e.* along the OX axis), of the laminate $X_{fi,k}$ from the closest stirrup ($\Delta X^{sf}_{i,\min}$). For this purpose, it is necessary to introduce other input parameters.

The parameters that need to be added to input parameters list are the following:

- s_s the spacing of the stirrups measured along the longitudinal axis of the beam;
- $\alpha_{fi}\left(\Delta X^{sf}_{i,\min}\right)$ the relation of the variation of the semi-conical surfaces' projecting angle α_{fi} with respect to the distance of the laminate from the closest stirrup, measured along the OX axis of the crack plane reference system.

The position of each i-th laminate, $X_{fi,k}$, along the OX axis and in correspondence of each k-th geometrical configuration can be calculate as shown in Block 2 of the previous Chapter 6.1.

Based on the parameters s_s, h_w and θ, the three possible configurations assumed by stirrups with respect to the crack are defined so as it was already done for the laminates (see Chapter 4 and Block 1 of Chapter 6.1) with the difference that, since the stirrups are orthogonal with respect to the beam axis, Eq. 4.2 modifies like follows:

$$N_{s,real} = \frac{h_w \cdot \cot\theta}{s_s} \tag{6.113}$$

where $N_{s,real}$ is the real number of stirrups that can intersect the crack.

After that, the integer number of stirrups that can cross the crack will be determined as exposed in Chapter 4 for the case of laminates: $N^{l}_{s,\text{int}}$ the lower integer of stirrups, $N^{h}_{s,\text{int}}$ the higher integer number of stirrups that can cross the crack, and $N_{s,odd}$ and $N_{s,ev}$ that are, respectively, the odd and even integer number of stirrups that can cross the crack.

At this point, a matrix $\underline{x}_s$, of dimension 3×2, can be built containing, in each row, the position of the first stirrup with respect to the crack origin and the corresponding number of stirrups, as given by Eq. 6.114:

$$(x_{s1}; N_s) = \begin{cases} \left[s_s ; N^{l}_{s,\text{int}} \right] \\ \left[\dfrac{h_w}{2} \cdot \dfrac{\sin(\theta+90)}{\sin\theta} - \dfrac{(N_{s,ev}-1)}{2} \cdot s_s ; N_{s,ev} \right] \\ \left[\dfrac{h_w}{2} \cdot \cot\theta - \dfrac{(N_{s,odd}-1)}{2} \cdot s_s ; N_{s,odd} \right] \end{cases} \tag{6.114}$$

in which h_w is the the height of the web.

Since the possible geometrical configurations of the stirrups with respect to the crack are three and the ones of the laminates are also three, there will be a total number of nine gometrical configurations. In the following, we will generically refer to one of those combinations of geometrical configurations.

Once the matrix $\underline{x}_s$ has been determined, for a generic geometric combination of disposition of stirrups and laminates with respect to the assumed crack, *i.e.* for a generic combination of the pairs $\left(x_{s1};N_s\right)$ and $\left(x_{f1};N_f\right)$, the position of each stirrup X_{si} along the OX axis can be calculated as follows:

$$X_{si}=\frac{1}{\sin\left(90+\theta\right)}\cdot\left[x_{s1}+\left(i-1\right)\cdot s_s\right] \tag{6.115}$$

and stored in a vector whose dimensions are $N_s\times 1$.

At this point, a matrix $\underline{\Delta X}^{sf}$ of dimensions $N_f\times N_s$ can be built containing, in each i-th row, referring to the i-th laminate, the distance ΔX_{ij}^{sf}, from the j-th stirrup for $j=1,...,N_s$, *i.e.*:

$$\Delta X_{ij}^{sf}=\left|X_{fi}-X_{sj}\right| \tag{6.116}$$

After that, for each laminate, the minimum value of ΔX_{ij}^{sf} should be determined as follows:

$$\Delta X_{i,\min}^{sf}=\min\Delta X_{i,j}^{sf} \tag{6.116}$$

and stored in the corresponding i-th row of another vector $\underline{\Delta X}_{\min}^{sf}$.

Only at that point, the angle between axis and generatrices of the semi-conical surface associated to the i-th laminate can be computed, based on the input relationship $\alpha_{fi}\left(\Delta X_{i,\min}^{sf}\right)$.

These calculations could be easily implemented in the algorithm already developed in Chapter 6.1.

7 Performance of the proposed Predictive Model

The Proposed Model (PM), as described in Chapter 6.1, *i.e.* neglecting the interaction between existing stirrups and laminates, was used to predict the NSM contribution for the shear resistance of the beams of the experimental program by Dias and Barros (2006). The average tensile strength of the concrete of the tested beams was estimated from the concrete average compressive strength at the age of the beam tests, and using the expressions proposed by the CEB-FIP model code 90 (1993), resulting f_{ctm} = 2.45 *MPa*. The results are listed in Table 7.1 and plotted in Figs. 7.1 to 7.3. For each beam of that experimental program, both the DM and the PM were applied to compare the experimentally recorded shear strengthening contribution of the distinct laminates' arrangements, $V_f^{\exp}$, with the corresponding ranges of possible analytical values. For the analysis of Table 7.1, the analytical values were obtained assuming for the shear crack angle, θ, the values measured in the tested beams, $\theta^{\exp}$, and listed in Table 7.1.

The model performance was also assessed by means of the ratios (in the following they are referred to as "*assessment ratios*"):

- $V_f^{\exp} / V_{f,\min}^{PM}$ of the experimental recording to the minimum value obtained by means of the PM;
- $V_f^{\exp} / V_{f,\max}^{PM}$ b of the experimental recording to the maximum value obtained by means of the PM;
- $V_f^{\exp} / V_{f,\min}^{DM}$ of the experimental recording to the minimum value obtained by means of the DM;
- $V_f^{\exp} / V_{f,\max}^{PM}$ of the experimental recording to the maximum value obtained by means of the DM.

The performance of the PM is absolutely satisfactory. In fact, for the series of beams with vertical laminates the average of the ratios $V_f^{\exp} / V_{f,\min}^{PM}$ and $V_f^{\exp} / V_{f,\max}^{PM}$ are respectively 0.99 and 0.56 meaning that, on average, the recorded values fall just on the lower bound of the analytical range $\left[V_{f,\min}^{PM}; V_{f,\max}^{PM}\right]$. For the series of beams with laminates at 60° the average value of the above two ratios are respectively 1.01 and 0.77 meaning that, as can be also gathered from Fig. 7.1, on average, the experimental recordings fall in between the lower and upper bound of the analytical values. For the series of beams with laminates disposed at 45° the average value of the ratio $V_f^{\exp} / V_{f,\min}^{PM}$ results to be less than unity because, the experimental value obtained in 2S_8LI45 beam was probably affected by some disturbance that did not allow the shear strengthening contribution of this NSM configuration to be fully mobilized. In fact, provided that, due to the interaction between subsequent laminates the rate $\Delta V_f^{\exp} / \Delta s_f$ decreases by diminishing s_f, it is unrealistic that passing from s_f of 220 mm (2S_5LI45 beam) to 138 mm (2S_8LI45 beam) the shear strength contribution decreases from 41.40 to 40.20 kN. At most, it should assume the same value of 41.40 kN.

On the contrary, the analytical range of values $\left[V_{f,\min}^{DM}; V_{f,\max}^{DM}\right]$ provided by the DM lies above the experimental recordings (see Figs. 7.1 to 7.3). This can be also gathered from the average values of the $V_f^{\exp} / V_{f,\min}^{DM}$ and $V_f^{\exp} / V_{f,\max}^{PM}$ ratios that are always less than unit (see Table 7.2).

Table 7.1 Values of V_f obtained from PM ($V_{f,k}^{PM}$) and DM ($V_{f,k}^{DM}$), and experimental recordings ($V_f^{\exp}$) for the experimental program by Dias & Barros 2006.

Beam label	s_f [mm]	β [°]	$\theta^{\exp}$ [°]	$V_{f,1}^{PM}$ [kN]	$V_{f,2}^{PM}$ [kN]	$V_{f,3}^{PM}$ [kN]	$V_{f,\min}^{PM}$ [kN]	$V_{f,\max}^{PM}$ [kN]	$V_{f,\min}^{DM}$ [kN]	$V_{f,\max}^{DM}$ [kN]	$V_f^{\exp}$ [kN]
2S_3LV	267	90	40	20.88	13.61	49.28	13.61	49.28	45.78	66.79	22.20
2S_5LV	160	90	40	48.80	46.38	51.78	46.38	51.78	85.74	94.93	25.20
2S_7LV	100	90	36	65.41	61.71	66.76	61.71	66.76	160.49	179.36	48.60
2S_3LI45	367	45	45	32.62	22.96	49.83	22.96	49.83	44.75	66.96	29.40
2S_5LI45	220	45	45	47.69	47.11	62.06	47.11	62.06	81.89	107.16	41.40
2S_8LI45	138	45	36	83.41	83.16	88.63	83.16	88.63	168.48	184.37	40.20
2S_3LI60	325	60	33	42.16	29.36	44.20	29.36	44.20	55.42	82.91	35.40
2S_5LI60	195	60	36	47.21	47.20	60.04	47.20	60.04	94.94	126.91	46.20
2S_7LI60	139	60	37	72.36	65.35	74.18	65.35	74.18	147.04	164.50	54.60

Table 7.2 Appraisal of the PM by comparison with the DM and the experimental recordings for the experimental program by Dias & Barros (2006).

Beam label	$V_f^{\exp}/V_{f,\min}^{PM}$ [ ]	$V_f^{\exp}/V_{f,\max}^{PM}$ [ ]	$V_f^{\exp}/V_{f,\min}^{DM}$ [ ]	$V_f^{\exp}/V_{f,\max}^{DM}$ [ ]
2S_3LV	1.63	0.45	0.48	0.33
2S_5LV	0.54	0.49	0.29	0.27
2S_7LV	0.79	0.73	0.30	0.27
average	**0.99**	**0.56**	**0.36**	**0.29**
2S_3LI45	1.28	0.59	0.66	0.44
2S_5LI45	0.88	0.67	0.51	0.39
2S_8LI45	0.48	0.45	0.24	0.22
average	**0.88**	**0.57**	**0.47**	**0.35**
2S_3LI60	1.21	0.80	0.64	0.43
2S_5LI60	0.98	0.77	0.49	0.36
2S_7LI60	0.84	0.74	0.37	0.33
average	**1.01**	**0.77**	**0.50**	**0.37**

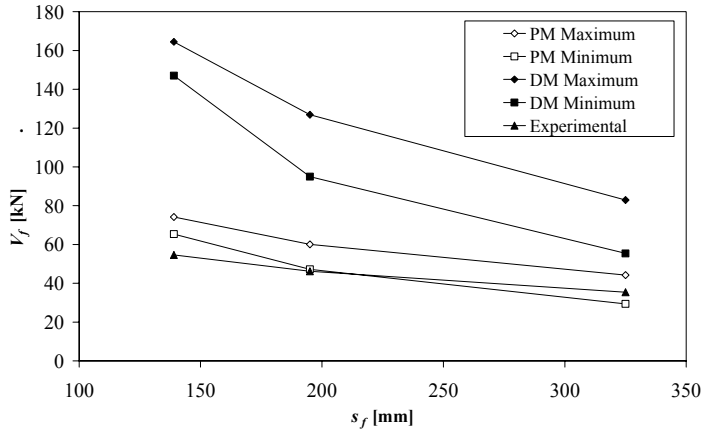

Fig. 7.1 – Experimental/analytical comparison of V_f for the beams with laminates at 60°.

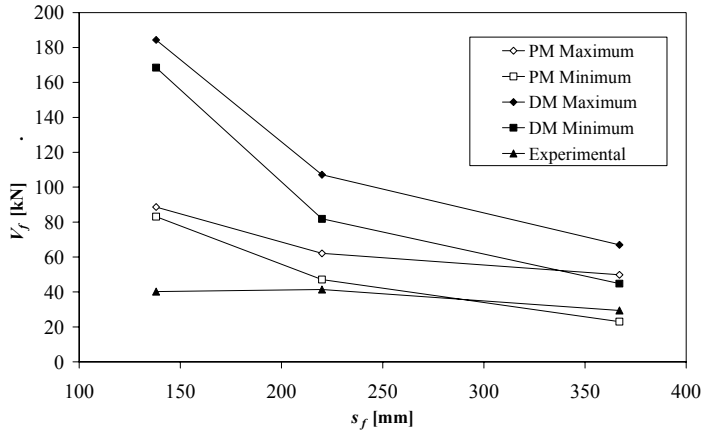

Fig. 7.2 – Experimental/analytical comparison of V_f for the beams with laminates at 45°.

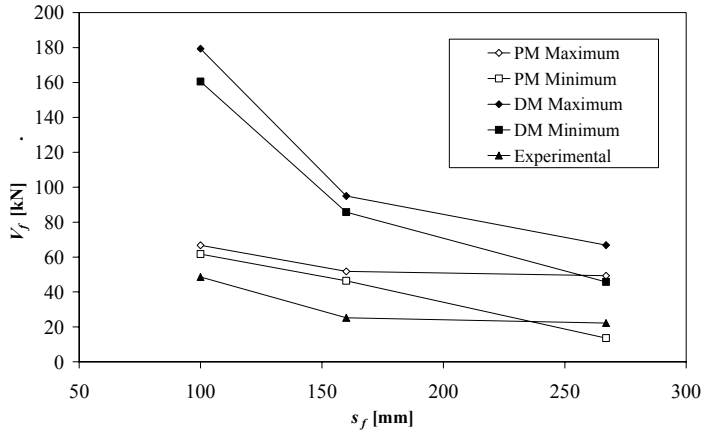

Fig. 7.3 – Experimental/analytical comparison of V_f for the beams with laminates at 45°.

To exclude the possibility of an erroneous experimental measurement of the critical shear crack inclination, θ^{exp}, the analytical values were also obtained assuming the constant value of θ = 45°. The resulting analytical values of the shear strength contribution V_f and the corresponding performance ratios are listed in Tables 7.3 and 7.4, respectively.

Since in some cases the experimentally-observed value of the shear crack angle was lower than 45°, when this latter value is assumed, the values of the available bond lengths L_{fi} and consequently the corresponding terms $V_{fi}^{p,cf}$ slightly decrease so as to justify the increment of the ratio $V_f^{\exp}/V_{f,\min}^{PM}$. Nonetheless, as can be gathered from the values listed in Table 7.4, the experimental values are located, on average, in between the analytical range provided by the PM *i.e.* $\left[V_{f,\min}^{PM};V_{f,\max}^{PM}\right]$.

Table 7.3 Values of V_f obtained from PM ($V_{f,k}^{PM}$) and DM ($V_{f,k}^{DM}$), and experimental recordings ($V_f^{\exp}$) for the experimental program by Dias and Barros (2006) assuming $\theta = 45°$.

Beam label	s_f [mm]	β [°]	$V_{f,1}^{PM}$ [kN]	$V_{f,2}^{PM}$ [kN]	$V_{f,3}^{PM}$ [kN]	$V_{f,\min}^{PM}$ [kN]	$V_{f,\max}^{PM}$ [kN]	$V_{f,\min}^{DM}$ [kN]	$V_{f,\max}^{DM}$ [kN]	$V_f^{\exp}$ [kN]
2S_3LV	267	90	7.49	4.36	60.24	4.36	60.24	29.02	60.83	22.20
2S_5LV	160	90	56.60	45.75	60.24	45.75	60.24	59.09	88.53	25.20
2S_7LV	100	90	48.69	48.69	74.51	48.69	74.51	102.64	174.97	48.60
2S_3LI45	367	45	32.62	22.96	49.83	22.96	49.83	44.75	66.96	29.40
2S_5LI45	220	45	47.69	47.11	62.06	47.11	62.06	81.89	107.16	41.40
2S_8LI45	138	45	71.00	68.83	73.07	68.83	73.07	145.81	150.18	40.20
2S_3LI60	325	60	22.85	14.97	46.76	14.97	46.76	45.98	69.02	35.40
2S_5LI60	195	60	41.99	41.48	51.83	41.48	51.83	87.79	102.36	46.20
2S_7LI60	139	60	55.95	53.88	68.22	53.88	68.22	127.20	133.30	54.60

Table 7.4 Appraisal of the PM by comparison with the DM and the experimental recordings for the experimental program by Dias and Barros (2006) assuming $\theta = 45°$.

Beam label	$V_f^{\exp}/V_{f,\min}^{PM}$ [ ]	$V_f^{\exp}/V_{f,\max}^{PM}$ [ ]	$V_f^{\exp}/V_{f,\min}^{DM}$ [ ]	$V_f^{\exp}/V_{f,\max}^{DM}$ [ ]
2S_3LV	5.09	0.37	0.76	0.36
2S_5LV	0.55	0.42	0.43	0.28
2S_7LV	1.00	0.65	0.47	0.28
average	**2.21**	**0.48**	**0.55**	**0.31**
2S_3LI45	1.28	0.59	0.66	0.44
2S_5LI45	0.88	0.67	0.51	0.39
2S_8LI45	0.58	0.55	0.28	0.27
average	**0.91**	**0.60**	**0.48**	**0.36**
2S_3LI60	2.36	0.76	0.77	0.51
2S_5LI60	1.11	0.89	0.53	0.45
2S_7LI60	1.01	0.80	0.43	0.41
average	**1.50**	**0.82**	**0.58**	**0.46**

The PM was also applied to estimate the experimental recordings regarding the program by De Lorenzis and Rizzo (2006). Those authors carried out an experimental program composed of RC beams shear-strengthened by both NSM CFRP laminates and rods. In fact, the technique of the structural strengthening by NSM CFRP elements was originally conceived contemplating the employment of rods (De Lorenzis and Nanni, 2001). In both cases, the failure mode reported by De Lorenzis & Rizzo is exactly the same observed by Dias & Barros *i.e.* the progressive detachment of the

concrete cover containing the glued CFRP elements. The concrete average tensile strength of the tested beams derived, according to the CEB-FIP model code 90 (1993), from the average splitting tensile strength, results to be f_{ctm} = 1.80 MPa, while the tensile strength of the CFRP elements, f_{fu}, is equal to 2068 MPa and 2214 MPa for the strips and rods, respectively.

The PM was applied faithfully to its original development, as delineated in Chapter 6.1, to the RC beams shear strengthened by NSM laminates. For the case of the RC beams strengthened by NSM rods, besides debonding, tensile rupture and concrete tensile fracture, the possibility of another failure mode affecting the NSM rods at ultimate, was contemplated, *i.e.* the splitting of the adhesive, whose occurrence was reported by De Lorenzis & Nanni (2002). Thus, for those cases, the Eq. 6.2 was modified as follows:

$$V_{fi}^{p} = \min\left\{V_{fi}^{p,db};\ V_{fi}^{p,tr};\ V_{fi}^{p,cf};V_{fi}^{p,spl}\right\} = \min\left\{\pi \,.\, d_b \,.\, L_{fi} \,.\, \tau_{b,rod}\left(L_{fi}\right);\ \pi \,.\, \frac{d_b^{\,2}}{4} \,.\, f_{fu};\ \left(\mathrm{A}_i^{nlin} + \mathrm{A}_i^{lin}\right) \,.\, \sin\left(\theta+\beta\right) \,.\, f_{ctm};\ \pi \,.\, d_b \,.\, L_{fi} \,.\, \tau_{spl,rod}\left(L_{fi}\right)\right\} \tag{7.1}$$

in which $V_{fi}^{p,spl}$ is the splitting-based contribution ascribed to the i-th rod parallely to its orientation, d_b is the nominal diameter of the adopted rod, $\tau_{b,rod}\left(L_{fi}\right)$ is the length-dependent average bond strength for the case of rods and $\tau_{spl,rod}\left(L_{fi}\right)$ is the length-dependent average bond strength contemplating the possibility for the rods to fail due to the adhesive splitting. The above relationships, $\tau_{b,rod}\left(L_{fi}\right)$ and $\tau_{spl,rod}\left(L_{fi}\right)$, calibrated on the basis of the test results reported by De Lorenzis & Nanni (2002), are as follows ($\tau_{b,rod}$ and $\tau_{spl,rod}$ in MPa and L_f in mm):

$$\tau_{b,rod}\left(L_f\right) = \begin{cases} 4.99 & 0 \le L_f < 114 \\ 15.10 - 2.13 \,.\, \ln L_f & 114 \le L_f \le 312 \\ 2.84 & L_f > 312 \end{cases} \tag{7.2}$$

and:

$$\tau_{spl,rod}\left(L_f\right) = \begin{cases} 8.73 & 0 \le L_f < 57 \\ 16.72 - 1.98 \,.\, \ln L_f & 57 \le L_f \le 312 \\ 5.36 & L_f > 312 \end{cases} \tag{7.3}$$

Indeed, as outlined by De Lorenzis & Nanni (2002), the phenomenon of the splitting of the adhesive shows a dependence on both the groove dimensions and the relative mechanical properties of adhesive and concrete but, since the reported failure mode of the beams was concrete tensile fracture, that issue was not further addressed.

The results, obtained by applying the PM $\left[V_{f,\min}^{PM};V_{f,\max}^{PM}\right]$ with a value of 45° for the shear crack angle, are listed, along with the experimental values, in Table 7.5. Moreover, the analytical ranges $\left[V_{f,\min}^{DM};V_{f,\max}^{DM}\right]$ and $\left[V_{f,\min}^{SPL};V_{f,\max}^{SPL}\right]$, obtained by applying the DM, respectively, with the debonding-based $\tau_{b,rod}\left(L_{fi}\right)$ and the splitting-based average bond strength $\tau_{spl,rod}\left(L_{fi}\right)$, are also reported.

The assessment ratios, as defined above, are listed in Table 7.6. It emerges that, on average, the upper bound $V_{f,\max}^{PM}$ provided by the PM underestimates the experimental recordings and such underestimation ranges between 22 and 45%.

The experimental recordings ascribed to the beams labeled NB90_73_a and NS90_73_a seem to be excessively high with respect to the others. In fact, for the beam NB90_73_a, the experimental value is almost twice as large as the one regarding the NB90_73_b beam that differs from the former only for the quality of the epoxy employed. If those two values are discarded, the above underestimation reduces to 6% for the beams shear strengthened by rods and 27% for those strengthened by laminates (see values in parentheses in Table 7.6). At the same time, the analytical ranges provided by the DM assuming both the debonding-based and splitting-based average bond strength, systematically overestimate the experimental recordings since the average values of the assessment ratios are both less than unit.

Table 7.5 Values of V_f obtained from PM and DM (considering both debonding and splitting) and experimental recordings ($V_f^{\exp}$) for the experimental program by De Lorenzis & Rizzo 2006 assuming $\theta = 45°$.

Beam label	s_f [mm]	β [°]	$V_{f,\min}^{PM}$ [kN]	$V_{f,\max}^{PM}$ [kN]	$V_{f,\min}^{DM}$ [kN]	$V_{f,\max}^{DM}$ [kN]	$V_{f,\min}^{SPL}$ [kN]	$V_{f,\max}^{SPL}$ [kN]	$V_f^{\exp}$ [kN]
NB90_73_a	73	90	16.99	28.83	32.33	39.74	53.94	63.51	54.20
NB90_73_b	73	90	16.99	28.83	32.33	39.74	53.94	63.51	26.40
NB90_45_b	45	90	26.70	31.94	56.44	59.96	92.93	98.28	28.60
NB45_146_a	146	45	21.72	25.69	32.22	36.97	49.52	60.12	39.10
NB45_73_a	73	45	29.93	30.80	68.69	69.65	108.60	109.66	28.00
NS90_73_a	73	90	16.99	31.18	138.46	171.56	-	-	50.50
NS45_146_a	146	45	21.72	25.69	113.04	150.23	-	-	32.70

Table 7.6 Appraisal of the PM by comparison with the DM (considering both debonding and splitting) and the experimental recordings for the experimental program by De Lorenzis & Rizzo 2006 assuming $\theta = 45°$.

Beam lebel	$V_f^{\exp}/V_{f,\min}^{PM}$ [ ]	$V_f^{\exp}/V_{f,\max}^{PM}$ [ ]	$V_f^{\exp}/V_{f,\min}^{DM}$ [ ]	$V_f^{\exp}/V_{f,\max}^{DM}$ [ ]	$V_f^{\exp}/V_{f,\min}^{SPL}$ [ ]	$V_f^{\exp}/V_{f,\max}^{SPL}$ [ ]
NB90_73_a*	3.19	1.88	1.68	1.36	1.00	0.85
NB90_73_b	1.55	0.92	0.82	0.66	0.49	0.42
NB90_45_b	1.07	0.90	0.51	0.48	0.31	0.29
NB45_146_a	1.80	1.52	1.21	1.06	0.79	0.65
NB45_73_a	0.94	0.91	0.41	0.40	0.26	0.26
average	**1.71 (1.34)**	**1.22 (1.06)**	**0.92 (0.74)**	**0.79 (0.65)**	**0.57 (0.46)**	**0.49 (0.40)**
NS90_73_a**	2.97	1.62	0.36	0.29	-	-
NS45_146_a	1.51	1.27	0.29	0.22	-	-
average	**2.24 (1.51)**	**1.45 (1.27)**	**0.33 (0.29)**	**0.26 (0.22)**	**-**	**-**

* NB = rods; ** NS = laminates

7.1 Conclusions

A new predictive model, originated from the need for a rational explanation to the features of the observed failure mechanisms affecting the behaviour at ultimate of RC beams shear strengthened by NSM CFRP laminates, was proposed. This model assumes as possible failure mechanisms debonding, tensile rupture of the laminates and concrete tensile fracture and allows the interaction between laminates to be accounted for. The comparisons with the debonding-based model showed that the proposed model provides a better estimation of the experimentally recorded NSM shear strength contribution, not only in the case of employment of laminates but also in the case of rods.

For the time being, the proposed model was appraised without taking into consideration the interaction between laminates and existing stirrups which also has a prominent influence on the failure of NSM shear strengthened RC beams. Further developments, in this respect, are desirable.

7.2 Acknowledgements

The authors of the present work wish to acknowledge the support provided by the "Empreiteiros Casais", S&P®, degussa® Portugal, and Secil (Unibetão, Braga). The study reported in this paper forms a part of the research program "CUTINSHEAR - Performance assessment of an innovative structural FRP strengthening technique using an integrated system based on optical fiber sensors" supported by FCT, POCTI/ECM/59033/2004. Also, this work was carried out under the auspices of the Italian DPC-ReLuis Project (repertory n. 540), Research Line 8.

References

ACI Committee 440 "*Guide for the Design and Construction of Externally Bonded FRP Systems for strengthening Concrete Structures*", Revised May 2002.

ACI Committee 318, "*Building code requirements for structural concrete and commentary*", American Concrete Institute, Reported by ACI Committee 118, 2002.

Australian Design Guideline for RC Structures retrofitted with FRP and metal plate: beams and slabs, Draft 3, submitted to Standard Australia, 2/2/06.

Barros, J.A.O., Dias, S.J.E. (2004) "*Experimental research of a new CFRP-based shear strengthening technique for reinforced concrete beams*" IBRACOM structural Journal, Vol. 1, N.1.

Barros, J.A.O., Dias, S.J.E. (2005) "*Shear Strengthening of RC Beams with Near-Surface-Mounted CFRP Laminates*", 7th International Symposium on Fiber Reinforced Polymer (FRP) Reinforcement for Concrete Structures (FRP7RCS), Kansas, USA, SP-230-47, 807-824.

Barros, J.A.O., Dias, S.J.E. (2006) "*Near Surface Mounted CFRP laminates for shear strengthening of concrete beams*", Journal Cement and Concrete Composites, 28(3), 276-292.

Barros J., Ferreira D., Fortes A., Dias S., (2006) "*Assessing the effectiveness of embedding CFRP laminates in the near surface for structural strengthening*", Construction and Building Materials Journal, Construction and Building Materials Journal, 20, 478-491.

Blaschko M., Zilch K., (1999) "*Rehabilitation of concrete structures with CFRP strips glued into slits*", Proceedings of the Twelfth International Conference of Composite Materials, ICCM 12, Paris, France (CD-ROM).

Blaschko M., (2001), "*Zum tragverhalten von betonbautelien mit in schlitze eingeklebten CFK-lamellen*", Bericht 8/2001 aus dem Konstructiven Ingenieurbau, TU München, 147 pp. (in German).

Blaschko M., (2003) "*Bond behavior of CFRP strips glued into slits*", proceedings FRP RCS-6, Singapore, World Scientific, 205-214.

Bousselham A., Chaalal O., (2004) "*Shear Strengthening Reinforced Concrete Beams with Fiber-Reinforced Polymer: Assessment of Influencing Parameters and Required Research*", ACI Structural Journal, Vol.101, Nº2, March-April, pp. 219-227.

CEB bulletin n° 201, "*Fastening to Concrete and Masonry Structures*", Thomas telford Services Ltd, London, 1994.

CEB bulletin n° 210, "*RC Elements under cyclic loading*", Thomas telford Services Ltd, London, 1996.

CEB-FIP Model Code 90, (1993) Bulletin d'Information N° 213/214, Final version printed by Th. Telford, London, (1993; ISBN 0-7277-1696-4; 460 pages)

CEN (1991), Eurocode 2: "*Design of concrete structures – Part 1-1: General rules and rules for buildings*" ENV 1992-1-1, Comitee Europeen de Normalization, Brussels, Belgium.

Chen, J.F. and Teng, J.G. (2003) "*Shear capacity of FRP-strengthened RC beams: FRP debonding*" Construction and Building Materials, Elsevier, 17, pp 27-41.

Chao S.Y., Chen J.F., Teng J.G., Hao Z., Chen J., (2005) "*Debonding in Reinforced Concrete Beams Shear Strengthened with Complete Fiber Reinforced Polymer Wraps*", Journal of Composites for Construction, ASCE September/October 2005/1.

CNR DT 200, (2004), "*Istruzioni per la Progettazione, l'Esecuzione ed il Controllo di Interventi di Consolidamento Statico mediante l'utilizzo di Composti Fibrorinforzati - Materiali, strutture di c.a. e di c.a.p., strutture murarie*", Roma, CNR 13 luglio 2004.

Cook, R.A., Doerr, G.T. and Klingner R.E., (1993) "*Bond Stress Model for Design of Adhesive Anchors*", ACI Structural Journal, Vol. 90, Nº5, September-October, pp.514-524.

Cook, Ronal A., Kunz, Jacob, Fuchs, Werner, Konz, Robert C., (1998) "*Behaviour and Design of Single Adhesive Anchors under Tensile Load in Uncracked Concrete*", ACI Structural Journal , Vol. 95, No. 1, January/February 1998, pp. 9-26.

De Lorenzis Laura, (2002), "*Strengthening of RC Structures with near surface mounted FRP rods*", Ph.D. Thesis, Department of Innovation Engineering, University of Lecce, Italy.

De Lorenzis, Laura and Nanni, Antonio, (2001), "*Shear strengthening of Reinforced Concrete Beams with Near-Surface Mounted Fiber-Reinforced Polymer Rods*", ACI Structural Journal, Vol. 98, N.1, pp. 60-68.

De Lorenzis, L. and Nanni, A. (2002), "*Bond between Near-Surface Mounted Fiber-Reinforced Polymer Rods and Concrete in Structural Strengthening*", ACI Structural Journal, Vol. 99, No. 2, March-April 2002, pp. 123-132.

De Lorenzis Laura (2004) "*Anchorage length of Near Surface Mounted Fiber-Reinforced Polymer Rods for Concrete Strengthening-Analytical Modeling*", ACI Structural Journal, Vol. 101, No. 3, May-June 2004, pp. 375-386.

De Lorenzis, Laura and Rizzo, Andrea, (2006), "*Behaviour and Capacity of RC Beams Strengthened in Shear with NSM FRP Reinforcement*" 2nd Int. fib Congress, Naples-Italy, June 5-8 2006, Paper ID 10-9 in CD.

Dias, S., Barros, J.A.O. (2004a) "*Materiais compósitos de CFRP no reforço ao corte de vigas de betão armado*", Relatório Técnico 04-DEC/E-03, Departamento de Engenharia Civil, Universidade do Minho, Fevereiro, 74 pp, 2004-a.

Dias, S., Barros, J. (2004b) "*CFRP no reforço ao corte de vigas de betão armado: investigação experimental e modelos analíticos*", Relatório Técnico 04-DEC/E-08, Departamento de Engenharia Civil, Universidade do Minho, Maio, 109 pp, 2004-b.

Dias, S.J.E. and Barros, J.A.O. (2005a), "*Reforço ao corte de vigas T de betão armado por inserção de laminados de CFRP (Shear strengthening of T cross section RC beams by NSM technique)*", 47º Brasilian Conference on Concrete – CBC2005, Olinda, Brazil, Paper 47CBC0415, p. VII.445 – VII.461, 2-7 September 2005. (in Portuguese)

Dias, S.J.E. and Barros, J.A.O., (2005b) "*Reforço ao corte de vigas T de betão armado usando a técnica NSM com laminados de CFRP*", Report No.05-DEC/E-23, Department of Civil Engineering, University of Minho, November.

Dias, S.J.E., and Barros, J.A.O. (2006) "*NSM CFRP Laminates for the Shear Strengthening of T Section RC Beams*", 2nd International *fib* Congress, Naples, 5-8 June 2006, Article 10-58 in CD,.

El-Hacha R., Rizkalla S.H., (2004) "*Near-Surface-Mounted Fiber-Reinforced Polymer Reinforcements for Flexural Strengthening of Concrete Structures*", ACI Structural Journal, Vol. 101, Nº5, September-October, pp.717-726

Eligehausen, R., Popov, E., Bertero, V.V. (1983) "*Local Bond Stress-Slip Relationships of Deformed Bars under Generalized Excitations*", Report N° 83/23, EERC, University of California at Berkeley, 162 pp.

fib – Bulletin 14. (2001) "*Externally bonded FRP reinforcement for RC structures*", Technical Report by Task Group 9.3 FRP (Fibre Reinforced Polymer) reinforcement for concrete structures, July, 2001, 130 pp.

fib Model Code "*Design and use of externally bonded fibre reinforced polymer reinforcement (FRP EBR) for reinforced concrete structures*", July 2001

Hillerborg *et al.* (1976) "*Analysis of crack formation and crack growth in concrete by means of fracture mechanics and finite elements*" Cement and Concrete Research, 6, 1976, 773-782.

Khalifa, A., Gold, W.J., Nanni, A. and Aziz, A.M.I. (1998) "*Contribution of externally bonded FRP to shear capacity of rc flexural members*", ASCE Journal of Composites for Construction, 2(4), 195-202.

Lima, João, ……. ,Master Thesis, (in preparation), University of Minho, Guimaraães, Portugal.

Liotta, Marc'Antonio, (2007) "*Shear strengthening of RC beams by externally bonded FRP: experiments and design equations*", PhD Thesis, Dept. of Structural Engrg. and Geotechnics, Univ. Sapienza of Roma, Rome, Italy, March 2007.

Monti, G., Renzelli, M., Luciani, P., (2003) "*FRP Adhesion to Uncracked and Cracked Concrete Zones*", Proceedings of the 6th International Symposium on Fibre-Reinforced Polymer (FRP) Reinforcement for Concrete Structures (FRPRCS-6), Singapore, July, 183-192.

Monti, G., Santinelli, F., Liotta, M.A., (2004) "*Mechanics of FRP Shear Strengthening of RC beams*", Proc. ECCM 11, Rhodes, Greece.

Monti, G., (2006) "*Fiber Reinforced Polymers in Design and Retrofit. Materials, adhesion, confinement*", Short Course Documentation, ROSE-School Pavia Italy, July 1-21 2006.

Monti, G., Liotta, Marc'Antonio, (2006) "*Tests and design equations for FRP-strengthening in shear*", Construction and Building Materials (2006), doi:10.1016/j.conbuildmat.2006.06.023.

Nanni, A., Di Ludovico, M., Parretti, R., (2004) "*Shear Strengthening of a PC Bridge Girder with NSM CFRP Rectangular Bars*", Advances in Structural Engineering, Vol. 7, No. 4.

Oehlers, D.J. and Seracino, R., (2004) "*Design of FRP and steel plated RC structures: retrofitting beams and slabs for strength, stiffness and ductility*", Elsevier. UK

Paretti, R., Nanni, A., (2004) "*Strengthening of RC members using near-surface mounted FRP composites: design overview*", Advances in Structural Engineering, 7(6), 569-483.

Park, R., Paulay, T., (1975) "*Reinforced Concrete Structures*", John Wiley and Sons, NY, 1975.

Priestley, M.J.N. and Seible, F., (1995) "*Design of seismic retrofit measures for concrete and masonry structures*", Construction and Buiding Materials, 9(6), pp. 365-377.

Sena-Cruz, J.M., Barros, J.A.O. (2002) "*Bond behaviour of carbon laminate strips into concrete by pull-out bending tests*", Proc. Int. Symposium Bond in Concrete-From Research to Standards, Budapest, Hungary, 614-621

Sena-Cruz, José Manuel, (2004) "*Strengthening of concrete structures by means of near-surface mounted CFRP laminate strips*", PhD Thesis, Dept. of Civil Eng., University of Minho, Guimarães, Portugal.

Sena-Cruz J.M., and Barros J.A.O. (2004a) "*Bond between near-surface mounted CFRP laminate strips and concrete in structural strengthening*", Journal of Composites for Construction, ASCE, 8(6), 519-527

Sena-Cruz, J.M. and Barros, J.A.O. (2004b) "*Modelling of bond between near-surface mounted CFRP laminate strips and concrete*", Computers & Structures, 82/17-19, 1513-1521.

Sena-Cruz, J.M.; Barros, J.A.O.; Azevedo, A.F,M.; Gettu, R., (2006), "*Bond behaviour of Near-Surface Mounted CFRP Laminate Strips under Monotonic and Cyclic Loading*", Journal of Composites for Construction, ASCE, 10(4), 295-303, July/August 2006.

Seracino, R., Raizal Saifulnaz, M.R. and Oehlers, D.J., (2006) "*Generic IC debonding resistances of EB and NSM plates*" Submitted to Journal of Composites for Construction, ASCE, provisionally accepted January 2006

Teng, J.G., Chen, J.F., Smith, S.T. and Lam, L., (2002) "*FRP strengthened RC Structures*", John Wiley and Sons Ltd., Chicester, England.

Teng, J.G., De Lorenzis, L., Wang, Bo, Rong, Li, Wong, T.N. and Lik, Lam, (2006) "*Debonding failures of RC beams Strengthened with Near Surface Mounted CFRP Strips*", Journal of Composites for Constructions, ASCE, March/April, pp.92-105.

Tompos, Eric J. and Frosch, Robert J. (2002) "*Influence of Beam Size, Longitudinal Reinforcement, and Stirrup Effectiveness on Concrete Shear Strength*", ACI Structural Journal, Vol. 99, N.5, pp.559-567.

Triantafillou, T.C., and Antonopoulos, C.P., (2000), "*Design of concrete flexural members strengthened in shear with FRP*", ASCE Journal of Composites for Construction, 4(4), pp. 198-205.

8 Appendices

8.1 Appendix A

Calculation of the force provided by one semi-conical surface

Hereinafter, we want to demonstrate that the operation of spreading the concrete mean tensile strength $\vec{f}_{ctm}$ throughout the semi-conical surface, integrating and then projecting in the direction of the axis of the semi-cone is equivalent to simply multiplying the area of the base of the semi-cone times the modulus of the tensile strength, see Fig. 9.1:

$$F_{vertical} = A_{base} \cdot f_{ctm} = \frac{\pi \cdot R^2}{2} \cdot f_{ctm} \tag{9.1}$$

where R is the radius of the basis of the semi-cone, and A_{base} is the area.

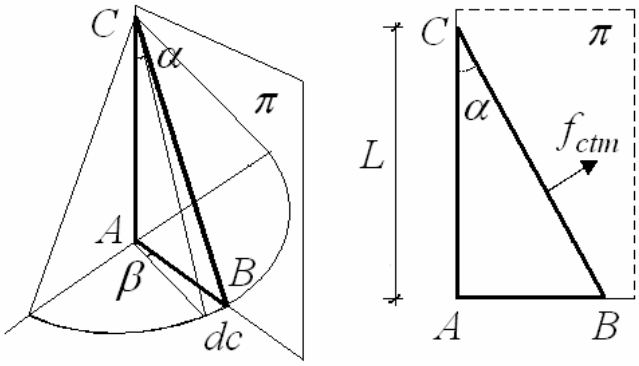

Fig. 9.1 – Force on the radial section of the semi-conical surface

The force parallel to the axis of the semi-cone and contributed by an infinitesimal slice of the semi-conical surface, is equal to the area of the slice of surface multiplied by the vertical component of the tensile strength:

$$dF_{vertical} = A_{slice} \cdot f_{ctm} \cdot \sin\alpha \tag{9.2}$$

$$dF_{vertical} = \left(\frac{L}{\cos\alpha} \cdot R \cdot d\beta \cdot \frac{1}{2} \right) \cdot f_{ctm} \cdot \sin\alpha = f_{ctm} \cdot \frac{1}{2} \cdot L \cdot \tan\alpha \cdot R \cdot d\beta = f_{ctm} \cdot \frac{R^2}{2} \cdot d\beta \tag{9.3}$$

that, integrating in β, yields:

$$F_{vertical,total} = \int_0^{\pi} f_{ctm} \cdot \frac{R^2}{2} \cdot d\beta = \frac{R^2}{2} \cdot f_{ctm} \cdot \int_0^{\pi} d\beta = \frac{\pi \cdot R^2}{2} \cdot f_{ctm} \tag{9.4}$$

That is exactly what we wanted to demonstrate.

Independency of the hypothesized shape of the surface

The independency of the shape of the surface, envelope of the traction isostatics, that from a pure analytical point of view constitutes the strength of the calculation method proposed, can be deduced as follows.

In the above Eq. 9.3, what happens in the plane π can be conveniently isolated, *i.e.*:

$$dF_{vertical} = \left(R \cdot d\beta \cdot \frac{1}{2} \right) \cdot \frac{L}{\cos\alpha} \cdot f_{ctm} \cdot \sin\alpha = \left(R \cdot d\beta \cdot \frac{1}{2} \right) \cdot dF_{vertical}^{\pi} \tag{9.5}$$

And the component provided by the section of the semi-cone contained in π, see Fig. 9.2:

$$dF_{vertical}^{\pi} = \int_0^s dl \cdot f_{ctm} \cdot \sin\alpha(l) \tag{9.6}$$

where l is a curvilinear one-dimensional reference system established along the generatrix of the semi-conical surface contained in the plane π and s is the total length of that generatrix.

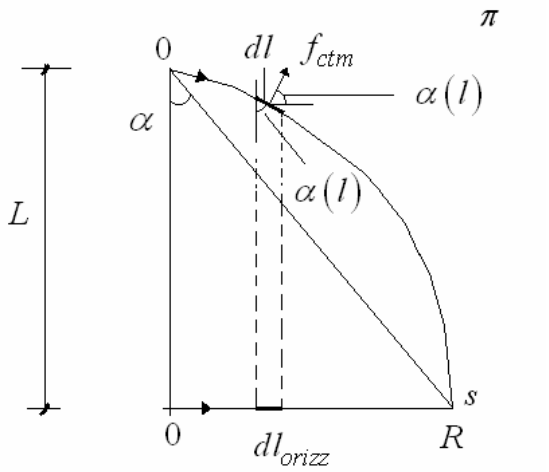

Fig. 9.2 – Independency of the shape of the surface

The above Eq. 9.6 can be re-written as follows:

$$dF_{vertical}^{\pi} = f_{ctm} \cdot \int_0^s dl \cdot \sin\alpha(l) = f_{ctm} \cdot \int_0^s dl_{orizz} = f_{ctm} \cdot L \cdot \tan\alpha \tag{9.7}$$

thus, the final expression of the infinitesimal vertical force is:

$$dF_{vertical} = \left(R \cdot d\beta \cdot \frac{1}{2} \right) \cdot f_{ctm} \cdot L \cdot \tan\alpha \tag{9.8}$$

Since Eq. 9.8 is exactly equal to Eq. 9.5, it is demonstrated that, even if the actual semi-conical surface is concave or convex, its linearization and the assumption of a unique value of the angle α does not modify the value of the vertical force.

Calculation of the length of the i-th Laminate

The formulae used to calculate the length of the i-th Laminate are derived by applying the Theorem of the Chord. That is valid for both the case in which the first laminate is positioned at s_f from the origin of the crack as in order to calculate $L_{tot,\min}$ (chapter 4) and in the more general case in which the first laminate is positioned at x_{f1} (paragraph 5.2).

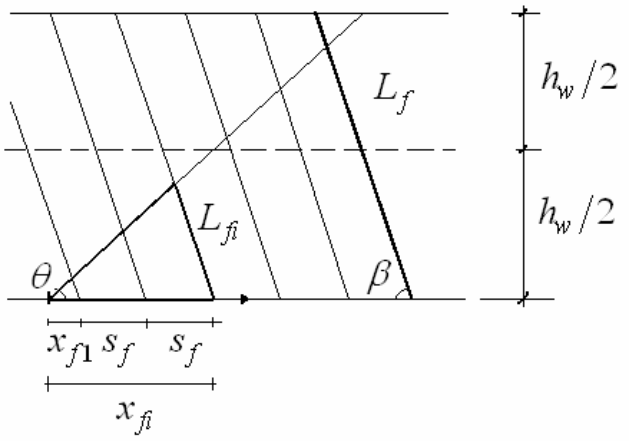

Fig. 9.3 – Application of the Chord Theorem to triangles

For a position x_{fi} of the laminate i-th laminate that is:

$$x_{fi} < \frac{h_w}{2} \cdot (\cot\theta + \cot\beta) \tag{9.9}$$

It results, by applying the Theorem of the Chord:

$$\frac{x_{f1} + (i-1)\cdot s_f}{\sin(\theta+\beta)} = \frac{L_{fi}}{\sin\theta} \quad \rightarrow \quad L_{fi} = \frac{\sin\theta}{\sin(\theta+\beta)} \cdot \left[x_{f1} + (i-1)\cdot s_f \right] \tag{9.10}$$

that yields:

$$L_{fi} = [x_{f1} + (i-1)\cdot s_f] \cdot \frac{\sin\theta}{\sin(\theta+\beta)} \quad \text{for} \quad x_{fi} < \frac{h_w}{2} \cdot (\cot\theta + \cot\beta) \tag{9.11}$$

While for a position x_{fi} of the laminate i-th laminate that is:

$$x_{fi} \geq \frac{h_w}{2} \cdot (\cot\theta + \cot\beta) \tag{9.12}$$

it results:

$$L_{fi} = L_f - \left[x_{f1} + (i-1)\cdot s_f \right] \cdot \frac{\sin\theta}{\sin(\theta+\beta)} \tag{9.13}$$

that yields:

$$L_{fi} = L_f - [x_{f1} + (i-1)\cdot s_f] \cdot \frac{\sin\theta}{\sin(\theta+\beta)} \quad \text{for} \quad x_{fi} \geq \frac{h_w}{2} \cdot (\cot\theta + \cot\beta) \tag{9.14}$$

Position of the first laminate $x_{f1,k}$

In the first configuration exhamined, the first laminate is positioned at a distance from the crack origin x_{f1}, equal to the spacing between laminates:

$$x_{f1,k} = s_f \tag{9.15}$$

The second geometrical configuration contemplates the possibility that the even number of laminates crossing the crack, $N_{f,ev}$, be disposed symmetrically with respect to the mean axis of the crack *i.e.* if the following condition is satisfied, see Fig. 9.4:

$$L_{f1} = L_{fN_{f,ev}} \tag{9.16}$$

.

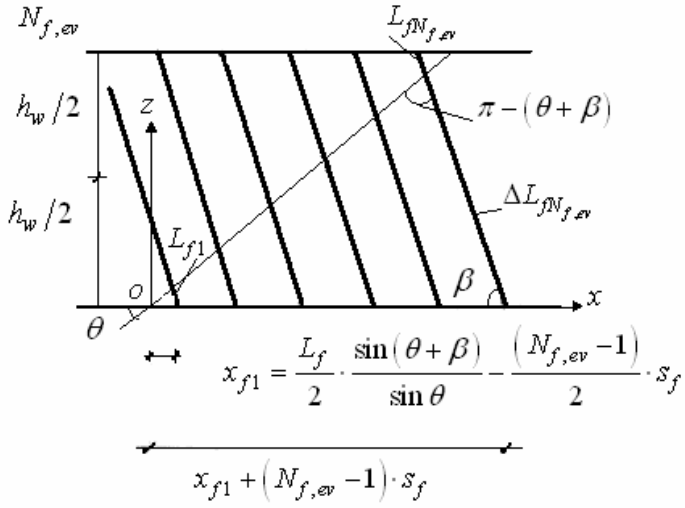

Fig. 9.4 – Symmetric disposition of an even number of laminates

From the figure above, the following developments can be deduced:
The effective length of the first laminate can be deduced as follows:

$$\frac{x_{f1}}{\sin(\beta+\theta)} = \frac{L_{f1}}{\sin\theta} \rightarrow L_{f1} = x_{f1}\cdot\frac{\sin\theta}{\sin(\theta+\beta)} \tag{9.17}$$

Moreover, the effective length of the laminate disposed symmetrically with respect to the axis of the crack can be obtained as follows:

$$L_{fN_{ev}} = L_f - \Delta L_{fN_{f,ev}} \tag{9.18}$$

$$\Delta L_{fN_{f,ev}} \rightarrow \frac{\Delta L_{fN_{f,ev}}}{\sin\theta} = \frac{x_{f1}+(N_{f,ev}-1)s_f}{\sin(\theta+\beta)} \rightarrow \Delta L_{fN_{f,ev}} = \frac{\sin\theta}{\sin(\theta+\beta)}\cdot\left[x_{f1}+(N_{f,ev}-1)\cdot s_f\right] \tag{9.19}$$

By introducing Eqs. 9.17-19, calculated as above in the governing condition, Eq. 9.16:

$$L_{f1} = L_{fN_{ev}} \rightarrow 2x_{f1}\frac{sen\,\theta}{sen\,(\theta+\beta)} = L_f - \frac{sen\,\theta}{sen\,(\theta+\beta)}(N_{ev}-1)s_f \tag{9.20}$$

Ultimately, the following expression is obtained:

$$x_{f1,2} = \frac{L_f}{2}\cdot\frac{\sin(\beta+\theta)}{\sin\theta} - \frac{(N_{f,ev}-1)}{2}\cdot s_f \tag{9.21}$$

The third configuration exhamined contemplates the possibility that the odd number of laminates, $N_{f,odd}$, be disposed in such a way that the middle laminate results of the maximum length possible. It has been deduced imposing that one of the laminates intersects the crack in correspondence of its mid point, *i.e.* according to Fig. 9.5 it is:

$$x_{f1} + \frac{\left(N_{f,odd} - 1\right)}{2} \cdot s_f = \frac{h_w}{2} \cdot \left(\cot\theta + \cot\beta\right) \tag{9.22}$$

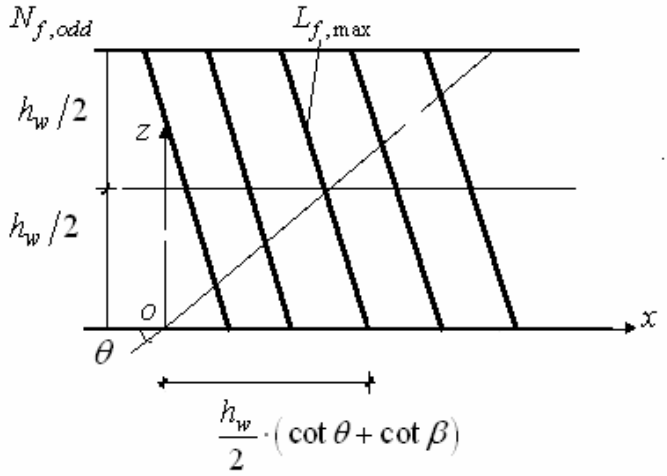

Fig. 9.5 – One of the odd number of laminates gets the highest length

From Eq. 9.22, the final formula can be obtained:

$$x_{f1,3} = \frac{h_w}{2} \cdot \left(\cot\theta + \cot\beta\right) - \frac{\left(N_{f,odd} - 1\right)}{2} \cdot s_f \tag{9.23}$$

8.2 Appendix B

Hereafter the test specimen geometry and the details of the materials employed are reported from the work by Teng *et al.* 2006.

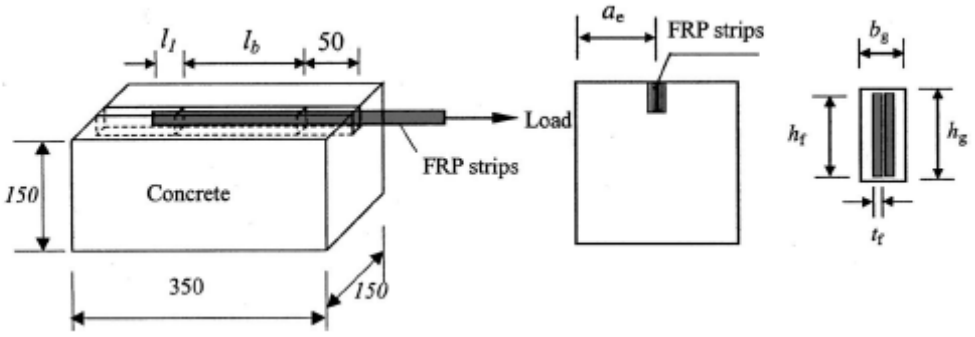

Fig. 9.6 – Specimen tested by Teng *et al.* 2006

The bonding test has been executed for different embedment lengths of the CFRP (l_b = 30; 100; 150; 200; 250), and for the materials shown in the following.

The concrete average cubic compressive strength ranged between 42 and 46 MPa, with an overall average of 44 MPa, and the average splitting tensile strength ranged between 3.1 and 3.7 MPa, with an overall average of 3.3 MPa.

The yield and ultimate strengths of the 8-mm steel bars, used as both compression and shear reinforcement, were 375 and 503 MPa, respectively, whereas the yield and ultimate strengths of the 12-mm steel bars used as tension reinforcement were 532 and 623 MPa, respectively. The corresponding yield strain of the tension reinforcement, computed with an assumed elastic modulus of 210 GPa, as strains were not measured in the tests, is equal to 2530.

The CFRP strips had a thickness, t_f , of 2 mm and a width, h_f, of 16 mm. Their ultimate tensile strength, f_u, and modulus of elasticity, E_f, as reported by the manufacturer, were equal, to 2068 MPa and 131 GPa, respectively. However, the value of E_f deduced from strain readings in the bond tests is 151 GPa. From the latter value of elastic modulus, the ultimate tensile strain of the CFRP strip can be computed as 1.37%. The strips had a surface texture obtained by peel-ply treatment.

The groove-filling material was a two-component epoxy adhesive with a mixing ratio of 2 resin: 1 hardener by weight. The elastic modulus and tensile strength averaged from five tensile tests conducted according to ASTM D638M-93 1993 are 2.62 GPa and 42.6 MPa, respectively.

Two CFRP strips were bonded together with the same adhesive used for groove filling, thus forming a double-strip bar whose total thickness was approximately equal to 5 mm i.e., 4 mm of CFRP plus about 1 mm of adhesive, whereas the width was still 16 mm. The use of such two-strip CFRP bars allowed strain gauges to be sandwiched between the two CFRP strips so that the strain gauges did not interfere with the interfacial behaviour of the NSM reinforcement and, in the meantime, were protected against mechanical damage due to interfacial movement.

Since the width-to-thickness ratio of the double-strip bar is more than 3 (4 considering only the CFRP), these double-strip bars may be considered as strips themselves.

8.3 Appendix C

Hereafter the details of the data concerning the beams' results used in chapter 5.4 are listed.

series	beam	t_f [mm]	w_f [mm]	E_f [GPa]	ß [°]	s_f [mm]	h_w [mm]	V_f [kN]	f_{ctm} [Mpa]
1st Dias/Barros	A10_VL	1,4	10	166,6	90	200	300	29,10	3,60
"	A10_IL	1,4	10	166,6	45	300	300	28,80	3,60
"	A12_VL	1,4	10	166,6	90	100	300	59,30	3,60
"	A12_IL	1,4	10	166,6	45	150	300	72,90	3,60
"	B10_VL	1,4	10	166,6	90	100	150	28,60	3,99
"	B10_IL	1,4	10	166,6	45	150	150	23,20	3,99
"	B12_VL	1,4	10	166,6	90	50	150	31,70	3,99
"	B12_IL	1,4	10	166,6	45	75	150	36,40	3,99
3rd Dias/Barros	2S_3LV	1,4	10	166,6	90	267	300	35,00	2,45
"	2S_5LV	1,4	10	166,6	90	160	300	50,00	2,45
"	2S_7LV	1,4	10	166,6	90	100	300	75,00	2,45
"	2S_3LI45	1,4	10	166,6	45	367	300	23,00	2,45
"	2S_5LI45	1,4	10	166,6	45	220	300	70,00	2,45
"	2S_8LI45	1,4	10	166,6	45	138	300	85,00	2,45
"	2S_3LI60	1,4	10	166,6	60	325	300	62,00	2,45
"	2S_5LI60	1,4	10	166,6	60	195	300	75,00	2,45
"	2S_7LI60	1,4	10	166,6	60	139	300	98,00	2,45
2nd Barros/Dias	CRFLV1	1,4	10	166,6	90	50	300	96,4	3,52
"	CRFLV2	1,4	10	166,6	90	50	300	100,9	3,52
"	CRFLI1	1,4	10	166,6	45	70	300	147,3	3,52
"	CFRLI2	1,4	10	166,6	45	70	300	143,2	3,52
"	CFRLI3	1,4	10	166,6	45	70	300	155,4	3,52
"	7SRFLV	1,4	10	166,6	90	150	300	66,7	3,52
"	7SRFLI	1,4	10	166,6	45	210	300	49,8	3,52
"	5SRFLV	1,4	10	166,6	90	90	300	20,2	3,52
"	5SRFLI	1,4	10	166,6	45	125	300	60,2	3,52

Fig. 9.7 – General Informations about the beams by Dias and Barros 2006

beam	$A_{tot,min}$ [mm^2]	$\nabla_{CR,vert}$ [kN]	V_f^{exp} [kN]	ΔV [%]
A10_VL	4933,91	17,76	29,10	-63,83
A10_IL	15370,13	39,13	28,80	26,39
A12_VL	14440,73	51,99	59,30	-14,07
A12_IL	19622,92	49,95	72,90	-45,94
B10_VL	1744,40	6,96	28,60	-310,91
B10_IL	1921,27	5,42	23,20	-328,00
B12_VL	5105,57	20,37	31,70	-55,61
B12_IL	8370,51	23,62	36,40	-54,13
2S_3LV	537,30	1,32	35,00	-2558,78
2S_5LV	9670,46	23,69	50,00	-111,04
2S_7LV	14440,74	35,38	75,00	-111,99
2S_3LI45	9271,43	16,06	23,00	-43,20
2S_5LI45	24660,52	42,72	70,00	-63,85
2S_8LI45	37424,94	64,84	85,00	-31,10
2S_3LI60	4116,47	8,73	62,00	-609,86
2S_5LI60	14505,34	30,78	75,00	-143,69
2S_7LI60	21210,52	45,00	98,00	-117,76
CRFLV1	20817,34	73,32	96,40	-31,48
CRFLV2	20817,34	73,32	100,90	-37,62
CRFLI1	43359,57	107,98	147,30	-36,41
CFRLI2	43359,57	107,98	143,20	-32,62
CFRLI3	43359,57	107,98	155,40	-43,91
7SRFLV	11101,29	39,10	66,70	-70,60
7SRFLI	25975,52	64,69	49,80	23,02
5SRFLV	14789,03	52,09	20,20	61,22
5SRFLI	38489,57	95,85	60,20	37,20
				-183,41

a)

beam	$A_{tot,mean}$ [mm^2]	$\nabla_{CR,vert}$ [kN]	V_f^{exp} [kN]	ΔV [%]
A10_VL	13413,88	48,29	29,10	39,74
A10_IL	20942,74	53,31	28,80	45,98
A12_VL	19400,77	69,84	59,30	15,10
A12_IL	27993,17	71,26	72,90	-2,30
B10_VL	2616,60	10,44	28,60	-173,94
B10_IL	4803,17	13,55	23,20	-71,20
B12_VL	6913,78	27,59	31,70	-14,91
B12_IL	9258,80	26,12	36,40	-39,34
2S_3LV	11369,94	27,86	35,00	-25,64
2S_5LV	15936,52	39,04	50,00	-28,06
2S_7LV	19555,13	47,91	75,00	-56,54
2S_3LI45	19513,14	33,80	23,00	31,96
2S_5LI45	29393,65	50,92	70,00	-37,47
2S_8LI45	38647,92	66,95	85,00	-26,95
2S_3LI60	12549,71	26,63	62,00	-132,84
2S_5LI60	18393,11	39,03	75,00	-92,18
2S_7LI60	24526,50	52,04	98,00	-88,32
CRFLV1	23800,77	83,82	96,40	-15,00
CRFLV2	23800,77	83,82	100,90	-20,37
CRFLI1	43475,48	108,27	147,30	-36,05
CFRLI2	43475,48	108,27	143,20	-32,26
CFRLI3	43475,48	108,27	155,40	-43,53
7SRFLV	16651,93	58,65	66,70	-13,73
7SRFLI	30631,80	76,28	49,80	34,72
5SRFLV	20139,46	70,93	20,20	71,52
5SRFLI	39673,45	98,80	60,20	39,07
				-25,87

b)

Fig. 9.8 – a) Minimum Total Area; b) Average Total Area

beam	$A_{tot,max}$ [mm^2]	$\nabla_{CR,vert}$ [kN]	V_f^{exp} [kN]	ΔV [%]
A10_VL	21893,86	78,82	29,10	63,08
A10_IL	26515,36	67,50	28,80	57,33
A12_VL	24360,81	87,70	59,30	32,38
A12_IL	36363,41	92,57	72,90	21,25
B10_VL	3488,80	13,92	28,60	-105,46
B10_IL	7685,06	21,68	23,20	-7,00
B12_VL	8722,00	34,80	31,70	8,91
B12_IL	10147,08	28,63	36,40	-27,15
2S_3LV	22202,58	54,40	35,00	35,66
2S_5LV	22202,58	54,40	50,00	8,08
2S_7LV	24669,53	60,44	75,00	-24,09
2S_3LI45	29754,84	51,55	23,00	55,38
2S_5LI45	34126,79	59,12	70,00	-18,40
2S_8LI45	39870,91	69,07	85,00	-23,06
2S_3LI60	20982,95	44,52	62,00	-39,26
2S_5LI60	22280,87	47,27	75,00	-58,65
2S_7LI60	27842,48	59,08	98,00	-65,89
CRFLV1	26784,20	94,33	96,40	-2,19
CRFLV2	26784,20	94,33	100,90	-6,96
CRFLI1	43591,39	108,56	147,30	-35,69
CFRLI2	43591,39	108,56	143,20	-31,91
CFRLI3	43591,39	108,56	155,40	-43,15
7SRFLV	22202,58	78,20	66,70	14,70
7SRFLI	35288,09	87,88	49,80	43,33
5SRFLV	25489,89	89,77	20,20	77,50
5SRFLI	40857,33	101,75	60,20	40,83
				-1,17

a)

Nanni et al.

beam	$V_{f\,R,vert}^{ana}$ [kN]	V_f^{exp} [kN]	DV [%]
A10_VL	55,39	29,10	47,46
A10_IL	52,39	28,80	45,03
A12_VL	110,78	59,30	46,47
A12_IL	132,87	72,90	45,13
B10_VL	37,94	28,60	24,61
B10_IL	40,24	23,20	42,34
B12_VL	75,87	31,70	58,22
B12_IL	95,84	36,40	62,02
2S_3LV	27,21	35,00	-28,64
2S_5LV	63,63	50,00	21,42
2S_7LV	110,78	75,00	32,30
2S_3LI45	47,34	23,00	51,42
2S_5LI45	87,96	70,00	20,42
2S_8LI45	151,66	85,00	43,95
2S_3LI60	49,78	62,00	-24,55
2S_5LI60	92,42	75,00	18,85
2S_7LI60	132,94	98,00	26,28
CRFLV1	251,76	96,4	61,71
CRFLV2	251,76	100,9	59,92
CRFLI1	303,49	147,3	51,47
CFRLI2	303,49	143,2	52,82
CFRLI3	303,49	155,4	48,80
7SRFLV	65,11	66,7	-2,44
7SRFLI	89,33	49,8	44,25
5SRFLV	137,39	20,2	85,30
5SRFLI	164,79	60,2	63,47
	mean value		38,39

b)

Fig. 9.9 – a) Maximum Total Area; b) Pure Debonding Model

8.4 Appendix D

Hereafter the details of the origin of some formulae present in the analytical development (see Chapter 6) of the proposed model are reported.

Block 2: Definition of the geometrical quantities and the ellipses' equations in the crack plane reference system $OXYZ$

Step 1: Determination of the position of each laminate and further informations necessary to write the equation of each semi-ellipse in its own local reference system

The position of each laminate, along the OX axis can be determined by applying the theorem of the Chord as already shown in Appendix A, see Fig. 9.10:

$$\frac{X_{fi}}{\sin\beta} = \frac{x_{f1} + (i-1)\cdot s_f}{\sin(\beta+\theta)} \tag{9.24}$$

$$X_{fi} = \frac{\sin\beta}{\sin(\beta+\theta)} \cdot \left[x_{f1} + (i-1)\cdot s_f \right] \tag{9.25}$$

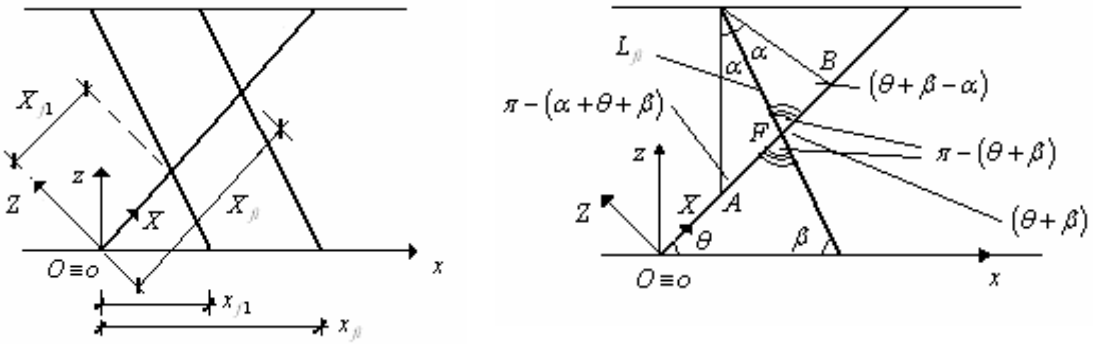

Fig. 9.10 – a) Position of each laminate in $OXYZ$; b) Determination of the major semi-axis

As regards the determination of the two semi-axes of the semi-ellipse associated with the i-th laminate, from Fig. 9.10, it results:

$$\overline{AF} = L_{fi} \cdot \frac{\sin\alpha_{fi}}{\sin\left(\alpha_{fi}+\beta+\theta\right)} \tag{9.26}$$

$$\overline{FB} = L_{fi} \cdot \frac{\sin\alpha_{fi}}{\sin\left(\theta+\beta-\alpha_{fi}\right)} \tag{9.27}$$

Thus the major semi-axis of i-th semi-ellipse is as follows:

$$a_i = \frac{L_{fi}}{2} \cdot \sin\alpha_{fi} \cdot \left[\frac{1}{\sin\left(\alpha_{fi} + \beta + \theta\right)} + \frac{1}{\sin\left(\theta + \beta - \alpha_{fi}\right)} \right] \tag{9.28}$$

The coordinates of another point P (*i.e.* the point of intersection with the vertical plane orthogonal to the web and having the laminate, as trace, in the plane OXZ) in the local reference system are as follows, see Fig. 9.11:

$$e_{1Pi} = X_{fi} - X_{oi} \tag{9.29}$$

$$e_{2Pi} = L_{fi} \cdot \tan\alpha_{fi} \tag{9.30}$$

It is necessary to detemine the coordinates of the auxiliary point P since, to write the equation of an ellipse, *i.e.* a second order curve, in its own local reference system, two conditions are required. In this case, the available informations are the coordinates of the auxilary point P (one condition) plus the length of the major semi-axis a_i (one condition).

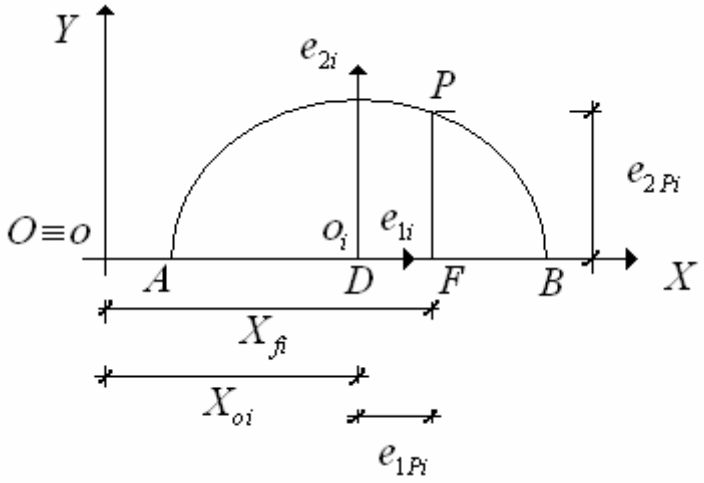

Fig. 9.11 – Local reference system $o_i e_{1i} e_{2i}$ of the i-th semi-ellipse

At this point the length of the minor semi-axis b_i can be easily determined by writing the equation of the ellipse in its local reference system $o_i e_{1i} e_{2i}$ (see Fig. 9.11), known the two conditions necessary to determine it:

$$\frac{e_{1Pi}^2}{a_i^2} + \frac{e_{2Pi}^2}{b_i^2} = 1 \tag{9.31}$$

$$b_i = \sqrt{\frac{a_i^2 \cdot e_{2Pi}^2}{\left(a_i^2 - e_{1Pi}^2\right)}} \tag{9.32}$$

As regards the determination of the position, X_{oi}, along the OX axis, of the center of the i-th semi-ellipse, (see Fig. 9.12) for:

$$x_{fi} < \frac{h_w}{2} \cdot \left(\cot\theta + \cot\beta\right) \tag{9.33}$$

it is:

$$X_{oi} = p_{fi} + a_i \tag{9.34}$$

From the application of the Theorem of the Chord, see Fig. 9.12:

$$p_{fi} = x_{fi} \cdot \frac{\sin\left(\beta - \alpha_{fi}\right)}{\sin\left(\theta + \beta - \alpha_{fi}\right)} \tag{9.35}$$

Introducing Eq. 9.35 into Eq. 9.34, it follows:

$$X_{oi} = x_{fi} \cdot \frac{\sin\left(\beta - \alpha_{fi}\right)}{\sin\left(\beta + \theta - \alpha_{fi}\right)} + a_i \quad \text{for} \quad \left(x_{fi} < \frac{h_w}{2} \cdot \left(\cot\theta + \cot\beta\right)\right) \tag{9.36}$$

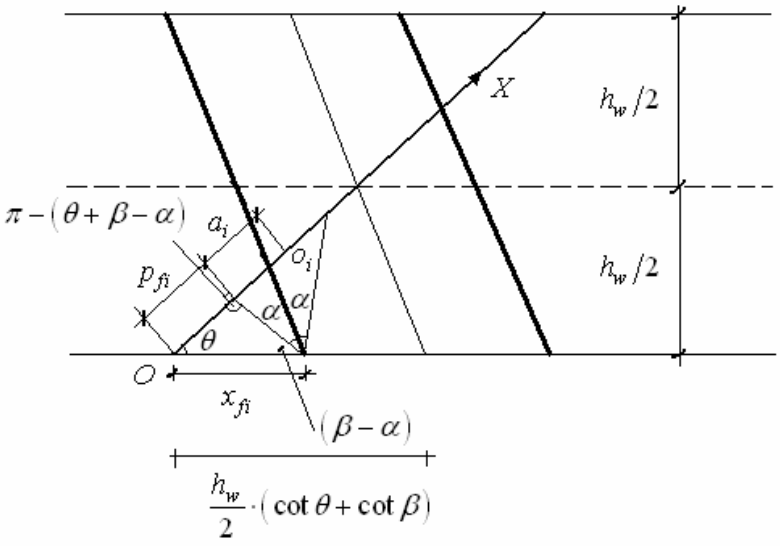

Fig. 9.12 – Determination of the position of the center of the i-th semi-ellipse along the OX axis for $x_{fi} < \frac{h_w}{2} \cdot \left(\cot\theta + \cot\beta\right)$

For laminates whose position in the global reference system is:

$$x_{fi} \geq \frac{h_w}{2} \cdot \left(\cot\theta + \cot\beta\right) \tag{9.37}$$

it is, see Fig. 9.13:

$$X_{oi} = L_d - \left(p_{fi} + a_i\right) \tag{9.38}$$

$$p_{fi} = p_o \cdot \frac{\sin\left(\beta - \alpha_{fi}\right)}{\sin\left(\theta + \beta - \alpha_{fi}\right)} \tag{9.39}$$

$$p_o = h_w \cdot \left(\cot\theta + \cot\beta\right) - x_{fi} \tag{9.40}$$

Substituting Eqs. 9.39 and 9.40 in Eq. 9.38, it results:

$$X_{oi} = \frac{h_w}{\sin\theta} - \frac{\sin\left(\beta - \alpha_{fi}\right)}{\sin\left(\theta + \beta - \alpha_{fi}\right)} \cdot \left[h_w \cdot \left(\cot\theta + \cot\beta\right) - x_{fi} \right] - a_i$$
$$\text{for } \left(x_{fi,k} \geq \frac{h_w}{2} \cdot \left(\cot\theta + \cot\beta\right) \right) \tag{9.41}$$

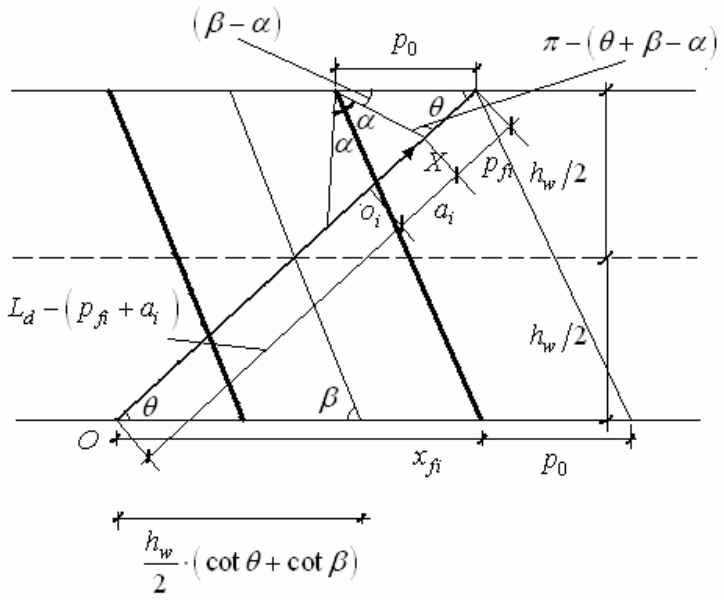

Fig. 9.13 – Determination of the position of the center of the i-th semi-ellipse along the OX axis for $x_{fi} \geq \frac{h_w}{2} \cdot \left(\cot\theta + \cot\beta\right)$

Step 2: determination of the equations of the ellipses in the global reference system

Once the equation of each ellipse is known in its own local reference system $o_i e_{1i} e_{2i}$, in the form:

$$\frac{e_{1i}^2}{a_i^2} + \frac{e_{2i}^2}{b_i^2} = 1 \tag{9.42}$$

changing the reference system, by means of the following equations, the several coefficients of the equation $E_i(\mathrm{X};\mathrm{Y})$ can be determined:

$$\begin{cases} X = X_{oi} + e_{1i} \\ Y = e_{2i} \end{cases} \tag{9.43}$$

From those substitutions it follows:

$$b_i^2 \cdot X^2 + a_i^2 \cdot Y^2 + \left(-2 \cdot X_{oi} \cdot b_i^2\right) \cdot X + \left(b_i^2 \cdot X_{oi}^2 - a_i^2 \cdot b_i^2\right) = 0 \tag{9.44}$$

And the following values of the coefficients:

$$E_{i1} = b_i^2 \tag{9.45}$$

$$E_{i2} = a_i^2 \tag{9.46}$$

$$E_{i3} = -2 \cdot b_i^2 \cdot X_{0i} \tag{9.47}$$

$$E_{i4} = b_i^2 \cdot X_{0i}^2 - a_i^2 \cdot b_i^2 \tag{9.48}$$

Block 5: Determination of the effective integration points $\underline{X}^{nlin1/2}$

The first condition of acceptance for the value $X_{ij}^{p1/2} \in \underline{X}^{p1/2}$ of the abscissa of the point of intersection between the i-th and j-th ellipses, to be accepted as limit of integration interval for the i-th semi-ellipse is that it belongs to the uppermost border line *i.e.*:

$$Y_i\left(X_{ij}^{p1/2}\right) \geq Y_h\left(X_{ij}^{p1/2}\right) \text{ for } h = 1,...,N_f \tag{9.49}$$

It means that, for the counter h varying between 1 and N_f, the value $Y_h\left(X_{ij}^{p1/2}\right)$ has to be minor or equal to the one assumed by the i-th ellipse $Y_i\left(X_{ij}^{p1/2}\right)$.

The equation of an ellipse is as follows:

$$E_i\left(X;Y\right) = E_{1i} \cdot \mathrm{X}^2 + E_{2i} \cdot \mathrm{Y}^2 + E_{3i} \cdot \mathrm{X} + E_{4i} = 0 \tag{9.50}$$

The positive value (the negative is not of interest for our method being the half-crack plane placed in the positive quadrant of the reference system OXY) assumed in correspondence of a general X value is equal to:

$$Y_i\left(X\right) = \sqrt{-\frac{\left[E_{1i} \cdot X^2 + E_{3i} \cdot X + E_{4i}\right]}{E_{2i}}} = \sqrt{\Delta_i\left(X\right)} \tag{9.51}$$

with:

- If the ellipse actually passes through that point and assumes a value different than zero, it results $\Delta_i\left(X\right) > 0$;
- If the ellipse does not pass through it, it results $\Delta_i\left(X\right) < 0$.

Provided that, the above condition of acceptance of $X_{ij}^{p1/2} \in \underline{X}^{p1/2}$ yields:

$$\sqrt{-\frac{\left[E_{1i} \cdot \left(X_{ij}^{p1/2}\right)^2 + E_{3i} \cdot \left(X_{ij}^{p1/2}\right) + E_{4i}\right]}{E_{2i}}} \geq \sqrt{-\frac{\left[E_{1h} \cdot \left(X_{ij}^{p1/2}\right)^2 + E_{3h}\left(X_{ij}^{p1/2}\right) + E_{4h}\right]}{E_{2h}}} \tag{9.52}$$

where the first member's determinant is positive because $X_{ij}^{p1/2}$ is the abscissa of a point through which the i-th ellipse actually passes, according to the calculation developed in Block 4, while the second can be higher, less than or equal to zero for $h = 1....N_f$ since, in eneral, the h-th ellipse can pass, can not pass or pass through that pont and assume null ordinate. Thus the above condition can be reported to the radicand of the square roots and the sign inverted, yielding:

$$\frac{\left[E_{1i} \cdot \left(X_{ij}^{p1/2}\right)^2 + E_{3i} \cdot \left(X_{ij}^{p1/2}\right) + E_{4i}\right]}{E_{2i}} \leq \frac{\left[E_{1h} \cdot \left(X_{ij}^{p1/2}\right)^2 + E_{3h}\left(X_{ij}^{p1/2}\right) + E_{4h}\right]}{E_{2h}} \tag{9.52}$$

And ultimately it provides:

$$Y_i\left(X_{ij}^{p1/2}\right) \geq Y_h\left(X_{ij}^{p1/2}\right) \quad \rightarrow \quad \left(\frac{E_{1i}}{E_{2i}} - \frac{E_{1h}}{E_{2h}}\right) \cdot \left(X_{ij}^{p1/2}\right)^2 + \left(\frac{E_{3i}}{E_{2i}} - \frac{E_{3h}}{E_{2h}}\right) \cdot \left(X_{ij}^{p1/2}\right) + \left(\frac{E_{4i}}{E_{2i}} - \frac{E_{4h}}{E_{2h}}\right) \leq 0 \tag{9.52}$$

8.5 Appendix E

It is necessary to check the effective reliability and generality of the algorithm developed (see Chapter 6). In particular it is necessary to see if for all the particular cases that can be encountered, the algorithm works without problems selecting appropriate couples of numbers defining the integration intervals. Note that, for the sake of rapidity, few attention has been paid to the quality of the drawings below, keeping in mind that they have to schematize semi-ellipses whose major semi-axis lies on the axis $Y = 0$. The general sequence of calculations, already explained in Blocks 5 and 6 of the above Chapter 6.1 follows, for both the *Linear* and *Non Linear* integration ranges, the several steps schematized by the flow chart of Fig. 6.11:

1. Do the auxiliary points lie within the area of interest for the relevant integration (*i.e. Linear* or *Non Linear*)?;
2. Do they lie on the upper border line?;
3. Do they effectively constitute useful extremities for the integration in *Linear* or *Non-Linear* range?;
4. Have the corresponding abscissa value already been stored, in the i-th row and for previous values of the j counter?

The calculations corresponding to each of the questions above, will particularize depending on the integration range *i.e.*: *Lin* or *Non-Lin*.

Case 1) two ellipses intersect each other along the line $Y = b_w/2$

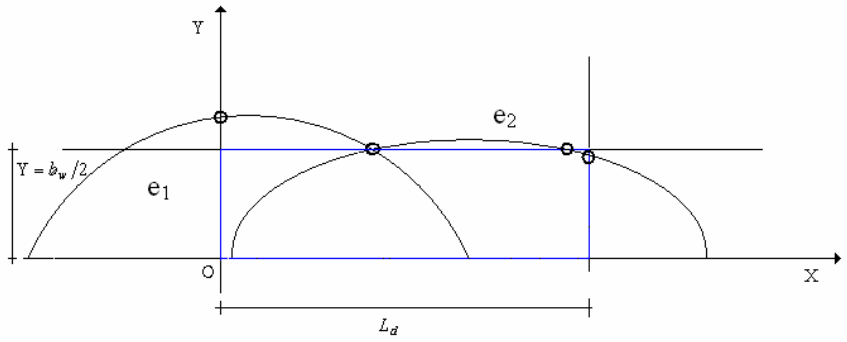

Fig. 9.5.1 – Case 1

The corresponding auxiliary matrices of the selected points are:

$$\underline{X}^{p1} = \begin{bmatrix} * & X_{12}^{p1} \\ X_{21}^{p1} & * \end{bmatrix}; \quad \underline{X}^{p2} = \begin{bmatrix} * & * \\ * & * \end{bmatrix}; \quad \underline{X}^{q} = \begin{bmatrix} X_{11}^{q} & X_{12}^{q} \\ X_{21}^{q} & X_{22}^{q} \end{bmatrix};$$

with $X_{12}^{q} = X_{21}^{q}$

$$\underline{G} = \begin{bmatrix} ...;\left(X_{o1} - a_1\right) & \left(X_{o1} + a_1\right) \\ ...;\left(X_{o2} - a_2\right) & \left(X_{o2} + a_2\right) \end{bmatrix}; \tag{9.5.1}$$

$$\underline{Y}^{e} = \begin{bmatrix} Y_{11}^{e} & * \\ * & Y_{22}^{e} \end{bmatrix}$$

with $Y_{11}^{e} > b_w/2$ and $Y_{22}^{e} < b_w/2$

The matrices built according to the calculations of Block 5:

$$\underline{X}^{nlin1}=\begin{bmatrix}* & *\\ * & *\end{bmatrix};\ \underline{X}^{nlin2}=\begin{bmatrix}* & *\\ * & *\end{bmatrix};\ \underline{X}^{nlin3}=\begin{bmatrix}* & *\\ * & X_{22}^{q}\end{bmatrix};$$
$$\underline{X}^{nlin4}=\begin{bmatrix}* & *\\ * & L_d\end{bmatrix};\ \underline{X}^{nlin5}=\begin{bmatrix}* & *\\ * & *\end{bmatrix};\ \underline{n}^{nlin}=\begin{bmatrix}0\\ 2\end{bmatrix};\ n^{nlin}=2$$
$$\text{and the final matrix is } \underline{X}^{nlin}=\begin{bmatrix}* & *\\ X_{22}^{q} & L_d\end{bmatrix} \tag{9.5.2}$$

and the matrix of the final areas:

$$\underline{\mathrm{A}}^{nlin}=\begin{bmatrix}*\\ \neq 0\end{bmatrix}$$

The auxiliary intersection point $X_{12}^{p1}=X_{21}^{p1}$ is discarded because it is outside of the relevant range of interest, $0<X_{ij,k}^{p1/2}<L_d$ and $0<Y_{i,k}\left(X_{ij,k}^{p1/2}\right)<\frac{b_w}{2}$. The point X_{11}^{q} is discarded because it is outside of the relevant range of interest while X_{12}^{q} and X_{21}^{q} are both inside the relevant range of interest and on the upper border line of the area to be calculated but they are not useful for the integration in the Non-Linear Range because they do not have, on the right and on the left side, respectively, a non linear branch that effectively constitutes border line. On the contrary, the abscissa of the point X_{22}^{q} results to be useful for the Non-Linear integration range because, on its right side, is followed by a non-linear branch enclosing the area to be calculated. As regards the vertices of the ellipses on the major semi-axis, $\left(X_{o1}-a_1\right)$ and $\left(X_{o2}+a_2\right)$ are discarded by the calculations of Block 5 because they are outside the relevant area of interest, *i.e.* $0\le\left(X_{oi,k}-a_{i,k}\right)\le L_d$ while $\left(X_{o1}+a_1\right)$ and $\left(X_{o2}-a_2\right)$ are discarded because the corresponding points do not lie on the upper border line of the area to be calculated. As to the points of intersection of the semi-ellipses with the lines $X=0$ and $X=L_d$, $Y_{11}^{e}=Y_1\left(X=0\right)$ is discarded because lying outside of the relevant range of interest for the Non Linear integration. On the contrary, $Y_{22}^{e}=Y_2\left(X=L_d\right)$ is accepted and copied in the corresponding cell of the matrix $\underline{X}^{nlin4}$ because it meets all of the acceptance conditions resulting an effective extremity of integration.

As regards the Linear range of integration:

$$\underline{X}^{lin1}=\begin{bmatrix}* & *\\ * & *\end{bmatrix};\ \underline{X}^{lin2}=\begin{bmatrix}* & *\\ * & *\end{bmatrix};\ \underline{X}^{lin3}=\begin{bmatrix}* & X_{12}^{q}\\ X_{21}^{q} & X_{22}^{q}\end{bmatrix};$$
$$\text{with } X_{12}^{e}=X_{21}^{e};\ \underline{X}^{lin4}=\begin{bmatrix}0 & *\\ * & *\end{bmatrix};\ \underline{n}^{lin}=\begin{bmatrix}2\\ 2\end{bmatrix};\ n^{lin}=2$$
$$\text{and the final matrix is } \underline{X}^{lin}=\begin{bmatrix}0 & X_{12}^{q}\\ X_{21}^{q} & X_{22}^{q}\end{bmatrix} \tag{9.5.3}$$

and the matrix of the final areas:

$$\underline{\mathrm{A}}^{lin}=\begin{bmatrix}\neq 0\\ \neq 0\end{bmatrix}$$

For the Linear integration, the abscissa value $X_{12}^{p1} = X_{21}^{p1}$ is discarded because, the corresponding point, lies on the line $Y = b_w/2$ and therefore outside the area of interest defined by: $0 < X_{ij,k}^{p1/2} < L_d$ and $Y_{i,k}\left(X_{ij,k}^{p1/2}\right) > \frac{b_w}{2}$. X_{12}^{e} and X_{22}^{e} are useful because they meet all of the conditions of acceptance (see Block 6 of Chapter 6.1) since they are within the area of interest, placed on the border line and useful for the Linear range integration. In fact, on their left side, the relevant semi-ellipse constitutes border line. X_{21}^{e} also meets all the acceptance conditions. Likewise, the auxiliary point $Y_{11}^{e} = Y_1\left(X = 0\right)$ is accepted because useful for the Linear integration range and the relevant value of the abscissa is copied in the corresponding cell of the matrix $\underline{X}^{lin4}$.

Hence the algorithm works satisfactorily.

Case 2) three (or more) ellipses intersect each other along the line $Y = b_w/2$

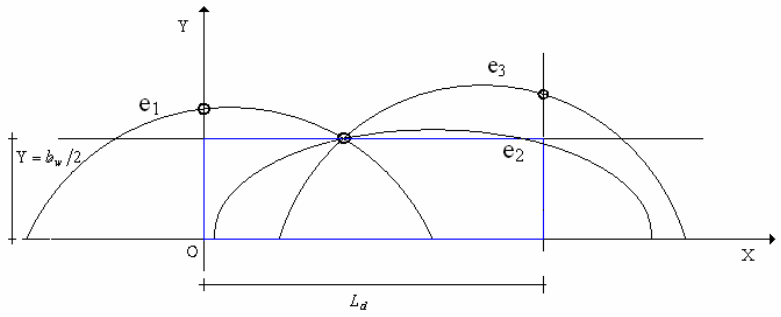

Fig. 9.5.2 – Case 2

The corresponding auxiliary matrices of the selected points are:

$$\underline{X}^{p1} = \begin{bmatrix} * & X_{12}^{p1} & X_{13}^{p1} \\ X_{21}^{p1} & * & X_{23}^{p1} \\ X_{31}^{p1} & X_{32}^{p1} & * \end{bmatrix}; \quad \underline{X}^{p2} = \begin{bmatrix} * & * & * \\ * & * & * \\ * & * & * \end{bmatrix}; \quad \underline{X}^{q} = \begin{bmatrix} X_{11}^{q} & X_{12}^{q} \\ X_{21}^{q} & X_{22}^{q} \\ X_{31}^{q} & X_{32}^{q} \end{bmatrix};$$

with $X_{12}^{p1} = X_{13}^{p1} = X_{21}^{p1} = X_{23}^{p1} = X_{31}^{p1} = X_{32}^{p1}$ and $X_{12}^{q} = X_{21}^{q} = X_{31}^{q}$

$$\underline{G} = \begin{bmatrix} .....\left(X_{o1} - a_1\right) & \left(X_{o1} + a_1\right) \\ .....\left(X_{o2} - a_2\right) & \left(X_{o2} + a_2\right) \\ .....\left(X_{o3} - a_3\right) & \left(X_{o3} + a_3\right) \end{bmatrix}; \tag{9.5.4}$$

$$\underline{Y}^{e} = \begin{bmatrix} Y_{11}^{e} & * \\ * & Y_{22}^{e} \\ * & Y_{32}^{e} \end{bmatrix}$$

with $Y_{11}^{e} > b_w/2$; $Y_{32}^{e} > b_w/2$ and $Y_{22}^{e} < b_w/2$

The matrices built according to the calculations of Block 5:

$$\underline{X}^{nlin1} = \begin{bmatrix} * & * & * \\ * & * & * \\ * & * & * \end{bmatrix}; \ \underline{X}^{nlin2} = \begin{bmatrix} * & * & * \\ * & * & * \\ * & * & * \end{bmatrix}; \ \underline{X}^{nlin3} = \begin{bmatrix} * & * \\ * & * \\ * & * \end{bmatrix};$$

$$\underline{X}^{nlin4} = \begin{bmatrix} * & * \\ * & * \\ * & * \end{bmatrix}; \ \underline{X}^{nlin5} = \begin{bmatrix} * & * \\ * & * \\ * & * \end{bmatrix}; \ \underline{n}^{nlin} = \begin{bmatrix} 0 \\ 0 \\ 0 \end{bmatrix}; \ n^{nlin} = 0 \tag{9.5.5}$$

and the final matrix $\underline{X}^{nlin}$ is not built at all

and the matrix of the final areas of the NLin:

$$\underline{\mathrm{A}}^{nlin} = \begin{bmatrix} * \\ * \\ * \end{bmatrix}$$

As regards the Linear range of integration:

$$\underline{X}^{lin1} = \begin{bmatrix} * & * & * \\ * & * & * \\ * & * & * \end{bmatrix}; \ \underline{X}^{lin2} = \begin{bmatrix} * & * & * \\ * & * & * \\ * & * & * \end{bmatrix}; \ \underline{X}^{lin3} = \begin{bmatrix} * & X_{12}^{q} \\ * & * \\ X_{31}^{q} & * \end{bmatrix};$$

with $X_{12}^{e} = X_{31}^{e}$; $\underline{X}^{lin4} = \begin{bmatrix} 0 & * \\ * & * \\ * & L_d \end{bmatrix}$; $\underline{n}^{lin} = \begin{bmatrix} 2 \\ 0 \\ 2 \end{bmatrix}$; $n^{lin} = 2$

and the final matrix is $\underline{X}^{lin} = \begin{bmatrix} 0 & X_{12}^{q} \\ * & * \\ X_{31}^{q} & L_d \end{bmatrix}$ (9.5.6)

and the matrix of the final areas in the Lin range:

$$\underline{\mathrm{A}}^{lin} = \begin{bmatrix} \neq 0 \\ * \\ \neq 0 \end{bmatrix}$$

Hence the algorithm works satisfactorily.

Case 3) three ellipses (e_1;e_2;e_3) intersect each other along the line $Y = 0$ and one (e_2) results to be completely inside the other (e_1)

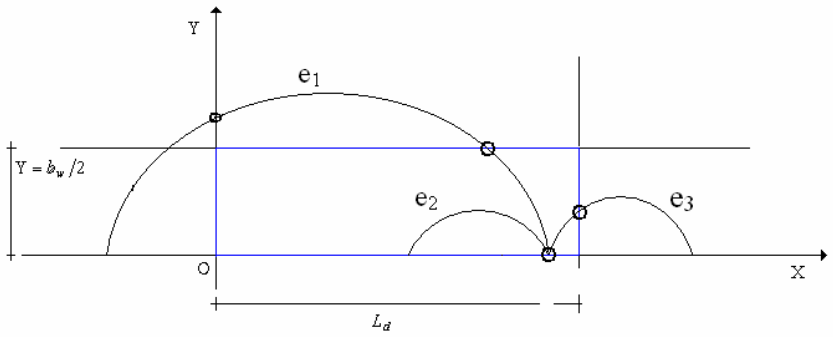

Fig. 9.5.3 – Case 3

The corresponding auxiliary matrices of the selected points are:

$$\underline{X}^{p1}=\begin{bmatrix}* & * & *\\ * & * & *\\ * & * & *\end{bmatrix};\ \underline{X}^{p2}=\begin{bmatrix}* & * & *\\ * & * & *\\ * & * & *\end{bmatrix};\ \underline{X}^{q}=\begin{bmatrix}X_{11}^{q} & X_{12}^{q}\\ * & *\\ * & *\end{bmatrix};$$

N.B.: even if they intersect each other along the X axis, the algorithm selects only intersection points with $Y>0$

$$\underline{G}=\begin{bmatrix}.....;\left(X_{o1}-a_1\right) & \left(X_{o1}+a_1\right)\\ .....;\left(X_{o2}-a_2\right) & \left(X_{o2}+a_2\right)\\ .....;\left(X_{o3}-a_3\right) & \left(X_{o3}+a_3\right)\end{bmatrix};\quad \underline{Y}^{e}=\begin{bmatrix}Y_{11}^{e} & *\\ * & *\\ * & Y_{32}^{e}\end{bmatrix} \tag{9.5.7}$$

with $\left(X_{o1}+a_1\right)=\left(X_{o2}+a_2\right)=\left(X_{o3}-a_3\right)$

and $Y_{11}^{e}>b_w/2$ and $Y_{22}^{e}<b_w/2$

The matrices of the effective selected points in the Non-Linear range are:

$$\underline{X}^{nlin1}=\begin{bmatrix}* & * & *\\ * & * & *\\ * & * & *\end{bmatrix};\ \underline{X}^{nlin2}=\begin{bmatrix}* & * & *\\ * & * & *\\ * & * & *\end{bmatrix};\ \underline{X}^{nlin3}=\begin{bmatrix}* & X_{12}^{q}\\ * & *\\ * & *\end{bmatrix};\ \underline{X}^{nlin4}=\begin{bmatrix}* & *\\ * & *\\ * & L_d\end{bmatrix}$$

$$\underline{X}^{nlin5}=\begin{bmatrix}* & \left(X_{o1}+a_1\right)\\ * & *\\ \left(X_{o3}-a_3\right) & *\end{bmatrix};\ \underline{n}^{nlin}=\begin{bmatrix}2\\0\\2\end{bmatrix};\ n^{nlin}=2\quad \text{with } \left(X_{o1}+a_1\right)=\left(X_{o3}-a_3\right) \tag{9.5.8}$$

and the final matrix is: $\underline{X}^{nlin}=\begin{bmatrix}X_{12}^{q} & \left(X_{o1}+a_1\right)\\ * & *\\ \left(X_{o3}-a_3\right) & L_d\end{bmatrix}$ and the final areas: $\underline{\mathrm{A}}^{nlin}=\begin{bmatrix}\neq 0\\ *\\ \neq 0\end{bmatrix}$

The matrices of the effective selected points in the Linear range are:

$$\underline{X}^{lin1}=\begin{bmatrix}* & * & *\\ * & * & *\\ * & * & *\end{bmatrix};\ \underline{X}^{lin2}=\begin{bmatrix}* & * & *\\ * & * & *\\ * & * & *\end{bmatrix};\ \underline{X}^{lin3}=\begin{bmatrix}* & X_{12}^{q}\\ * & *\\ * & *\end{bmatrix};\ \underline{X}^{lin4}=\begin{bmatrix}0 & *\\ * & *\\ * & *\end{bmatrix}$$

$$\underline{n}^{lin}=\begin{bmatrix}2\\0\\0\end{bmatrix};\ n^{lin}=2 \text{ and the final matrices: } \underline{X}^{lin}=\begin{bmatrix}0 & X_{12}^{q}\\ * & *\\ * & *\end{bmatrix};\ \underline{\mathrm{A}}^{lin}=\begin{bmatrix}\neq 0\\ *\\ *\end{bmatrix} \tag{9.5.9}$$

Hence the algorithm works satisfactorily.

Case 4) one ellipse (e_1) is tangent to the straight line $Y=b_w/2$ and the other (e_2) intersects it in correspondence of the tangent point

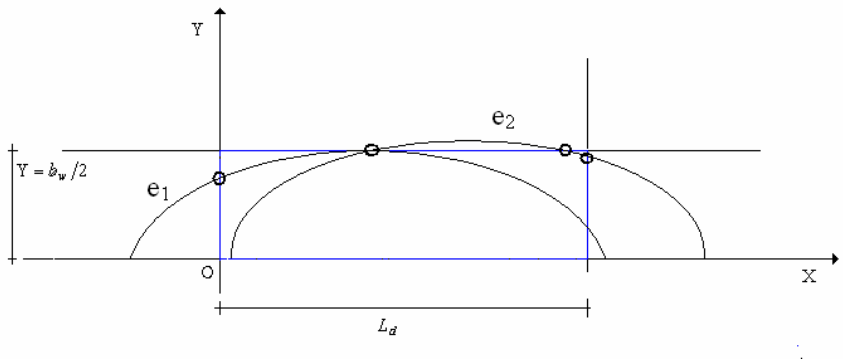

Fig. 9.5.4 – Case 4

The auxiliary matrices are:

$$\underline{X}^{p1}=\begin{bmatrix} * & X_{12}^{p1} \\ X_{21}^{p1} & * \end{bmatrix};\ \underline{X}^{p2}=\begin{bmatrix} * & * \\ * & * \end{bmatrix};\ \underline{X}^{q}=\begin{bmatrix} X_{11}^{q} & X_{12}^{q} \\ X_{21}^{q} & X_{22}^{q} \end{bmatrix};$$

with $X_{11}^{q}=X_{12}^{q}=X_{21}^{q}$

$$\underline{Y}^{e}=\begin{bmatrix} Y_{11}^{e} & Y_{12}^{e} \\ * & Y_{22}^{e} \end{bmatrix};\quad \underline{G}=\begin{bmatrix} ...;\left(X_{o1}-a_1\right)^{*} & \left(X_{o1}+a_1\right)^{*} \\ ...;\left(X_{o2}-a_2\right)^{*} & \left(X_{o2}+a_2\right)^{*} \end{bmatrix} \tag{9.5.10}$$

with $Y_{11}^{e}<b_w/2$ and $Y_{12}^{e};\ Y_{22}^{e}<b_w/2$

The Non-Linear range matrices:

$$\underline{X}^{nlin1}=\begin{bmatrix} * & * \\ * & * \end{bmatrix};\ \underline{X}^{nlin2}=\begin{bmatrix} * & * \\ * & * \end{bmatrix};\ \underline{X}^{nlin3}=\begin{bmatrix} X_{11}^{q} & * \\ * & X_{22}^{q} \end{bmatrix}\ \text{with}\ X_{11}^{q}=X_{21}^{q}$$

$$\underline{X}^{nlin4}=\begin{bmatrix} 0 & * \\ * & L_d \end{bmatrix};\underline{X}^{nlin5}=\begin{bmatrix} * & * \\ * & * \end{bmatrix};\ \underline{n}^{nlin}=\begin{bmatrix} 2 \\ 2 \end{bmatrix};\ n^{nlin}=2 \tag{9.5.11}$$

and the final matrices: $\underline{X}^{nlin}=\begin{bmatrix} 0 & X_{11}^{q} \\ X_{22}^{q} & L_d \end{bmatrix};\underline{\mathrm{A}}^{nlin}=\begin{bmatrix} \neq 0 \\ \neq 0 \end{bmatrix}$

As regards the Linear range of integration:

$$\underline{X}^{lin1}=\begin{bmatrix} * & * \\ * & * \end{bmatrix};\ \underline{X}^{lin2}=\begin{bmatrix} * & * \\ * & * \end{bmatrix};\ \underline{X}^{lin3}=\begin{bmatrix} * & * \\ X_{21}^{q} & X_{22}^{q} \end{bmatrix};\ \underline{X}^{lin4}=\begin{bmatrix} * & * \\ * & * \end{bmatrix}$$

$$\underline{n}^{lin}=\begin{bmatrix} 0 \\ 2 \end{bmatrix};\ n^{lin}=2 \tag{9.5.12}$$

and the final matrices $\underline{X}^{lin}=\begin{bmatrix} * & * \\ X_{21}^{q} & X_{22}^{q} \end{bmatrix};\underline{\mathrm{A}}^{lin}=\begin{bmatrix} * \\ \neq 0 \end{bmatrix}$

Hence the performance is satisfactory.

Case 5) one ellipse (e_2) is tangent to the straight line $Y=b_w/2$ and the other (e_1) intersects it both in correspondence of the tangency point and in the right vertex along the X axis.

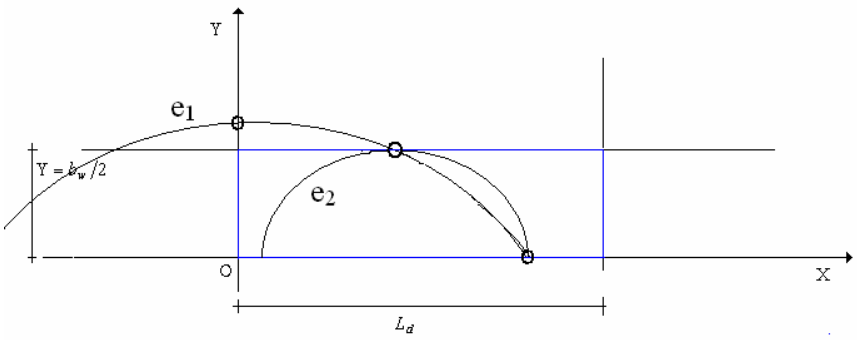

Fig. 9.5.5 – Case 5

The auxiliary matrices are:

$$\underline{X}^{p1}=\begin{bmatrix} * & X_{12}^{p1} \\ X_{21}^{p1} & * \end{bmatrix};\ \underline{X}^{p2}=\begin{bmatrix} * & * \\ * & * \end{bmatrix};\ \underline{X}^{q}=\begin{bmatrix} X_{11}^{q} & X_{12}^{q} \\ X_{21}^{q} & X_{22}^{q} \end{bmatrix};\ \underline{Y}^{e}=\begin{bmatrix} Y_{11}^{e} & * \\ * & * \end{bmatrix}$$

$$\text{with: } X_{12}^{p1}=X_{21}^{p1}=X_{21}^{q}=X_{22}^{q}=X_{12}^{q} \text{ and with: } Y_{11}^{e}>b_w/2 \qquad (9.5.13)$$

$$\underline{G}=\begin{bmatrix} .....\left(X_{o1}-a_1\right) & \left(X_{o1}+a_1\right) \\ .....\left(X_{o2}-a_2\right) & \left(X_{o2}+a_2\right) \end{bmatrix};\ \text{with } \left(X_{o1}+a_1\right)=\left(X_{o2}+a_2\right)$$

In that case, even if we have two real distinct roots of the Eq. (6.28) contemplating the possibility of two distinct real intersection points because of the intersection between the two ellipses in X_{12}^{p1} and their tangency in $X_{o2}+a_2 = X_{o1}+a_1$, the algorithm behind the determination of the auxiliary matrices $\underline{X}^{p1}$ and $\underline{X}^{p2}$ discards the second solution $X_{o2}+a_2=X_{o1}+a_1$ because the corresponding ordinate is equal to zero for both the 1st $Y_1\left(X_{o1}+a_1\right)=0$ and 2nd $Y_2\left(X_{o2}+a_2\right)=0$ ellipses.

The Non-Linear range matrices:

$$\underline{X}^{nlin1}=\begin{bmatrix} * & * \\ * & * \end{bmatrix};\ \underline{X}^{nlin2}=\begin{bmatrix} * & * \\ * & * \end{bmatrix};\ \underline{X}^{nlin3}=\begin{bmatrix} * & * \\ * & X_{22}^{q} \end{bmatrix};\ \underline{X}^{nlin4}=\begin{bmatrix} * & * \\ * & * \end{bmatrix}$$

$$\underline{X}^{nlin5}=\begin{bmatrix} * & * \\ * & \left(X_{o2}+a_2\right) \end{bmatrix};\ \underline{n}^{nlin}=\begin{bmatrix} 0 \\ 2 \end{bmatrix};\ n^{nlin}=2 \qquad (9.5.14)$$

$$\text{and the final matrices: } \underline{X}^{nlin}=\begin{bmatrix} * & * \\ X_{22}^{q} & \left(X_{o2}+a_2\right) \end{bmatrix};\ \underline{\mathrm{A}}^{nlin}=\begin{bmatrix} * \\ \neq 0 \end{bmatrix}$$

As regards the Linear range of integration:

$$\underline{X}^{lin1}=\begin{bmatrix} * & * \\ * & * \end{bmatrix};\ \underline{X}^{lin2}=\begin{bmatrix} * & * \\ * & * \end{bmatrix};\ \underline{X}^{lin3}=\begin{bmatrix} * & X_{12}^{q} \\ * & * \end{bmatrix};\ \underline{X}^{lin4}=\begin{bmatrix} 0 & * \\ * & * \end{bmatrix};\ \underline{n}^{lin}=\begin{bmatrix} 2 \\ 0 \end{bmatrix};\ n^{lin}=2$$

$$\text{and the final matrix is } \underline{X}^{lin}=\begin{bmatrix} 0 & X_{12}^{q} \\ * & * \end{bmatrix};\ \underline{\mathrm{A}}^{lin}=\begin{bmatrix} \neq 0 \\ * \end{bmatrix} \qquad (9.5.15)$$

Hence the performance is satisfactory.

Case 6) one ellipse (e_2) is tangent to the straight line $Y=b_w/2$ and the other (e_1) intersects it in correspondence of the tangency point.

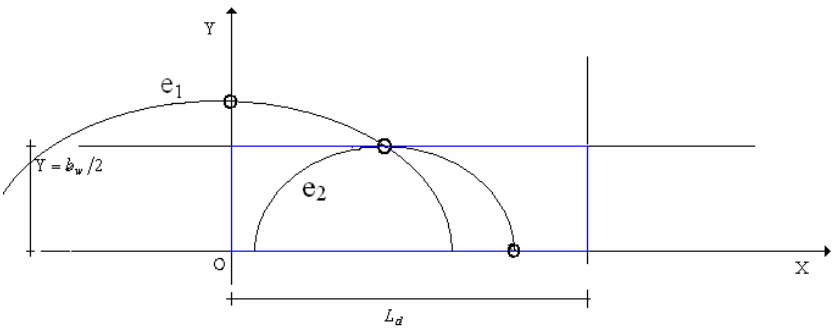

Fig. 9.5.6 – Case 6

The auxiliary matrices are:

$$\underline{X}^{p1}=\begin{bmatrix} * & X_{12}^{p1} \\ X_{21}^{p1} & * \end{bmatrix};\ \underline{X}^{p2}=\begin{bmatrix} * & * \\ * & * \end{bmatrix};\ \underline{X}^{q}=\begin{bmatrix} X_{11}^{q} & X_{12}^{q} \\ X_{21}^{q} & X_{22}^{q} \end{bmatrix};\ \underline{Y}^{e}=\begin{bmatrix} Y_{11}^{e} & * \\ * & * \end{bmatrix}$$

$$\text{with } X_{12}^{p1}=X_{21}^{p1}=X_{21}^{q}=X_{22}^{q} \text{ and with } \quad Y_{11}^{e}>b_w/2 \tag{9.5.16}$$

$$\underline{G}=\begin{bmatrix} .....\left(X_{o1}-a_1\right) & \left(X_{o1}+a_1\right) \\ .....\left(X_{o2}-a_2\right) & \left(X_{o2}+a_2\right) \end{bmatrix};$$

The Non Linear range matrices:

$$\underline{X}^{nlin1}=\begin{bmatrix} * & * \\ * & * \end{bmatrix};\ \underline{X}^{nlin2}=\begin{bmatrix} * & * \\ * & * \end{bmatrix};\ \underline{X}^{nlin3}=\begin{bmatrix} * & * \\ * & X_{22}^{q} \end{bmatrix};\ \underline{X}^{nlin4}=\begin{bmatrix} * & * \\ * & * \end{bmatrix}$$

$$\underline{X}^{nlin5}=\begin{bmatrix} * & * \\ * & \left(X_{o2}+a_2\right) \end{bmatrix};\ \underline{n}^{nlin}=\begin{bmatrix} 0 \\ 2 \end{bmatrix};\ n^{nlin}=2 \tag{9.5.17}$$

$$\text{and the final matrices: } \underline{X}^{nlin}=\begin{bmatrix} * & * \\ X_{22}^{q} & \left(X_{o2}+a_2\right) \end{bmatrix};\ \underline{\mathrm{A}}^{nlin}=\begin{bmatrix} * \\ \neq 0 \end{bmatrix}$$

As regards the Linear range of integration:

$$\underline{X}^{lin1}=\begin{bmatrix} * & * \\ * & * \end{bmatrix};\ \underline{X}^{lin2}=\begin{bmatrix} * & * \\ * & * \end{bmatrix};\ \underline{X}^{lin3}=\begin{bmatrix} * & X_{12}^{q} \\ * & * \end{bmatrix};\ \underline{X}^{lin4}=\begin{bmatrix} 0 & * \\ * & * \end{bmatrix};\ \underline{n}^{lin}=\begin{bmatrix} 2 \\ 0 \end{bmatrix};\ n^{lin}=2$$

$$\text{and the final matrices: } \underline{X}^{lin}=\begin{bmatrix} 0 & X_{12}^{q} \\ * & * \end{bmatrix};\ \underline{\mathrm{A}}^{lin}=\begin{bmatrix} \neq 0 \\ * \end{bmatrix} \tag{9.5.18}$$

Hence the performance is satisfactory.

Case 7) one ellipse (e_2) is tangent to the straight line $Y=b_w/2$ and the other (e_1) intersects it both in correspondence of the tangency point and in another point.

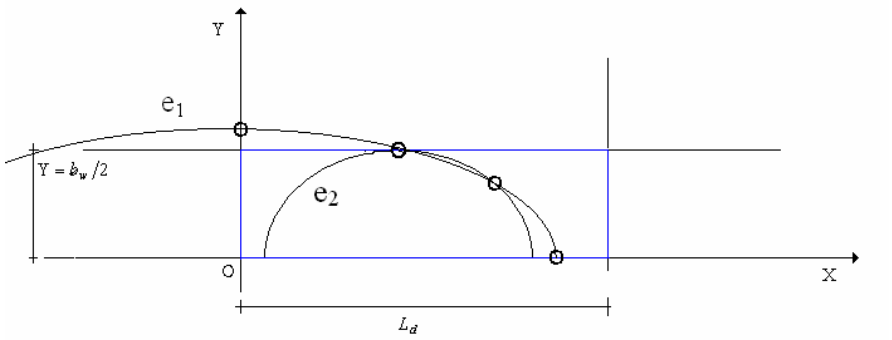

Fig. 9.5.7 – Case 7

Since the semi-conical surfaces are intersected by the same plane, thus the ratio between the minor and the major semi-axis is constant, this situation can occur rarely but it is worth taking that eventuality into consideration in order for the algorithm to be as much general as possible. This is also useful in order to face further future developments with confidence about the reliability and generality of the model.

The auxiliary matrices are:

$$\underline{X}^{p1}=\begin{bmatrix} * & X_{12}^{p1} \\ X_{21}^{p1} & * \end{bmatrix};\ \underline{X}^{p2}=\begin{bmatrix} * & X_{12}^{p2} \\ X_{21}^{p2} & * \end{bmatrix};\ \underline{X}^{q}=\begin{bmatrix} X_{11}^{q} & X_{12}^{q} \\ X_{21}^{q} & X_{22}^{q} \end{bmatrix};\ \underline{Y}^{e}=\begin{bmatrix} Y_{11}^{e} & * \\ * & * \end{bmatrix} \text{ with } \quad Y_{11}^{e} > b_w/2$$

$$\text{with } X_{12}^{p1}=X_{21}^{p1}=X_{21}^{q}=X_{22}^{q}=X_{12}^{q} \text{ and } X_{12}^{p2}=X_{21}^{p2}>X_{12}^{p1}=X_{21}^{p1} \text{ and } X_{11}^{q}<0 \tag{9.5.19}$$

$$\underline{G}=\begin{bmatrix} ...;\left(X_{o1}-a_1\right) & \left(X_{o1}+a_1\right) \\ ...;\left(X_{o2}-a_2\right) & \left(X_{o2}+a_2\right) \end{bmatrix};$$

The Non-Linear range matrices:

$$\underline{X}^{nlin1}=\begin{bmatrix} * & * \\ * & * \end{bmatrix};\ \underline{X}^{nlin2}=\begin{bmatrix} * & X_{12}^{p2} \\ X_{21}^{p2} & * \end{bmatrix};\ \underline{X}^{nlin3}=\begin{bmatrix} * & * \\ * & X_{22}^{q} \end{bmatrix};\ \underline{X}^{nlin4}=\begin{bmatrix} * & * \\ * & * \end{bmatrix}$$

$$\underline{X}^{nlin5}=\begin{bmatrix} * & \left(X_{o1}+a_1\right) \\ * & * \end{bmatrix};\ \underline{n}^{nlin}=\begin{bmatrix} 2 \\ 2 \end{bmatrix};\quad n^{nlin}=2 \tag{9.5.20}$$

$$\text{and the final matrices: is } \underline{X}^{nlin}=\begin{bmatrix} X_{12}^{p2} & \left(X_{o1}+a_1\right) \\ X_{22}^{q} & X_{21}^{p2} \end{bmatrix};\ \underline{\mathrm{A}}^{nlin}=\begin{bmatrix} \neq 0 \\ \neq 0 \end{bmatrix}$$

The first intersection point's abscissa is discarded because outside the range of interest while the second one's is accepted by the algorithm $0<X_{12}^{p2}=X_{21}^{p2}<L_d$ and $0<Y\left(X_{12}^{p2}\right)<b_w/2$.

As regards the Linear range of integration:

$$\underline{X}^{lin1}=\begin{bmatrix} * & * \\ * & * \end{bmatrix};\ \underline{X}^{lin2}=\begin{bmatrix} * & * \\ * & * \end{bmatrix};\ \underline{X}^{lin3}=\begin{bmatrix} * & X_{12}^{q} \\ * & * \end{bmatrix};$$

$$\underline{X}^{lin4}=\begin{bmatrix} 0 & * \\ * & * \end{bmatrix};\ \underline{n}^{lin}=\begin{bmatrix} 2 \\ 0 \end{bmatrix};\ n^{lin}=2 \tag{9.5.21}$$

$$\text{and the final matrices: } \underline{X}^{lin}=\begin{bmatrix} 0 & X_{12}^{q} \\ * & * \end{bmatrix};\ \underline{\mathrm{A}}^{lin}=\begin{bmatrix} \neq 0 \\ * \end{bmatrix}$$

Hence the performance is satisfactory.

Case 8) one ellipse passes through the point of coordinates $\left[0; b_w/2\right]$

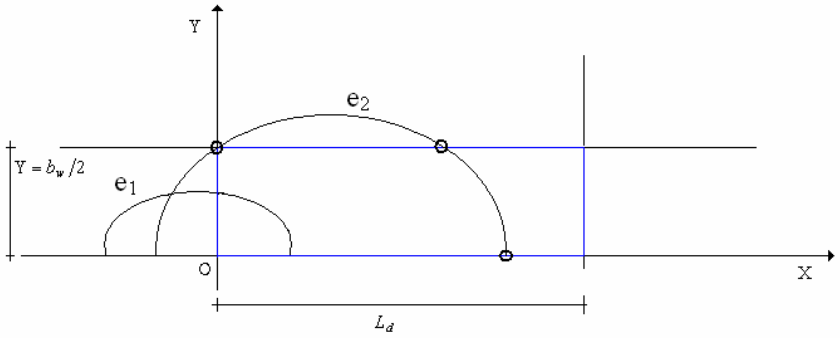

Fig. 9.5.8 – Case 8

The auxiliary matrices are:

$$\underline{X}^{p1} = \begin{bmatrix} * & X_{12}^{p1} \\ X_{21}^{p1} & * \end{bmatrix}; \; \underline{X}^{p2} = \begin{bmatrix} * & * \\ * & * \end{bmatrix}; \; \underline{X}^{q} = \begin{bmatrix} * & * \\ X_{21}^{q} & X_{22}^{q} \end{bmatrix}; \; \underline{Y}^{e} = \begin{bmatrix} Y_{11}^{e} & * \\ Y_{21}^{e} & * \end{bmatrix}$$

$$\text{with } X_{12}^{p1} = X_{21}^{p1} < 0 \text{ and } X_{21}^{q} = 0; \quad Y_{11}^{e} < b_w/2 \quad \text{and} \quad Y_{21}^{e} = b_w/2 \tag{9.5.22}$$

$$\underline{G} = \begin{bmatrix} .....\left(X_{o1} - a_1\right) & \left(X_{o1} + a_1\right) \\ .....\left(X_{o2} - a_2\right) & \left(X_{o2} + a_2\right) \end{bmatrix};$$

The Non-Linear range matrices:

$$\underline{X}^{nlin1} = \begin{bmatrix} * & * \\ * & * \end{bmatrix}; \; \underline{X}^{nlin2} = \begin{bmatrix} * & * \\ * & * \end{bmatrix}; \; \underline{X}^{nlin3} = \begin{bmatrix} * & * \\ * & X_{22}^{q} \end{bmatrix}; \; \underline{X}^{nlin4} = \begin{bmatrix} * & * \\ * & * \end{bmatrix}^{nlin}$$

$$\underline{X}^{nlin5} = \begin{bmatrix} * & * \\ * & \left(X_{o2} + a_2\right) \end{bmatrix}; \; \underline{n}^{nlin} = \begin{bmatrix} 0 \\ 2 \end{bmatrix}; \quad n^{nlin} = 2 \tag{9.5.23}$$

$$\text{and the final matrices: } \underline{X}^{nlin} = \begin{bmatrix} * & * \\ X_{22}^{q} & \left(X_{o2} + a_2\right) \end{bmatrix}; \underline{\mathrm{A}}^{nlin} = \begin{bmatrix} * \\ \neq 0 \end{bmatrix}$$

As regards the Linear range of integration:

$$\underline{X}^{lin1} = \begin{bmatrix} * & * \\ * & * \end{bmatrix}; \; \underline{X}^{lin2} = \begin{bmatrix} * & * \\ * & * \end{bmatrix}; \; \underline{X}^{lin3} = \begin{bmatrix} * & * \\ X_{21}^{q} & X_{22}^{q} \end{bmatrix};$$

$$\underline{X}^{lin4} = \begin{bmatrix} * & * \\ * & * \end{bmatrix}; \; \underline{n}^{lin} = \begin{bmatrix} 0 \\ 2 \end{bmatrix}; \; n^{lin} = 2 \tag{9.5.24}$$

$$\text{and the final matrices: } \underline{X}^{lin} = \begin{bmatrix} * & * \\ X_{21}^{q} & X_{22}^{q} \end{bmatrix}; \underline{\mathrm{A}}^{lin} = \begin{bmatrix} * \\ \neq 0 \end{bmatrix}$$

Hence the performance is satisfactory.

Case 9) two ellipses intersect each other on the axis $X = 0$ above the line $Y = b_w/2$

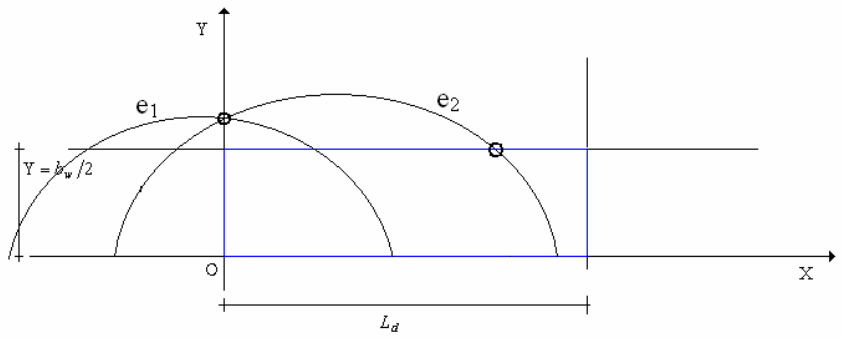

Fig. 9.5.9 – Case 9

The auxiliary matrices are:

$$\underline{X}^{p1}=\begin{bmatrix} * & X_{12}^{p1} \\ X_{21}^{p1} & * \end{bmatrix};\ \underline{X}^{p2}=\begin{bmatrix} * & * \\ * & * \end{bmatrix};\ \underline{X}^{q}=\begin{bmatrix} X_{11}^{q} & X_{12}^{q} \\ X_{21}^{q} & X_{22}^{q} \end{bmatrix};$$

with $X_{12}^{p1}=X_{21}^{p1}=0\ ;\ X_{11}^{q}<0;\ X_{21}^{q}<0\ ;\ 0<X_{12}^{q}\ ;\ X_{22}^{q}<L_d$

$$\underline{G}=\begin{bmatrix} .....\left(X_{o1}-a_1\right) & \left(X_{o1}+a_1\right) \\ .....\left(X_{o2}-a_2\right) & \left(X_{o2}+a_2\right) \end{bmatrix};\qquad (9.5.25)$$

with $\left(X_{o2}+a_2\right)>\left(X_{o1}+a_1\right)$ and $0<\left(X_{o2}+a_2\right)\ ;\ \left(X_{o1}+a_1\right)<L_d$

$$\underline{Y}^{e}=\begin{bmatrix} Y_{11}^{e} & * \\ Y_{21}^{e} & * \end{bmatrix}\ \text{with}\quad Y_{11}^{e}>b_w/2\ \text{ and }\ Y_{21}^{e}>b_w/2$$

The Non Linear range matrices:

$$\underline{X}^{nlin1}=\begin{bmatrix} * & * \\ * & * \end{bmatrix};\ \underline{X}^{nlin2}=\begin{bmatrix} * & * \\ * & * \end{bmatrix};\ \underline{X}^{nlin3}=\begin{bmatrix} * & * \\ * & X_{22}^{q} \end{bmatrix};\ \underline{X}^{nlin4}=\begin{bmatrix} * & * \\ * & * \end{bmatrix}$$

$$\underline{X}^{nlin5}=\begin{bmatrix} * & * \\ * & \left(X_{o2}+a_2\right) \end{bmatrix};\ \underline{n}^{nlin}=\begin{bmatrix} 0 \\ 2 \end{bmatrix};\quad n^{nlin}=2 \qquad (9.5.26)$$

and the final matrices: $\underline{X}^{nlin}=\begin{bmatrix} * & * \\ X_{22}^{q} & \left(X_{o2}+a_2\right) \end{bmatrix};\ \underline{\mathrm{A}}^{nlin}=\begin{bmatrix} * \\ \neq 0 \end{bmatrix}^{nlin}$

As regards the Linear range of integration:

$$\underline{X}^{lin1}=\begin{bmatrix} * & * \\ * & * \end{bmatrix}\ ;\ \underline{X}^{lin2}=\begin{bmatrix} * & * \\ * & * \end{bmatrix}\ ;\ \underline{X}^{lin3}=\begin{bmatrix} * & * \\ * & X_{22}^{q} \end{bmatrix};$$

$$\underline{X}^{lin4}=\begin{bmatrix} * & * \\ 0 & * \end{bmatrix};\ \underline{n}^{lin}=\begin{bmatrix} 0 \\ 2 \end{bmatrix}\ ;\ n^{lin}=2 \qquad (9.5.27)$$

and the final matrices: $\underline{X}^{lin}=\begin{bmatrix} * & * \\ 0 & X_{22}^{q} \end{bmatrix}\ ;\ \underline{\mathrm{A}}^{lin}=\begin{bmatrix} * \\ \neq 0 \end{bmatrix}$

Hence the performance is satisfactory.

Case 10) two ellipses intersect each other within the range of interest *i.e.*: $Y>b_w/2$ and $0<X<L_d$

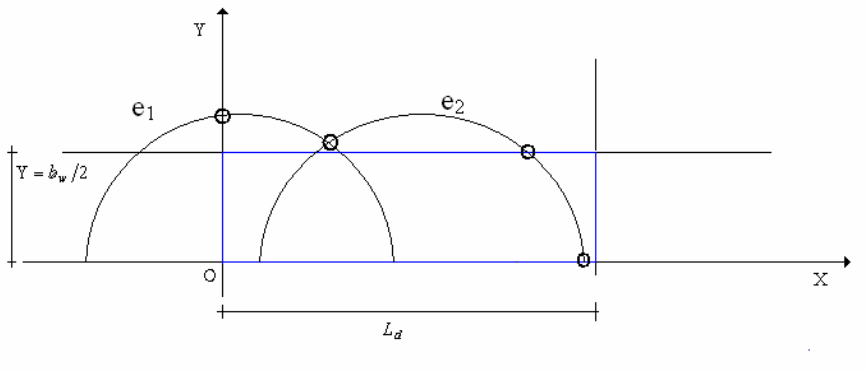

Fig. 9.5.10 – Case 10

The auxiliary matrices are:

$$\underline{X}^{p1}=\begin{bmatrix} * & X_{12}^{p1} \\ X_{21}^{p1} & * \end{bmatrix};\ \underline{X}^{p2}=\begin{bmatrix} * & * \\ * & * \end{bmatrix};\ \underline{X}^{q}=\begin{bmatrix} X_{11}^{q} & X_{12}^{q} \\ X_{21}^{q} & X_{22}^{q} \end{bmatrix};$$

$$\text{with}\ \ 0<X_{12}^{p1}=X_{21}^{p1}<L_d\ \ \text{and}\ \ Y\left(X_{12}^{p1}\right)>b_w/2$$

$$\underline{G}=\begin{bmatrix} .....\left(X_{o1}-a_1\right) & \left(X_{o1}+a_1\right) \\ .....\left(X_{o2}-a_2\right) & \left(X_{o2}+a_2\right) \end{bmatrix};\qquad (9.5.28)$$

$$\underline{Y}^{e}=\begin{bmatrix} Y_{11}^{e} & * \\ * & * \end{bmatrix}\ \text{with}\ \ Y_{11}^{e}>b_w/2$$

The Non Linear range matrices:

$$\underline{X}^{nlin1}=\begin{bmatrix} * & * \\ * & * \end{bmatrix};\ \underline{X}^{nlin2}=\begin{bmatrix} * & * \\ * & * \end{bmatrix};\ \underline{X}^{nlin3}=\begin{bmatrix} * & * \\ * & X_{22}^{q} \end{bmatrix};\ \underline{X}^{nlin4}=\begin{bmatrix} * & * \\ * & * \end{bmatrix}$$

$$\underline{X}^{nlin5}=\begin{bmatrix} * & * \\ * & \left(X_{o2}+a_2\right) \end{bmatrix};\ \underline{n}^{nlin}=\begin{bmatrix} 0 \\ 2 \end{bmatrix};\ \ n^{nlin}=2 \qquad (9.5.29)$$

$$\text{and the final matrices:}\ \underline{X}^{nlin}=\begin{bmatrix} * & * \\ X_{22}^{q} & \left(X_{o2}+a_2\right) \end{bmatrix};\ \underline{\mathrm{A}}^{nlin}=\begin{bmatrix} * \\ \neq 0 \end{bmatrix}$$

As regards the Linear range of integration:

$$\underline{X}^{lin1}=\begin{bmatrix} * & X_{12}^{p1} \\ X_{21}^{p1} & * \end{bmatrix};\ \underline{X}^{lin1}=\begin{bmatrix} * & * \\ * & * \end{bmatrix};\ \underline{X}^{lin3}=\begin{bmatrix} * & * \\ * & X_{22}^{q} \end{bmatrix};$$

$$\underline{X}^{lin4}=\begin{bmatrix} 0 & * \\ * & * \end{bmatrix};\ \underline{n}^{lin}=\begin{bmatrix} 2 \\ 2 \end{bmatrix};\ n^{lin}=2 \qquad (9.5.30)$$

$$\text{and the final matrices:}\ \underline{X}^{lin}=\begin{bmatrix} 0 & X_{12}^{p1} \\ X_{21}^{p1} & X_{22}^{q} \end{bmatrix};\ \underline{\mathrm{A}}^{lin}=\begin{bmatrix} \neq 0 \\ \neq 0 \end{bmatrix}$$

Hence the performance is satisfactory.

Case 11) one ellipse is tangent to the straight line $Y=b_w/2$ in the point $\left[0;b_w/2\right]$:

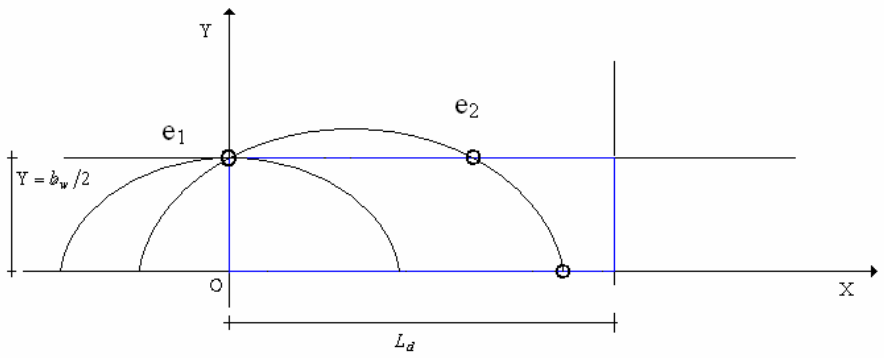

Fig. 9.5.11 – Case 11

The auxiliary matrices are:

$$\underline{X}^{p1}=\begin{bmatrix} * & X_{12}^{p1} \\ X_{21}^{p1} & * \end{bmatrix};\ \underline{X}^{p2}=\begin{bmatrix} * & * \\ * & * \end{bmatrix};\ \underline{X}^{q}=\begin{bmatrix} X_{11}^{q} & X_{12}^{q} \\ X_{21}^{q} & X_{22}^{q} \end{bmatrix};\ \underline{Y}^{e}=\begin{bmatrix} Y_{11}^{e} & * \\ Y_{21}^{e} & * \end{bmatrix}$$

$$\text{with } X_{11}^{q}=X_{12}^{q}=X_{21}^{q}=X_{12}^{p1}=X_{21}^{p1}=0 \text{ and with } Y_{11}^{e}=Y_{21}^{e}=b_w/2 \qquad (9.5.31)$$

$$\underline{G}=\begin{bmatrix} .....\left(X_{o1}-a_1\right) & \left(X_{o1}+a_1\right) \\ .....\left(X_{o2}-a_2\right) & \left(X_{o2}+a_2\right) \end{bmatrix};$$

The Non Linear range matrices:

$$\underline{X}^{nlin1}=\begin{bmatrix} * & * \\ * & * \end{bmatrix};\ \underline{X}^{nlin2}=\begin{bmatrix} * & * \\ * & * \end{bmatrix};\ \underline{X}^{nlin3}=\begin{bmatrix} * & * \\ * & X_{22}^{q} \end{bmatrix};\ \underline{X}^{nlin4}=\begin{bmatrix} * & * \\ * & * \end{bmatrix}$$

$$\underline{X}^{nlin5}=\begin{bmatrix} * & * \\ * & \left(X_{o2}+a_2\right) \end{bmatrix};\ \underline{n}^{nlin}=\begin{bmatrix} 0 \\ 2 \end{bmatrix};\quad n^{nlin}=2 \qquad (9.5.32)$$

$$\text{and the final matrices: } \underline{X}^{nlin}=\begin{bmatrix} * & * \\ X_{22}^{q} & \left(X_{o2}+a_2\right) \end{bmatrix};\ \underline{\mathrm{A}}^{nlin}=\begin{bmatrix} * \\ \neq 0 \end{bmatrix}$$

As regards the Linear range of integration:

$$\underline{X}^{lin1}=\begin{bmatrix} * & * \\ * & * \end{bmatrix};\ \underline{X}^{lin2}=\begin{bmatrix} * & * \\ * & * \end{bmatrix};\ \underline{X}^{lin3}=\begin{bmatrix} * & * \\ X_{21}^{q} & X_{22}^{q} \end{bmatrix};$$

$$\underline{X}^{lin4}=\begin{bmatrix} * & * \\ * & * \end{bmatrix};\ \underline{n}^{lin}=\begin{bmatrix} 0 \\ 2 \end{bmatrix};\ n^{lin}=2 \qquad (9.5.33)$$

$$\text{and the final matrices: } \underline{X}^{lin}=\begin{bmatrix} * & * \\ X_{21}^{q} & X_{22}^{q} \end{bmatrix};\ \underline{\mathrm{A}}^{lin}=\begin{bmatrix} * \\ \neq 0 \end{bmatrix}$$

Hence the performance is satisfactory.

Case 12) one ellipse (e_1) passes through the point $[0;0]$; another (e_4) is tangent to the straight line $Y=b_w/2$ in the point $[L_d;b_w/2]$; and two (e_2;e_3) are completely inside the range of interest $0<X<L_d$ and $0<Y<b_w/2$

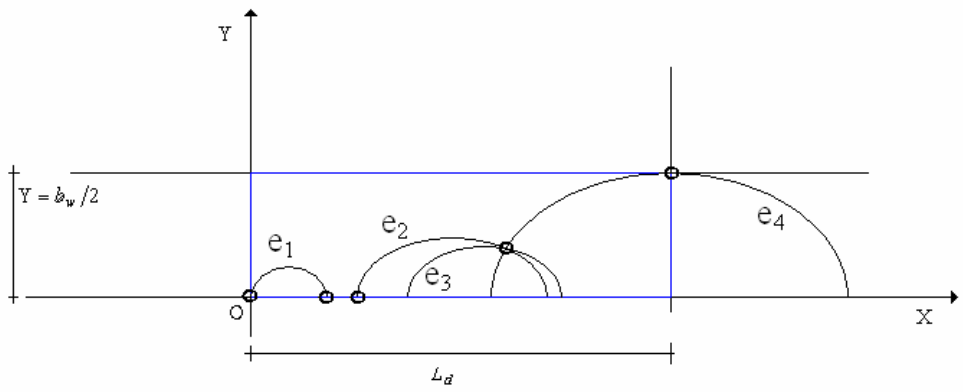

Fig. 9.5.12 – Case 12

The auxiliary matrices are:

$$\underline{X}^{p1} = \begin{bmatrix} * & * & * & * \\ * & * & X_{23}^{p1} & X_{24}^{p1} \\ * & X_{32}^{p1} & * & X_{34}^{p1} \\ * & X_{42}^{p1} & X_{43}^{p1} & * \end{bmatrix}; \quad \underline{X}^{p1} = \begin{bmatrix} * & * & * & * \\ * & * & * & * \\ * & * & * & * \\ * & * & * & * \end{bmatrix}; \quad \underline{X}^{q} = \begin{bmatrix} * & * \\ * & * \\ * & * \\ X_{41}^{q} & X_{42}^{q} \end{bmatrix};$$

with $X_{41}^{q} = X_{42}^{q} = L_d$ and $X_{23}^{p1} = X_{24}^{p1} = X_{34}^{p1} = X_{32}^{p1} = X_{42}^{p1} = X_{43}^{p1}$

$$\underline{G} = \begin{bmatrix} .....\left(X_{o1} - a_1\right) & \left(X_{o1} + a_1\right) \\ .....\left(X_{o2} - a_2\right) & \left(X_{o2} + a_2\right) \\ .....\left(X_{o3} - a_3\right) & \left(X_{o3} + a_3\right) \\ .....\left(X_{o4} - a_4\right) & \left(X_{o4} + a_4\right) \end{bmatrix}; \tag{9.5.34}$$

with $\left(X_{o1} - a_1\right) = 0$ and $\left(X_{o4} + a_4\right) > L_d$

$$\underline{Y}^{e} = \begin{bmatrix} Y_{11}^{e} & * \\ * & * \\ * & * \\ * & Y_{42}^{e} \end{bmatrix} \text{ with } \quad Y_{42}^{e} = b_w/2 \text{ and } \quad Y_{11}^{e} = 0$$

The Non Linear range matrices:

$$\underline{X}^{nlin1}=\begin{bmatrix}* & * & * & *\\ * & * & X_{23}^{p1} & *\\ * & * & * & *\\ * & X_{42}^{p1} & * & *\end{bmatrix};\ \underline{X}^{nlin2}=\begin{bmatrix}* & * & * & *\\ * & * & * & *\\ * & * & * & *\\ * & * & * & *\end{bmatrix};$$

$$\underline{X}^{nlin3}=\begin{bmatrix}* & *\\ * & *\\ * & *\\ X_{41}^{q} & *\end{bmatrix};\ \underline{X}^{nlin4}=\begin{bmatrix}* & *\\ * & *\\ * & *\\ * & *\end{bmatrix}$$

$$\underline{X}^{nlin5}=\begin{bmatrix}(X_{o1}-a_1) & (X_{o1}+a_1)\\ (X_{o2}-a_2) & *\\ * & *\\ * & *\end{bmatrix};\ \underline{n}^{nlin}=\begin{bmatrix}2\\2\\0\\2\end{bmatrix};\quad n^{nlin}=2 \tag{9.5.35}$$

and the final matrices: $\underline{X}^{nlin}=\begin{bmatrix}(X_{o1}-a_1) & (X_{o1}+a_1)\\ (X_{o2}-a_2) & X_{23}^{p1}\\ * & *\\ X_{42}^{p1} & X_{41}^{q}\end{bmatrix};\ \underline{\mathrm{A}}^{nlin}=\begin{bmatrix}\neq 0\\ \neq 0\\ *\\ \neq 0\end{bmatrix}$

As regards the Linear range of integration:

$$\underline{X}^{lin1}=\begin{bmatrix}* & * & * & *\\ * & * & * & *\\ * & * & * & *\\ * & * & * & *\end{bmatrix};\ \underline{X}^{lin2}=\begin{bmatrix}* & * & * & *\\ * & * & * & *\\ * & * & * & *\\ * & * & * & *\end{bmatrix};\ \underline{X}^{lin3}=\begin{bmatrix}* & *\\ * & *\\ * & *\\ * & *\end{bmatrix};$$

$$\underline{X}^{lin4}=\begin{bmatrix}* & *\\ * & *\\ * & *\\ * & *\end{bmatrix};\ \underline{n}^{lin}=\begin{bmatrix}0\\0\\0\\0\end{bmatrix};\ n^{lin}=0 \tag{9.5.36}$$

and the final matrices: $\underline{X}^{lin}=\begin{bmatrix}*\\*\\*\\*\end{bmatrix};\ \underline{\mathrm{A}}^{lin}=\begin{bmatrix}*\\*\\*\\*\end{bmatrix}$

Hence the performance is satisfactory.

Case 13) one ellipse (e_1) passes through $[0;0]$; another (e_3) passes through the points $\left[0;\frac{b_w}{2}\right]$ and $\left[L_d;\frac{b_w}{2}\right]$; another ($e_4$) is tangent to the straight line $Y=b_w/2$ in the point $[L_d;b_w/2]$; and one (e_2) is completely inside the range of interest $0<X<L_d$ and $0<Y<b_w/2$

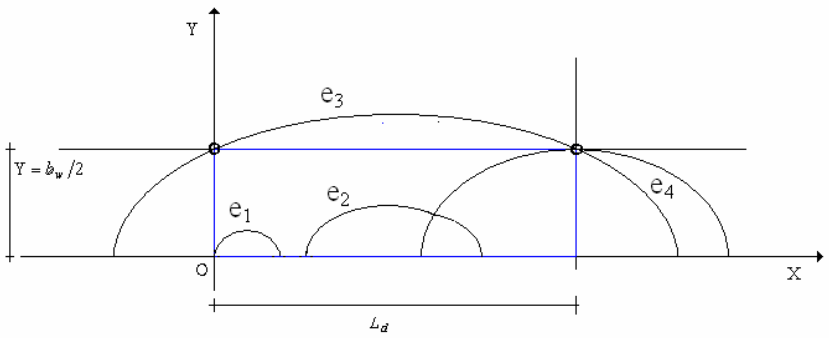

Fig. 9.5.13 – Case 13

The auxiliary matrices are:

$$\underline{X}^{p1}=\begin{bmatrix} * & * & * & * \\ * & * & * & X_{24}^{p1} \\ * & * & * & X_{34}^{p1} \\ * & X_{42}^{p1} & X_{43}^{p1} & * \end{bmatrix};\ \underline{X}^{p2}=\begin{bmatrix} * & * & * & * \\ * & * & * & * \\ * & * & * & * \\ * & * & * & * \end{bmatrix};\ \underline{X}^{q}=\begin{bmatrix} * & * \\ * & * \\ X_{31}^{q} & X_{32}^{q} \\ X_{41}^{q} & X_{42}^{q} \end{bmatrix};$$

with $X_{43}^{p1}=X_{34}^{p1}=L_d$ and $X_{31}^{q}=0$ and $X_{41}^{q}=X_{42}^{q}=X_{32}^{q}=L_d$

$$\underline{G}=\begin{bmatrix} .....\left(X_{o1}-a_1\right) & \left(X_{o1}+a_1\right) \\ .....\left(X_{o2}-a_2\right) & \left(X_{o2}+a_2\right) \\ .....\left(X_{o3}-a_3\right) & \left(X_{o3}+a_3\right) \\ .....\left(X_{o4}-a_4\right) & \left(X_{o4}+a_4\right) \end{bmatrix}; \tag{9.5.37}$$

$$\underline{Y}^{e}=\begin{bmatrix} Y_{11}^{e} & * \\ * & * \\ Y_{31}^{e} & Y_{32}^{e} \\ * & Y_{42}^{e} \end{bmatrix} \text{ with } \quad Y_{11}^{e}=0 \quad \text{and} \quad Y_{31}^{e}=Y_{32}^{e}=Y_{42}^{e}=b_w/2$$

The Non Linear range matrices:

$$\underline{X}^{nlin1}=\begin{bmatrix} * & * & * & * \\ * & * & * & * \\ * & * & * & * \\ * & * & * & * \end{bmatrix};\ \underline{X}^{nlin2}=\begin{bmatrix} * & * & * & * \\ * & * & * & * \\ * & * & * & * \\ * & * & * & * \end{bmatrix};\ \underline{X}^{nlin3}=\begin{bmatrix} * & * \\ * & * \\ * & * \\ * & * \end{bmatrix};\ \underline{X}^{nlin4}=\begin{bmatrix} * & * \\ * & * \\ * & * \\ * & * \end{bmatrix}$$

$$\underline{X}^{nlin5}=\begin{bmatrix} * & * \\ * & * \\ * & * \\ * & * \end{bmatrix};\ \underline{n}^{nlin}=\begin{bmatrix} 0 \\ 0 \\ 0 \\ 0 \end{bmatrix};\quad n^{nlin}=0 \tag{9.5.38}$$

and the final matrices: $\underline{X}^{nlin}=\begin{bmatrix} * \\ * \\ * \\ * \end{bmatrix};\ \underline{\mathrm{A}}^{nlin}=\begin{bmatrix} * \\ * \\ * \\ * \end{bmatrix}$

As regards the Linear range of integration:

$$\underline{X}^{lin1} = \begin{bmatrix} * & * & * & * \\ * & * & * & * \\ * & * & * & * \\ * & * & * & * \end{bmatrix}; \underline{X}^{lin2} = \begin{bmatrix} * & * & * & * \\ * & * & * & * \\ * & * & * & * \\ * & * & * & * \end{bmatrix}; \underline{X}^{lin3} = \begin{bmatrix} * & * \\ * & * \\ X_{31}^{q} & X_{32}^{q} \\ * & * \end{bmatrix};$$

with $X_{31}^{q} = 0$ and $X_{32}^{q} = L_d$

$$\underline{X}^{lin4} = \begin{bmatrix} * & * \\ * & * \\ * & * \\ * & * \end{bmatrix}; \underline{n}^{lin} = \begin{bmatrix} 0 \\ 0 \\ 2 \\ 0 \end{bmatrix}; n^{lin} = 2 \tag{9.5.39}$$

and the final matrices: $\underline{X}^{lin} = \begin{bmatrix} * & * \\ * & * \\ 0 & L_d \\ * & * \end{bmatrix}; \underline{\mathrm{A}}^{lin} = \begin{bmatrix} * \\ * \\ \neq 0 \\ * \end{bmatrix}$ and $\frac{\mathrm{A}_{tot}}{2} = \frac{b_w}{2} L_d$

Hence the performance is satisfactory.

Case 14) one ellipse (e_1) passes through $[0;0]$; another (e_3) passes through the points $\left[0;\frac{b_w}{2}\right]$ and $\left[L_d;\frac{b_w}{2}\right]$; another ($e_4$) is tangent to the straight line $Y = b_w/2$ in the point $[L_d;b_w/2]$; and one (e_2) crosses the range of interest $0 < X < L_d$ and $0 < Y < b_w/2$.

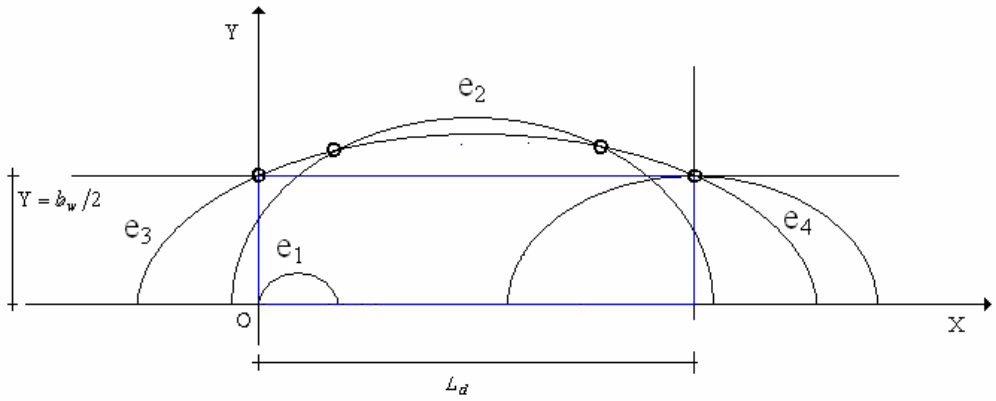

Fig. 9.5.14 – Case 14

The auxiliary matrices are:

$$\underline{X}^{p1}=\begin{bmatrix} * & * & * & * \\ * & * & X_{23}^{p1} & X_{24}^{p1} \\ * & X_{32}^{p1} & * & X_{34}^{p1} \\ * & X_{42}^{p1} & X_{43}^{p1} & * \end{bmatrix};\ \underline{X}^{p2}=\begin{bmatrix} * & * & * & * \\ * & * & X_{23}^{p2} & * \\ * & X_{32}^{p2} & * & * \\ * & * & * & * \end{bmatrix};\ \underline{X}^{q}=\begin{bmatrix} * & * \\ X_{21}^{q} & X_{22}^{q} \\ X_{31}^{q} & X_{32}^{q} \\ X_{41}^{q} & X_{42}^{q} \end{bmatrix};$$

with $X_{43}^{p1}=X_{34}^{p1}=L_d$ and $X_{31}^{q}=0$ and $X_{41}^{q}=X_{42}^{q}=X_{32}^{q}=L_d$

$$\underline{G}=\begin{bmatrix} .....\left(X_{o1}-a_1\right) & \left(X_{o1}+a_1\right) \\ .....\left(X_{o2}-a_2\right) & \left(X_{o2}+a_2\right) \\ .....\left(X_{o3}-a_3\right) & \left(X_{o3}+a_3\right) \\ .....\left(X_{o4}-a_4\right) & \left(X_{o4}+a_4\right) \end{bmatrix};\qquad (9.5.40)$$

$$\underline{Y}^{e}=\begin{bmatrix} Y_{11}^{e} & * \\ Y_{21}^{e} & Y_{22}^{e} \\ Y_{31}^{e} & Y_{32}^{e} \\ * & Y_{42}^{e} \end{bmatrix}\ \text{with}\quad Y_{11}^{e}=0\quad\text{and}\quad Y_{31}^{e}=Y_{32}^{e}=Y_{42}^{e}=b_w/2\ \text{and}$$

$0<Y_{21}^{e}<b_w/2\quad 0<Y_{22}^{e}<b_w/2$

The Non Linear range matrices:

$$\underline{X}^{nlin1}=\begin{bmatrix} * & * & * & * \\ * & * & * & * \\ * & * & * & * \\ * & * & * & * \end{bmatrix};\ \underline{X}^{nlin2}=\begin{bmatrix} * & * & * & * \\ * & * & * & * \\ * & * & * & * \\ * & * & * & * \end{bmatrix};\underline{X}^{nlin3}=\begin{bmatrix} * & * \\ * & * \\ * & * \\ * & * \end{bmatrix};\underline{X}^{nlin4}=\begin{bmatrix} * & * \\ * & * \\ * & * \\ * & * \end{bmatrix}$$

$$\underline{X}^{nlin5}=\begin{bmatrix} * & * \\ * & * \\ * & * \\ * & * \end{bmatrix};\ \underline{n}^{nlin}=\begin{bmatrix} 0 \\ 0 \\ 0 \\ 0 \end{bmatrix};\quad n^{nlin}=0\ \text{and the final matrices:}\ \underline{X}^{nlin}=\begin{bmatrix} * \\ * \\ * \\ * \end{bmatrix};\ \underline{\mathrm{A}}^{nlin}=\begin{bmatrix} * \\ * \\ * \\ * \end{bmatrix}\qquad (9.5.41)$$

As regards the Linear range of integration:

$$\underline{X}^{lin1}=\begin{bmatrix} * & * & * & * \\ * & * & X_{23}^{p1} & * \\ * & X_{32}^{p1} & * & * \\ * & * & * & * \end{bmatrix};\ \underline{X}^{lin2}=\begin{bmatrix} * & * & * & * \\ * & * & X_{23}^{p2} & * \\ * & X_{32}^{p2} & * & * \\ * & * & * & * \end{bmatrix};\ \underline{X}^{lin3}=\begin{bmatrix} * & * \\ * & * \\ X_{31}^{q} & X_{32}^{q} \\ * & * \end{bmatrix};$$

with $X_{31}^{q}=0$ and $X_{32}^{q}=L_d$; $\underline{X}^{lin4}=\begin{bmatrix} * & * \\ * & * \\ * & * \\ * & * \end{bmatrix};\ \underline{n}^{lin}=\begin{bmatrix} 0 \\ 2 \\ 4 \\ 0 \end{bmatrix}$; $n^{lin}=4\qquad (9.5.42)$

and the final matrices: $\underline{X}^{lin}=\begin{bmatrix} * & * & * & * \\ X_{23}^{p1} & X_{23}^{p2} & * & * \\ X_{31}^{q} & X_{32}^{p1} & X_{32}^{p2} & X_{32}^{q} \\ * & * & * & * \end{bmatrix};\underline{\mathrm{A}}^{lin}=\begin{bmatrix} * \\ \neq 0 \\ \neq 0 \\ * \end{bmatrix}$ and $\frac{\mathrm{A}_{tot}}{2}=\frac{b_w}{2}L_d$

Hence the performance is satisfactory.

Case 15) one ellipse (e_1) passes through $[0;0]$ and is completely external to the area of interest $0 < X < L_d$ and $0 < Y < b_w/2$.

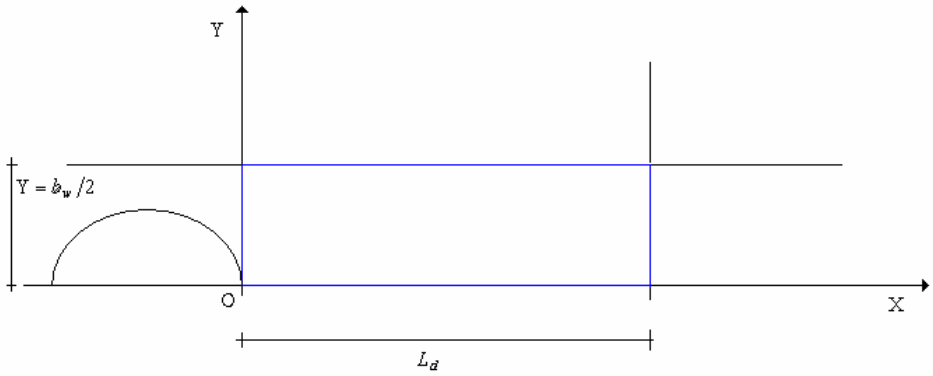

Fig. 9.5.15 – Case 15

This case can never happen (it is definitely impossible) but the algorithm is organised in such a way that even in that impossible eventuality, it would discard the auxiliary point $(X_{o1} + a_1)$ hence providing a satisfactory performance as well.

Case 16) two ellipses are tangent to each other in a point with $0 < X < L_d$ and $0 < Y < b_w/2$:

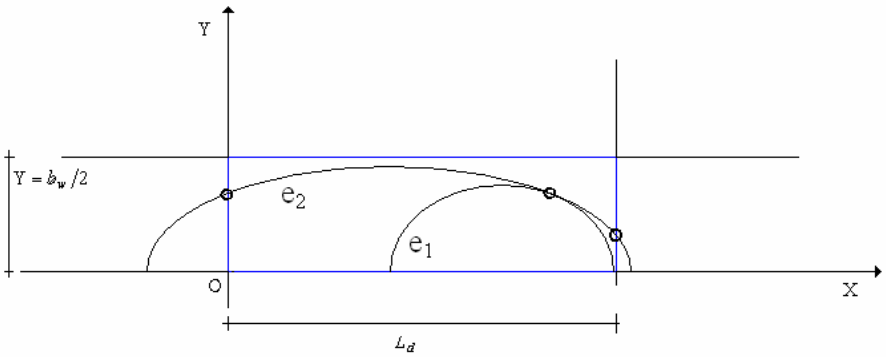

Fig. 9.5.16 – Case 16

The auxiliary matrices are:

$$\underline{X}^{p1} = \begin{bmatrix} * & * \\ * & * \end{bmatrix}; \underline{X}^{p2} = \begin{bmatrix} * & * \\ * & * \end{bmatrix}; \underline{X}^{q} = \begin{bmatrix} * & * \\ * & * \end{bmatrix}; \underline{G} = \begin{bmatrix} .....(X_{o1} - a_1) & (X_{o1} + a_1) \\ .....(X_{o2} - a_2) & (X_{o2} + a_2) \end{bmatrix};$$
$$\underline{Y}^{e} = \begin{bmatrix} * & * \\ Y_{21}^{e} & Y_{22}^{e} \end{bmatrix} \text{ with } Y_{21}^{e} < b_w/2;\ Y_{22}^{e} < b_w/2 \tag{9.5.43}$$

The algorithm discards the tangency point because is not useful for our purposes.

The Non Linear range matrices:

$$\underline{X}^{nlin1}=\begin{bmatrix}* & *\\ * & *\end{bmatrix};\ \underline{X}^{nlin2}=\begin{bmatrix}* & *\\ * & *\end{bmatrix};\ \underline{X}^{nlin3}=\begin{bmatrix}* & *\\ * & *\end{bmatrix};\ \underline{X}^{nlin4}=\begin{bmatrix}* & *\\ X_{21}^{e} & X_{22}^{e}\end{bmatrix}$$

$$\underline{X}^{nlin5}=\begin{bmatrix}* & *\\ * & *\end{bmatrix};\ \text{with } X_{21}^{e}=0\ ;\ X_{22}^{e}=L_d\ ;\ \underline{n}^{nlin}=\begin{bmatrix}0\\ 2\end{bmatrix};\quad n^{nlin}=2 \tag{9.5.44}$$

$$\text{and the final matrices: } \underline{X}^{nlin}=\begin{bmatrix}* & *\\ X_{21}^{e} & X_{22}^{e}\end{bmatrix};\ \underline{\mathrm{A}}^{nlin}=\begin{bmatrix}*\\ \neq 0\end{bmatrix}$$

As regards the Linear range of integration:

$$\underline{X}^{lin1}=\begin{bmatrix}* & *\\ * & *\end{bmatrix};\ \underline{X}^{lin2}=\begin{bmatrix}* & *\\ * & *\end{bmatrix};\ \underline{X}^{lin3}=\begin{bmatrix}* & *\\ * & *\end{bmatrix};$$

$$\underline{X}^{lin4}=\begin{bmatrix}* & *\\ * & *\end{bmatrix};\ \underline{n}^{lin}=\begin{bmatrix}0\\ 0\end{bmatrix}\ ;\ n^{lin}=0 \tag{9.5.45}$$

$$\text{and the final matrices: } \underline{X}^{lin}=\begin{bmatrix}*\\ *\end{bmatrix};\ \underline{\mathrm{A}}^{lin}=\begin{bmatrix}*\\ *\end{bmatrix}$$

Hence the performance is satisfactory.

Case 17) two ellipses are tangent to each other in a point with $0<X<L_d$ and $Y=b_w/2$:

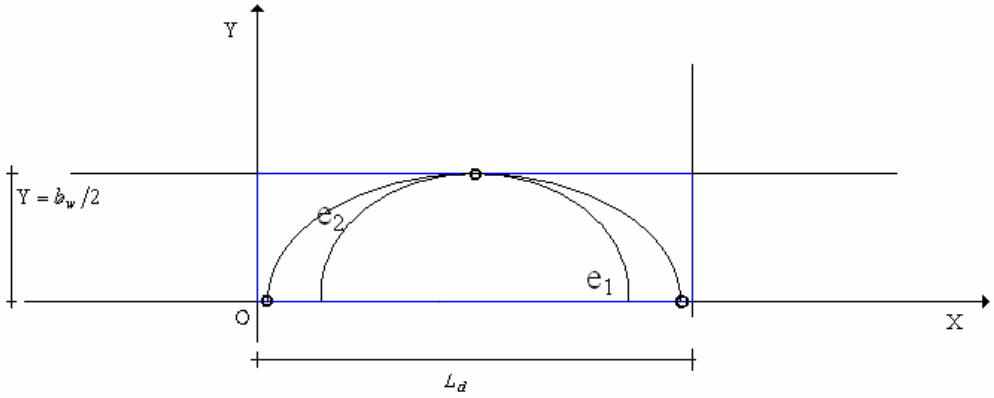

Fig. 9.5.17 – Case 17

The auxiliary matrices are:

$$\underline{X}^{p1}=\begin{bmatrix}* & *\\ * & *\end{bmatrix};\ \underline{X}^{p2}=\begin{bmatrix}* & *\\ * & *\end{bmatrix};\ \underline{X}^{q}=\begin{bmatrix}X_{11}^{q} & X_{12}^{q}\\ X_{21}^{q} & X_{22}^{q}\end{bmatrix};$$

$$\text{with } X_{11}^{q}=X_{12}^{q}=X_{21}^{q}=X_{22}^{q} \tag{9.5.46}$$

$$\underline{G}=\begin{bmatrix}.....\left(X_{o1}-a_1\right) & \left(X_{o1}+a_1\right)\\ .....\left(X_{o2}-a_2\right) & \left(X_{o2}+a_2\right)\end{bmatrix};\ \underline{Y}^{e}=\begin{bmatrix}* & *\\ * & *\end{bmatrix}$$

The Non Linear range matrices:

$$\underline{X}^{nlin1}=\begin{bmatrix}* & *\\ * & *\end{bmatrix};\ \underline{X}^{nlin2}=\begin{bmatrix}* & *\\ * & *\end{bmatrix};\ \underline{X}^{nlin3}=\begin{bmatrix}* & *\\ X_{21}^{q} & X_{22}^{q}\end{bmatrix};\ \underline{X}^{nlin4}=\begin{bmatrix}* & *\\ * & *\end{bmatrix}$$

$$\underline{X}^{nlin5}=\begin{bmatrix}* & *\\ \left(X_{o2}-a_2\right) & \left(X_{o2}+a_2\right)\end{bmatrix};\ \underline{n}^{nlin}=\begin{bmatrix}0\\ 4\end{bmatrix};\quad n^{nlin}=4 \tag{9.5.47}$$

and the final matrices: $\underline{X}^{nlin}=\begin{bmatrix}* & * & * & *\\ \left(X_{o2}-a_2\right) & X_{21}^{q} & X_{22}^{q} & \left(X_{o2}+a_2\right)\end{bmatrix};\ \underline{\mathrm{A}}^{nlin}=\begin{bmatrix}*\\ \neq 0\end{bmatrix}$

As regards the Linear range of integration:

$$\underline{X}^{lin1}=\begin{bmatrix}* & *\\ * & *\end{bmatrix};\ \underline{X}^{lin2}=\begin{bmatrix}* & *\\ * & *\end{bmatrix};\ \underline{X}^{lin3}=\begin{bmatrix}* & *\\ * & *\end{bmatrix};$$

$$\underline{X}^{lin4}=\begin{bmatrix}* & *\\ * & *\end{bmatrix};\ \underline{n}^{lin}=\begin{bmatrix}0\\ 0\end{bmatrix};\ n^{lin}=0 \tag{9.5.48}$$

and the final matrices: $\underline{X}^{lin}=\begin{bmatrix}*\\ *\end{bmatrix};\ \underline{\mathrm{A}}^{lin}=\begin{bmatrix}*\\ *\end{bmatrix}$

Hence the performance is satisfactory.

Case 18) one ellipse (e_1) is tangent internally to another (e_1) and a third one intersects the previous ones in the tangency point.

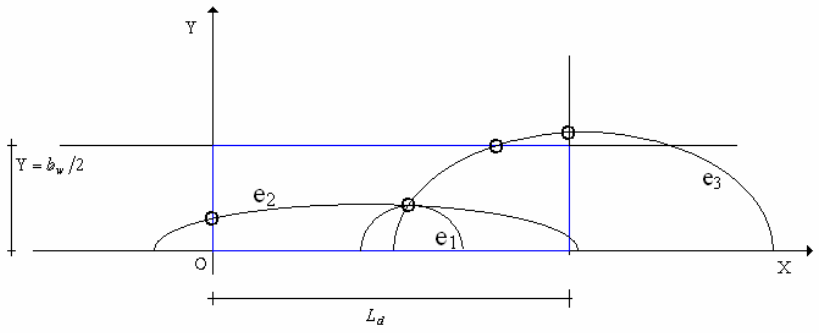

Fig. 9.5.18 – Case 18

The auxiliary matrices are:

$$\underline{X}^{p1}=\begin{bmatrix}* & * & X_{13}^{p1}\\ * & * & X_{23}^{p1}\\ X_{31}^{p1} & X_{32}^{p1} & *\end{bmatrix};\ \underline{X}^{p2}=\begin{bmatrix}* & * & *\\ * & * & *\\ * & * & *\end{bmatrix};\ \underline{X}^{q}=\begin{bmatrix}* & *\\ * & *\\ X_{31}^{q} & X_{32}^{q}\end{bmatrix};$$

$$\text{with}\quad X_{13}^{p1}=X_{23}^{p1}=X_{31}^{p1}=X_{32}^{p1};\ \underline{G}=\begin{bmatrix}.....\left(X_{o1}-a_1\right) & \left(X_{o1}+a_1\right)\\ .....\left(X_{o2}-a_2\right) & \left(X_{o2}+a_2\right)\\ .....\left(X_{o3}-a_3\right) & \left(X_{o3}+a_3\right)\end{bmatrix}; \tag{9.5.49}$$

$$\underline{Y}^{e}=\begin{bmatrix}* & *\\ Y_{21}^{e} & Y_{22}^{e}\\ * & Y_{32}^{e}\end{bmatrix}\ \text{with}\quad Y_{21}^{e}<b_w/2;\ Y_{22}^{e}<b_w/2\ \text{ and }\quad Y_{32}^{e}>b_w/2$$

The Non Linear range matrices:

$$\underline{X}^{nlin1}=\begin{bmatrix} * & * & * \\ * & * & X_{23}^{p1} \\ X_{31}^{p1} & * & * \end{bmatrix};\ \underline{X}^{nlin2}=\begin{bmatrix} * & * & * \\ * & * & * \\ * & * & * \end{bmatrix};\ \underline{X}^{nlin3}=\begin{bmatrix} * & * \\ * & * \\ X_{31}^{q} & * \end{bmatrix};\ \underline{X}^{nlin4}=\begin{bmatrix} * & * \\ X_{21}^{e} & * \\ * & * \end{bmatrix}$$

$$\underline{X}^{nlin5}=\begin{bmatrix} * & * \\ * & * \\ * & * \end{bmatrix};\ \underline{n}^{nlin}=\begin{bmatrix} 0 \\ 2 \\ 2 \end{bmatrix};\ n^{nlin}=2 \text{ and the final matrices: } \underline{X}^{nlin}=\begin{bmatrix} * & * \\ X_{21}^{e} & X_{23}^{p1} \\ X_{31}^{p1} & X_{31}^{q} \end{bmatrix};\ \underline{\mathrm{A}}^{nlin}=\begin{bmatrix} * \\ \neq 0 \\ \neq 0 \end{bmatrix} \tag{9.5.50}$$

As regards the Linear range of integration:

$$\underline{X}^{lin1}=\begin{bmatrix} * & * & * \\ * & * & * \\ * & * & * \end{bmatrix};\ \underline{X}^{lin2}=\begin{bmatrix} * & * & * \\ * & * & * \\ * & * & * \end{bmatrix};\ \underline{X}^{lin3}=\begin{bmatrix} * & * \\ * & * \\ X_{31}^{q} & * \end{bmatrix};\ \underline{X}^{lin4}=\begin{bmatrix} * & * \\ * & * \\ * & X_{32}^{e} \end{bmatrix};\ \text{with } X_{32}^{e}=L_d$$

$$\underline{n}^{lin}=\begin{bmatrix} 0 \\ 0 \\ 2 \end{bmatrix};\ n^{lin}=2 \text{ and the final matrices: } \underline{X}^{lin}=\begin{bmatrix} * & * \\ * & * \\ X_{31}^{q} & X_{32}^{e} \end{bmatrix};\ \underline{\mathrm{A}}^{lin}=\begin{bmatrix} * \\ * \\ \neq 0 \end{bmatrix} \tag{9.5.51}$$

Hence the performance is satisfactory.

By analyzing the previous cases 16th and 18th it arises the reason why it is better, in the selection of the auxiliary intersection points between ellipses, to discard the abscissa of the tangency points. The reasons are:

1. They are not useful integration points because the tangency can be or between two ellipses resulting one completely inside the other (case 16th) or one completely external to the other and tangent in one of the vertices along X (see case 3rd);
2. If the double point of tangency is included in the auxiliary matrices $\underline{X}^{p1}$ and $\underline{X}^{p2}$, when the algorithm has to select the effective intersection points for the Non Linear integration, there might be problems of lack of generality.

The second reason can be easily shown by means of the above cases 16th and 18th. In fact, if the double identical root is included in the $\underline{X}^{p1/2}$, for the 16th case, the auxiliary matrices would be:

$$\underline{X}^{p1}=\begin{bmatrix} * & X_{12}^{p1} \\ X_{21}^{p1} & * \end{bmatrix};\ \underline{X}^{p2}=\begin{bmatrix} * & X_{12}^{p2} \\ X_{21}^{p2} & * \end{bmatrix};\ \underline{X}^{q}=\begin{bmatrix} * & * \\ * & * \end{bmatrix};$$

$$\text{with } X_{12}^{p1}=X_{21}^{p1}=X_{12}^{p2}=X_{21}^{p2}$$

$$\underline{G}=\begin{bmatrix} .....(X_{o1}-a_1) & (X_{o1}+a_1) \\ .....(X_{o2}-a_2) & (X_{o2}+a_2) \end{bmatrix};$$

$$\underline{Y}^{e}=\begin{bmatrix} * & * \\ Y_{21}^{e} & Y_{22}^{e} \end{bmatrix} \text{ with } Y_{21}^{e}<b_w/2;\ Y_{22}^{e}<b_w/2 \tag{9.5.52}$$

And the matrices for the Non Linear range:

$$\underline{X}^{nlin1}=\begin{bmatrix} * & * \\ X_{12}^{p1} & * \end{bmatrix};\ \underline{X}^{nlin2}=\begin{bmatrix} * & * \\ X_{12}^{p2} & * \end{bmatrix};\ \underline{X}^{nlin3}=\begin{bmatrix} * & * \\ * & * \end{bmatrix};$$
$$\text{with } X_{12}^{p1}=X_{12}^{p2};\ \underline{X}^{nlin5}=\begin{bmatrix} * & * \\ * & * \end{bmatrix};\underline{X}^{nlin4}=\begin{bmatrix} * & * \\ X_{21}^{e} & X_{22}^{e} \end{bmatrix}$$
$$\text{with } X_{21}^{e}=0;\ X_{22}^{e}=L_d;\ \underline{n}^{nlin}=\begin{bmatrix} 0 \\ 4 \end{bmatrix};\ n^{nlin}=4 \qquad (9.5.53)$$
$$\text{and the final matrices: } \underline{X}^{nlin}=\begin{bmatrix} * & * & * & * \\ X_{21}^{e} & X_{12}^{p1} & X_{12}^{p2} & X_{22}^{e} \end{bmatrix};\ \underline{\mathrm{A}}^{nlin}=\begin{bmatrix} * \\ \neq 0 \end{bmatrix}$$

Hence, for the 2nd ellipse, there would be two couples of effective points and the algorithm would be working properly.

For case 18th, it the auxiliary matrices would be:

$$\underline{X}^{p1}=\begin{bmatrix} * & X_{12}^{p1} & X_{13}^{p1} \\ X_{21}^{p1} & * & X_{23}^{p1} \\ X_{31}^{p1} & X_{32}^{p1} & * \end{bmatrix};\ \underline{X}^{p2}=\begin{bmatrix} * & X_{12}^{p2} & * \\ X_{21}^{p2} & * & * \\ * & * & * \end{bmatrix};\ \underline{X}^{q}=\begin{bmatrix} * & * \\ * & * \\ X_{31}^{q} & X_{32}^{q} \end{bmatrix};$$
$$\text{with } X_{13}^{p1}=X_{23}^{p1}=X_{31}^{p1}=X_{32}^{p1}=X_{12}^{p1}=X_{12}^{p2}=X_{21}^{p1}=X_{21}^{p2}$$
$$\underline{G}=\begin{bmatrix} .....\left(X_{o1}-a_1\right) & \left(X_{o1}+a_1\right) \\ .....\left(X_{o2}-a_2\right) & \left(X_{o2}+a_2\right) \\ .....\left(X_{o3}-a_3\right) & \left(X_{o3}+a_3\right) \end{bmatrix}; \qquad (9.5.54)$$
$$\underline{Y}^{e}=\begin{bmatrix} * & * \\ Y_{21}^{e} & Y_{22}^{e} \\ * & Y_{32}^{e} \end{bmatrix} \text{ with } \quad Y_{21}^{e}<b_w/2;\ Y_{22}^{e}<b_w/2 \text{ and } \quad Y_{32}^{e}>b_w/2$$

And the matrices of the effective integration points in the Non Linear case would be:

$$\underline{X}^{nlin1}=\begin{bmatrix} * & * & * \\ X_{21}^{p1} & * & * \\ X_{31}^{p1} & * & * \end{bmatrix};\ \underline{X}^{nlin2}=\begin{bmatrix} * & * & * \\ X_{21}^{p2} & * & * \\ * & * & * \end{bmatrix};\ \text{with } X_{21}^{p1}=X_{21}^{p2};\ \underline{X}^{nlin3}=\begin{bmatrix} * & * \\ * & * \\ X_{31}^{q} & * \end{bmatrix};$$
$$\underline{X}^{nlin4}=\begin{bmatrix} * & * \\ X_{21}^{e} & * \\ * & * \end{bmatrix};\ \underline{X}^{nlin5}=\begin{bmatrix} * & * \\ * & * \\ * & * \end{bmatrix};\underline{n}^{nlin}=\begin{bmatrix} 0 \\ 3 \\ 2 \end{bmatrix};\ n^{nlin}=3 \qquad (9.5.55)$$
$$\text{and the final matrix: } \underline{X}^{nlin}=\begin{bmatrix} * & * & * \\ X_{21}^{e} & X_{21}^{p1} & X_{21}^{p2} \\ X_{31}^{p1} & X_{31}^{q} & * \end{bmatrix}$$

But this would create problems because we have to determine couples of effective abscissa values.

A solution could be to check, while building the matrix $\underline{X}^{p2}$, if in the i-th row, a value that results valid is not equal to someone else already existing in the corresponding i-th row of the matrix $\underline{X}^{p1}$ but this would, again, return an odd number of effective points for the case 16th thus, since those tangency points are not necessary for the final integration, is better to discard them from the beginning. Those considerations are also valid for intersections between ellipses lying above the line $Y=b_w/2$.